Collapse Assessment of Steel Plate Shear Walls

Armin Farahbakhshtooli

A Thesis

In the Department

of

Building, Civil and Environmental Engineering

Presented in Partial Fulfillment of the Requirements

For the Degree of

Doctor of Philosophy (Civil Engineering) at

Concordia University

Montréal, Québec, Canada

July 2020

CONCORDIA UNIVERSITY

School of Graduate Studies

This is to certify that the thesis prepared

By: Armin Farahbakhshtooli

Entitled: Collapse Assessment of Steel Plate Shear Walls

and submitted in partial fulfillment of the requirements for the degree of

Doctor of Philosophy (Civil Engineering)

complies with the regulations of the university and meets the accepted standards with respect to originality and quality.

Signed by the final examining committee:

_____ Chair
Dr. Rajamohan Ganesan

_____ External Examiner
Dr. Sreekanta Das

_____ External to Program
Dr. Sivakumar Narayanswamy

_____ Examiner
Dr. Lucia Tirca

_____ Examiner
Dr. Khaled Galal

_____ Thesis Supervisor
Dr. Anjan Bhowmick

Approved by _____
Dr. Michelle Nokken, Graduate Program Director

Wednesday 2020-07-15

_____
Dr. Mourad Debbabi, Dean
Gina Cody School of Engineering and Computer Science

ABSTRACT

Collapse Assessment of Steel Plate Shear Walls

Armin Farahbakhshtooli, Ph.D.

Concordia University, 2020

Steel Plate Shear Walls (SPSWs) are commonly used in low- to high-rise buildings as the lateral load resisting system. Most commonly used SPSWs in multi-storey buildings are unstiffened, stiffened, and composite SPSWs. Unlike unstiffened SPSWs, very little research has been conducted to assess the seismic performance of stiffened and composite SPSWs. The stiffened and composite SPSWs have been proved to provide higher level of ductility due to the fact that they can prevent the buckling of thin infill plate, while increasing the initial stiffness and energy absorbance capacity of the whole system. The objective of current study is to assess the seismic performance and collapse capacity of stiffened and composite SPSWs. In the current research work, two types of composite SPSWs (traditional and innovative) are considered. In innovative composite SPSW, there is a small gap between reinforced concrete (RC) panel and surrounding boundary members, while in traditional one, RC panel is in direct contact with surrounding boundary members. In the first step, a reliable macro-modelling approach was developed for each type of SPSWs considered in this study. The validity of the proposed macro models was then investigated against available experimental data. Several multi-storey stiffened and composite SPSWs were designed according to CSA S16-14 and NBC 2015. To estimate the seismic response parameters (i.e., ductility-related force modification factor and overstrength-related force modification factor) for designing stiffened and composite SPSWs, nonlinear static pushover analysis and incremental dynamic analysis (IDA) have been performed on all archetypes using OpenSees following the procedure presented in FEMA P695. Quantification of seismic parameters of stiffened and composite SPSWs, including period-based ductility, overstrength, and collapse margin ratio has been conducted to better understand the seismic response and collapse capacity of the SPSW system. The results showed that all archetypes provide significant safety margin

against collapse (large collapse margin ratio values) and satisfy the requirements of FEMA P695. Seismic response sensitivity of traditional composite SPSWs to the variation of post-yielding parameters (i.e., ductility capacity and post-cap stiffness ratio) in infill plate and variation of post-cracking parameters (i.e., shear strain correspond to maximum shear stress, yielding shear strain, and residual stress) in shear behavior adopted for RC panel are further investigated. The study showed that the capacity of composite SPSW is more sensitive to the variation of post-yielding parameters of the infill plate, while the variation of post-cracking parameters of the concrete panel has a minor effect on overall performance of the composite SPSW system.

Steel plate shear wall with regularly spaced circular perforations has recently been developed. While the current edition of AISC 341-16 and CSA S16-14 have adopted perforated SPSW in their design standards, no simple numerical model is currently available for this SPSW system. In this study, a reliable macro-modelling approach was developed for regularly spaced circular perforation and was validated against available experimental results. Nonlinear seismic response of perforated SPSWs was studied through conducting a series of time history and incremental dynamic analysis to better understand the overall performance of the system when subjected to strong ground motions.

Acknowledgements

First and foremost, I would like to thank my supervisor, Dr. Anjan Bhowmick for his support, help, and guidance throughout this research study. His continuous encouragement has provided me with the confidence to learn and progress all the time. His dynamism, vision, sincerity and motivation have deeply inspired me. He taught me the way to carry out the research and to present the research works as clearly as possible. It was a great privilege and honour to work and study under his guidance.

I will be failing in my duty if I do not mention special thanks to my friends Shadnoush Pashaei Farahani, Hamid Arabzadeh, Shadman Hosseinzadeh, Siamak Pejmanfar, Siamak Delir Jafarzadeh, Ali Shirani, and Ali Gohari for their help, endless support and valuable hints throughout this research study.

I would like to acknowledge the financial support from Gina Cody School of Engineering and Computer Science, Concordia University, Montreal and Natural Sciences and Engineering Research Council of Canada (NSERC). Their support is gratefully acknowledged.

Finally, I would like to thank my main pillars in my life, my parents, without whom, I would not be definitely achieving this success. Also, I would like to acknowledge my brothers for their invaluable supporting over the past four years throughout my study.

Dedication

To my lovely parents,

& To my Brothers

Co-Authorship

This thesis has been prepared in accordance with the regulations for a sandwich thesis format. This research presents numerical work carried out solely by Armin Farahbakhshtooli. Advice and guidance provided for the whole thesis by the academic supervisor Dr. Anjan Bhowmick. This thesis consists of the following chapters:

- Chapter 3

  Farahbakhshtooli, A., and Bhowmick, AK. (2019). "Seismic Collapse Assessment of Stiffened Steel Plate Shear Walls using FEMA P695 Methodology", Journal of Engineering Structures, 200: 1–19.

- Chapter 4

  Farahbakhshtooli, A., and Bhowmick, AK. (2019). "Seismic Collapse Assessment of Composite Plate Shear Walls", ASCE Journal of Structural Engineering, accepted (In Press).

- Chapter 5

  Farahbakhshtooli, A., and Bhowmick, AK. (2020). "Nonlinear Seismic Analysis of Perforated Steel Plate Shear Walls using a Macro-model", Journal of Thin-Walled Structures, submitted and is under review.

TABLE OF CONTENTS

List of tables

List of Figures

Chapter 1
Introduction

1.1 Background and Problem Definition

Steel plate shear walls (SPSWs) have been widely used as primary load carrying system in many buildings in Japan and United States. Three common types of SPSWs that are widely used in construction of multi-storey buildings are unstiffened, stiffened, and composite SPSWs. Unstiffened SPSW consists of a thin infill plate and is connected to the surrounding boundary elements (beams and columns) using fillet welds or bolts. A significant number of analytical as well as experimental studies have been conducted on unstiffened SPSWs to assess the overall performance of the system (Driver et al. 1997; Roberts and Sabouri-Ghomi 1991; Bhowmick et al. 2008; Choi and Park 2010). It has been shown that unstiffened SPSWs are capable of resisting applied lateral loads by forming the tension field action in the infill plate. The main disadvantage of unstiffened SPSW is the buckling of compression zone in the infill plate due to relatively small lateral force, which results in significant reduction in stiffness, strength, and energy dissipation capacity of the whole system. To postpone the buckling of infill plate, two general methods can be used. First method is to install series of horizontal and vertical stiffeners on thin infill plate to prevent the overall buckling of the infill plate. However, adding stiffeners will impose additional cost to the construction. In addition, both unstiffened and stiffened SPSWs experience larger inelastic rotation in their connections when subjected to cyclic loading (Allen and Bulson 1980). The second method is to attach a reinforced concrete (RC) panel to one or both sides of the thin infill plate. This system is known as composite plate shear wall (C-PSW) and can mitigate most disadvantages of both stiffened and unstiffened SPSWs. Moreover, presence of RC panel reduces the vulnerability of the system against fire and blast loads. To the best of authors' knowledge, very limited research has been done on C-PSWs. Research on C-PSWs started from experimental study of Zhao and Astaneh-Asl (2004) on two different configurations of C-PSWs, denoted as "Traditional" and "Innovative". In innovative C-PSWs, there is a small gap between RC panel and surrounding boundary elements, while in traditional one, RC panel is in direct contact with surrounding boundary members.

This research will focus on the seismic performance of composite and stiffened steel plate shear walls and assessing the validity of seismic performance factors (i.e., ductility-related force modification factor ,R_d, of 5.0 and overstrength-related force modification factor ,R_0, of 1.6 that are used for designing of unstiffened SPSWs) for designing of composite and stiffened SPSWs.

Past studies has shown that infill plate thickness requirement for SPSW (i.e., solid unstiffened, stiffened, and composite) to resist storey shear is usually low, especially in low-to-mid-rise buildings. From constructability point of view, it is often observed that the minimum plate thickness used in construction is larger than the required infill plate thickness. When larger than required infill plate thickness is used, the demand on surrounding boundary members will increase significantly and consequently will increase the sizes of boundary members. To overcome this problem, researchers have proposed several alternatives such as using light-gauge shear walls with cold rolled infill plates (Berman and Bruneau 2005), using low-yield strength steel (Soltani et al. 2017), introducing vertical slit, introducing perforation such as circular perforation (Vian and 2004; Purba 2006; Bhowmick et al. 2014; Shekastehband et al. 2017; Ali et al. 2018), or rectangular perforation (Sabouri-Ghomi et al. 2016; Sabouri-Ghomi and Mamazizi 2015; Barkhordari et al. 2014). The later solution is appealing for civil engineering community since it can accommodate the need for utility to pass through infill plate without any damage to the whole system and ease handling and installation of the infill plate in the site. This study will focus on developing a reliable macro-modelling approach to better understand the overall performance of perforated SPSWs when subjected to strong ground motions.

1.2 Research Significance and Motivation

Analytical and numerical modelling are more recently considered and used by many researchers since they are less expensive and more effective in modelling different aspect of structures addressing many drawbacks caused by experimental tests such as huge amount of expenses, scaling method, and etc. The numerical modelling approach shown to be capable of capturing experimental events with great level of accuracy while these approaches provide the user with more control over the failure modes, loading protocols, and collapse criteria assessment. The literature indicates lack of macro-modelling approach in predicting the inelastic behavior of unstiffened (i.e., perforated), stiffened and composite SPSWs. As will be discussed later, these

macro-models are key, not only to facilitate evaluating the overall response of the system, but also to help better understand the performance data in accordance with new seismic performance standards and assessment approaches. [e.g., ASCE 41-17 (ASCE 2017), FEMA P695 (FEMA 2009), and FEMA 356 (FEMA 2000)].

The recent capacity design methodology introduced by (Berman and Bruneau 2008) dictates an efficient while feasible designing and detailing of the elements and components of the structure to ensure a stable and predictable behavior of the whole system during seismic events. Meanwhile, any sudden strength loss and non-ductile failure modes needs to be avoided. Therefore, SPSW system should provide a ductile performance in a seismic event and be able to sustain large reversible cycles of inelastic deformations without significant degradation in strength. Past experiments on unstiffened SPSW systems represented that significant tearing occurrence in the infill plate can attribute in significant strength loss in whole building and cause global instability. To postpone the global instability and control the maximum interstorey drift, RC panel can be attached to one or both sides of infill plate. Presence of RC panel has significant impact in maintaining the global stability of the whole system in relatively large interstorey drift when extensive web tearing occurs in thin infill plate and the system is losing a significant portion of both strength and stiffness.

1.3 Objectives and Scope of the Work

The main objective of this research is to investigate the seismic performance of steel shear walls (i.e., perforated unstiffened, stiffened, and composite SPSWs) while taking into consideration the deficiency of some existing buildings designed based on the previous code provisions. The following sub-objectives are also considered for the present research:

- Development and validation of precise modelling approaches to reliably predict the nonlinear responses of both stiffened and composite SPSWs.

- Development and validation of a new modelling approach to simulate the effects of gap existence between RC panel and surrounding boundary elements for innovative C-PSWs.

- Incremental dynamic analysis and seismic assessment of stiffened and composite SPSWs using the proposed method by FEMA P695 (FEMA 2009).

- Assess the seismic response sensitivity of stiffened and composite SPSWs to the variation

of post-yielding parameters (i.e., ductility capacity and post-cap stiffness ratio) in the infill plate.

- Assess the seismic response sensitivity of C-PSWs to variation of post-cracking parameters in the RC panel.

- Develop a reliable macro-modelling approach for regularly-spaced circular perforations and validate against available experimental tests.

- Investigate the demand reduction in the boundary members due to existence of perforation and compare the differences with solid infill plate.

- conduct a series of time history analyses to assess the sensitivity of perforated SPSWs response to the changes in hole diameter

1.4 The Thesis Layout

The thesis is divided into six chapters as following:

- Chapter 1 consists of introduction; research significance and motivation; objectives and scope of work including a brief literature review.
- Chapter 2 includes the literature review including the numerical micro and macro models proposed for the simulation of the seismic behavior of unstiffened (i.e., solid and perforated), stiffened, and composite SPSWs; common failure modes of steel shear walls.
- Chapter 3 investigates "Seismic Collapse Assessment of Stiffened Steel Plate Shear Walls using FEMA P695 Methodology". This chapter discusses the different types of buckling (i.e., global and local buckling) that might occur in stiffened SPSWs along with the requirements to prevent unanticipated behaviors. Developing numerical model and conducting a series of seismic analysis to evaluate the performance of stiffened SPSWs when subjected to strong ground motions.
- Chapter 4 consist of "Seismic Collapse Assessment of Composite Plate Shear Walls". The proposed numerical models of traditional and innovative C-PSWs including detail description of the modelling procedure for reinforced concrete (RC) panel, infill plate, and surrounding boundary members are provided in this chapter.

- Chapter 5 investigates the "Nonlinear Seismic Analysis of Perforated Steel Plate Shear Walls using a Macro-model". This chapter evaluates the seismic force demand in different levels of studied archetypes and assess the contribution of each component (i.e., infill plates and boundary members) in resisting the storey shear.
- Chapter 6 includes the summary of the research project, the main contributions, conclusions, and the recommendations for future work.

Chapter 2
General Background

2.1 Introduction

In past three decades, unstiffened steel plate shear walls (SPSWs) have been used as a primary load carrying system in a number of buildings in Japan and United states. The SPSW resembles to a vertical plate girder which is extended along the height of the building. Thin infill plate is connected to surrounding boundary elements using fillet welds or bolts and acts similar to the web of the plate girder. The columns which are known as vertical boundary elements are performing like the flanges of the plate while the beams are acting like the stiffeners installed on the web of the plate girder. The main difference between a SPSW and plate girder is that columns in SPSW are carrying a significant amount of axial loads. This issue makes the SPSW more complicated compare with plate girder. In addition, unstiffened SPSW is buckled elastically in the early stages of loading and tension field action forms in infill plate to resist applied loads. Buckling of infill plate in elastic region can decrease initial elastic stiffness as well as energy absorbance in the system. To solve this issue, thin infill plate can be stiffened or thick infill plate can be implemented instead of thin one to prevent elastic buckling in order to increase the system's initial stiffness as well as energy absorbance capacity. Thick infill plates are not practical and have many disadvantages such as more costs, higher demands on boundary elements, and higher weight which results in larger seismic forces applied on the system. In order to avoid these disadvantages, stiffened plate can be implemented instead of thick plate to enhance the overall performance of the system. One major issue associated with all three defined types of SPSW systems (i.e. unstiffened, stiffened, thick steel plate shear walls) is the large inelastic deformation of the panel which result in large cyclic rotation in the connection of boundary elements. Thus, beam to column connections are more susceptible to damage during severe loading condition. To address this issue, reinforced concrete panel (RC panel) is attached to one or both sides of thin infill plate. RC panel provides lateral bracing for infill plate to prevent elastic buckling of the plate. Also, it contributes in resisting lateral loads by increasing the strength and stiffness of the system. The extra stiffness added to the system due to participation of RC panel in resisting lateral loads, can be considered as a

compensation for stiffness loss due to plate yielding and plate tearing. In 2004, Zhao and Astaneh-Asl investigated the performance of composite plate shear walls (C-PSWs) by conducting hysteretic cyclic loading analyses on two common types of C-PSW (Zhao and Astaneh-Asl 2004).

2.2 Literature Review

Infill plates provide high stiffness and strength for entire system through post buckling behavior and tension field action. Prior to key research conducted on SPSWs in 1980s, buckling of infill plate was considered as the limit state in designing of SPSWs. However, several experimental and analytical results conducted on the SPSWs indicate that ductility and energy dissipation capacity of the system during post buckling behavior of infill plates are substantial (Thorburn et al. 1983; Timler and Kulak 1983; Driver et al. 1997, Roberts and Sabouri-Ghomi 1991). Based on the findings reported by researchers, Canadian Standards Association steel design provided design procedure for SPSWs by allowing infill plate to buckle (CSA 2014). Post buckling strength and tension field action are two primary features of SPSW system which will be described as follow. Infill plate does not contribute in resisting gravity loads and experiences only shear deformation when the system is subjected to lateral loads. Thus, the infill plate is subjected to pure shear. By using Mohr circle concept, it is clear that principal compressive and tensile stresses are oriented at a 45 degree with regards to the direction of loading. The buckling stress of infill plates is dependent on various parameters like slenderness ratio (ratio of height to thickness, ratio of width to thickness) and initial imperfection created in thin infill plate during handling and installation in the field. The compressive stress corresponds to onset of buckling is relatively small due to large slenderness ratio associated with typical infill plates. Thus, buckling of thin infill plate initiates in early stages of loading and fold lines form perpendicular to the direction of principal compressive stresses (parallel with principal tensile stresses). After buckling, infill plate is not capable of carrying compressive stresses which are higher than the allowable value corresponds to onset of buckling. At this point, lateral loads are transferred through infill plate by the principal tensile stresses. This post buckling behavior is known as tension field action. This mechanism was first recognized in aerospace engineering (Wagner 1931) and implemented in building construction during design process of plate girders (Basler 1961).

The first study on unstiffened thin SPSW was performed by Thorburn et al. (1983). The researchers introduced two analytical models to represent the behavior of unstiffened thin SPSW, namely the *Strip Model* and the *Equivalent Truss Model.* Those models considered the post-buckling strength of SPSW, adopting the original work on plate girder webs subjected to shear studied earlier by Basler (1961) and the theory of diagonal tension field action by Wagner (1931), given that the wall infill plate was allowed to buckle in shear and form a diagonal tension field to resist the applied lateral loads. In the *Strip Model*, the infill plate was replaced by a series of tension strips (equal width), pin-ended, inclined in the direction of the tension field. Fig. 2.1 illustrates the strip model used to represent any typical storey and the inclination angle of the tension field α was:

$$tan^4\alpha = \left[\frac{1 + \frac{L\,.\,t_p}{2\,.\,A_c}}{1 + \frac{h\,.\,t_p}{A_b}}\right] \tag{2.1}$$

where L is the frame bay width, h is the frame storey height, t_p is the panel thickness, and A_b and A_c are gross-sectional area of the storey beam and column, repectively.

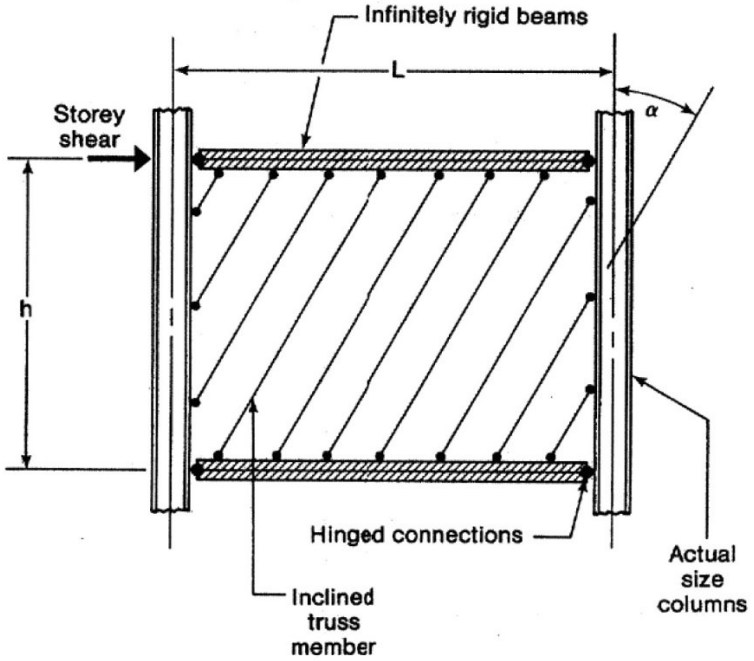

Fig. 2.1. Schematic of SPSW strip model (Thorburn et al. 1983)

The researchers also conducted analytical studies to determine the number of strips per panel that would adequately represent the infill plate behavior, and concluded that 10 strips per panel would be sufficient to represent the infill plate behavior for all shear walls investigated.

Timler and Kulak (1983) tested a single storey, full scale, thin SPSW specimen to verify the analytical work of Thorburn et al. (1983). The test specimen, shown in Fig. 2.2, consisted of two SPSW panels of 3750 mm bay width by 2500 mm storey height and 5 mm thick and vertically oriented beams W460X144 and horizontally oriented columns W310X129 connected by pinned joints at the four extreme corners and continuous joints at the middle intersections. A 6 mm thick "fish plate" was used to connect a 5 mm thick infill plate to the boundary frame. The specimen was loaded by quasi-static cyclic loading until it reached the maximum permissible serviceability drift limit.

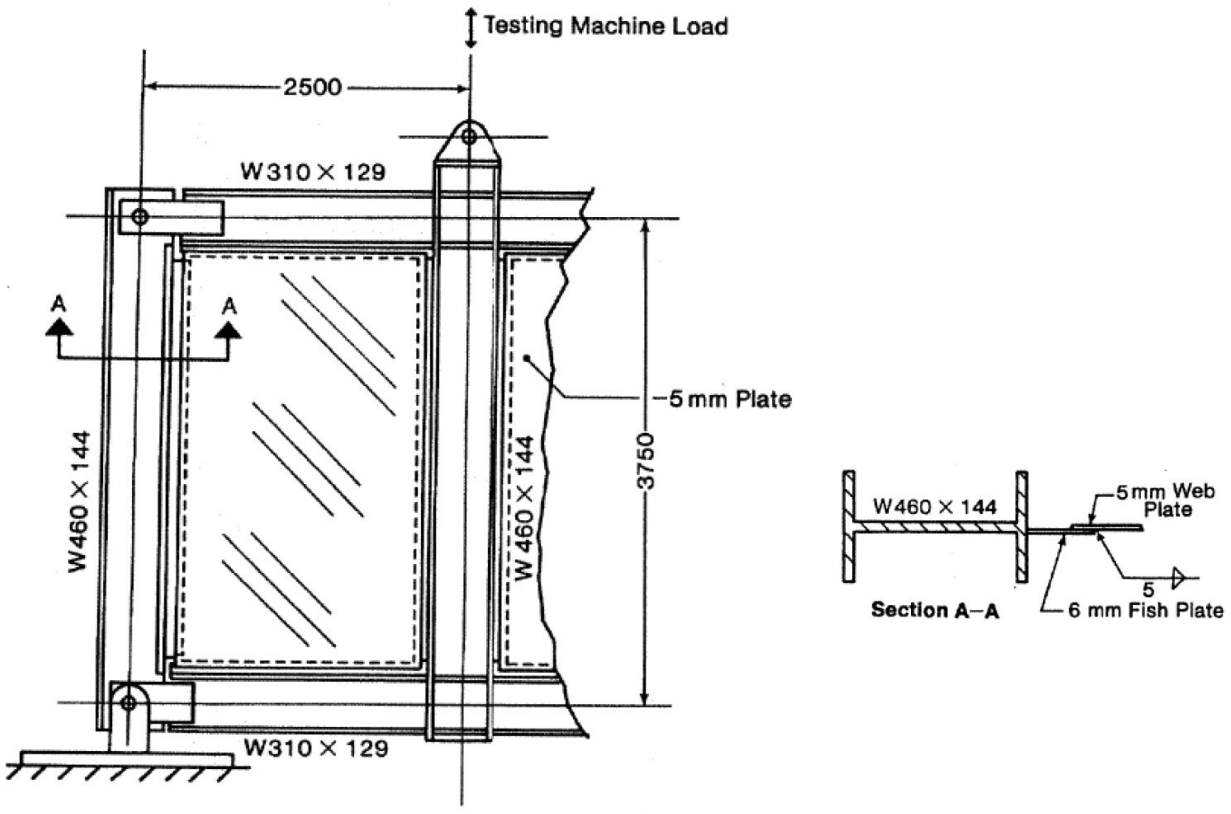

Fig. 2.2. Schematic of test specimen (Timler and Kulak 1983)

Further study on unstiffened SPSW system was conducted to investigate the effects of beam to column connection on overall performance of the system. The results indicate that the overall performance of the system is not sensitive to the type of beam to column connection (simple or rigid) since the infill plate is fully connected to the boundary frame using fillet welds or bolts (Caccese et al. 1993).

Roberts and Sabouri-Ghomi (1991) investigated the hysteretic characteristics of solid unstiffened plate shear panels. Six unstiffened SPSW specimens were subjected to quasi-static cyclic loading tests. All the specimens exhibited adequate ductility and stable S-shaped behavior during tests. A new analytical model was proposed which takes into account the shear buckling of plate, plate yielding as well as plastic hinges formation in boundary members.

Roberts and Sabouri-Ghomi (1992) performed tests to investigate the hysteretic characteristics of unstiffened steel plate shear panels with centrally placed circular openings. Quasi-static cyclic loading tests were conducted on sixteen specimens with panel dimensions (width b and depth d) of either 300×300 mm or 450×300 mm, panel thickness h of either 0.83 mm or 1.23 mm and diameter of the central circular openings D of $0, 60, 105, or\ 150$ mm. Results were correlated with results presented in Roberts and Sabouri-Ghomi (1991) for a similar specimen but with solid panel. The ratio of ultimate strength and stiffness of perforated and solid panels is plotted in Fig. 2.3 where the ultimate strength and stiffness of panels decrease as size of perforation increase. The researchers recommended that the ultimate strength and stiffness of a perforated panel can be conservatively approximated by applying a linear reduction factor as follow:

$$\frac{V_{yp.perf}}{V_{yp}} = \frac{K_{perf}}{K_{panel}} = \left[1 - \frac{D}{d}\right] \tag{2.2}$$

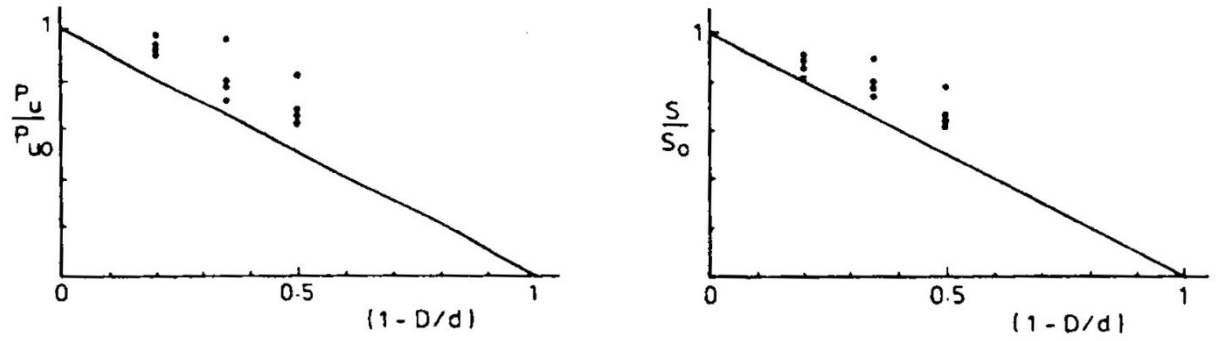

Fig. 2.3. Variation of strength and stiffness of shear panels with size of openings (Roberts and Sabouri-Ghomi 1992)

A large multi-storey steel plate shear wall with 7.4m height and 3.05m width was subjected to quasi-static cyclic loading (Fig. 2.4). Equal lateral loads were applied at all the storey levels during cyclic analysis and first storey displacement was considered as the control point. The test terminated due to rupture of west column since this column experienced severe local buckling. A finite element model was also developed for the specimen to predict the behavior of the system. The deformed shape of the SPSW model when loaded to a base shear of approximately 2200 kN is shown in Fig. 2.5. Fig. 2.6 compares the storey shear versus interstorey displacement of the experimental and the monotonic finite element model results. A good agreement between the two was observed up to a storey shear of about 400 kN (one-eight of the maximum value attained). However, at higher levels, some discrepancy was observed due to geometric nonlinearity effects, which were not taken into account in the finite element model, and the cyclic loading applied to the tested specimen that soften the structure. The finite element model overestimated the stiffness of the system. In addition to finite element model, Driver et al. (1997) developed a strip-based macro-model to investigate the behavior of four-storey SPSW. The plane-frame strip model of the tested specimen is plotted in Fig. 2.7 where each infill plate is simulated using 10 strips at the calculated tension field angle. The researchers reported that a tension inclination angle of 45 degree generally can be used in strip model. The strip model captured well the envelope of the cyclic test curves results as shown in the Fig. 2.8, but it underestimated the initial stiffness of the specimen.

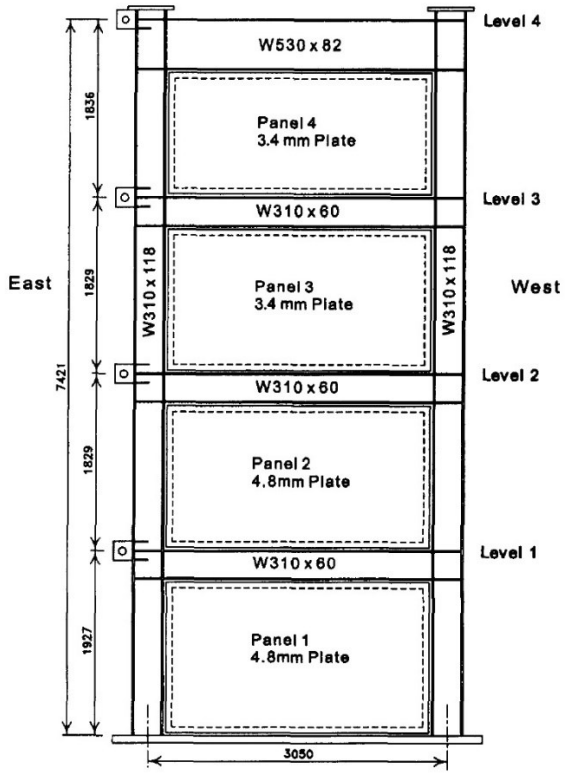

Fig. 2.4. Schematic of test specimen – North elevation (Driver et al. 1997)

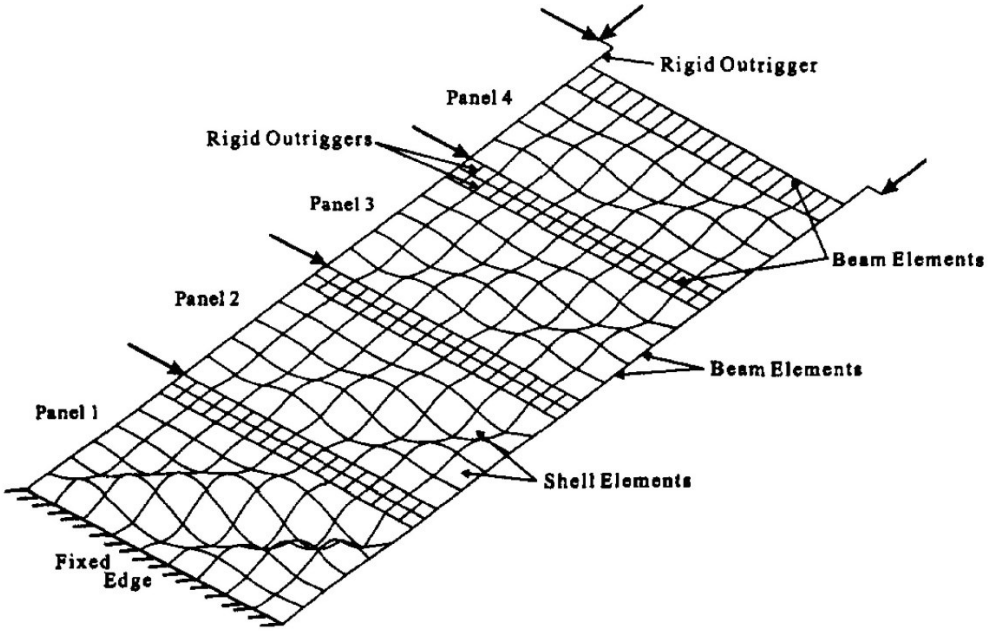

Fig. 2.5. Finite element model of test specimen – deformation scale factor = 5 (Driver et al 1997)

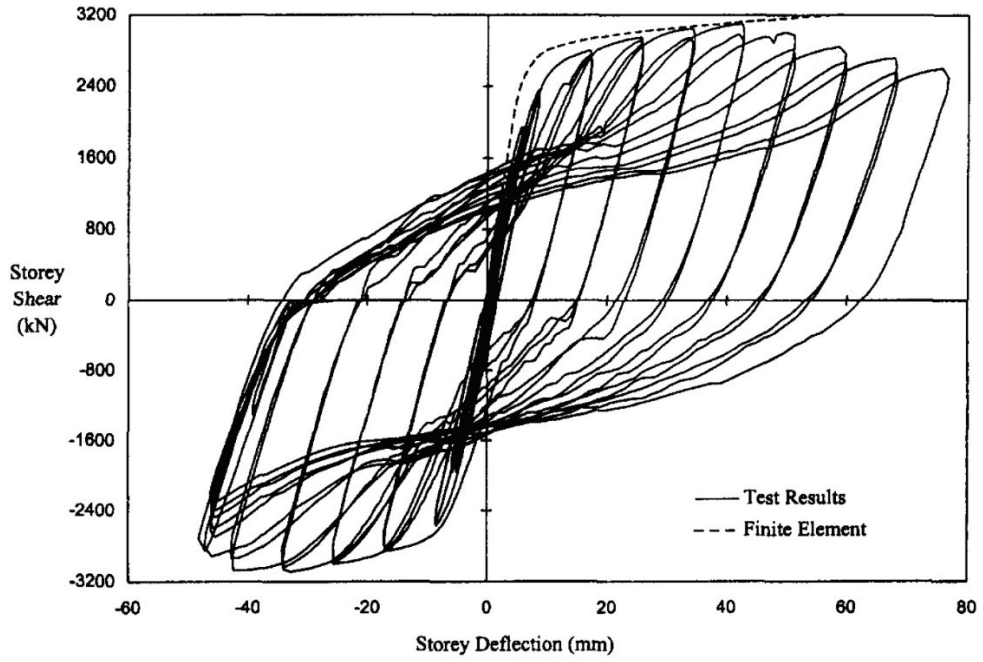

Fig. 2.6. Comparison of experimental and monotonic finite element model results (Driver et al. 1997)

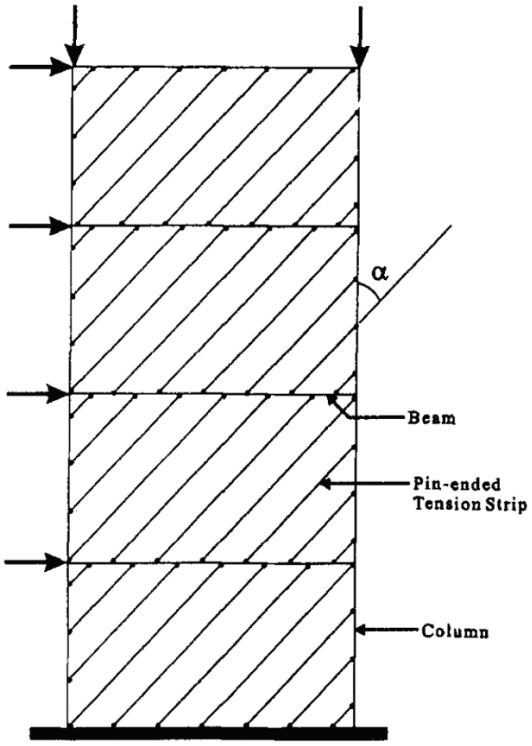

Fig. 2.7. Plane-frame strip model of test specimen (Driver et al. 1997)

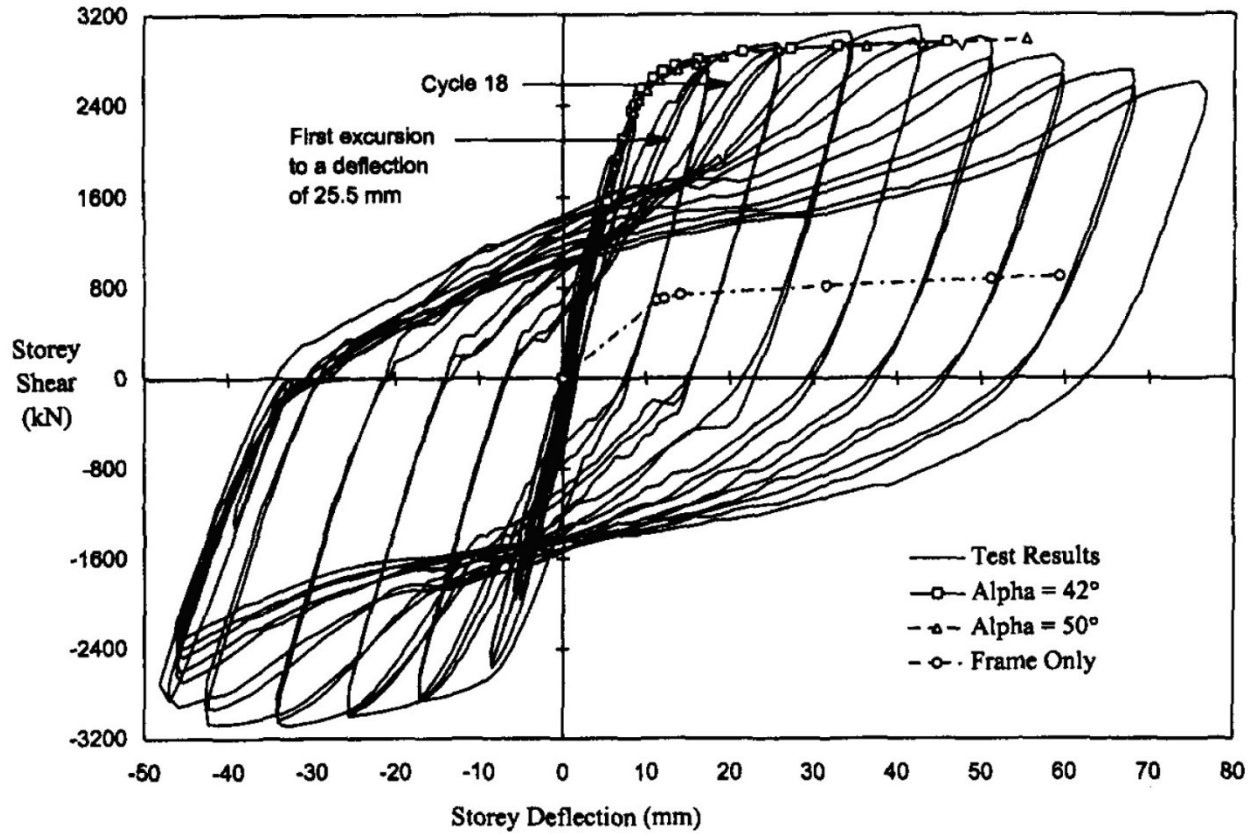

Fig. 2.8. Comparison of strip model analysis with experimental results (Driver et al. 1997)

Three 1-storey SPSWs with low yield strength infill plate and reduced beam section (RBS) at the beam ends were tested by Vian and Bruneau (2004). Three specimens were labeled as P, CR, and S2 which stand for perforated without cutout corner-reinforced, non-perforated with cutout corner-reinforced, and non-perforated without cutout corner-reinforced (solid) infill plates, respectively. All the SPSWs exhibited ductile behavior and stable S-shape hysteresis loops. Specimens "P" and "CR" were intended to accommodate the need for utility systems to pass through the infill plate. The final designs of the three specimens are plotted in Fig. 2.9. Tests were ceased due to bottom flange fracture at both RBS locations of the lower HBE at 3% interstorey drift. Results indicate that installation of low yield strength (LYS) infill plate instead of regular hot-rolled steel plate results in stiffness reduction of entire system as well as decreasing demand (forces that are applied to boundary members due to tension field action in plate) on boundary frames. The perforated panel specimen with regular hot-rolled infill plates can be an appropriate substitute for non-perforated LYS infill plates where LYS steel is not readily available in the

market since they decrease the system overall stiffness as well as overstrength in the system (Vian and Bruneau 2004).

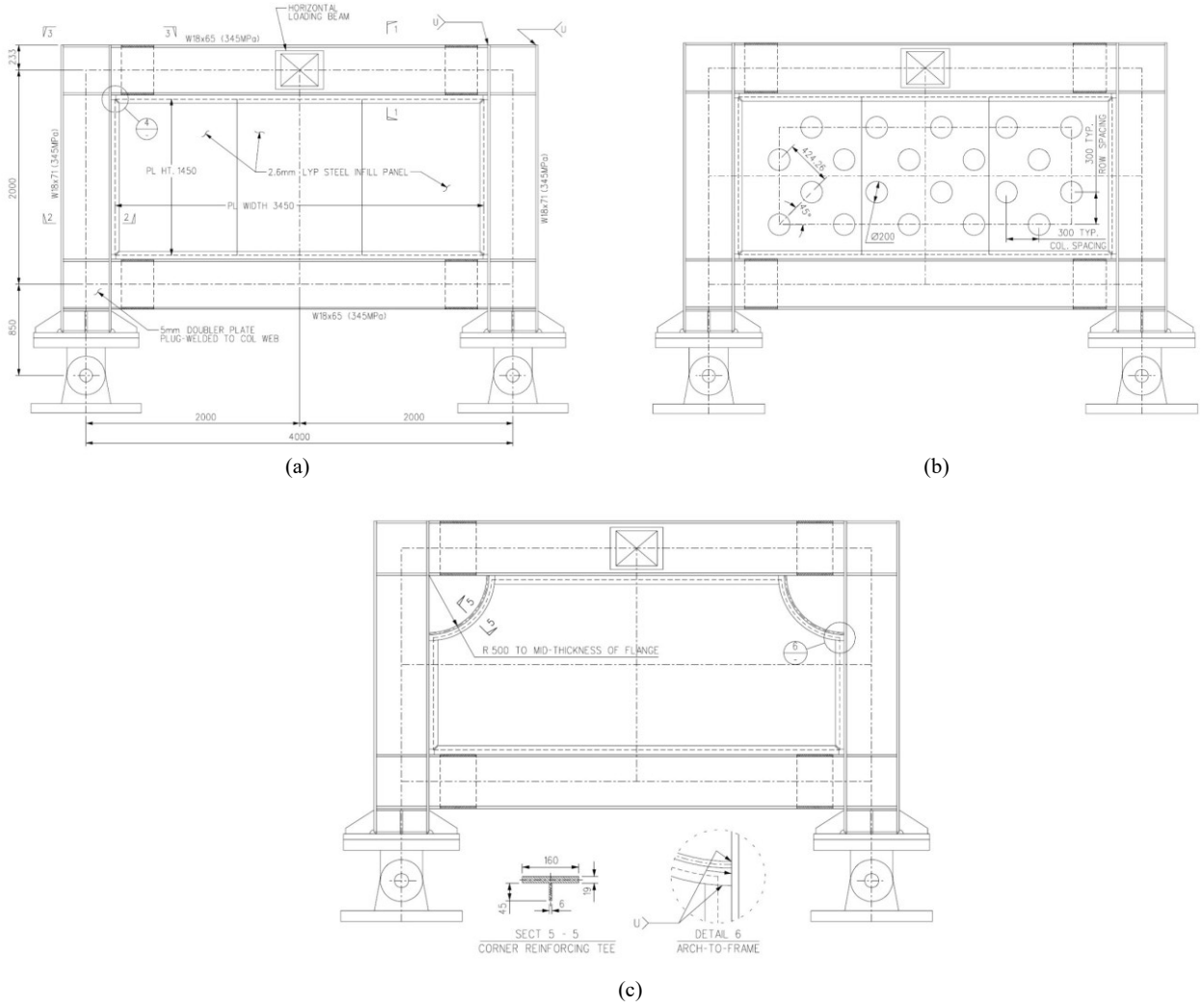

Fig. 2.9. Basic specimen dimensions (Vian and Bruneau 2004): (a) specimen S; (b) specimen P; (c) specimen CR

Choi and Park (2010) developed a finite element model for infill plate with rigid boundary elements. Based on the analysis results, the hysteretic behavior of infill plate was idealized as an equivalent stress-strain relationship for strips in macroscopic modelling of SPSWs (Fig. 2.10). Proposed stress-strain relationship was verified against several available experimental results (Fig. 2.11). The main weakness point associated with the newly developed material model is that it is not capable of considering deterioration in infill plate due to plate tearing. Thus, this material

model overestimates the specimen capacity in last cycles of loading especially in the case of severe plate tearing.

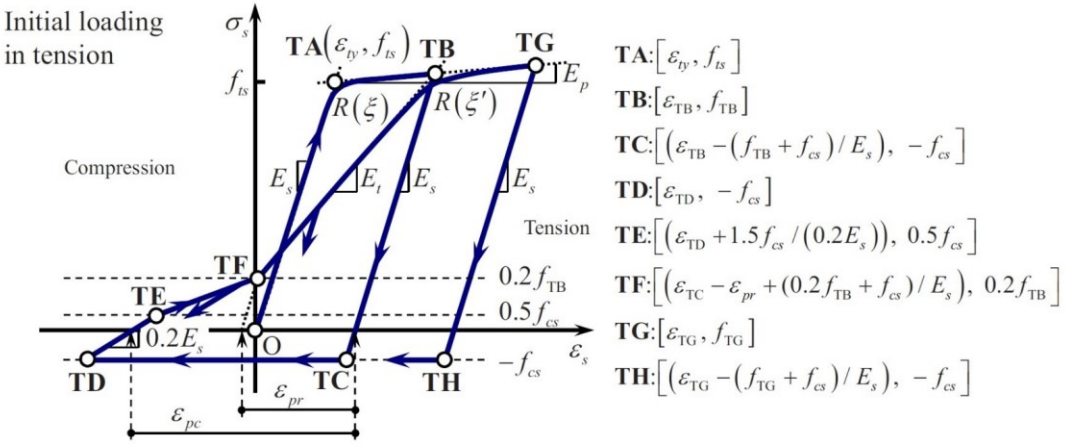

(a)

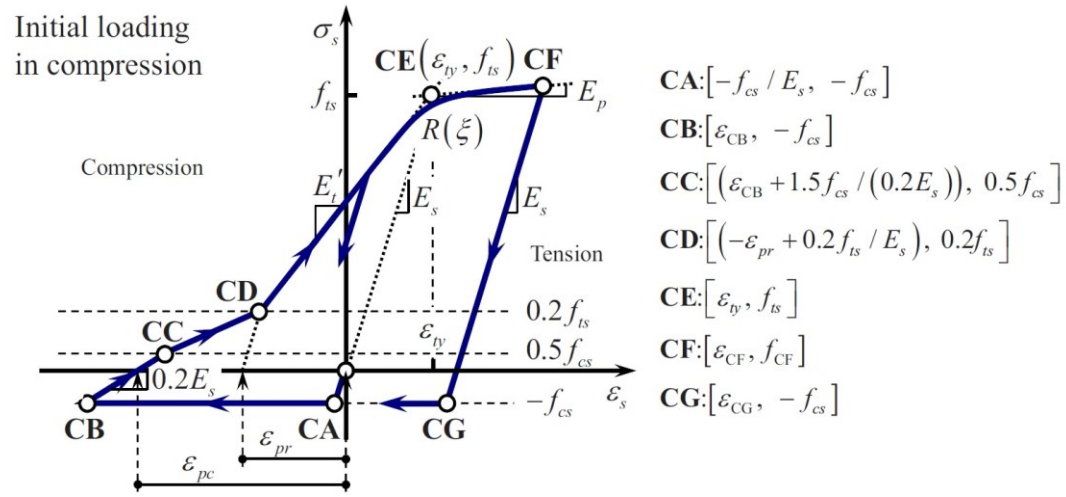

(b)

Fig. 2.10. Proposed stress-strain relationships for strip elements (Choi and Park 2010): (a) initial loading in compression; (b) initial loading in tension

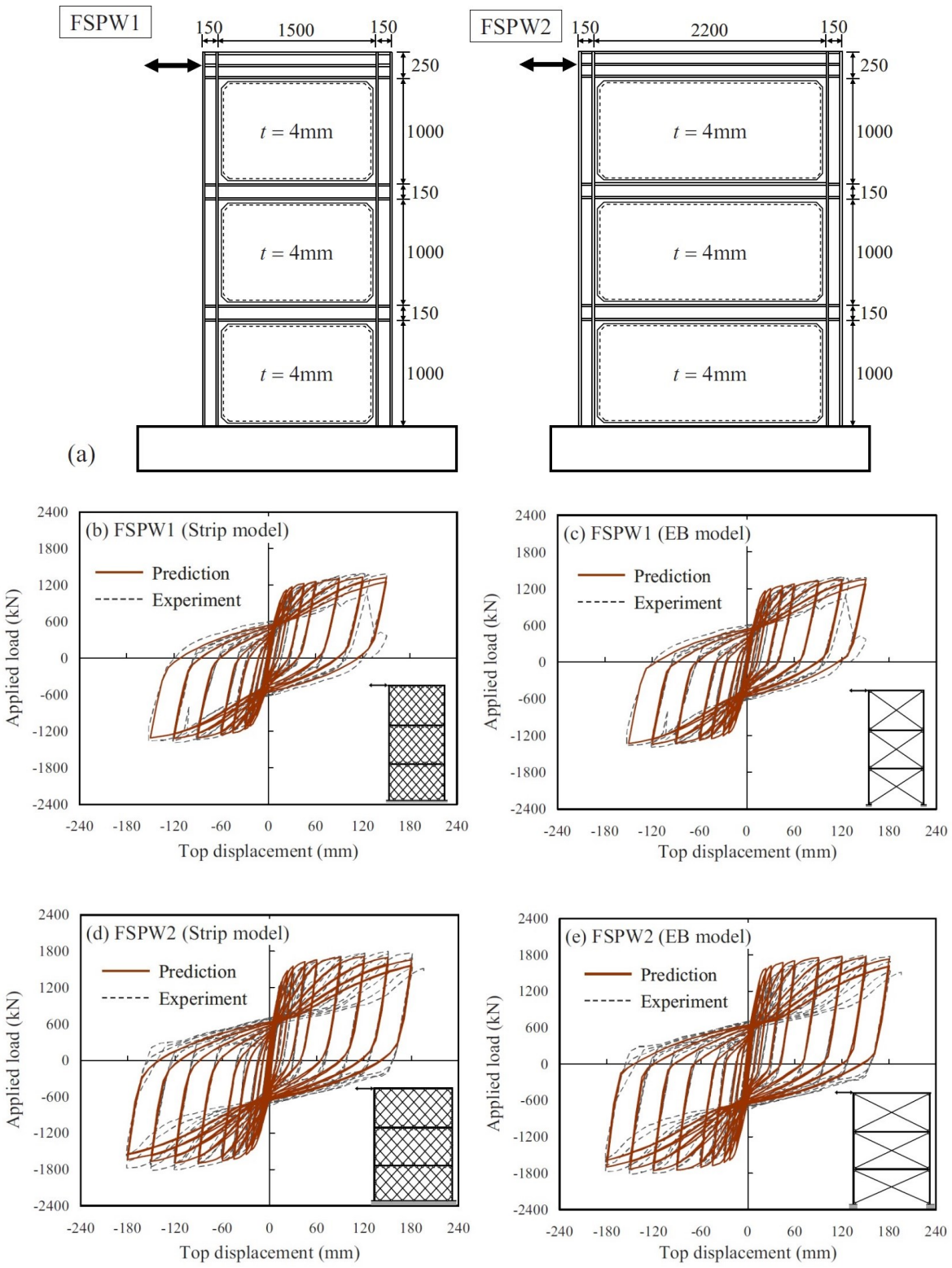

Fig. 2.11. Predictions for FSPW 1 and FSPW 2 tested by Choi and Park (2008): (a) dimensions of test specimens; (b) FSPW 1 (tension strip model); (c) FSPW 1 (equivalent tension brace model); (d) FSPW 2 (tension strip model); (e) FSPW 2 (equivalent tension brace model)

Berman and Bruneau (2003) performed plastic analysis of steel plate shear walls using the standard strip model as a basis to obtain the ultimate strength of single and multi-storey SPSWs with either simple or rigid connections. Two types of plastic collapse mechanism were considered, namely: a uniform collapse mechanism and a soft-storey collapse mechanism (Fig. 2.12). The resulting general equation for the ultimate strength of SPSWs (for the desirable uniform collapse mechanism case) is expressed as follow:

$$\sum_{i=1}^{n_s} V_i\, h_i = 2M_{pc1} + 2M_{pcn} + \sum_{i=1}^{n_s-1} M_{pbi} + \sum_{i=1}^{n_s} \frac{1}{2}\, F_y\, L\, h_i\, (t_i - t_{i+1})\sin(2\alpha) \tag{2.3}$$

where V_i is the storey shear force at the i-th storey; h_i is the storey elevation from the base; M_{pc1} and M_{pcn} are the first and top storey column (VBE) plastic moment, respectively; F_y is the infill plate yield stress; L is the bay width; h_i is the storey height; t_i is the plate thickness at the i-th storey; α is the tension field action angle from the vertical; and n_s is the total number of stories. The equation provides simple checks of results from more advanced computer models used to analyze SPSWs.

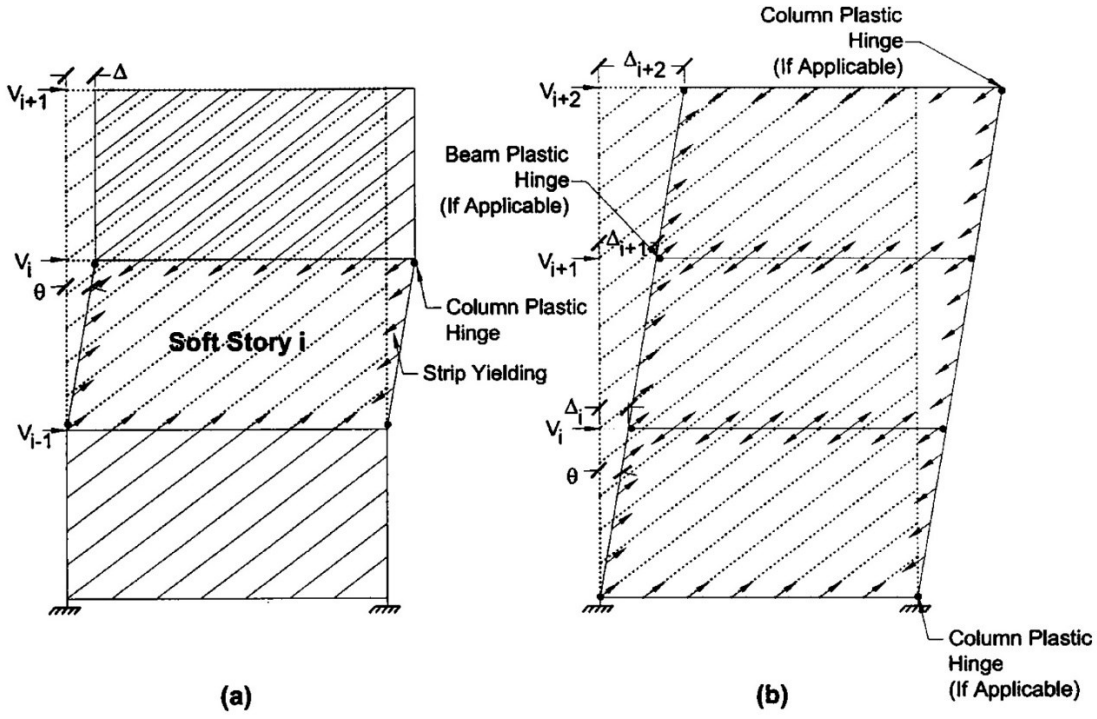

Fig. 2.12. Examples of plastic collapse mechanisms for multi-storey steel plate shear walls (Berman and Bruneau 2003)

While Eq. (2.3) was derived for the uniform collapse mechanism of multi-storey SPSW with rigid connection (Fig. 2.12-b), the equation can easily be adapted to other cases considered. For example, to estimate the ultimate strength of SPSW having the soft storey mechanism shown in Fig. 2.12-a, one can exclude the third component on the right side of the equation and remove the summation from the remaining equation. To calculate the ultimate strength of multi-storey SPSWs with simple connections, the first three parts on the right side of the equation should be canceled out.

Berman and Bruneau (2008) proposed a new method of designing vertical boundary members using capacity design method. New proposed procedure uses uniform plastic collapse mechanism and linear beam analysis to approximate the applied design loads on VBEs. Based on capacity design and fundamentals of plastic collapse mechanism, surrounding boundary members are designed based on inward forces resulting from uniform yielding of infill plates along the height the building (Fig. 2.13). Under the corresponding loads, plastic hinges are allowed to be formed at both ends of the beams in all stories as well as at the bottom of the columns in the first storey. The structure will collapse when plastic hinges are formed at both ends of columns in the first storey. As shown in Fig. 2.14, Moment and axial force diagram for VBEs calculated using new suggested procedure agrees well with pushover analyses results obtained for two example of SPSW systems.

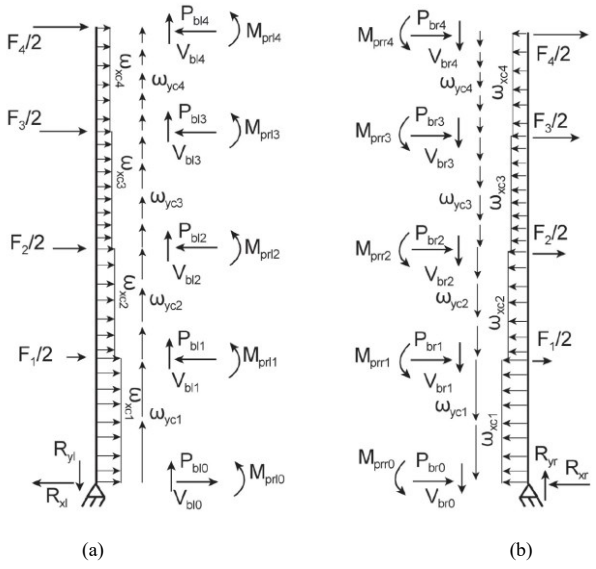

Fig. 2.13. VBE free body diagram (Berman and Bruneau 2008)

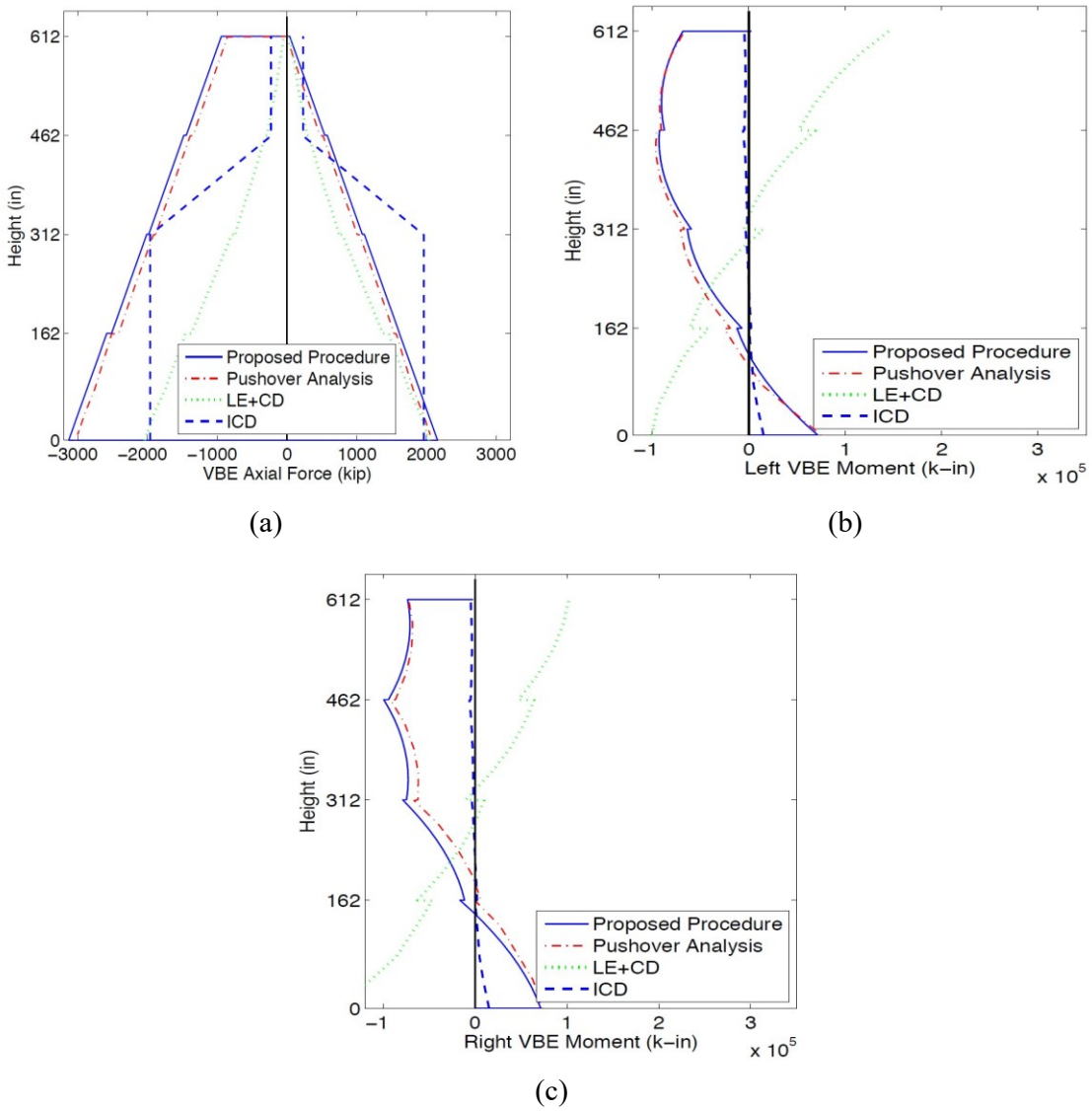

Fig. 2.14. Comparison of VBE demands from various methods for SPSW (Berman and Bruneau 2008): (a) axial force; (b) bending moment for left VBE; (c) bending moment for right VBE

Rahai and Hatami (2009) investigated the effects of variation in middle beam rigidity, shear studs spacing, and beam to column connection on overall performance of the composite plate shear walls (C-PSWs). For this aim, two parallel studies of numerical and experimental have been conducted. For numerical simulation, 42 detailed finite element models were developed by changing the three aforementioned parameters (i.e. middle beam rigidity, shear studs spacing, and beam to column connection). To assess the effect of shear studs spacing in overall performance of the system, 3 C-PSW specimens with 2m width and 1m height and varying shear studs spacing

were constructed and subjected to cyclic loading condition. The results (both experimental and numerical results) indicated that by increasing the shear studs spacing up to a specific value, energy absorption capacity of the system decreases (Fig. 2.15).

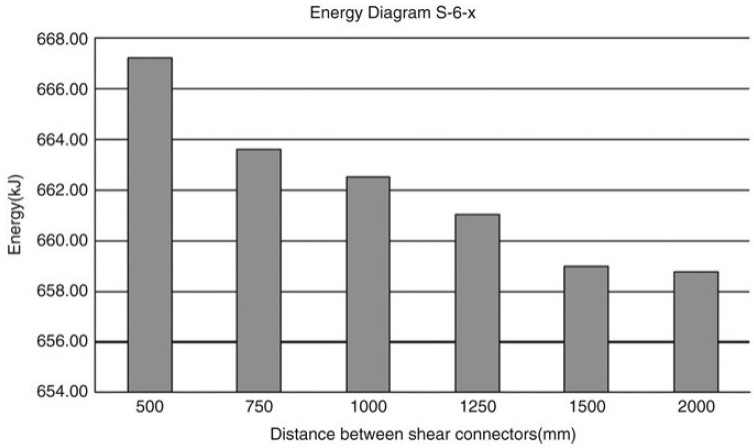

Fig. 2.15. Energy absorption (for a 60 mm thickness of concrete) (Rahai and Hatami 2009)

In addition, to investigate the effect of middle-beam rigidity on overall performance of C-PSW, a four-storey model was studied. Fig. 2.16 and Fig. 2.17 show the lateral displacement at the 1st and 4th storey level for stiffened and non-stiffened walls as a function of moment of inertia of the middle beam. In this study, the analysis was carried out using three common methods (i.e., substitution of the plate with a truss model, finite element, and classic method) related to steel plate shear walls. As shown in the figure, the curves resulting from truss modelling of steel shear walls showed very different values compared to those obtained from finite element or classic methods. Based on the results obtained from finite element or classic method, changing the middle beam rigidity has an insignificant impact on the behavior of C-PSWs.

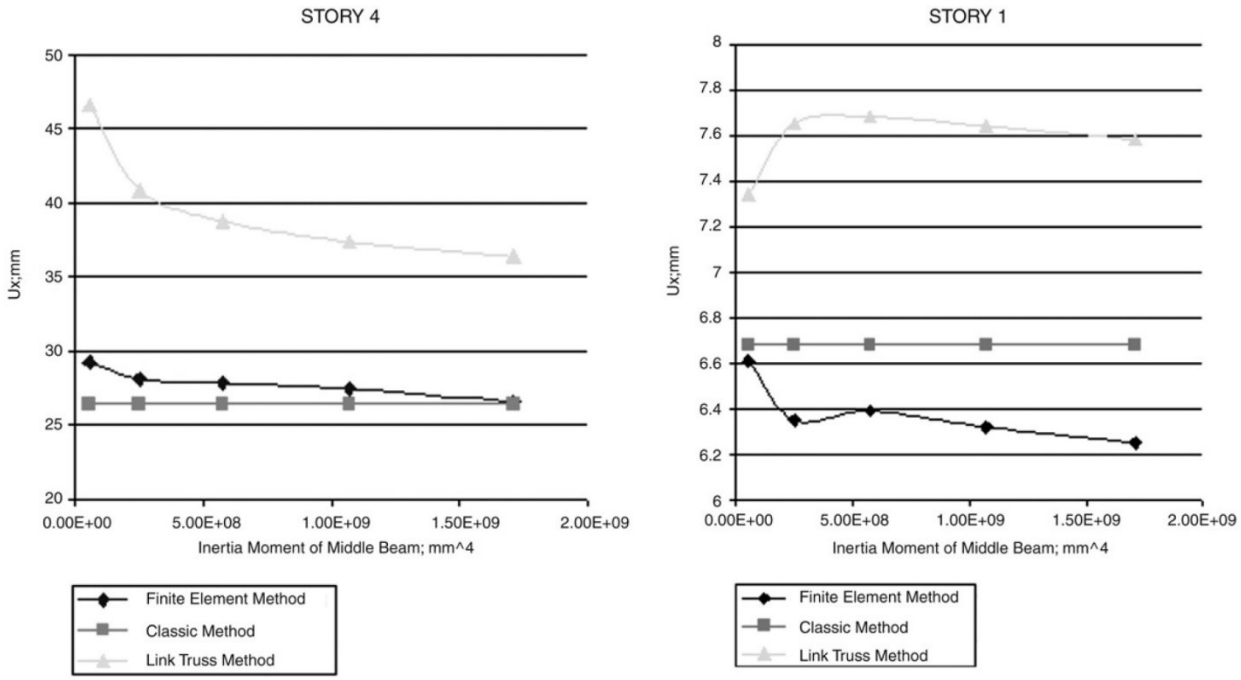

Fig. 2.16. Lateral displacement of non-stiffened shear wall (Rahai and Hatami 2009)

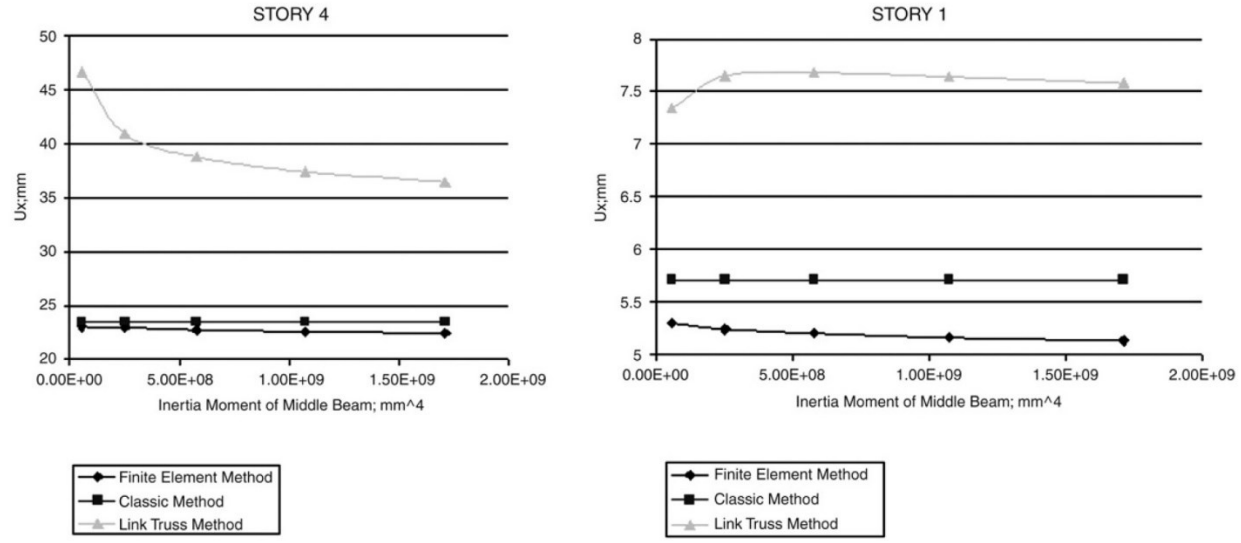

Fig. 2.17. Lateral displacement of stiffened shear wall (Rahai and Hatami 2009)

Gholipour and Alinia (2016) assessed the overall performance of SPSWs with regards to bay width variation. Several SPSWs ranging from low-rise to high-rise buildings with three different bay width (i.e., small, medium, and large) were designed and subjected to pushover analysis. The

results indicated that bay width variation highly affects the deformation mode of the entire system. For small bay width, the structure mainly deforms in flexural mode while for medium and large bay width, the structure deforms in a combination of flexure and shear modes (Fig. 2.18). In addition, further analysis indicates that in small bay width, plastic hinges are formed in boundary members prior to plate yielding which is an undesirable outcome in designing of SPSWs. To avoid this undesirable behavior, larger cross section should be considered for vertical boundary elements (VBEs) in small bay width which in turn increase the construction cost and decrease effective bay width in the system. They represented that by choosing larger bay width especially in high-rise buildings, the behavior of the system changes from pure flexure mode to a combination of flexure and shear which postpone the plastic hinges formation in boundary elements. Consequently, appropriate selection of bay width causes a considerable reduction of VBE sections especially in high-rise buildings.

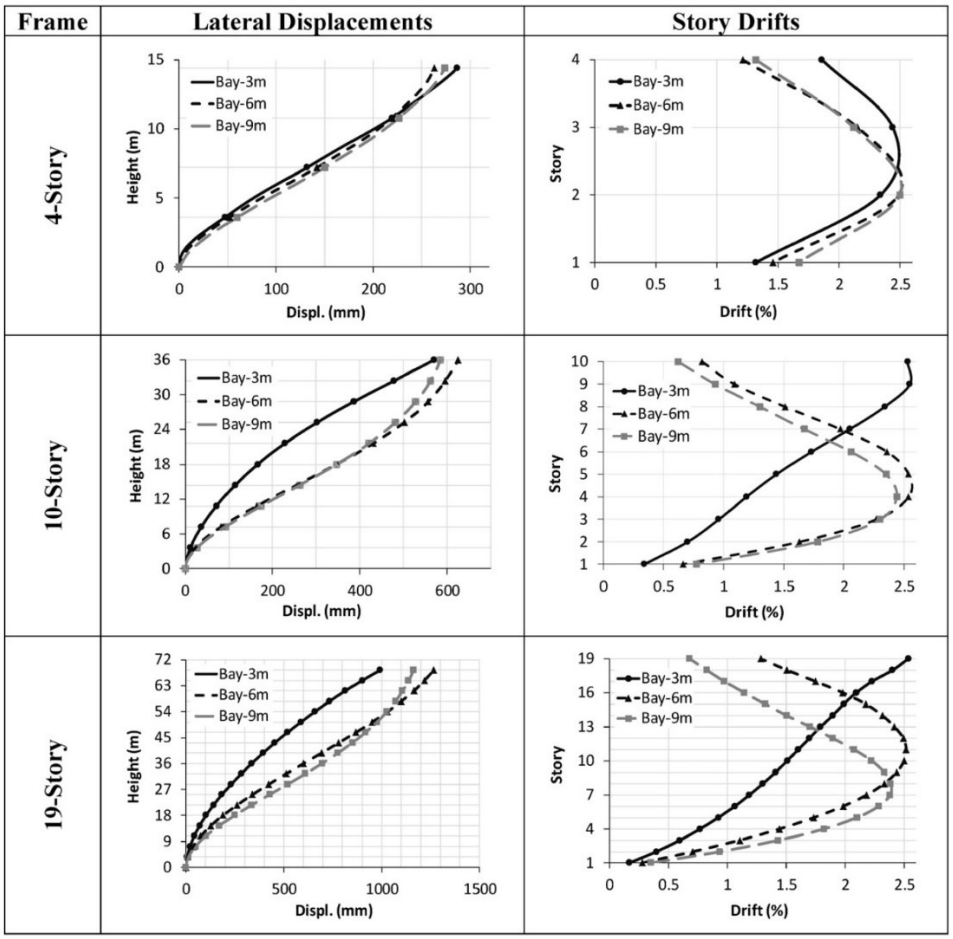

Fig. 2.18. Lateral displacements and storey drifts at ultimate load (Gholipour and Alinia 2016)

Dey and Bhowmick (2016) assessed the seismic behavior of C-PSWs. For this aim, nonlinear seismic responses of a 4-storey and a 6-storey C-PSWs were studied. Fig. 2.19 presents the contribution of infill plate, boundary column, and the reinforced concrete (RC) panel in resisting total storey shear in both 4-storey and 6-storey C-PSWs under both real and artificial ground motions. The results indicated that boundary members and reinforced concrete together can contribute in resisting 30% of the total shear applied on the structure while AISC341-16 (AISC 2016) ignores the contribution of reinforced concrete panel in resisting lateral loads. Based on plate buckling theory, two simple equations were proposed to find the minimum RC panel thickness as well as maximum allowable shear studs spacing to ensure that shear yielding occurs prior to local and global buckling of the infill plate.

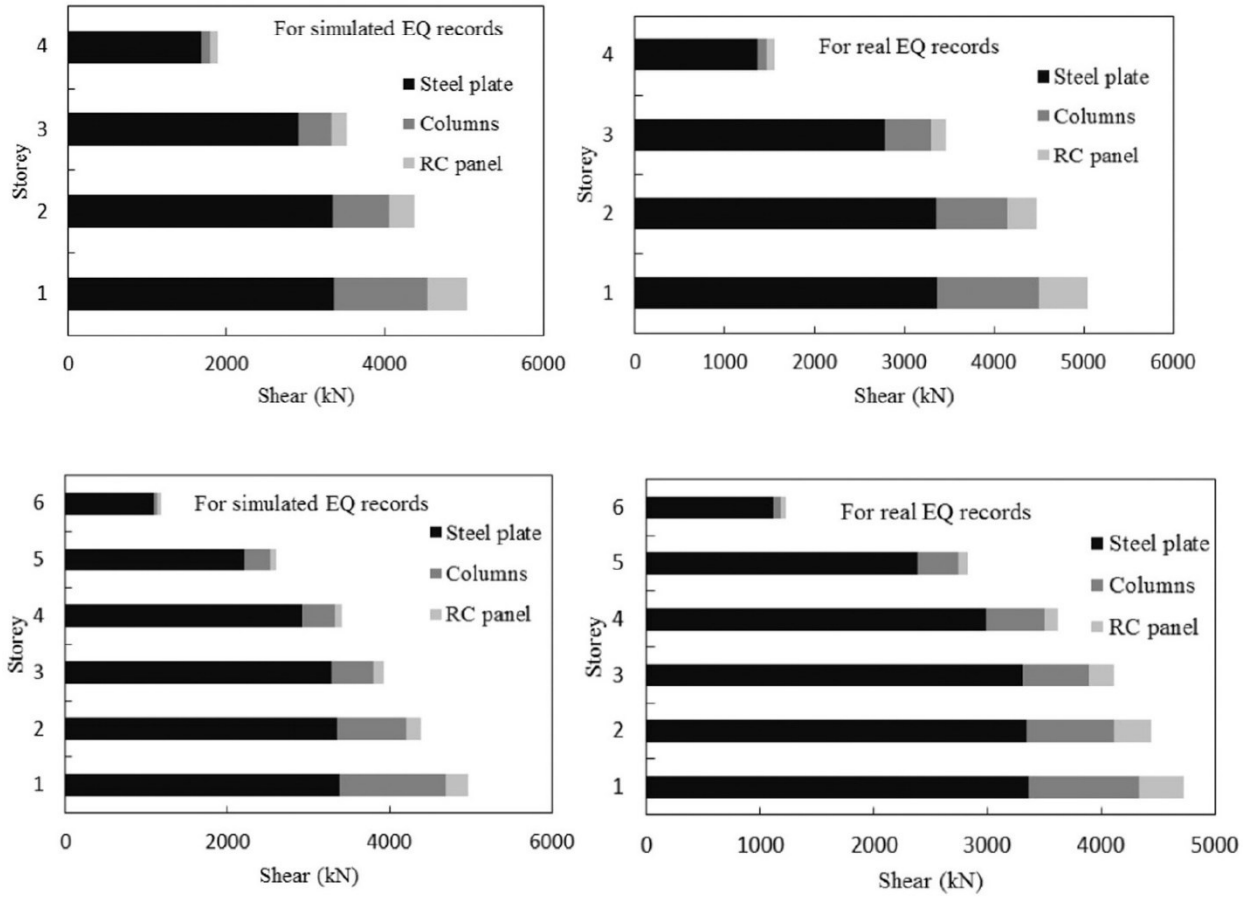

Fig. 2.19. Average peak storey shear contributions of 4-storey and 6-stoey C-PSWs (Dey and Bhowmick 2016)

Alinia and Shirazi (2009) developed several finite element models to assess the performance of stiffened SPSWs by focusing on finding the optimum stiffener's dimensions (i.e., thickness and height of stiffeners). By utilizing numerous finite element results, they proposed empirical relationships to address the optimum dimensions of stiffeners. Fig. 2.20 shows the in-plane displacements of a typical plate having various optimised stiffeners arrangements. As shown, the initial stiffness of all stiffened plates, which relate to their initial linear elastic parts, was identical. After buckling however, which occurred at different loads for different cases, the curves branched away. This means that by increasing the number of stiffeners, plate became more rigid and less ductile.

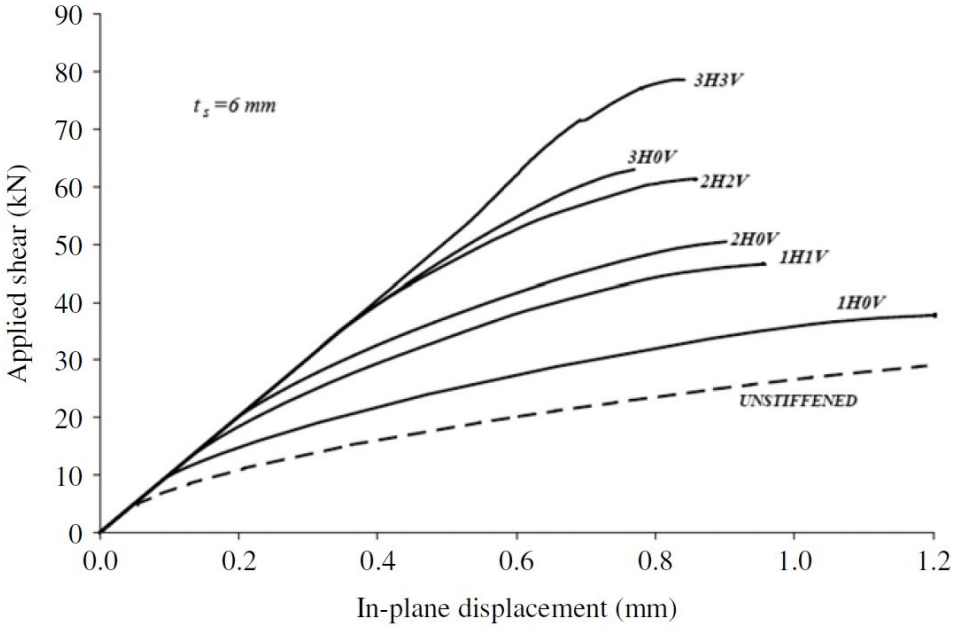

Fig. 2.20. In-plane-displacement curves for the $1000 \times 1000 \times 1.25$ mm plate with optimised stiffener arrangements (Alinia and Shirazi 2019)

Purba and Bruneau (2014-a) developed new deterioration models for SPSW components to assess the seismic performance of SPSW systems by considering two different design philosophies for infill plates. For this aim, they referred to a design procedure that is adopted for designing of SPSWs in Canadian standard for the design of steel structures (CSA 2014). In the Canadian standard, it is specified that infill plate must be designed to resist entire storey shear in the building. This procedure ignores the contribution of boundary elements in resisting lateral loads which in

turn result in larger overstrength factor for the system. To clarify this issue, they addressed the research conducted by Qu and Bruneau (2009) where they demonstrated that the contribution of boundary elements in resisting lateral loads can be up to 50% for panel aspect ratio of 2. Thus, two different design philosophies were considered in the design of SPSW systems. The first design philosophy was the design procedure illustrated in Canadian standard while the second philosophy was based on the contribution of boundary members in resisting lateral loads and eliminate the overstrength in the system by means of optimum design. In the first step, the research has been conducted to select a deterioration model for SPSW components. Between many deterioration models developed to model the deterioration of structural components, force-deformation capacity of structural components suggested by FEMA 356, Ibarra and Krawinkler model (2005), and Song and Pincheira (2000) were introduced and discussed. Final adopted backbone curve is similar to the concept of FEMA 356 and capable of considering moderate to severe pinching effect in infill plate due to plate tearing. To accurately quantify degradation parameters in each component of SPSW system, a comprehensive literature review was conducted to investigate the different types of failure in boundary members as well as infill plate. Totally 36 conventional slender unstiffened SPSW systems were chosen and the type of failure in each test were determined. Web tearing, flexural and shear failure of boundary elements, and instability of boundary elements (IBEs) were the main sources of deterioration in SPSW components during the experiment. Shear failure and IBEs are unlikely to occur in a SPSW in which boundary members are designed according to capacity design method and satisfy the requirements of seismically compact section to prevent local buckling of web and flanges. Thus, the calibration process has been conducted against four specimens ranging from one to four storey SPSWs which are reflecting extensive web tearing (3-storey tested by Choi and Park), Flexural failure of boundary elements (1-storey tested by Vian and Bruneau), and combination of both failures (4-storey Driver et al, 2-storey Qu and Bruneau) (Choi and Park, 2008). For each experiment, the deterioration model adopted for infill plate and boundary members were obtained during calibration process. Finally, the most conservative deterioration model among the obtained models for each type of failure (web tearing or flexural failure) were considered for seismic collapse assessment of SPSW systems (Fig. 2.21).

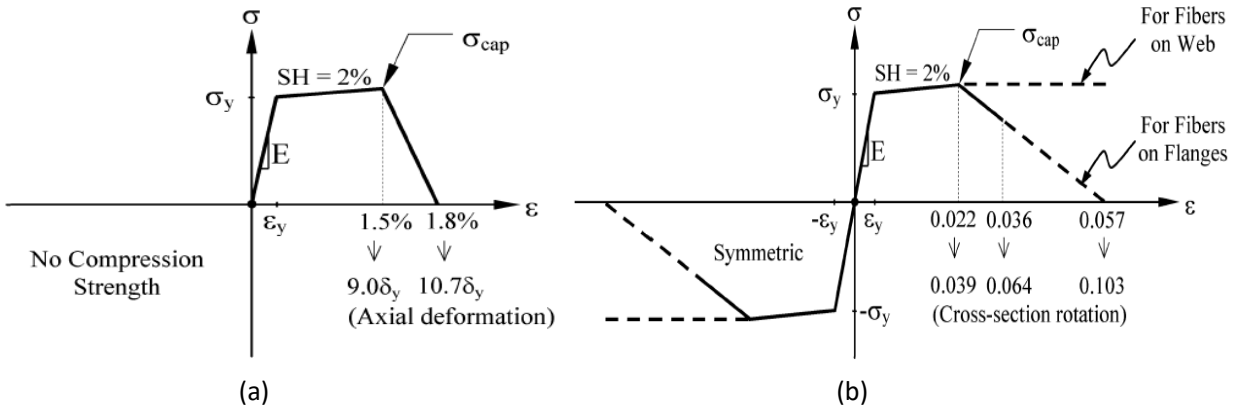

Fig. 2.21. Final degradation models (Purba and Bruneau 2014): (a) strips; (b) boundary elements

Purba and Bruneau (2014-b) in the second paper assessed the seismic performance of unstiffened SPSWs in which the infill plates are designed using two different design philosophies. The assessment was first conducted on SPSWs which are designed by neglecting the contribution of boundary elements in designing lateral loads (called conventional design procedure). This procedure was again repeated for SPSWs which are designed on the basis of sharing storey shear between infill plate and boundary members in each storey (called balanced design procedure). 12 SPSW archetypes were designed with various structural configuration (i.e., panel aspect ratio, intensity level of seismic weight, and number of stories). Based on the assessments, seismic performance factors (i.e., response modification factor, overstrength factor, and deflection amplification factor) for both types of designed SPSWs were obtained and compared. Static pushover analyses have been performed on all SPSWs and the results were extracted. The most noteworthy result taken from pushover analyses, is the overstrength provided in each building. Overstrength is defined as the maximum strength of the building taken from pushover analysis divided by design base shear. Overstrength obtained for SPSWs with conventional design procedure is changing from 2.3 to 3.1 since in this case, boundary members are acting as a back-up for entire system and provide extra strength and stiffness for the system while the overstrength obtained for SPSWs with balanced design procedure is near to 1 due to sharing the storey shear between boundary members and infill plate. By taking advantages of symmetric plan and leaning column concept, whole the building can be represented by a single SPSW system. Thus, 2-D analytical model for all SPSWs were developed by using the strip concept for modelling of infill

plate (Fig. 2.22). Suggested deterioration material model for boundary members and infill plate which have been addressed in the first paper were assigned to the components in the 2-D analytical model. To accurately assess the seismic performance of the models, a suite of ground motions was chosen for IDA analyses (44 ground motion). The IDA analyses have been conducted using maximum interstorey drift as the engineering demand parameter (EDP) and 5% damped spectral acceleration of the buildings first-mode period, was used as intensity measure (IM). The derived IDA curves for each archetype were used to calculate the probability of collapse using FEMA P695 methodology (FEMA 2009). FEMA P695 provides a rational basis to evaluate the accuracy of adopted response modification factor for a specific type of load resisting system by assessing the probability of collapse under maximum considered earthquake (MCE). Potential of collapse in a specific structure known as collapse margin ratio (CMR) can be calculated by dividing median collapse capacity, S_{CT}, by S_{MT} which is the response spectrum of MCE ground motions at the fundamental period of the given structure. By adjusting CMR value derived from IDA analyses to consider the frequency content of selected ground motions using spectral shape factor, adjusted collapse margin ratio (ACMR) is calculated for a specific building. The calculated ACMR for each archetype must be greater than the allowable value specified in FEMA P695 to ensure that R-factor considered in the design of the building satisfy the requirements of the code.

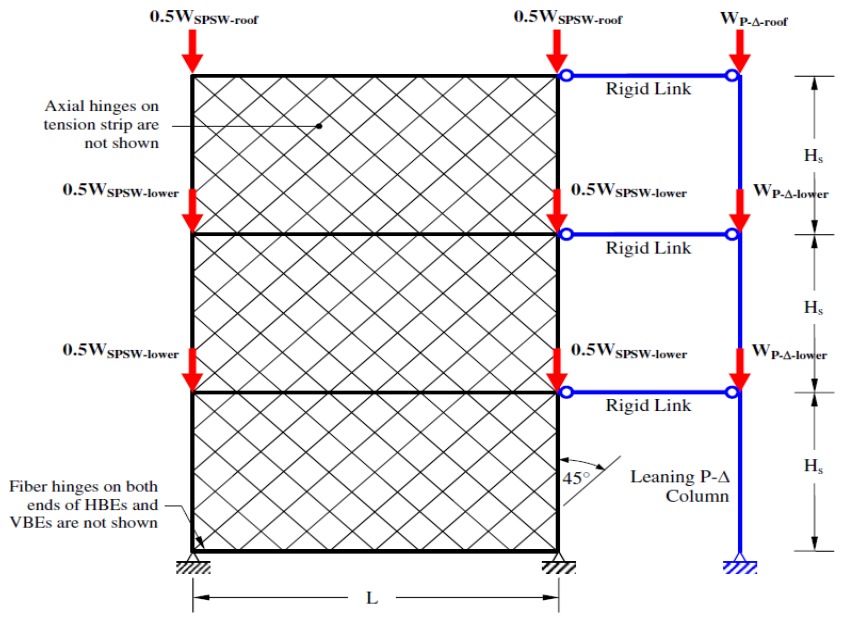

Fig. 2.22. Nonlinear model for collapse simulation: example structural model of three-storey archetype (Purba and Bruneau 2014)

All conventional archetypes met FEMA P695 (FEMA 2009) performance criteria for R-factor of 7 considered in the design. On the other hand, balanced design archetypes with R-factor of 7 did not met the requirements of FEMA P695. The authors proposed the use of R-factor 5 instead of 7 when the contribution of boundary elements are also considered in design process to resist storey shear (balanced design procedure). The results indicated that balanced designed archetypes will probably suffer from extensive damages to structural and non-structural components due to larger interstorey drifts compared to the same archetype designed based on conventional procedure. The authors also assessed the sensitivity of each archetype to the variation of structural configurations (i.e., panel aspect ratio, intensity level of the seismic weight, and number of stories). Concluding remarks are categorized as follow:

• **Panel aspect ratio**: two different panel aspect ratio of 1 and 2 were considered in this research. Based on the findings reported by Qu and Bruneau (2009), overstrength factor increases as panel aspect ratio increases. Hence, by increasing the panel aspect ratio, CMR increases. For instance, the CMR derived for 3-storey SPSWs with panel aspect ratio of 1 and 2 were compared. CMR for SW310 (i.e., three storey archetype with panel aspect ratio of 1) was found to be 2.1 which is 12.5% smaller than that of SW320 (i.e., three storey archetype with panel aspect ratio of 2) (Fig. 2.23).

• **Number of Stories**: In general, CMR increases as the number of stories increases (Fig. 2.23). However, CMR increment does not linearly correspond with increase in the number of the stories. Thus, for SPSW systems in which all of them are designed with a specific procedure (balanced or conventional procedure), long-period archetype has lower probability of collapse compare with short-period one when both are subjected to a same intensity of a specific ground motion.

• **Intensity level of seismic weight**: Two different categories were considered to investigate the effect of seismic weight variation on overall performance of the system. For the first group, SPSW systems have been designed by assuming that one-sixth of total seismic weight in each floor were sustained by single 2-D analytical model developed for SPSW system. For the second group, one half of the total seismic weight in each floor was assumed to be resisted by single 2-D SPSW. The first and second groups were denoted as low and high seismic weight respectively. The results indicated that derived CMR for archetypes located in the high seismic weight group are larger than

that in low seismic weight group (Fig. 2.23). Larger axial force demand on vertical boundary elements will result in larger cross section for VBEs in the SPSW systems located in the second group. Pushover analyses reveals that the onset of degradation in the first group occurs sooner than that in second group. To address this difference, Purba and Bruneau (2014) investigated the behavior of deep and shallow cross sections when subjected to the combination of axial force and bending moment. They found that distance between neutral axis and center of gravity increases as the axial force increases. Thus, in deep cross sections, onset of degradation is postponed since the distance between furthest fibers from the neutral axis is more in case of deep cross sections.

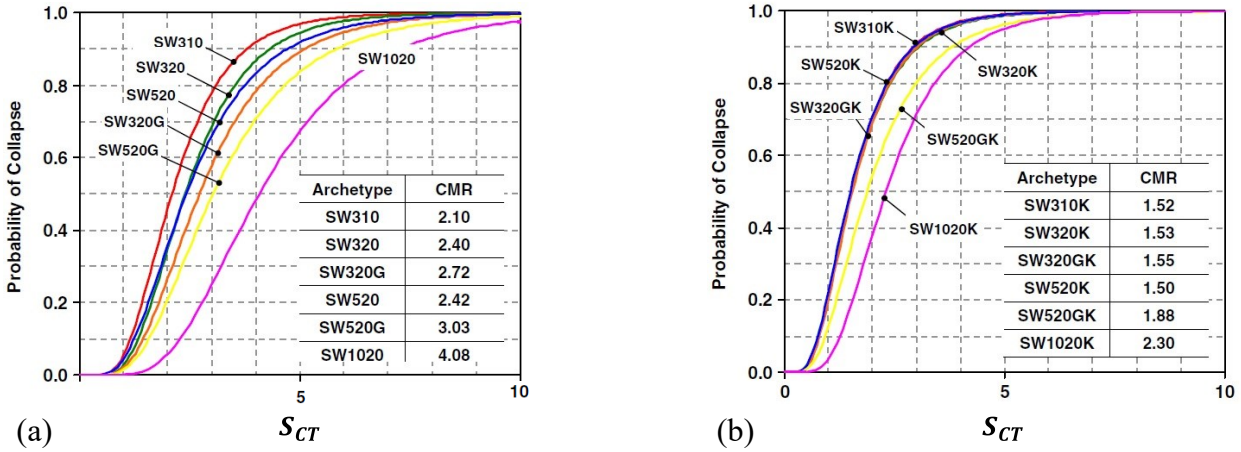

Fig. 2.23. Collapse fragility curves for archetypes with various configurations (Purba and Bruneau 2014): (a) conventional design case; (b) balanced design case

Zhao and Astaneh-Asl (2004) conducted experimental study to investigate the cyclic behavior of composite plate shear walls (C-PSWs). C-PSWs are generally consist of thin steel infill plate which is connected to surrounding boundary elements (vertical and horizontal boundary elements) using bolts or welds. In addition, reinforced concrete (RC) panel is attached to one or both sides of infill plate using bolts to ensure that yielding of infill plate occurs prior to its global or local buckling through providing bracing to prevent out-of-plane buckling of thin infill plate (Fig. 2.24).

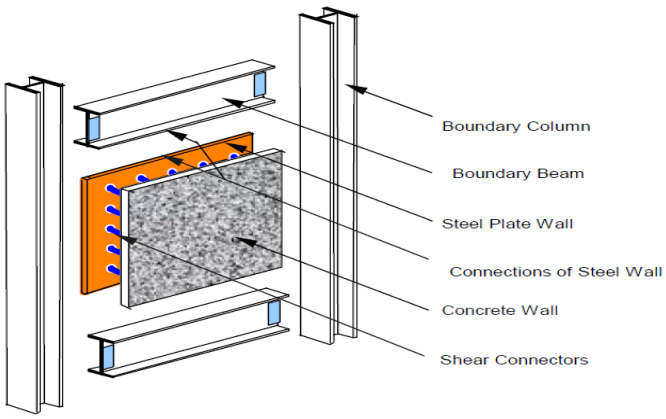

Fig. 2.24. Main components of a typical composite shear walls (Zhao and Astaneh-Asl 2002)

Zhao and Astaneh-Asl (2004) focused on two common configurations of C-PSWs denoted as "Traditional" and "Innovative". The only difference is that in traditional C-PSW, the RC panel is in direct contact with boundary elements while in innovative one, there is a gap between RC panel and boundary elements (Fig. 2.25). Thus, for traditional C-PSW, both steel shear wall and reinforced concrete are active (from the beginning of loading) and provide stiffness and strength for the entire system. However, concrete panel can severely damage in relatively small lateral displacement. On the other hand, reinforced concrete panel does not contribute in resisting lateral loads from the beginning since there is a gap between RC panel and boundary members. As long as the gap is not closed, RC panel does not contribute in resisting applied load, so it continues to provide bracing for thin infill plate as the primary function. Under large lateral displacement, the gap is closed at the corners, so reinforced concrete engaged in providing additional stiffness and strength for the entire system and compensate the loss of stiffness and strength in the system due to plate tearing. Zhao and Astaneh-Asl (2002) indicated that the extent of damage to RC panel in an innovative system is much less than that for traditional system (Fig. 2.26). To quantify this result, two half-scale 3-storey specimens with and without gap were fabricated by a local fabricator and delivered to the test site (University of California Civil Engineering Laboratories). Both specimens were subjected to a similar cyclic loading pattern specified in American Institute of Steel Construction for qualifying tests of beam-to-column and link-to-column connections. The results indicated that installation of RC panel on a thin infill plate cased the hysteretic curve to change from "S" shape to "Spindle" shape which increase the energy dissipation capacity of the system. In addition, both specimens exhibit smooth and stable hysteresis curves.

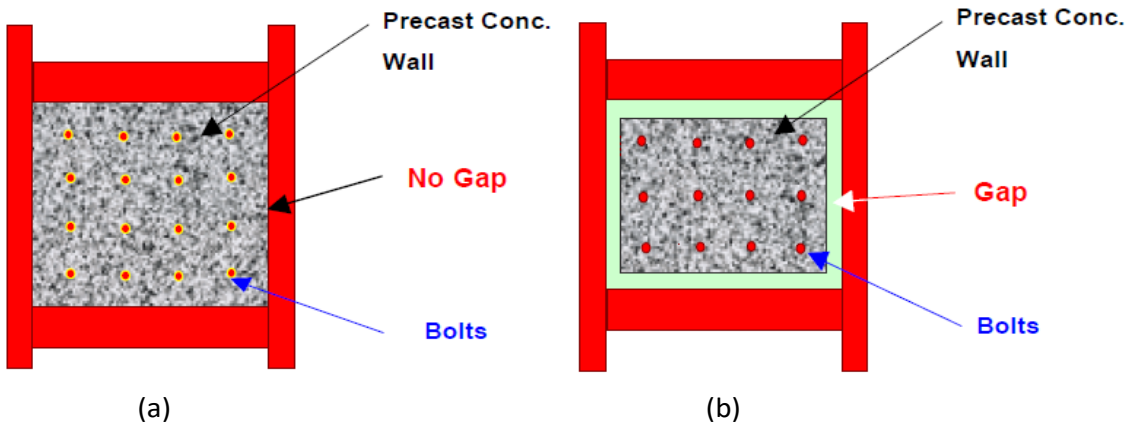

Fig. 2.25. Two common types of composite plate shear wall (Zhao and Astaneh-Asl 2002): (a) traditional C-PSW; (b) innovative C-PSW

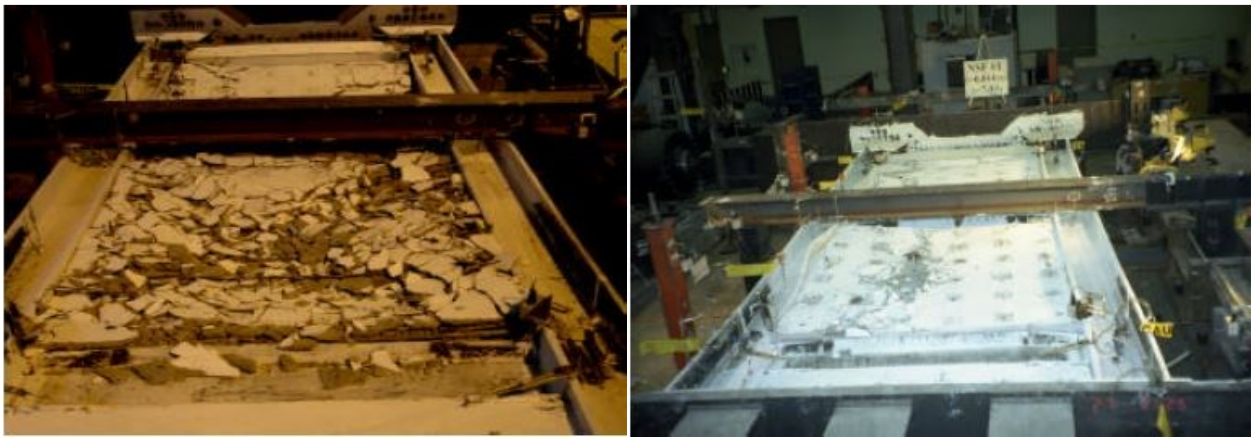

Fig. 2.26. Comparison of damage to concrete wall in traditional and innovative system for same level of drift (Zhao and Astaneh-Asl 2002): (a) traditional C-PSW; (b) innovative C-PSW

Main components of test setup are: actuator, top loading beam, bottom reaction beam, RC reaction blocks and bracings. Top loading beam was installed on the top of the specimen to transfer the horizontal cyclic load and displacement to the specimen. Bottom reaction beam was designed to transfer shear forces as well as overturning moment to the RC reaction blocks. Pre-stressed reaction blocks were used to transfer the loads to the laboratory floor. Bracing were provided in different locations in the model to prevent out-of-plane buckling of boundary elements. Fig. 2.27 shows the general configuration of test setup and the specimen installed in it.

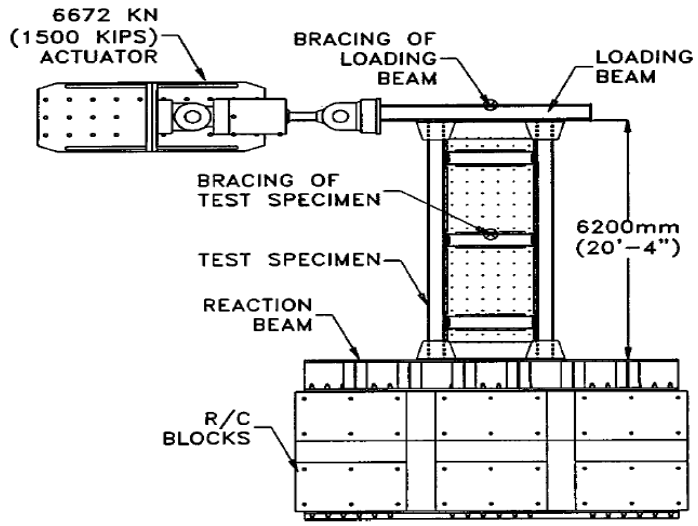

Fig. 2.27. Test specimen inside test setup (Zhao and Astaneh-Asl 2002)

Prior to conduct cyclic loading, a numerical analysis was performed to obtain the first significant yielding in the system. Obtained value was then verified during the test. Several linear variable displacement transducer (LVDTs) were installed on the centerline of the boundary members, corner of infill plates, and corner of panel zones to monitor the movements. Fig. 2.28 exhibits the locations of the installed global and local LVDTs on the specimens. Based on the monitored results, panel zone deformation, infill panel deformation, and the rotation of beam-to-column connection could be measured. Furthermore, a number of strain gauges were installed at different locations on the web and flanges of the boundary elements to capture the initiation of local buckling.

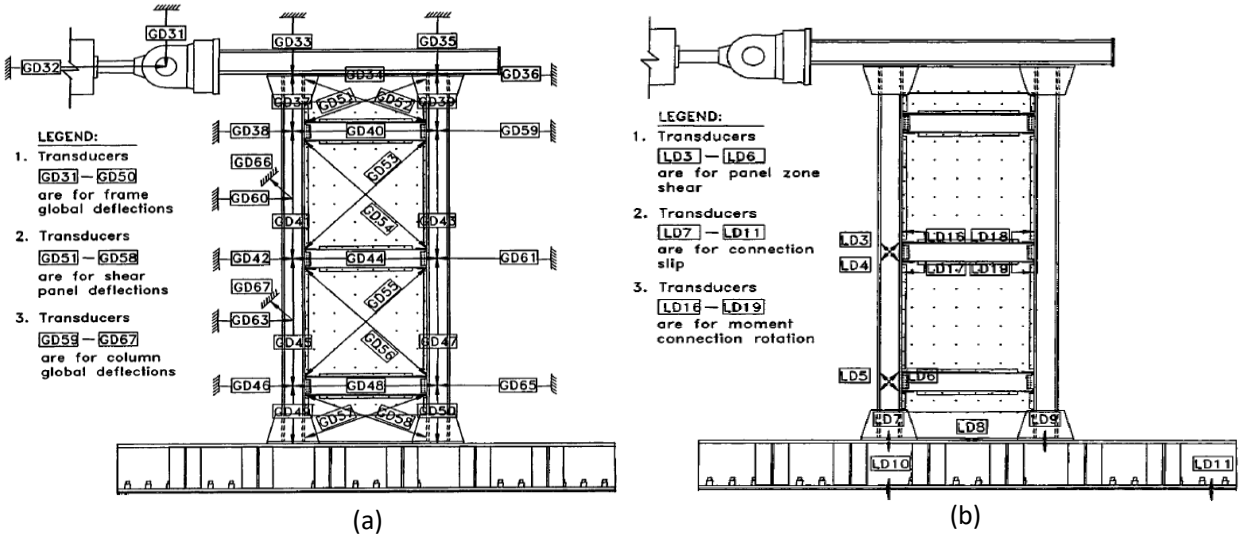

Fig. 2.28. LVDT's location on the specimens (Zhao and Astaneh-Asl 2002): (a) global displacement transducers; (b) local displacement transducers

Purba and Bruneau (2006) investigated the individual perforated strip strength to calculate the overall strength of unstiffened perforated SPSWs. By using finite element model, Purba and Bruneau (2006) analyzed a series of single perforated strips with a dimension of 2000 x 400 mm and with perforation diameters *D* from 10 mm to 300 mm (Fig. 2.29). along with various boundary conditions and plate thickness in order to understand the behavior of complete perforated SPSW. Later, a series of single-storey SPSW with different perforation diameter, with different plate thickness were analysed using nonlinear pushover analysis. It was observed that the behavior of individual strip can accurately predict the behavior of complete perforated SPSW provided the holes diameter is less than 60% of the strip width. In addition, it was reported that no interaction exists between adjacent strips which could affect the stress distribution within an individual strip i.e., each strip in SPSW behaves independently.

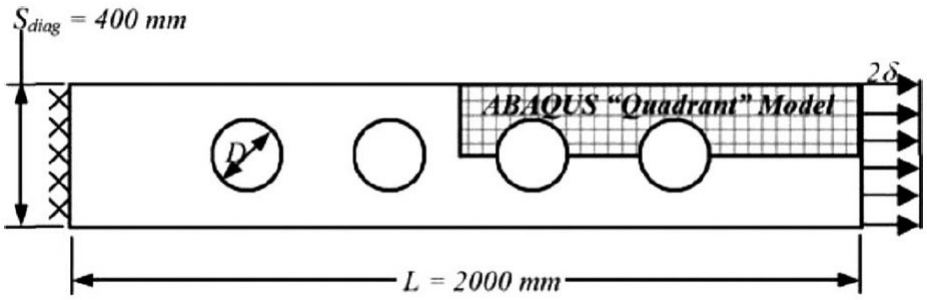

(a)

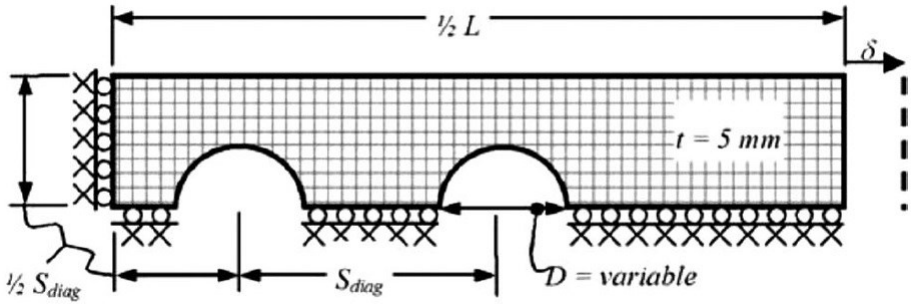

(b)

Fig. 2.29. Individual perforated strip (Purba and Bruneau 2006): (a) geometry of perforated strip; (b) finite element model

Roberts and Sabouri-Ghomi (1992) had proposed Eq. 2.4) to estimate the shear strength of perforated SPSWs with single circular perforation located at the center of the infill plate.

$$V_r = 0.42\, F_y\, t\, L_{cf}\, (1 - \frac{D}{S_{diag}}) \qquad 2.4)$$

Purba and Bruneau (2006) reassessed the applicability of Eq. (2.4) to estimate the shear strength of SPSW with regularly-spaced circular perforations by applying a factor to the equation. They analyzed several solid and perforated SPSWs with same characteristics (i.e., material and geometric properties, loading, element type, and initial imperfection). The infill panel strength was determined by subtracting the strength of bare frame for both solid and perforated systems. Infill plate strength ratio (i.e., shear strength of perforated to solid infill plate) versus perforation ratio

(D/S_{diag}) was plotted and a linear relationship was observed. Finally, Eq. (2.5) was proposed to estimate the shear strength of perforated SPSW with regularly-spaced circular perforations.

$$V_{perf} = \left(1 - 0.7\frac{D}{S_{diag}}\right)V_{solid} \tag{2.5}$$

2.3 Common Failure Modes of Steel Shear Walls

Purba and Bruneau (2014) conducted a comprehensive literature review to investigate the different types of failure in boundary members as well as infill plate. Totally 36 conventional slender unstiffened SPSW systems were chosen and the type of failure in each test were determined. Web tearing, flexural and shear failure of boundary elements, and instability of boundary elements were the main sources of deterioration in SPSW components during the experiment. Each type of failure is clarified as follows:

- Web tearing (WT): WT causes significant deterioration in the whole system when web tearing propagate in a significant region in the panel which unable a part of the panel to develop tension field action (Fig. 2.30).
- Flexural failure of boundary members: Plastic hinges formation at the ends of boundary members due to local buckling of web or flanges, weld fracture between HBEs and VBEs or VBEs and their base, fracture of boundary members especially in HBEs with reduced beam section (RBS) at the two ends (Fig. 2.31)
- Shear failure: Shear failure is characterized by shear yielding of a significant length across the web of VBEs, which causes lower-than-expected VBE plastic moments and can result in significant VBE inward deformations (i.e., hour-glass shape deformations) (Fig. 2.32)
- Instability of boundary elements (IBEs): IBEs occur due to out-of-plane buckling about weak axis or lateral torsional buckling of VBEs. Global instability reported in past experiments was associated with out-of-plane (weak-axis) buckling of VBEs or lateral torsional buckling of HBEs (Fig. 2.33). Shear failure and IBEs are unlikely to occur in a SPSW in which boundary members are designed according to capacity design method

and satisfy the requirements of seismically compact section to prevent local buckling of web and flanges.

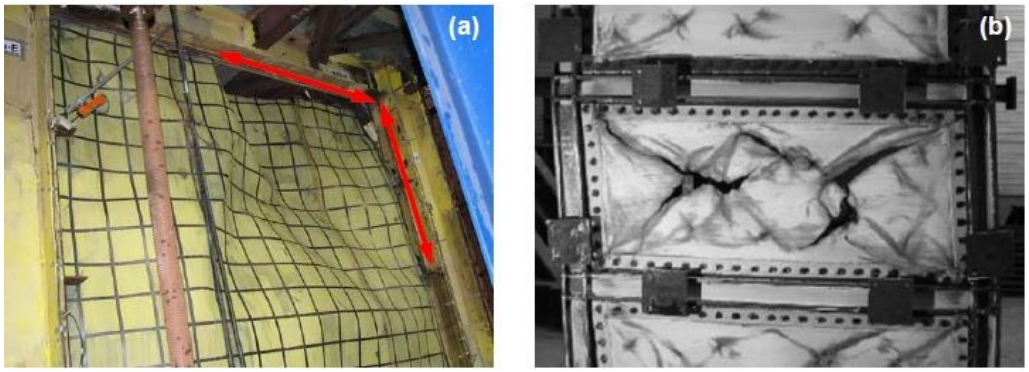

Fig. 2.30. Web tearing creating strength deterioration: (a) Web tearing along vertical and horizontal fish plates (Qu and Bruneau 2009); (b) Web tearing across the infill plates (Choi and Park 2008)

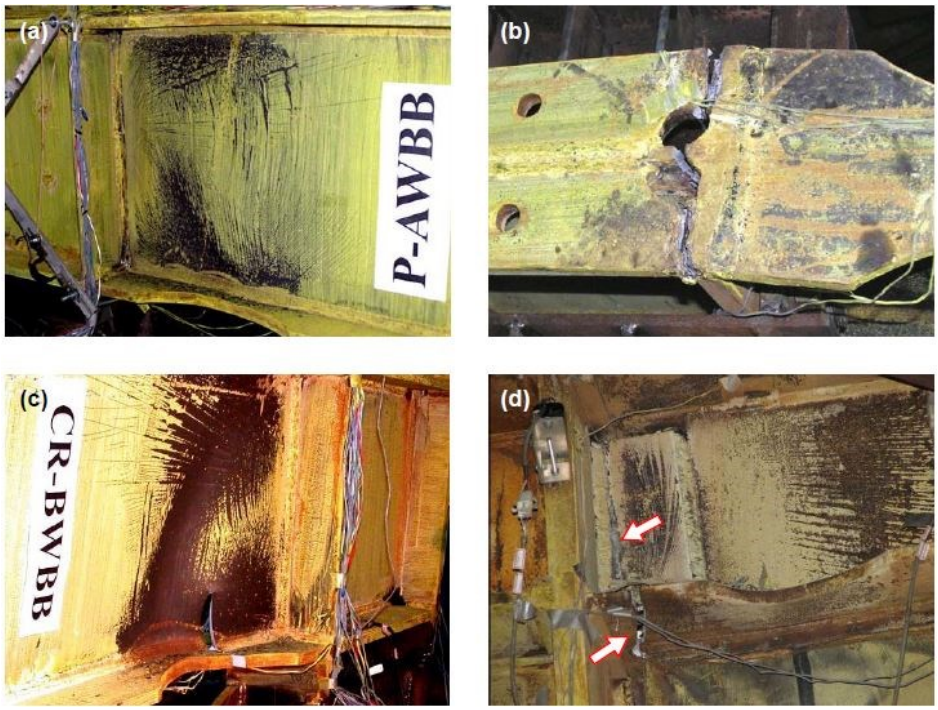

Fig. 2.31. Flexural failure of boundary elements: (a) Plastic hinge development; (b) Weld connection fracture; (c) Fracture at RBS connection (the first three photos from Vian and Bruneau 2004); (d) Shear tab fracture (Qu and Bruneau 2009)

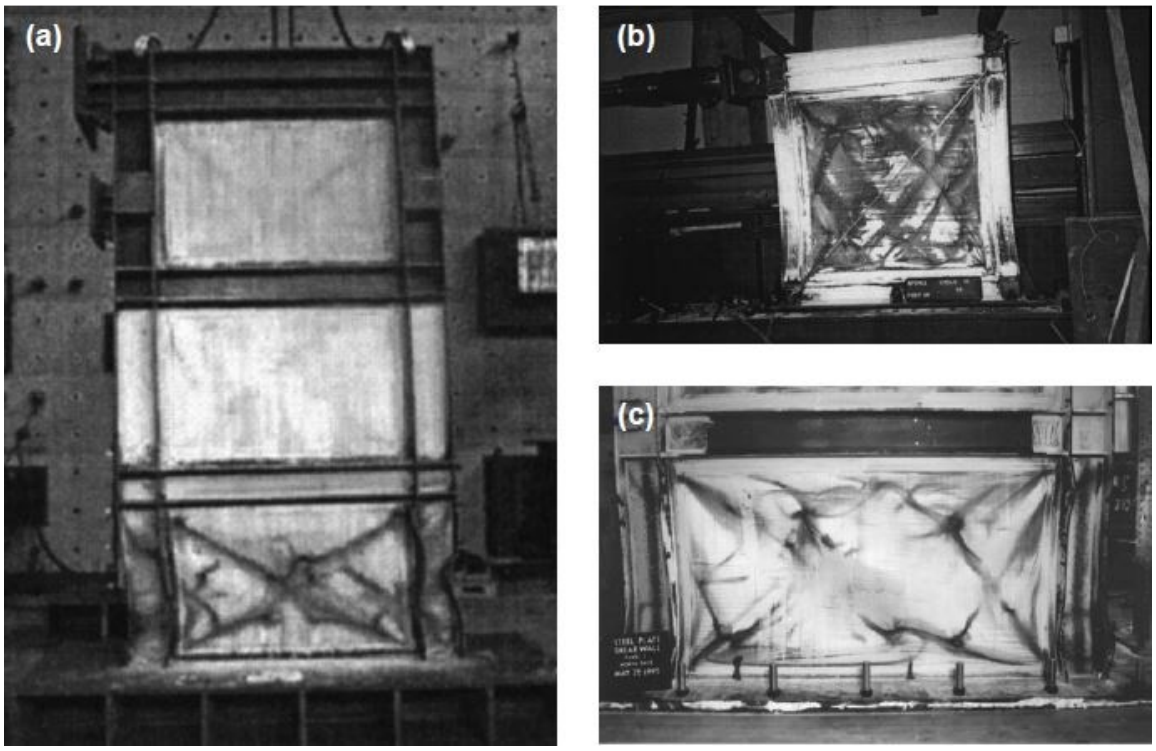

Fig. 2.32. Shear failure of boundary elements: (a) Shear yielding with excessive local buckling (Park et al. 2007); (b) Hour-Glass shape deformation (Lubell et al. 2000); (c) Shear yielding at the base of 4-storey specimen (Driver et al. 1997)

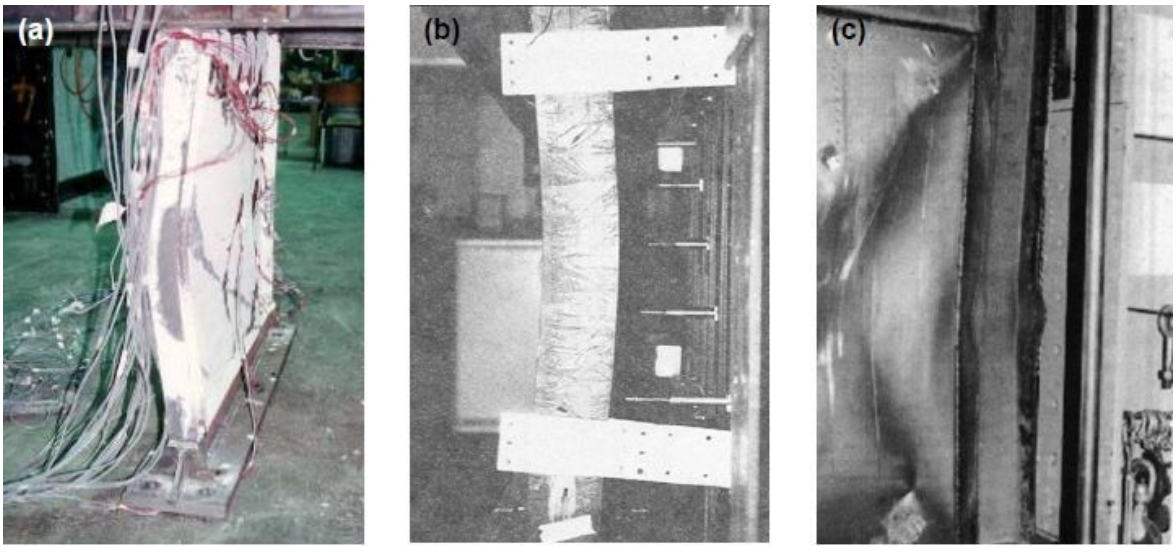

Fig. 2.33. Instability of first storey vertical boundary elements: (a) Out-of-plane buckling in 4-storey SPSW specimen (Kharrazi et al. 2011); (b) Out-of-plane buckling in 3-storey SPSW specimen (Caccese et al. 1993); (c) VBE local buckling in 2-storey SPSW specimen that lead to global instability (Elgaaly 1998)

2.4 Response Assessment of Steel Shear Walls

In order to study the behavior of SPSWs and its failure modes, a review of affecting parameters on SPSW behavior should be discussed as it relates to wall response. Typically, the seismic performance of a SPSW system can be evaluated experimentally through assessing its hysteretic lateral force-displacement relationship. Many experimental studies have been conducted in the recent decades to investigate the lateral behavior of steel shear walls. Although experimental testing is seen to be the most evident approach to assess the performance of a steel shear wall, numerical simulations found to be a valuable tool for parametric studies and collapse assessments of SPSW systems in multi-storey buildings.

Regarding the numerical simulation, investigation of inelastic response of SPSW systems involves using a reliable modelling approach that is capable of coupling important interactions and response parameters. The setup and check of the model requires substantial technical expertise in the numerical modelling, especially when the entire building has to be modelled and analyzed, and not just the structural wall. A variety of software tools are available that employ non-linear finite element methods for the analysis of steel shear walls.

Detailed solid finite element (FE) models (i.e. ANSYS, ABAQUS) using built-in constitutive models are able to capture the local stress-strain responses, quantify low cycle fatigue, in addition to the global force-displacement responses. These programs require the definition of several material parameters according to the constitutive model and failure envelope used. Additional parameters to drive the nonlinear solution algorithms to convergence are also of major importance. Fiber-based models are also often used to calibrate the nonlinear stiffness and strength properties of fiber elements (i.e., OpenSees, SeismoStruct) that could be used in a computationally effective way to assess the global nonlinear response of a complete building structures (i.e. formation of plastic hinges). The predictions of both FE and Fiber models need to be compared to experimental data to validate their performance for both ductile (flexural) and brittle (shear) failure mechanisms.

The main objective of many recent studies was to develop and validate micro/macro models for steel shear walls subjected to cyclic reversals. Some also developed simplified models that can be used by engineering practitioners. Modelling approaches addressing the required elements and

corresponding material constitutive models were explained in detail, and the process for calibration of parameters was highlighted in some cases. As for simulation of steel shear wall system, the numerical models have to be able to efficiently approximate the effect of distributed loads acting on boundary elements due to formation of tension field action in infill plate.

Chapter 3

Seismic Collapse Assessment of Stiffened Steel Plate Shear Walls using FEMA P695 Methodology

3.1 Abstract

Unlike unstiffened steel plate shear walls (SPSWs), very little research has been conducted to assess the seismic performance of stiffened SPSWs. This paper presents a new component strength deterioration model for stiffened infill plate to evaluate the seismic performance of stiffened SPSWs using FEMA P695 procedure. The newly developed component strength deterioration model is first validated against the available experimental results. A total of three multi-storey (7-, 10-, and 13-storey) stiffened SPSWs with panel aspect ratio of 1.39 are then analysed using the proposed component strength deterioration model. Static pushover and incremental dynamic analyses using a suite of 44 ground motions compatible to Western Canada are conducted for all archetypes. Adjusted collapse margin ratios obtained for stiffened SPSWs designed with similar response parameters of those for unstiffened SPSWs are compared with allowable limits given in FEMA P695. The results indicate that currently recommended seismic response modification factor, ductility related force modification factor and overstrength related force modification factor, for unstiffened SPSW can be used for design of stiffened SPSW. In addition, seismic response parameters such as variation of maximum interstorey drift and shear demand in different components of stiffened SPSW, boundary columns and infill plates, are estimated in all stories for all designed archetypes during incremental dynamic analysis. Furthermore, seismic response sensitivity of stiffened SPSWs to the variation of post-yielding parameters (i.e., ductility capacity and post-cap stiffness ratio) in infill plate is investigated. Sensitivity analysis shows that the capacity of stiffened SPSW is more sensitive to ductility capacity changes, while the variation of post-cap stiffness has a lesser effect on overall performance of the system.

Key words: Stiffened SPSW; FEMA P695; Incremental dynamic analysis; Seismic response parameters; Strength deterioration model.

3.2 Introduction

Unstiffened steel plate shear walls (SPSWs) have widely been used as a primary load carrying system in many buildings in Japan and North America. The SPSW resembles to a vertical plate girder. In SPSW, thin infill plate is connected to surrounding boundary members using fillet welds or bolts and acts similar to web of the plate girder. The columns, which are known as vertical boundary elements (VBEs), perform like the flanges of the plate girder, whereas beams act like the stiffeners installed on the web of the plate girder. The design process of SPSWs is quite complicated than that for plate girders since the columns in SPSW are carrying significant amount of axial force. A significant number of numerical as well as experimental studies have been conducted on the behavior of unstiffened SPSW systems (Bhowmick et al. 2008; Berman et al. 2011; Choi and Park 2010; Driver et al. 1997; Roberts and Sabouri-Ghomi 1991). These studies all showed the effectiveness of the system in resisting applied lateral loads by forming the tension field action (TFA). The main drawback of the unstiffened SPSW system is the buckling of thin infill plate in relatively small compressive stresses, which results in significant reduction in energy dissipation capacity and initial stiffness of the whole system. One available approach to prevent buckling of the infill plate is to replace it with a thicker one. However, this method is not practical and has many disadvantages, such as more cost, higher demands on boundary elements, and higher seismic weight, resulting in higher seismic forces on the system. Another option is to install a series of horizontal and vertical stiffeners on thin infill plate to prevent buckling of infill plate. Sabouri-Ghomi and Asad-Sajjadi (2012) tested two one storey similar SPSWs with and without stiffeners. Their tests indicated that stiffener's installation caused 26% increase in energy dissipation capacity of the whole system. In addition, initial elastic stiffness of the system increased by 51%, whereas the maximum strength increased about 2%. Takahashi et al. (1973) conducted several tests on stiffened SPSWs with various infill plate thicknesses and different stiffeners dimensions. They indicated that by sufficiently stiffening the infill plate, hysteretic loops of an SPSW can be transformed from S-shape in unstiffened to spindle-shape in stiffened SPSW. This transformation significantly increases the energy dissipation capacity of the whole system. Alinia and Shirazi (2009) conducted finite element analysis to assess the performance of stiffened SPSWs by focusing on finding the optimum stiffener's dimensions (i.e., thickness and height of stiffeners). From the finite element analysis results, they proposed empirical relationships to

determine the optimum dimensions of stiffeners. In addition, they indicated that increasing the number of stiffeners will result in more rigid and less ductile behavior of SPSW. Rahmzadeh et al. (2016) proposed a general equation to calculate the tension field angle in both stiffened and unstiffened SPSW systems. This formulation is capable of calculating tension field angle for stiffened SPSW with various numbers of stiffeners as well as different stiffeners arrangement. In addition, by using the theory of incomplete diagonal tension, several equations were proposed to calculate ultimate shear capacity of stiffened infill plate and inward forces exerted on boundary elements.

Unlike unstiffened SPSW, only few numerical as well as experimental studies are available for stiffened SPSWs. Design guidelines for steel plate shear walls in North American steel standards (AISC 341-16; CSA S16-14) are based on research on unstiffened SPSWs. Thus, the seismic force modification factors adopted in the corresponding building codes (ASCE 7-16; NBC 2015) are obtained from studies on unstiffened SPSWs. Recently, another steel shear walls system, composite plate shear walls (C-PSWs), has been adopted in AISC 341-16 (AISC 2016) and ASCE 7-16 (2016) and the seismic response modification factors for C-PSWs are different than SPSWs., The behavior of stiffened SPSW is more similar to C-PSW than unstiffened SPSW, since in both systems, shear yielding of infill plate can be reached, whereas in unstiffened SPSW, elastic buckling occurs in the infill plate at a load which is quite smaller than that causes shear yielding in the infill plate. It is thus important to evaluate seismic response modification factors for stiffened SPSW. At the time of this writing, there is no recommendation in NBC (2015) regarding seismic response modification factors (ductility-related force modification factor, R_d, and overstrength-related force modification factor, R_o, in Canada) for designing of stiffened SPSWs. It is up to the engineers to select appropriate seismic response modification factors when designing stiffened SPSW. One approach would be to use the same R-factors as used in the design of unstiffened SPSW. This paper investigates the accuracy of this approach by quantifying the seismic response modification factors for stiffened SPSWs using the FEMA P695 (FEMA 2009) methodology. FEMA P695 (FEMA 2009) provides a rational basis to evaluate the accuracy of adopted response modification factors for a specific type of load resisting system by assessing the probability of collapse under maximum considered earthquake (MCE). However, this methodology requires accurate and efficient structural numerical models to be used in the collapse analysis of the lateral load resisting system. In most of the numerical modelling studies conducted on SPSWs, a bilinear

relationship was assigned to strips in tension zone for modelling the infill plate and the effect of degradation in the infill plate due to plate tearing was not considered (Choi and Park 2010; Driver et al. 1997; Roberts and Sabouri-Ghomi 1991). Also, when conducting fragility analysis, it is not suitable to adopt refined analysis. Thus, a macro- model for simulation of the behavior of stiffened SPSWs subjected to earthquake loads needs to be developed. In this study, a component strength deterioration model for stiffened infill plate is developed to evaluate the seismic collapse performance of stiffened SPSWs using FEMA P695 (FEMA 2009) procedure. Using *Open System for Earthquake Engineering Simulation* (*OpenSees*) software (McKenna et al. 2013), the accuracy of the proposed macro-modelling approach is validated against available experimental results in the literature. Three multi-storey (7-, 10-, and 13-storey) stiffened SPSWs were designed using the same seismic force modification factors as of unstiffened one. Nonlinear incremental dynamic analysis (IDA) was carried out on all designed archetypes using a group of 44 artificial ground motions that were developed for western Canada by Atkinson (2009). Furthermore, nonlinear time history analysis (NTHA) was done on all designed archetypes in design level using the same group of 44 artificial ground motions that were used for incremental dynamic analysis. In addition, Maximum contribution of various structural components (i.e., infill plate and boundary elements) in resisting applied lateral loads are assessed and depicted in the figures for comparison. Finally, a sensitivity study is carried out on different variant models in each building to investigate the extent of variation in the capacity of the whole system due to the variation of post-yielding parameters in infill plate. Variant models in each building are developed using different combination of post-yielding parameters in the infill plate.

3.3 Buckling of Stiffened SPSW System

Infill plate under pure shear can buckle in two modes: (1) global buckling and (2) local buckling. Stiffeners are designed in such a way that local buckling occurs prior to global buckling to achieve better structural performance and increase the critical elastic stress correspond to onset of buckling in infill plate. In order to force the infill plate to buckle in subpanel (local buckling mode), a minimum moment of inertia is required for horizontal and vertical stiffeners. Global buckling occurs when the stiffeners are very slender (low moment of inertia). In addition, to utilize the whole capacity of stiffened infill plate, spacing between horizontal and vertical stiffeners must be calculated in such a way that shear yielding of infill plate happens prior to local buckling of

infill plate in subpanels. The following two subsections will address on finding shear stress in infill plate.

3.3.1 Global Buckling Mode

Critical shear stress onset of global buckling can be derived with the assumption of orthotropic stiffness of infill plate. This means that the stiffened SPSW can be considered to have two different stiffness in two global directions. Exact solution for long orthotropic simply supported plates in shear can be employed to calculate the global shear stress,τ_{crg} (Allen and Bulson 1980; Timoshenko and Gere 1961), which is given in Eq. (3.1).

$$\tau_{crg} = \frac{K_g \, \pi^2}{h^2 \, t} \, (D_x)^{0.75} \, (D_y)^{0.25} \tag{3.1}$$

where t is the infill plate thickness; h is the panel's height; K_g is the global buckling factor that is the function of D_x (flexural stiffness for bending about x-axis) and D_y (flexural stiffness for bending about y-axis). The minimum value of K_g for plate to frame connection of pinned and rigid is 3.64 and 6.9, respectively. In order to have a conservative design, the value of τ_{crg} is calculated with the assumption of pinned connection of plate to frame since this assumption will result in smaller value for onset of global buckling in infill plate. Flexural stiffness for bending about x-axis and y-axis are calculated using following equations:

$$D_x = \frac{E_s \, I_x}{s_x} + \frac{E_s \, t^3}{12 \, (1 - \vartheta^2)} \tag{3.2}$$

$$D_y = \frac{E_s \, I_y}{s_y} + \frac{E_s \, t^3}{12 \, (1 - \vartheta^2)} \tag{3.3}$$

where E_s is the modulus of elasticity of infill plate; s_x is spacing between vertical stiffeners; s_y is spacing between horizontal stiffeners; I_x and I_y are the stiffener's moment of inertia about x-axis and y-axis, respectively; ϑ is the Poisson's ratio of steel plate.

3.3.2 Local Buckling Mode

The critical shear buckling stress corresponding to onset of local buckling in sub panels can be obtained using Eq. (3.4) (Galambos 1998)

$$\tau_{crl} = \frac{K_l \, \pi^2 \, E_s}{12 \, (1 - \vartheta^2)} \, (\frac{t}{s_x})^2 \tag{3.4}$$

where K_l is the local buckling factor, which is a function of subpanel's aspect ratio and can be calculated using Eq. (3.5):

$$k_l = \begin{pmatrix} 5.35 + 4\left(\frac{s_x}{s_y}\right)^2 & if \ \left(\frac{s_y}{s_x}\right) \geq 1 \\ 4 + 5.35\left(\frac{s_x}{s_y}\right)^2 & if \ \left(\frac{s_y}{s_x}\right) \leq 1 \end{pmatrix} \tag{3.5}$$

3.3.3 Stiffener's Requirements

To make sure that local buckling in subpanels occurs prior to global buckling of infill plate, following equation must be satisfied:

$$\tau_{crg} > \tau_{crl} \tag{3.6}$$

By substituting Eqs. (3.1), (3.2), (3.3), and (3.4) in Eq. (3.6), the following equation can be derived:

$$\frac{K_g \, \pi^2}{h^2 \, t} \, (\frac{E_s \, I_x}{s_x} + \frac{E_s \, t^3}{12 \, (1 - \vartheta^2)})^{0.75} \, (\frac{E_s \, I_y}{s_y} + \frac{E_s \, t^3}{12 \, (1 - \vartheta^2)})^{0.25} > \frac{K_l \, \pi^2 \, E_s}{12 \, (1 - \vartheta^2)} \, (\frac{t}{s_x})^2 \tag{3.7}$$

Eq. (3.7) provides the minimum required moment of inertia for stiffeners to ensure that local buckling happens prior to global buckling. To simplify Eq. (3.7), vertical and horizontal stiffeners are assumed to be equally spaced ($s_x = s_y = s$) and have an equal moment of inertia in both directions ($I_x = I_y = I$). Eq. (3.8) represents the simplified form of Eq. (3.7).

$$I > 0.916 \left(\frac{K_l \, h^2}{s \, K_g} - s\right) t^3 \tag{3.8}$$

Other requirement is that the spacing between horizontal and vertical stiffeners should be determined in such a way that shear yielding of subpanels happens prior to local buckling. To ensure shear yielding, the following equation must be satisfied:

$$\tau_{crl} > \tau_{sy} \tag{3.9}$$

where τ_{sy} is the shear yield stress of infill plate, which is calculated based on Von Mises yield criterion and is equal to $\sigma_y/\sqrt{3}$, where σ_y is the yield strength of the steel infill plate. Maximum spacing required for stiffeners to guarantee shear yielding occurrence in sub panels is derived using Eq. (3.10):

$$s_{max} = 4.777\, t \sqrt{\frac{E_s}{\sigma_y}} \tag{3.10}$$

Eq. (3.8) is proposed by Sabouri-Ghomi et al. (2008) to find the minimum required moment of inertia for stiffeners to ensure local buckling occurrence prior to global buckling in the infill plate. The accuracy of the proposed equation was assessed using several FE models. They concluded that Eq. (3.8) might be useful in determining design criteria for stiffened SPSW systems, if a proper calibration factor is implemented. In the absence of any calibration factor and to provide more conservative approach, AISC Steel design guide 20 (Sabelli and Bruneau 2007) suggests that stiffeners should reduce plate slenderness in order to meet the following limits:

$$I \geq s\, t^3 J \tag{3.11}$$

$$J = 2.5 \left(\frac{h}{s}\right)^2 - 2 \geq 0.5 \tag{3.12}$$

where J is the required ratio of rigidity of one transverse stiffener to the plate rigidity. In addition, AISC Steel design guide 20 (Sabelli and Bruneau 2007) suggests the following limitation for plates with vertical and horizontal stiffeners to ensure full shear yielding of subpanels.

$$s_{max} = 3.82\, t \sqrt{\frac{E_s}{\sigma_y}} \tag{3.13}$$

In order to find the minimum moment of inertia for stiffeners to ensure local buckling in subpanels, the authors suggest using either Eq. (3.8) or Eq. (3.11), whichever is greater. Regarding the maximum spacing between stiffeners to ensure full shear yielding in subpanels, it is conservative to use Eq. (3.13) instead of Eq. (3.10) to provide smaller spacing between stiffeners.

3.4 Modelling Approach

This section presents development of deterioration models for SPSWs with both unstiffened and stiffened infill plates. First, details of the development of unstiffened SPSW are described, which are then extended for stiffened SPSW.

3.4.1 Unstiffened Steel Plate Shear Wall

Infill plates do not contribute in resisting gravity loads and experience only shear deformation when the system is subjected to lateral loads. Thus, infill plate is subjected to pure shear when the applied lateral load is smaller than a specific critical load. By using Mohr circle concept, it is clear that principal tensile and compressive stresses are oriented at a 45^0 and 135^0 respectively with respect to the direction of loading, as indicated in Fig. 3.1. When applied lateral load exceeds the specific allowable limit, infill plate buckles. The buckling stress of infill plate depends on various parameters like slenderness ratio (ratio of height to thickness, ratio of width to thickness), out-of-plane bracing, and initial imperfection developed in the thin infill plate during handling and installation in the field. Compressive stress corresponding to onset of buckling is relatively small due to large slenderness ratio associated with typical infill plates (unstiffened). Therefore, buckling of thin infill plate initiates in the early stages of loading and fold lines form perpendicular to the direction of principal compressive stresses (parallel with principal tensile stresses). After buckling, the infill plate is not capable of carrying compressive stresses which are higher than allowable limit corresponding to onset of buckling. At this point, lateral forces are transferred through infill plate by the principal tensile stresses. This post buckling behavior is known as tension field action.

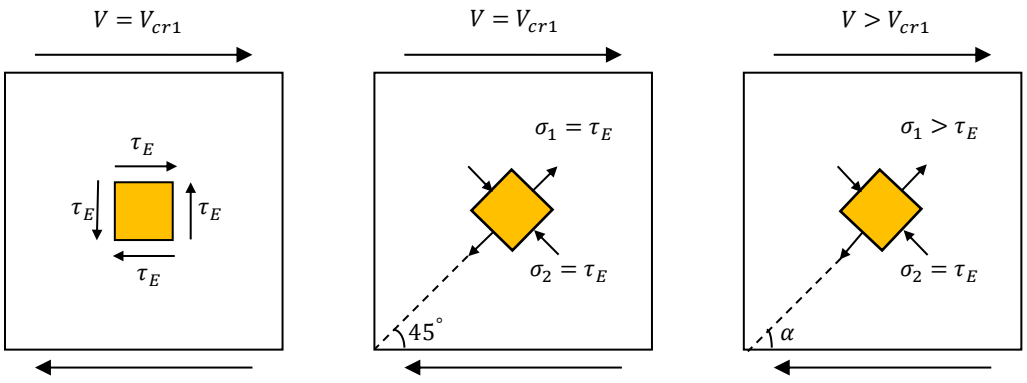

Fig. 3.1. Mohr circle concept and orientation of stresses acting on unstiffened infill plate during different stages of loading.

Thorburn et al. (1983) proposed an analytical model to predict the behavior of unstiffened SPSW systems. Appropriateness of proposed analytical model was experimentally confirmed by Timler and Kulak (1983). The proposed analytical model consists of series of parallel truss elements known as strips oriented in the direction of tension field angle, α, to resist applied lateral loads. By using the principal of least work, inclination angle of truss elements measured from vertical direction can be calculated as (Timler and Kulak 1983):

$$tan^4\alpha = \frac{1 + \frac{tL}{2\,A_c}}{1 + th_c\left[\frac{1}{A_b} + \frac{h_c^3}{360\,I_c\,L}\right]} \tag{3.14}$$

where A_b is the cross sectional area of horizontal boundary element (HBE); A_c is the cross sectional area of vertical boundary element (VBE); L is the distance between VBE centerlines; h_c is the distance between HBE centerlines; I_c is the moment of inertia of VBE. A minimum of 10 truss elements is required to accurately represent the actual behavior of infill plate in each storey and to approximate the effect of distributed loads acting on boundary elements due to formation of tension field action in infill plate (Thorburn et al. 1983). Width of each truss element is calculated using $(L\cos\propto + h_c \sin\alpha)$ divided by total number of strips in each storey. The length of beam segments required to locate n strips equally spaced, is calculated using $(L + h_c \tan\alpha)$ divided by total number of strips in the storey of interest. Since tension field angle is a function of geometric properties of surrounding boundary members and infill plate thickness, it varies along the height of building due to variation of infill plate thickness and surrounding boundary member's

properties. Thus, in case of multi-storey SPSW, variation of inclination angle along the height of building will result in staggered node points on the beam, which lead to creation of artificial bending moment acting on beam due to differential pulling forces from yielding of infill plate in adjacent stories. To avoid this phenomenon and for practical purposes, the average of tension field angle along the height of multi-storey SPSW is used instead of calculated tension field angle in each storey level. This will provide common nodes at beam level in adjacent stories. Such a slight variation has no significant impact on overall performance of SPSW system (Dastfan and Driver 2008). A general configuration of truss elements and their connections to surrounding boundary members is depicted in Fig. 3.2(b) for unstiffened SPSW system.

Fig. 3.2(c) shows the stress-strain relationship considered for truss members to represent the behavior of unstiffened infill plate. As shown in Fig. 3.2(c), a trilinear material model for tension and bilinear material model for compression zone are considered. Trilinear material model considered in tension zone is capable of considering the wide range of possible behaviors that infill plate can experience during excitations such as elastic, yielding, strain hardening, and degradation due to web tearing. In order to define bilinear relationship in the compression zone, as shown in Fig. 3.2(c), elastic buckling stress, τ_E , and corresponding strain are calculated. According to the plate buckling theory, elastic buckling stress is calculated as:

$$\tau_E = \frac{K_s \pi^2 E_s}{12 (1 - \vartheta^2)} (\frac{t}{L})^2 \tag{3.15}$$

$$k_s = \begin{pmatrix} 5.6 + 8.98\left(\frac{L}{h}\right)^2 & if \ \left(\frac{L}{h}\right) \geq 1 \\ 8.98 + 5.6\left(\frac{L}{h}\right)^2 & if \ \left(\frac{L}{h}\right) \leq 1 \end{pmatrix} \tag{3.16}$$

where k_s is the buckling coefficient and is a function of unstiffened infill plate panel aspect ratio. It is worth mentioning that τ_E is the maximum compressive stress resisted by unstiffened thin infill plate prior to buckling.

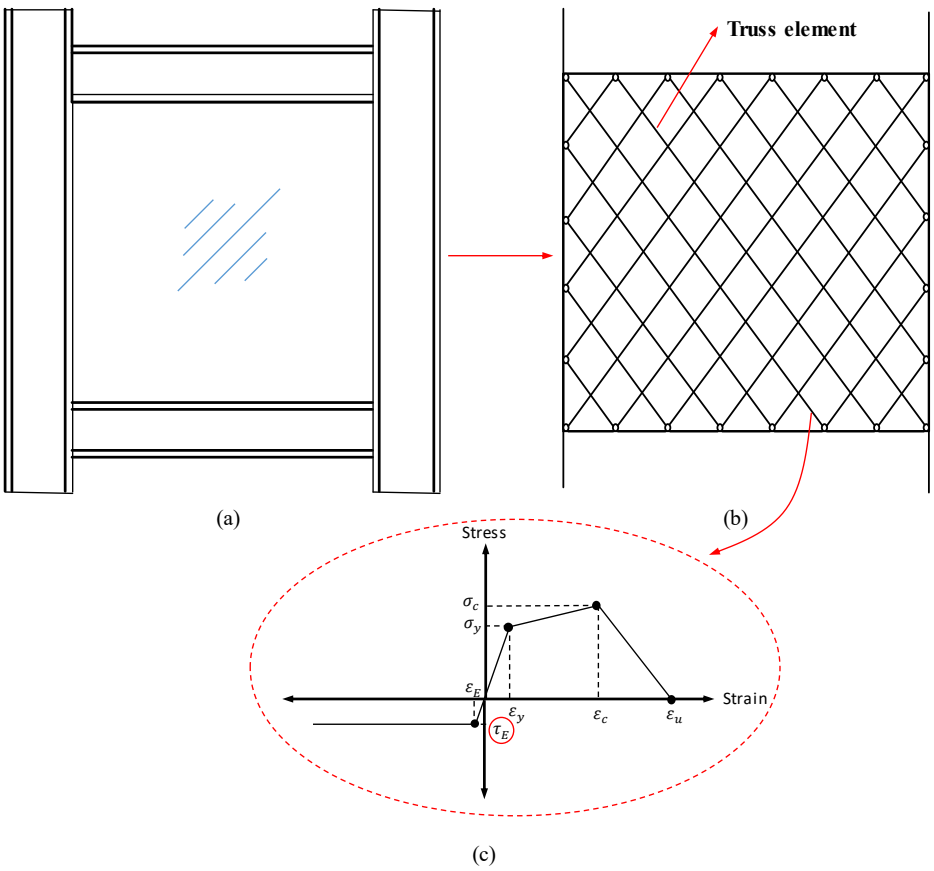

Fig. 3.2. (a) Sample configuration of unstiffened SPSW; (b) strip model for infill plate; (c) stress-strain relationship for strips in unstiffened infill plate.

3.4.2 Stiffened Steel Plate Shear Wall

By satisfying equations ((3.8), (3.11), and (3.13)) in stiffened SPSW, shear yielding of infill plate will occur prior to local and global buckling of infill plate, which leads to higher initial stiffness and higher energy absorbance in the whole system. Stiffened SPSWs are capable of developing significant compressive forces in addition to tensile forces that can be developed in unstiffened SPSWs. Thus, the design of surrounding boundary members does not include such large flexural forces that are present in unstiffened one. Fig. 3.3(a) and Fig. 3.3(b) present the general configuration of stiffened SPSW along with newly proposed strength deterioration model for stiffened infill plate. Stress-strain relationship assigned to strips for the infill plate is shown in Fig. 3.3(c).

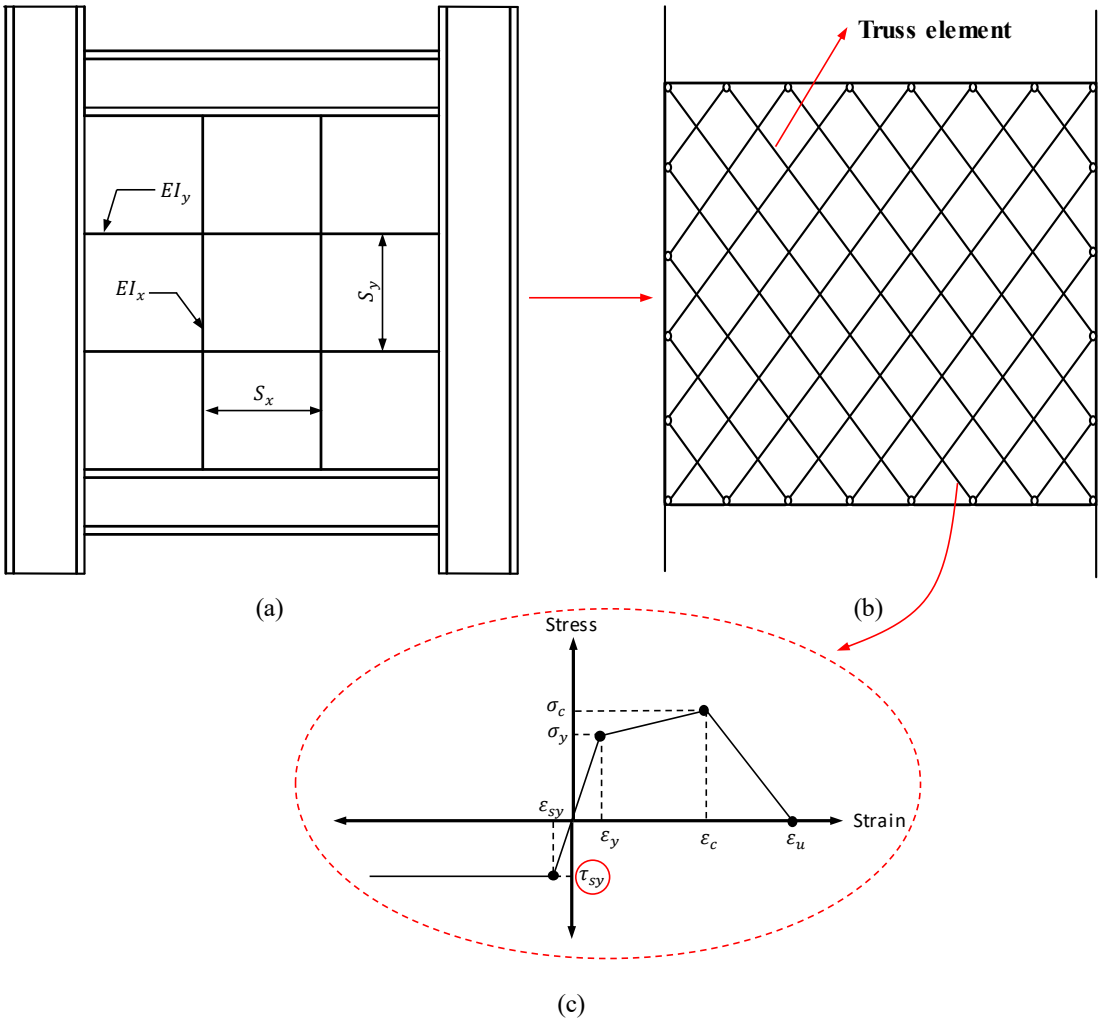

Fig. 3.3. (a) Sample configuration of stiffened SPSW; (b) strip model for infill plate; (c) stress-strain relationship for strips in stiffened infill plate.

Tension zone in stiffened SPSW is similar to unstiffened one which follows a trilinear material model in tension. The only difference is that in the proposed macro-model for infill plate, the effect of fully stiffened SPSW system is considered in the assigned stress-strain relationship for each strip. Hence, instead of modelling horizontal and vertical stiffeners directly, the effect of fully stiffened condition (shear yielding occurrence prior to global and local buckling) is applied by substituting elastic buckling shear stress, τ_E, with shear yield stress, τ_{sy}, in the assigned stress-strain relationship for strips. In the case of stiffened SPSW, since shear yield stress is much higher than elastic buckling stress ($\tau_{sy} > \tau_E$), tension field action will form in stiffened infill plate with a delay in comparison with unstiffened infill plate (Fig. 3.4). Thus, due to late activation of tension

field action and the degree in which the infill plate is stiffened, the tension field angle in stiffened infill plate may differ from the tension field angle which is proposed by Thorburn et al. (1983) for unstiffened system. The angle at which this tension field action forms in stiffened SPSW is not well established yet. AISC Design Guide 20 (Sabelli and Bruneau 2007) proposed two equations to calculate the tension field angle in stiffened SPSW and the one which produces higher resultant forces be used for design purposes. The first equation is derived for unstiffened SPSW and is given in Eq. (3.14) and the second equation is based on plate girder design (Berman and Bruneau 2005):

$$\tan(\alpha) = \frac{s_x}{s_y} \tag{3.17}$$

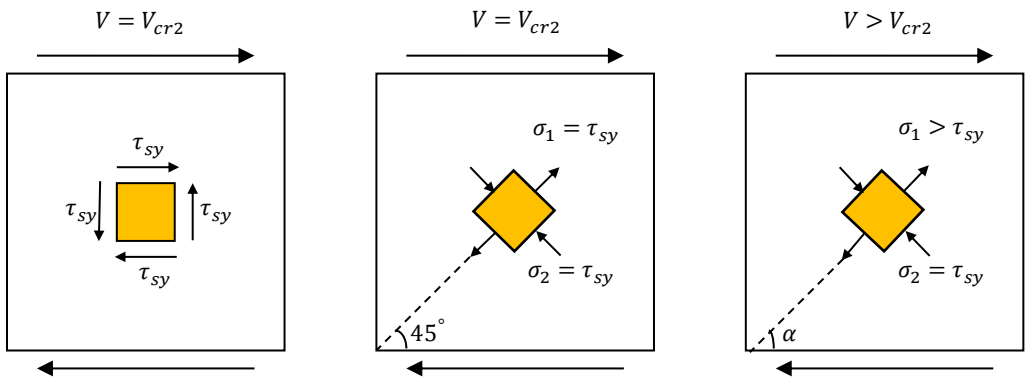

Fig. 3.4. Mohr circle concept and orientation of stresses acting on sufficiently stiffened infill plate during different stages of loading.

For boundary members, a displacement-based fiber element (distributed-plasticity) in which Menegotto-Pinto steel material with *OpenSees* (McKenna et al. 2013) default parameters were used to simulate the cyclic strain hardening as well as Bauschinger effect. One of the main features of displacement-based fiber elements is their capability to account for axial-flexural interaction, which is important for boundary members as they are subjected to high axial force due to gravity loads and inward forces resulting from yielding of infill plate.

3.5 Model Validation

The proposed numerical model in this study is validated by comparing results of numerical analysis of two single storey similar SPSW systems with and without stiffeners with the reported experimental results. This section briefly summarizes each experimental program.

3.5.1 Unstiffened SPSW Tested by Sabouri and Sajjadi (2012)

The unstiffened SPSW specimen had infill plate thickness of 2 mm and panel aspect ratio of 1.47, which can be considered as an average panel aspect ratio based on the lower and upper limits of 0.8 and 2.5 in AISC 341-16 (AISC 2016). For unstiffened SPSW, during the test, the first significant yielding occurred at the storey shear displacement of 1.7mm (0.18% drift). The maximum load carrying capacity of the system was 789.6 kN, which happened at a storey shear displacement of 39 mm (4.06% drift). In order to prevent the zipping effects, four small stiffeners were installed at the corners of the infill plate. Web tearing in plate was developed initially in the triangular region surrounded by stiffeners and boundary elements and then started to propagate out of the triangular region. In addition, plastic hinges were developed at the top and bottom of the columns during the experiment. General configuration of the unstiffened single storey SPSW is shown in Fig. 3.5(a). Fig. 3.5(b) presents the performance of the proposed numerical model under cyclic loading, which agrees well with the experimental results. Thus, the proposed model can accurately capture post-yielding behavior of the panel as well as the point associated with significant yielding in the SPSW system. In addition, average pinching effect observed during experiment due to plate tearing is captured by the numerical model.

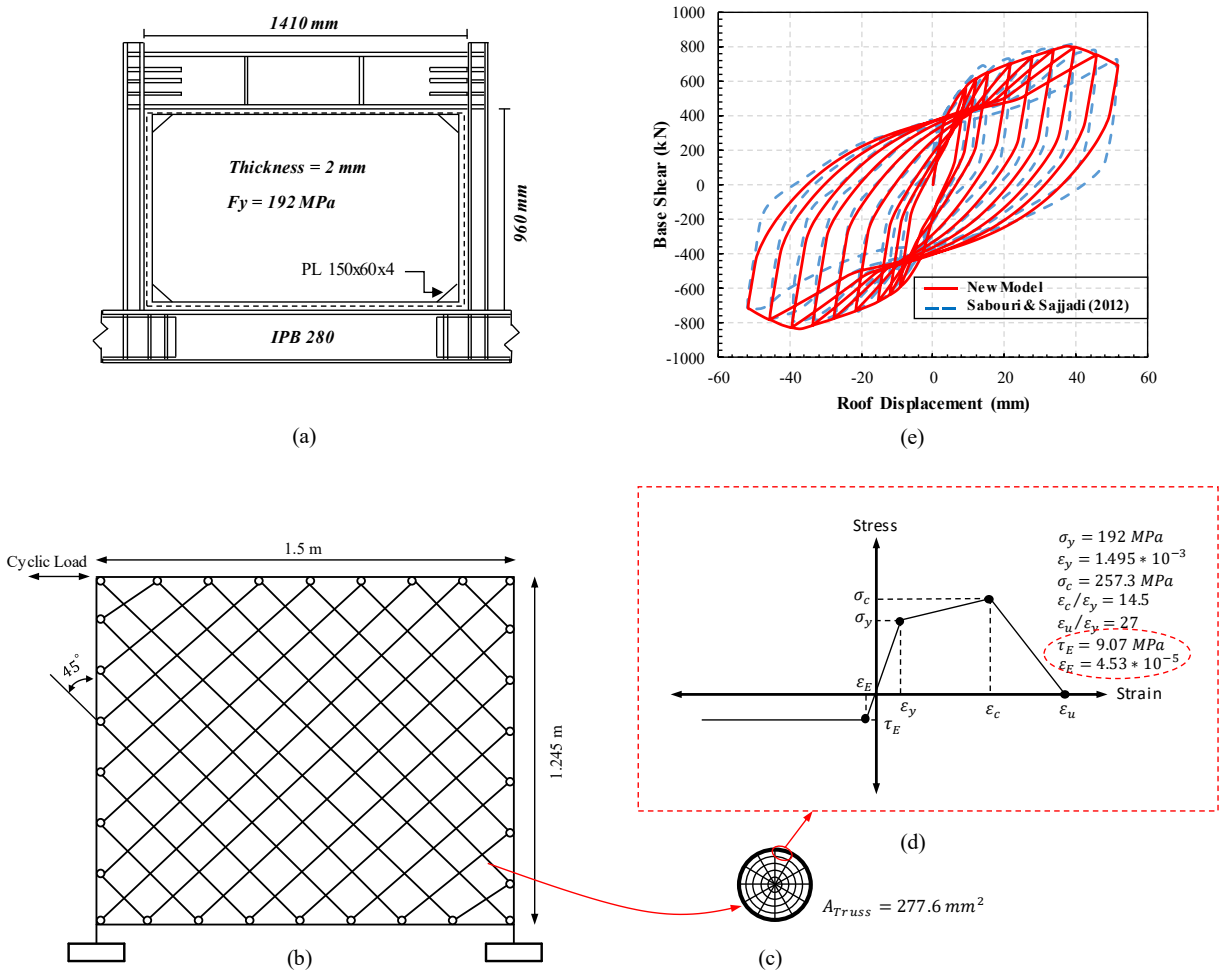

Fig. 3.5. Validation of numerical model: (a) unstiffened specimen tested by Sabouri and Sajjadi (2012); (b) strip model for infill plate; (c) cross section of each truss member along with fiber discretization; (d) stress-strain relationship for strips in an unstiffened infill plate; (e) comparison of numerical model with experimental result of Sabouri and Sajjadi (2012).

3.5.2 Stiffened SPSW Tested by Sabouri and Sajjadi (2012)

During the cyclic test of stiffened SPSW, first significant yielding was observed at a storey shear displacement of 1.58 mm. Sabouri and Sajjadi (2012) reported initiation of local buckling in one of the sub steel plates at the storey shear displacement of 2.7mm (0.28% drift), but they did not specify whether the local buckling happens prior to shear yielding or after the shear yielding.

Maximum shear capacity of 808 kN was reached at shear displacement of 34.05 mm and maximum interstorey of 6.44% was recorded at the end of the test for the stiffened specimen. At storey shear displacement of 21.6 mm (2.25% drift), minor tearing occurred in one of the middle

sub panels and the tearing propagated within the subpanel by increasing the shear displacement. SPSW strength decreased when the sub steel plates lost their continuity due to extensive web tearing. General configuration of stiffened SPSW system along with spacing between horizontal and vertical stiffeners is depicted in Fig. 3.6(a). The measured (obtained from experimental results) and predicted (obtained from *OpenSees*) base shears are plotted against roof displacements in Fig. 3.6(e). As shown in Fig. 3.6(e), there is a good agreement between results from the numerical model and that from the test. Yield point, capping point, slight pinching, and degradation backbone curve until the end of the experiment are captured precisely by the developed numerical model.

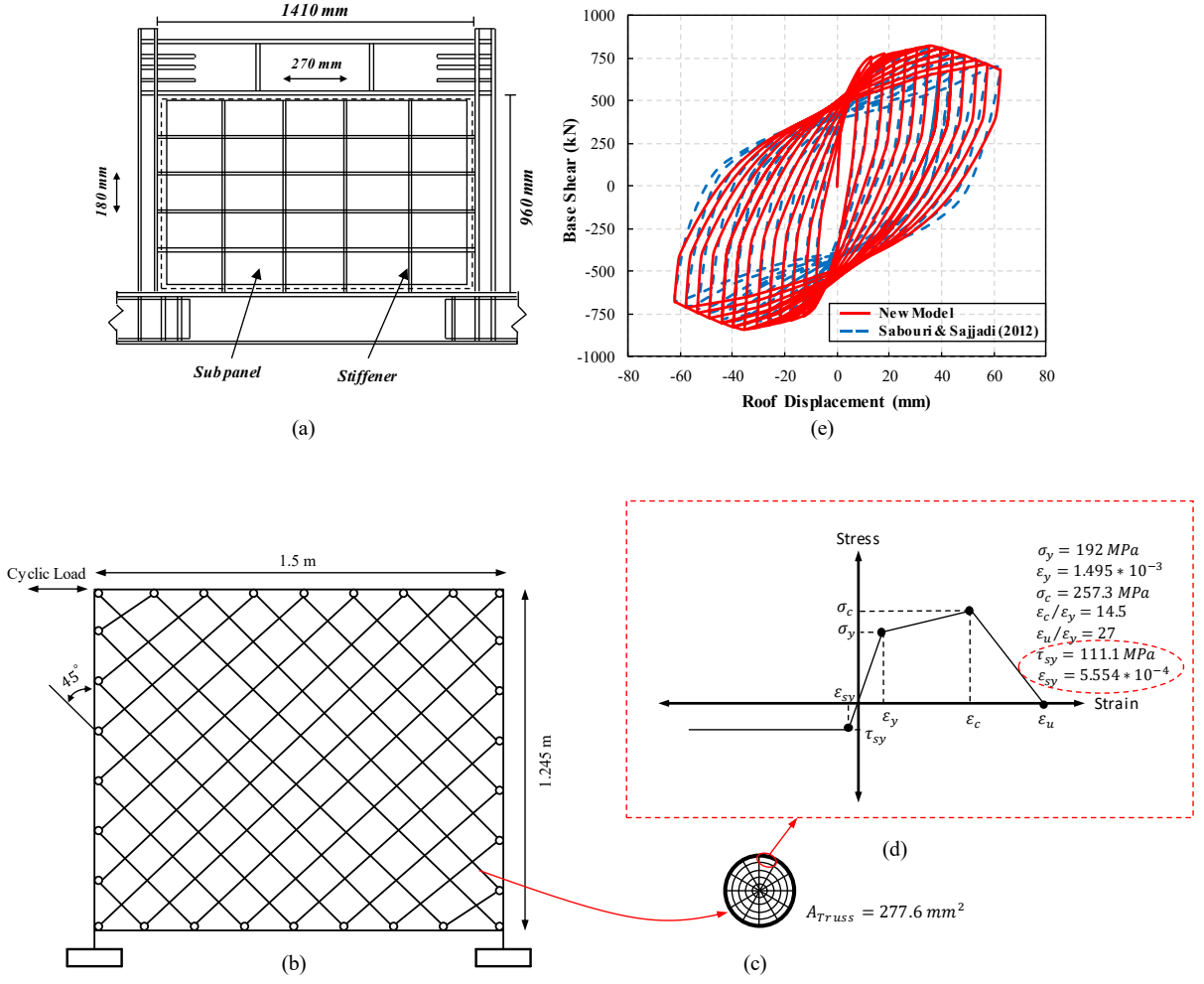

Fig. 3.6. Validation of numerical model: (a) stiffened specimen tested by Sabouri and Sajjadi (2012); (b) strip model for infill plate; (c) cross section of each truss member along with fiber discretization; (d) stress-strain relationship for strips in stiffened infill plate; (e) comparison of numerical model with experimental result of Sabouri and Sajjadi (2012).

3.6 Selected Stiffened Steel Plate Shear Walls

The buildings studied herein, are three multi-storey (7-, 10-, and 13-storey) stiffened SPSW systems. These buildings are hypothetical residential buildings located in Vancouver, Canada and share a 30x30 symmetric square plan in which two stiffened SPSW systems resist applied lateral loads in each direction (Fig. 3.7). All archetypes were designed according to CSA S16-14 (CSA 2014) and NBC (2015). A dead load of 4.1 kPa for each floor and 3.3 kPa for roof level was considered. Live load on all floors was taken as 2.4 kPa (other than roof level). The snow load was calculated to be 1.64 kPa at the roof level for all archetypes. A minimum thickness of 2 mm was considered during design process of stiffened infill plates. In order to ensure shear yielding occurrence in subpanels prior to local or global buckling of infill plate, horizontal and vertical stiffeners were installed on infill plates. The stiffeners have spacing of 200 mm, which was found adequate to ensure shear yielding of the steel plate.

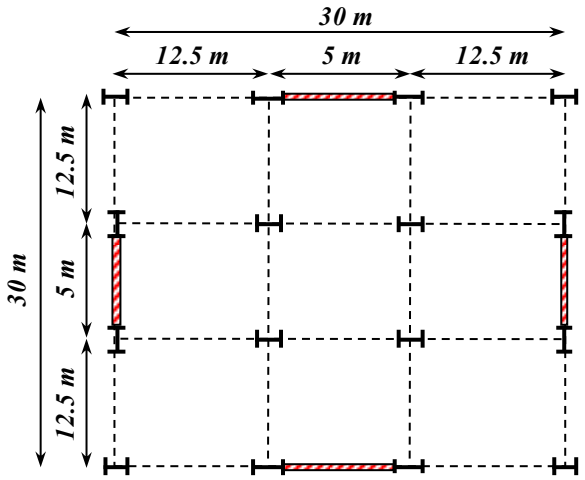

Fig. 3.7. Plan view of sample buildings.

The "gravity-leaning-column" elements are employed in this study in all archetypes for performance assessment purposes. These columns are not a part of the lateral load resisting system, but their presence is crucial to simulate the destabilizing effects from the gravity load assigned to the columns. Fig. 3.8 shows a two-dimensional nonlinear model of a 7-storey stiffened SPSW along with gravity columns. As discussed earlier, in the developed macro-model, instead of

modelling the horizontal and vertical stiffeners directly, the effects of fully stiffened condition were applied in the stress-strain relationship adopted for the infill plate.

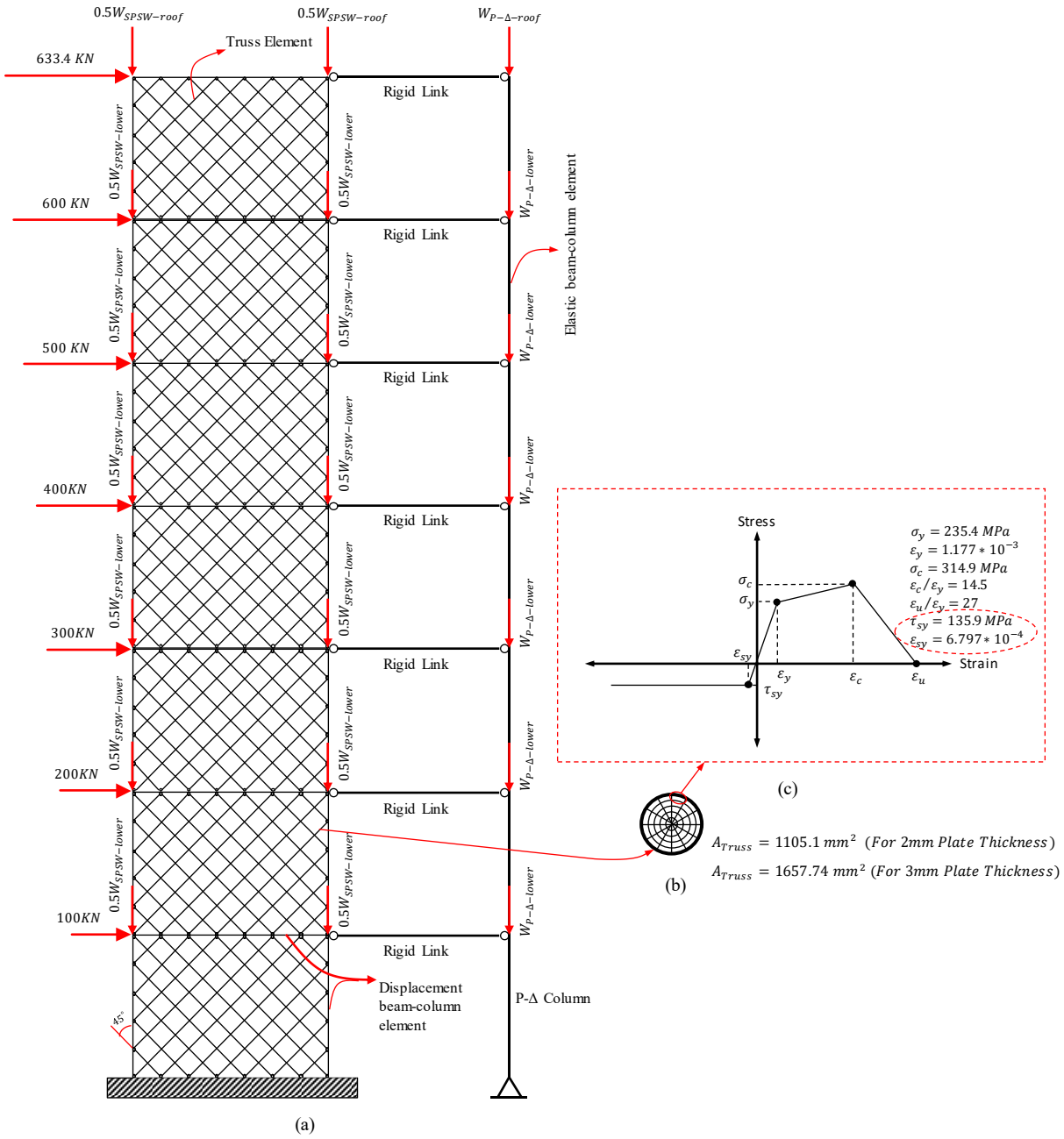

Fig. 3.8. (a) Nonlinear model used for collapse simulation: example structural model of 7-storey archetype; (b) cross section of each truss member along with fiber discretization; (c) stress-strain relationship for strips in stiffened infill plate.

To design stiffened SPSWs, equivalent static force procedure presented in NBC (2015) was employed to determine the storey shear in each level. All archetypes were designed using the same seismic response modification factors as of unstiffened SPSWs since these factors are currently not quantified for stiffened SPSW in NBC (2015). Thus, ductility-related force modification factor, R_d, of 5.0 and overstrength-related force modification factor, R_o , of 1.6 were utilized to design stiffened SPSWs. Seismic design base shear (V_d), as shown in Table 3.1, calculated according to equivalent lateral force method in NBC (2015) were 1243.7 kN, 1502.7 kN, and 1616.2 kN for 7-, 10-, and 13-storey stiffened SPSWs, respectively.

Table 3.1. Storey weight and design base shear of SPSW archetypes

Archetype	Level	$W_{SPSW}(kN)$	$W_{P-\Delta}(kN)$	$W_{total}(kN)$	$V_d(kN)$
7	Roof	405.78	1263.72	1669.5	1243.7
	Lower	579.69	1805.31	2385	
10	Roof	405.78	1263.72	1669.5	1502.7
	Lower	579.69	1805.31	2385	
13	Roof	405.78	1263.72	1669.5	1616.2
	Lower	579.69	1805.31	2385	

Note: W_{SPSW} = gravity loads on SPSW; $W_{P-\Delta}$ = gravity loads on $P-\Delta$ leaning column; W_{total} = total gravity load ($= W_{SPSW} + W_{P-\Delta}$)

In each storey, the total shear was assumed to be resisted by the stiffened infill plate only. As presented in steel design guide 20 (Sabelli and Bruneau 2007), the design shear strength of stiffened SPSW is calculated based on shear yielding of stiffened infill plate as follows:

$$V_r = 0.6\,\emptyset\,F_y\,t_w\,L_{cf} \tag{3.18}$$

where $\emptyset = 0.9$; F_y is specified yield stress of infill plate; t_w is the plate thickness; L_{cf} is the clear length of the panel between VBE flanges.

The capacity design procedure proposed by Berman and Bruneau (2008) was employed to design surrounding boundary members. This procedure is based on uniform collapse mechanism, which includes uniform yielding of infill plates in all stories along the height of the building as well as plastic hinges formation at the ends of HBEs. In addition, plastic hinges are allowed to be formed at the base of boundary columns in the first storey. Based on derivation from Berman and

Bruneau (2003), the following equation must be satisfied to ensure occurrence of uniform collapse mechanism in the system.

$$\sum_{i=1}^{n_s} F_i\, H_i = \sum_{i=0}^{n_s} M_{prli} + \sum_{i=0}^{n_s} M_{prri} + \sum_{i=1}^{n_s} \frac{1}{2}\,(t_{wi} - t_{wi+1}) F_y\, L\, H_i \sin(2\alpha_i) \tag{3.19}$$

where F_i is the applied lateral load in each level to cause the mechanism; H_i is the height from base to the storey level of interest; M_{prli} and M_{prri} are reduced plastic moment capacity at the HBE ends in each level for left and right end respectively. To employ Eq. (3.19) in calculating applied lateral loads that cause this mechanism, a relationship between lateral loads is needed to be assumed (relationship between F_1, F_2, and etc.). For this purpose, a load pattern equal to that calculated using the equivalent static force procedure presented in NBC (2015) is employed. Table 3.2, Table 3.3, and Table 3.4 present selected boundary members and infill plate thicknesses for all archetypes.

As discussed, in the proposed macro-modelling approach, instead of modelling horizontal and vertical stiffeners directly, the effect of fully stiffened condition is applied in the stress-strain relationship adopted for the strips. Thus, any configuration of stiffeners that satisfy equations (3.8), (3.11), and (3.13) can be considered as a sufficiently stiffened SPSW system (it means that shear yielding of infill plate occurs prior to local or global buckling) and can be modelled using the proposed approach.

Table 3.2. Design summary of 7-storey stiffened SPSW

Storey	$t_w\,(mm)$	HBE section	VBE section
7	2	W360x287	W360x509
6	2	W310x67	W360x592
5	2	W310x67	W360x634
4	2	W310x67	W360x634
3	2	W310x67	W360x634
2	3	W360x179	W360x634
1	3	W310x79	W360x818
0	NA	W360x382	NA

Table 3.3. Design summary of 10-storey stiffened SPSW

Storey	$t_w\,(mm)$	HBE section	VBE section
10	2	W360x287	W360x509
9	2	W310x67	W360x634
8	2	W310x67	W360x677
7	2	W310x67	W360x744
6	2	W310x67	W360x744
5	3	W360x179	W360x744
4	3	W310x79	W360x744
3	3	W310x79	W360x744
2	3	W310x79	W360x744
1	3	W310x79	W360x900
0	NA	W360x382	NA

Table 3.4. Design summary of 13-storey stiffened SPSW

Storey	$t_w\,(mm)$	HBE section	VBE section
13	2	W360x314	W1000x296
12	2	W310x67	W1000x412
11	2	W310x67	W1000x483
10	2	W310x67	W1000x539
9	2	W310x67	W1000x554
8	2	W310x67	W1000x591
7	3	W360x179	W1000x642
6	3	W310x79	W1000x748
5	3	W310x79	W1000x748
4	3	W310x79	W1000x748
3	3	W310x79	W1000x748
2	3	W310x79	W1000x883
1	3	W310x79	W40x655 [a]
0	NA	W360x421	NA

[a] Imperial designation

3.7 Analysis of Stiffened SPSWs

3.7.1 Static Pushover Analysis

Nonlinear pushover analysis was performed on all stiffened SPSW archetypes to extract system overstrength factor, Ω, and period-based ductility, μ_T. These two factors are calculated using the following equations:

$$\Omega = \frac{V_{max}}{V_d} \tag{3.20}$$

$$\mu_T = \frac{\delta_u}{\delta_{y,eff}} \tag{3.21}$$

where V_{max} is the maximum base shear obtained from nonlinear pushover analysis; V_d is the design base shear; δ_u is the ultimate roof displacement of the building corresponding to 20% strength loss from maximum strength; $\delta_{y,eff}$ is the yield roof displacement and is calculated according to Eq. (3.22):

$$\delta_{y,eff} = C_0 \frac{V_{max}}{W} \left[\frac{g}{4\pi^2}\right] (\max(T, T_1))^2 \tag{3.22}$$

where C_0 is a modification factor to relate the spectral displacement of an equivalent single-degree-of-freedom (SDOF) system to the roof displacement of multi-degree-of-freedom (MDOF) system calculated according to ASCE 41-06 (ASCE 2006). V_{max}/W is the maximum base shear normalized by building weight, g is the gravity constant, T is the upper limit of fundamental period of the system calculated based on empirical equation (i.e., $2 * T_a$ in NBC 2015 for shear walls), and T_1 is the fundamental period of archetype model computed using eigenvalue analysis. The lateral loads for pushover analyses were obtained from the equivalent static force procedure presented in NBC (2015). Fig. 3.8(a) shows the lateral load patterns used for pushover analysis of 7-storey stiffened SPSW. Fig. 3.9 presents the results of pushover analysis for all studied archetypes. All the designed stiffened SPSWs showed highly ductile and stable performance during pushover analysis. From the pushover curves the period-based ductility (μ_T) was calculated as 7, 6.6, and 7.5 for 7-, 10-, and 13-storey stiffened SPSWs, respectively. In addition, system

overstrength factor (Ω) was calculated as 3.3, 2.8, and 2.8 for 7-, 10-, and 13-storey stiffened SPSWs, respectively (these values are shown in Table 3.6).

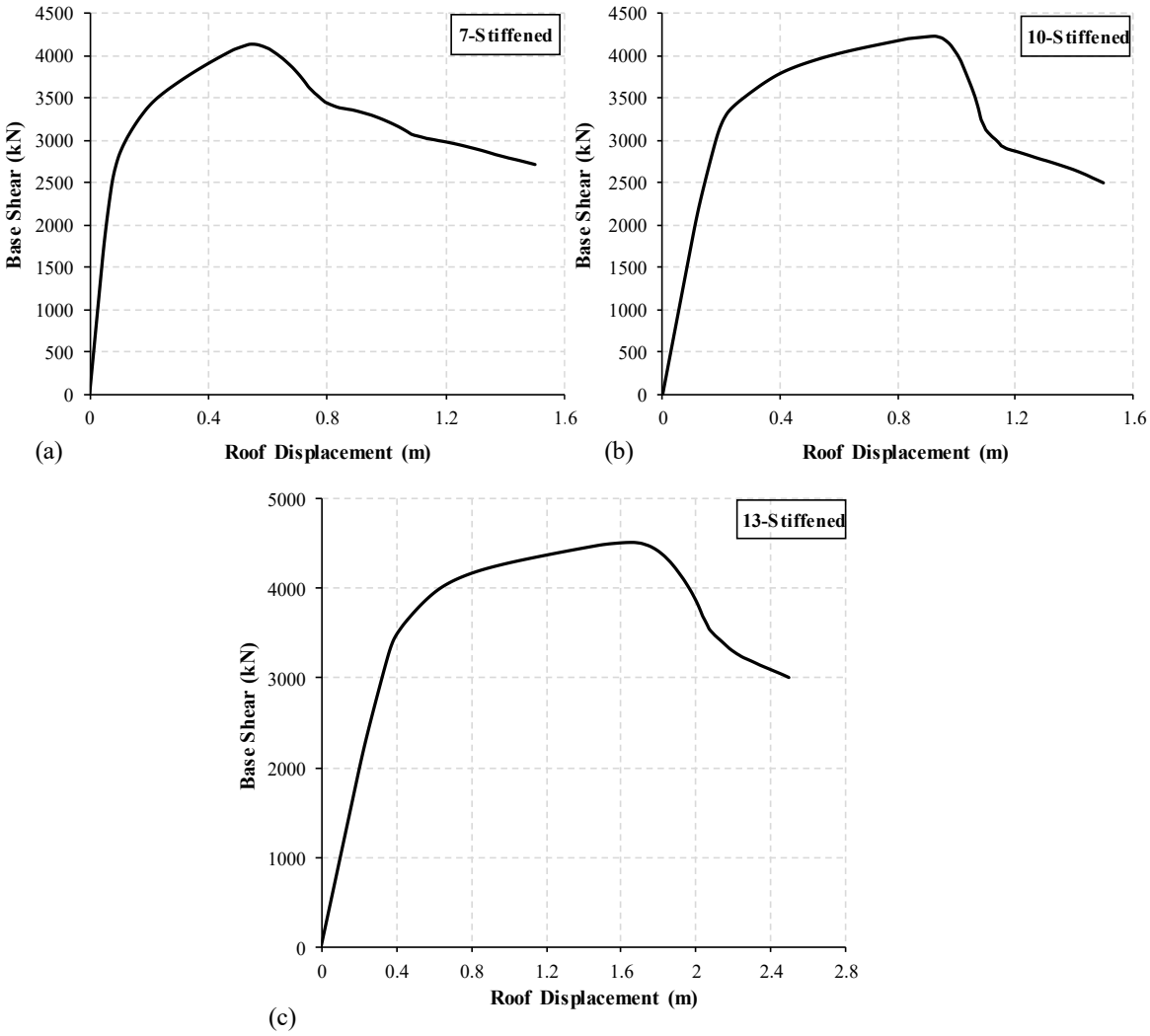

Fig. 3.9. Monotonic pushover analysis results.

3.7.2 Ground Motion Selection and Scaling

FEMA P695 (FEMA 2009) prescribes using a group of 44 ground motions to reliably assess the probability of collapse for a given archetype. In western Canada, due to lack of real accelerograms, a set of 44 spectrum-compatible artificial ground motions were used to assess the seismic performance of each archetype. These artificial ground motions are developed for western Canada by Atkinson (2009). Table 3.5 provides several major characteristics of each ground

motion such as magnitude (M), closest distance to fault rupture (R_{fault}), peak ground acceleration (PGA), and the ratio of maximum velocity to maximum acceleration $\left(\frac{v}{a}\right)$. Fig. 3.10 shows four sample selected unscaled artificial ground motions used in this study for IDA and NTHA.

Table 3.5. Characteristics of selected unscaled ground motions

Event	M	$R_{fault}\,(km)$	PGA (g)	v/a	**Event**	M	$R_{fault}\,(km)$	PGA (g)	v/a
west6c2.1	6.5	19.7	0.223	0.0959	west7c1.19	7.5	21.6	0.433	0.1032
west6c2.2	6.5	19.7	0.27	0.087	west7c1.20	7.5	21.6	0.309	0.0989
west6c2.4	6.5	21.6	0.222	0.0799	west7c1.22	7.5	20.3	0.341	0.1044
west6c2.5	6.5	21.6	0.244	0.0776	west7c1.23	7.5	20.3	0.325	0.1596
west6c2.10	6.5	21.6	0.174	0.0788	west7c1.25	7.5	18.1	0.58	0.0949
west6c2.11	6.5	21.6	0.184	0.0848	west7c1.26	7.5	18.1	0.516	0.11
west6c2.16	6.5	21.8	0.239	0.0753	west7c1.31	7.5	26.3	0.33	0.0811
west6c2.17	6.5	21.8	0.176	0.1013	west7c1.32	7.5	26.3	0.284	0.1289
west6c2.22	6.5	25.8	0.168	0.0676	west7c1.34	7.5	26.3	0.179	0.1224
west6c2.23	6.5	25.8	0.208	0.0968	west7c1.35	7.5	26.3	0.248	0.109
west6c2.37	6.5	27.8	0.183	0.076	west7c1.37	7.5	26.3	0.245	0.1182
west6c2.38	6.5	27.8	0.204	0.0854	west7c1.38	7.5	26.3	0.229	0.0928
west7c1.1	7.5	16.4	0.522	0.112	west7c1.40	7.5	26.3	0.262	0.0815
west7c1.2	7.5	16.4	0.588	0.0793	west7c1.41	7.5	26.3	0.22	0.1371
west7c1.4	7.5	17.1	0.327	0.0931	west7c1.43	7.5	26.3	0.185	0.1376
west7c1.5	7.5	17.1	0.284	0.108	west7c1.44	7.5	26.3	0.276	0.1103
west7c1.10	7.5	17.1	0.342	0.1067	west7c2.1	7.5	47.4	0.162	0.1321
west7c1.11	7.5	17.1	0.413	0.1106	west7c2.2	7.5	47.4	0.189	0.1293
west7c1.13	7.5	17.1	0.351	0.0704	west7c2.4	7.5	45.7	0.253	0.1108
west7c1.14	7.5	17.1	0.32	0.1297	west7c2.5	7.5	45.7	0.197	0.1319
west7c1.16	7.5	21.6	0.294	0.1208	west7c2.13	7.5	30.2	0.203	0.208
west7c1.17	7.5	21.6	0.392	0.1165	west7c2.14	7.5	30.2	0.256	0.0984

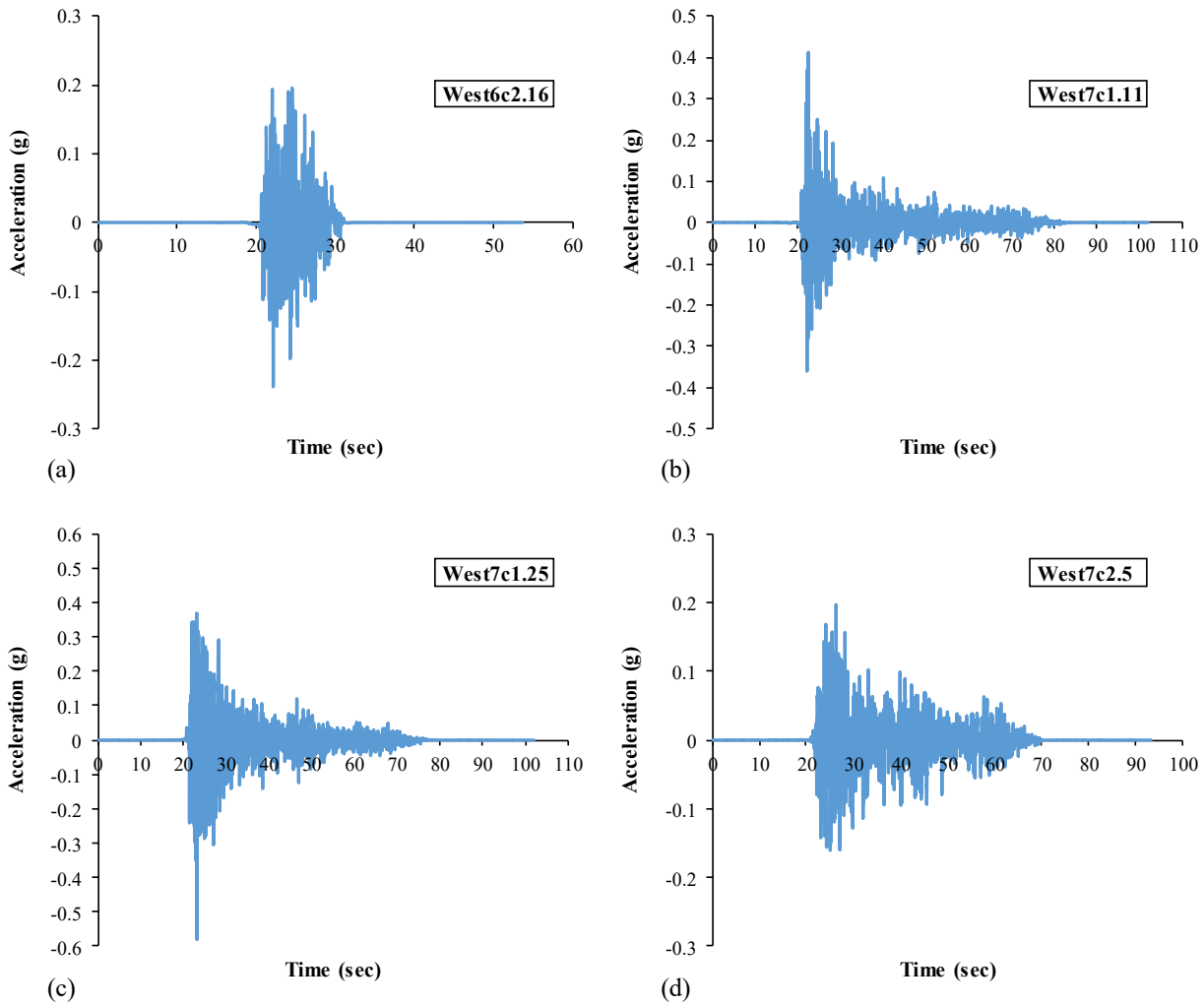

Fig. 3.10. Sample time histories of selected ground motions.

Each ground motion was scaled using ASCE/SEI-7 (ASCE 2016) method such that within the interval of $0.2T_1$ to $1.5T_1$, where T_1 is the fundamental period of the vibration obtained from modal analysis in *OpenSees*, mean spectrum taken from response spectra of a set of ground motions (at least seven ground motions) fit or be above the uniform hazard spectrum (UHS). Fig. 3.11(a,b), present response spectra of 44 ground motions together with design spectrum and mean spectrum for two different cases of unscaled and scaled, respectively.

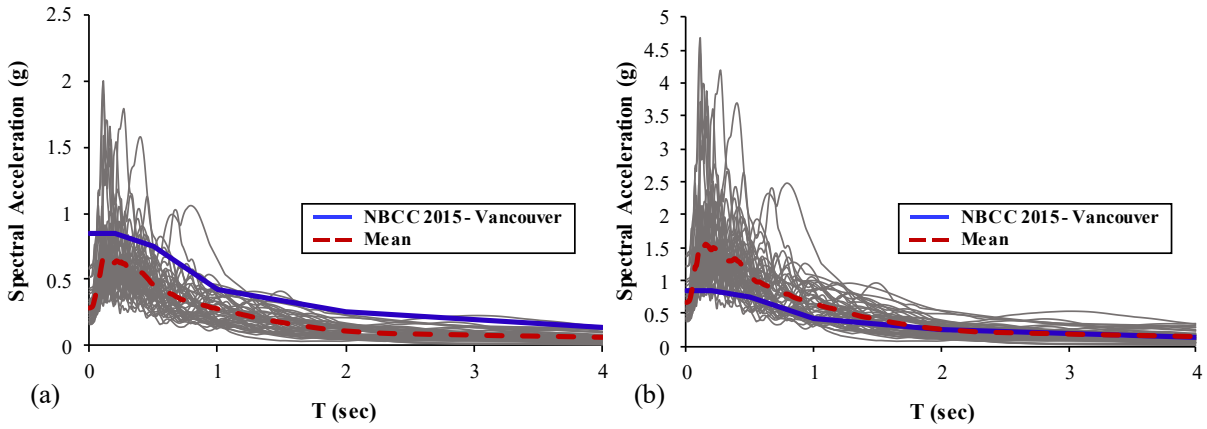

Fig. 3.11. Response spectra of 44 ground motions along with mean and design spectrum: (a) unscaled ground motions; (b) scaled ground motions.

3.7.3 Incremental Dynamic Analysis and Fragility Curves

Inelastic demand for stiffened SPSW archetypes were determined using incremental dynamic analysis (IDA). Incremental dynamic analysis method was first developed by Luco and Cornell (1998) and later explained in detail by Vamvatsikos and Cornell (2002). In IDA procedure, nonlinear dynamic analyses of a structural model are carried out under a group of ground motions and the intensity measure selected for each ground motion for collapse assessment is incrementally increased until the collapse of the system reaches (e.g., global dynamic instability). Although, multiplication of ground motion using a scale factor does not necessarily result in realizable ground motion, it can provide a wide range of valuable feedback regarding the performance of the system starting from elastic to final global dynamic instability. Incremental dynamic analyses have been performed using 5% damped spectral acceleration at fundamental period of the structure as intensity measure (IM) and maximum interstorey drift as engineering demand parameter (EDP). The IDA curves resulting from 44 ground motions for each archetype along with 16th, 50th, and 84th percentile IDA curves are presented in Fig. 3.12. Collapse fragility function was developed for each archetype based on the results obtained from incremental dynamic analysis. The IM value corresponding to initiation of collapse for each ground motion is calculated using the IDA results and a cumulative distribution function is fitted to resulting IM values (Fig. 3.12). Fig. 3.12(b,d,f) present probability of collapse under different level of spectral acceleration intensity. The median collapse spectral acceleration intensity, S_{CT}, the spectral acceleration intensity at which 22 ground

motions cause collapse in the structure, is calculated as 2.76, 1.41, and 0.95 for 7-, 10-, and 13-storey stiffened SPSWs, respectively. The term "Discrete Probability" in Fig. 3.12 refers to the ratio of collapse cases to the total number of analyses for each IM level, and the term "Cumulative Distribution" refers to theoretical cumulative distribution function, which is calculated based on a normal distribution with a specified median and standard deviation. Collapse margin ratio (CMR), a primary parameter in quantifying the collapse safety of the structure, is calculated as (S_{CT}/S_{MT}), where S_{MT} is the response spectrum of maximum considered earthquake (MCE) at the fundamental period of a given archetype.

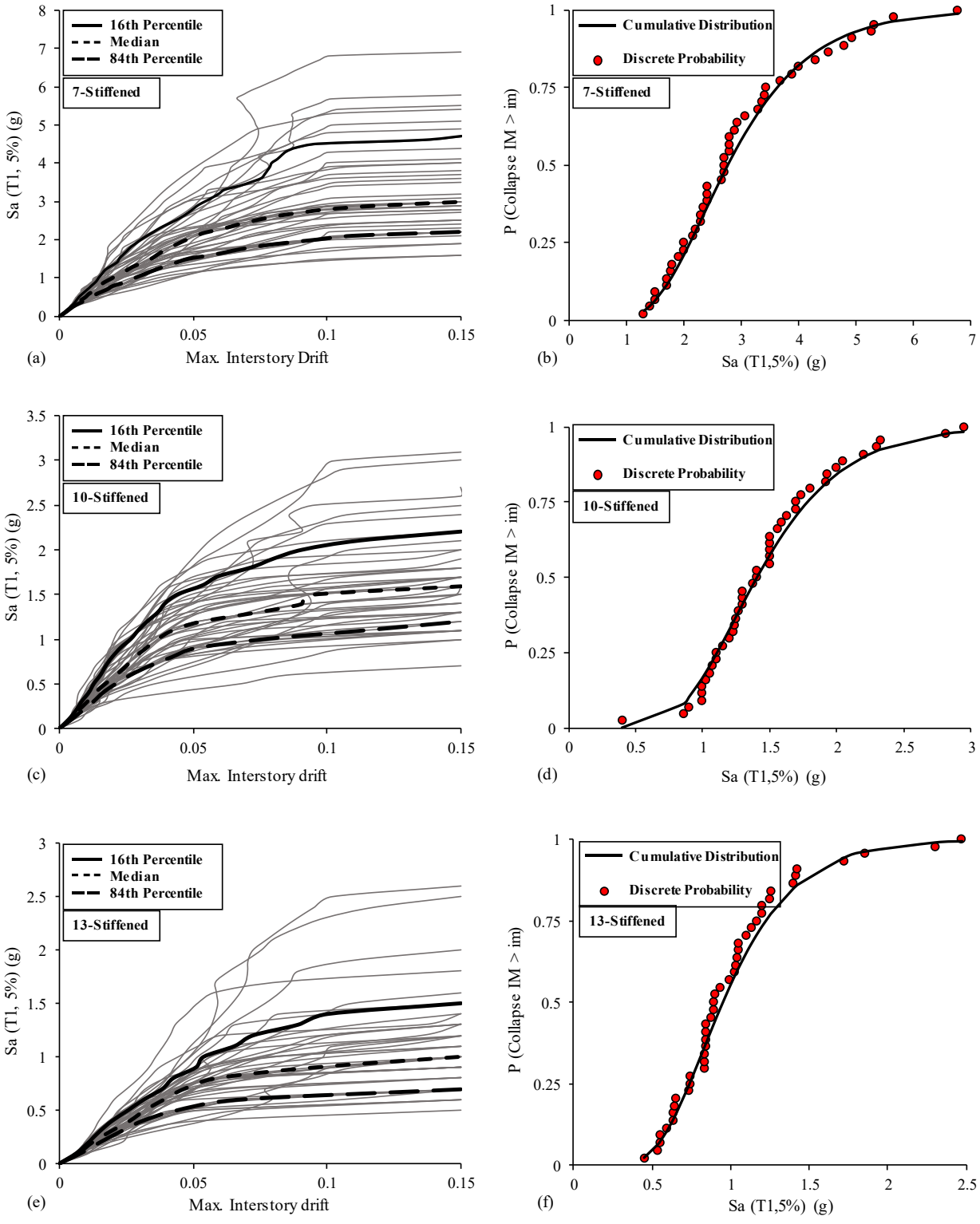

Fig. 3.12. IDA results and corresponding derived fragility curves for all archetypes.

3.7.4 Collapse Performance Evaluation

In order to account for the effects of spectral shape on collapse capacity of the structure, CMR is modified by multiplying a factor known as spectral shape factor (SSF) to obtain adjusted collapse margin ratio (ACMR). SSF is a function of fundamental period, T, period-based ductility, μ_T, and seismic design category, which is assumed to be D_{max} in this study. For performance evaluation purposes, uncertainties related to design requirements (β_{DR}), modelling (β_{MDL}), test data (β_{TD}) chosen for verification of numerical model, and record to record variability (β_{RTR}) must be quantified based on the guideline provided by FEMA P695 (FEMA 2009) methodology.

Uncertainty related to design requirements: Design requirements uncertainty refers to the completeness and robustness of the design procedure followed to design stiffened SPSW. In this study, the design guidelines provided in CSA S16-14 (CSA 2014) and NBC (2015) were followed to design stiffened SPSW. CSA S16-14 (CSA 2014) provides sufficient design requirements to ensure a safety margin against unanticipated failure modes. Thus, in the current study, design requirements uncertainty was rated as B (good) and the corresponding value of 0.2 was assigned.

Uncertainty related to Modelling: This uncertainty refers to capability of developed analytical model to cover the wide range of possible failure modes in the system. Based on the study performed by Purba and Bruneau (2014), web tearing of thin infill plate and flexural failure of boundary members are main sources of degradation in SPSW systems. Developed analytical model was capable of considering both sources of degradation in the system. Hence, the nonlinear model development in this study was rated as B (good) and the corresponding value associated with modelling uncertainty was assumed to be 0.2.

Uncertainty related to test data: This uncertainty refers to the reliability of the test data which are used for verification purposes and total number of experiments that are used for verification. At the time of this writing, very limited numbers of experimental studies have been performed on stiffened SPSW systems. On the other hand, in unstiffened SPSW, total numbers of tested specimens are less than 50, which are also quite less than other lateral load resisting systems (e.g., moment resisting frames). In the current study, test data was rated as C (fair) and corresponding value associated with test data uncertainty was assumed to be 0.35.

Uncertainty related to record-to-record variability: Record-to-record uncertainty is due to the variation in response of a single archetype to a group of ground motions. This variability is mainly due to the variation in frequency content and dynamic characteristics of different ground motions. A fixed value of $\beta_{RTR} = 0.4$ is considered for structures with significant period elongation (i.e., period-based ductility, $\mu_T \geq 3$). For most of the systems with limited ductility, the same record-to-record uncertainty as of ductile systems can be used since most of the systems will experience a significant period elongation before collapse.

Total system collapse uncertainty is calculated based on combination of aforementioned four sources of uncertainties as follows:

$$\beta_{TOT} = \sqrt{\beta_{RTR}^2 + \beta_{DR}^2 + \beta_{TD}^2 + \beta_{MDL}^2} \tag{3.23}$$

Based on the given values for each uncertainty, total system uncertainty of 0.6 is obtained using Eq. (3.23). Acceptable value of adjusted collapse margin ratio ($ACMR_{10\%}$) is based on total system collapse uncertainty, β_{TOT}, and established values of acceptable probabilities of collapse, which is normally assumed to be 10% probability of collapse under maximum considered earthquake (MCE) for assessing the performance of a group of archetypes. According to the table provided by FEMA P695 (FEMA 2009), the acceptable ACMR for 10% probability of collapse under MCE ground motions for β_{TOT} of 0.6 is 2.16. As indicated in Table 3.6, all archetypes successfully passed the performance criterion prescribed by FEMA P695 (FEMA 2009) procedure. As shown in Table 3.6, the smallest calculated CMR value of 3.79 (for 13-storey stiffened SPSW) passes the allowable adjusted collapse margin ratio (ACMR) given by FEMA P695 (FEMA 2009). Thus, the seismic force modification factors (R_d of 5.0 and R_0 of 1.6) used for designing the selected stiffened SPSWs are found adequate. Currently, R_d of 5.0 is the highest ductility factor assigned to any lateral load resisting system in NBC (2015). The seismic force modification factors suggested by building codes are based on engineering judgments with adequate safety to account for any uncertainty in design and construction. Since the hierarchical modes of failure in both stiffened and unstiffened SPSWs are same: steel infill plate yielding as the main ductile fuse, followed by yielding at the end of steel beams and finally plastic hinging at the base of columns, same seismic force modifications factors (R_d of 5.0 and R_0 of 1.6) can be used for both stiffened and unstiffened SPSWs.

Table 3.6. Summary of the results obtained from pushover and IDA analyses for all structural configurations

Archetype	Pushover results						IDA results			Performance evaluation		
	$\Delta_y(mm)$	$\Delta_u(mm)$	μ_T	$V_d\ (KN)$	$V_{max}\ (KN)$	Ω_0	$S_{MT}\ (g)$	$S_{CT}\ (g)$	CMR	SSF	ACMR	Pass/fail
7	132.5	937	7.07	1243.7	4126.5	3.3	0.504	2.76	5.48	1.323	7.25	Pass
10	161.7	1074	6.64	1502.7	4231.4	2.8	0.356	1.41	3.96	1.35	5.34	Pass
13	272.9	2059	7.5	1616.2	4520	2.8	0.251	0.95	3.79	1.421	5.39	Pass

3.8 Results from Nonlinear Time History Analysis

Since interstorey drift is an important indicator of structure's functionality in performance-based earthquake engineering, the variation of maximum interstorey drift in every storey is recorded for each ground motion and is plotted in two different styles (i.e., profile and boxplot) for each archetype. As shown, the box represents a range (Q16 – Q84) between 16th percentile and 84th percentile. The solid line inside the box represents the median of the data at the corresponding storey. Two lines located outside of the box are used to indicate the upper and lower bound of the data. As can be seen in Fig. 3.13, maximum interstorey drift in all stories for all archetypes are quite less than the allowable drift limit of 2.5%, as prescribed by NBC (2015).

Maximum shear contribution of each individual component, infill plate and boundary columns, was extracted for each ground motion through post-processing of statistical data resulting from NTHA. The maximum shear contribution of each structural element is indicated in the form of boxplot in Fig. 3.14. As shown in the Fig. 3.14, the values are normalized based on maximum storey shear resulting from each ground motion. As can be seen from Fig. 3.14, in 7- and 10-storey stiffened SPSW system, the participation of infill plate in resisting the applied forces are quite larger than those resisted by boundary columns in all stories, whereas in 13-storey stiffened SPSW system, the contribution of boundary columns in resisting the applied lateral forces is close to the corresponding values obtained for infill plate in the same storey and in several cases, the participation of boundary columns is significantly larger than that for infill plate (first storey of 13-storey stiffened SPSW). Thus, based on the results indicated in Fig. 3.14, the contribution of boundary columns is quite significant in most of the stories in all archetypes. However, in the current design of stiffened SPSWs, the total shear is assumed to be resisted by stiffened infill plate and the contribution of surrounding columns is ignored. The same observation was reported by Qu and Bruneau (2009) for unstiffened SPSW, where they demonstrated that the participation of boundary columns in resisting lateral loads can be up to 50% for panel aspect ratio of 2.0. Purba and Bruneau (2014) indicated that several unstiffened SPSW systems that are designed based on the storey shear shared between the infill plate and the boundary columns were not able to satisfy the requirements suggested by FEMA P695 (FEMA 2009). Thus, neglecting the contribution of boundary columns in design process of unstiffened and stiffened SPSWs will lead to more stable

performance and provide a reliable backup system for primary load carrying component (i.e., infill plate).

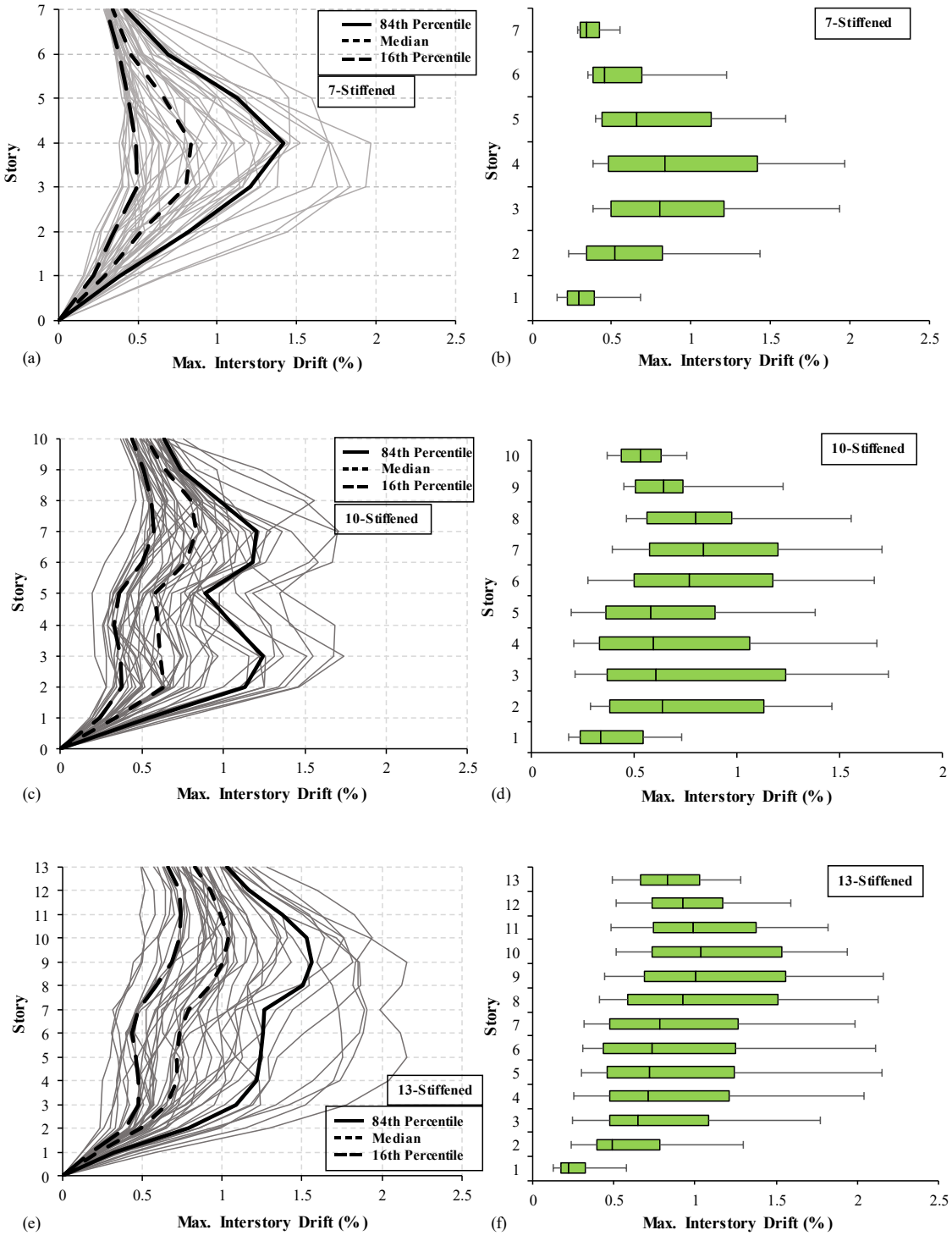

Fig. 3.13. Interstorey drifts of all archetypes under 44 ground motions at design level.

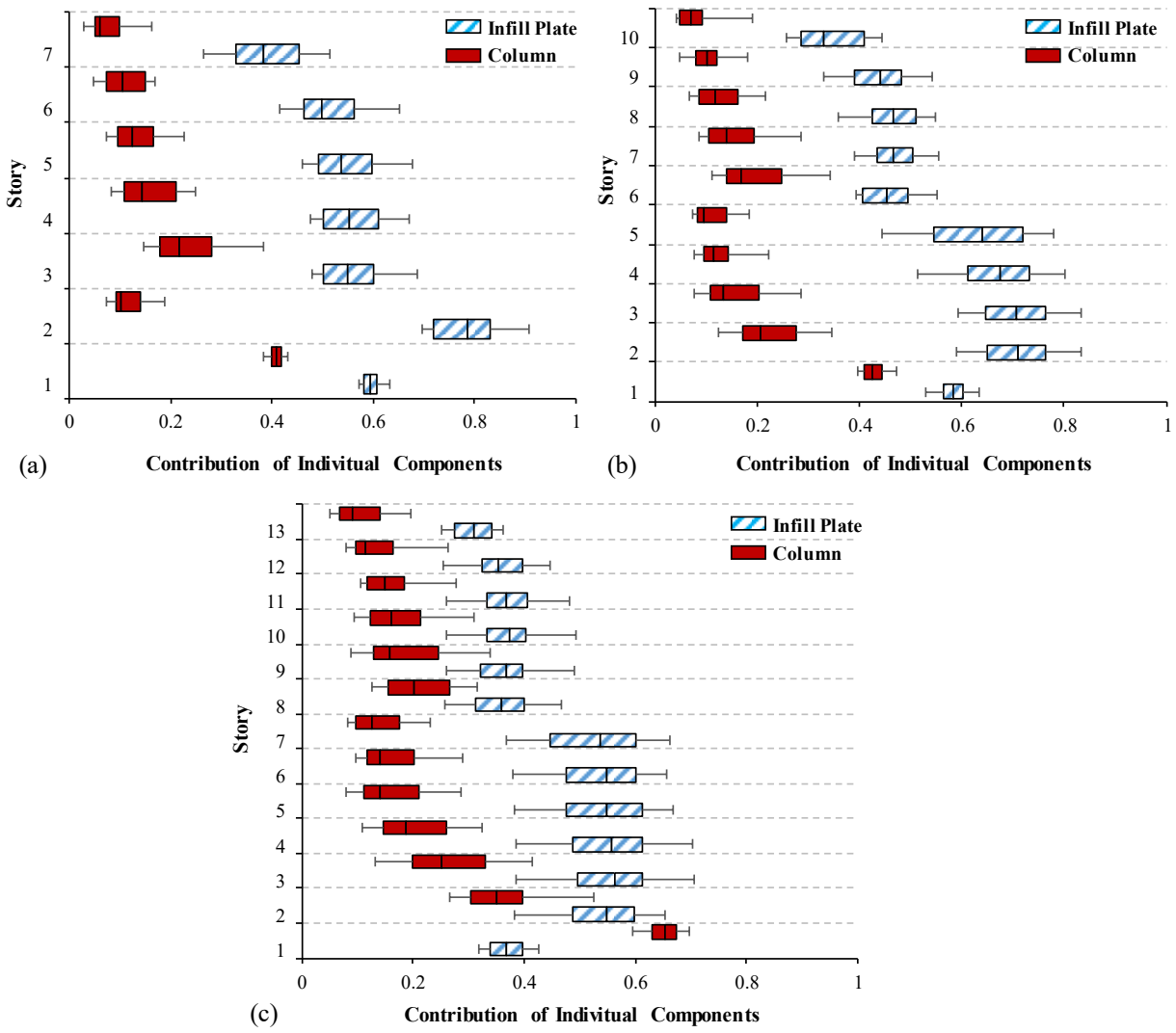

Fig. 3.14. Maximum shear contribution of individual structural components subjected to 44 ground motions.

3.9 Sensitivity Assessment for Variation of Infill Plate Parameters

It is understood that post yielding parameters (i.e., ductility capacity and post-cap stiffness ratio) in the deterioration model can vary. It is thus important to investigate the effect of variation of these parameters on collapse performance of stiffened SPSWs. Ductility capacity is defined as the ratio of strain at capping point to the yield strain, $\varepsilon_c/\varepsilon_y$, in stress-strain relationship for strips in infill plate (see Fig. 3.3(c)). Post-cap stiffness ratio is defined as the slope of the degrading line normalized by modulus of elasticity of steel ($\alpha = (\sigma_c/(\varepsilon_u - \varepsilon_c))/E$). Purba and Bruneau (2014)

estimated these two post-yielding parameters from calibration of four selected unstiffened SPSW tests. This section presents sensitivity assessment for variation of these two post-yielding parameters selected previously for the deterioration model for the stiffened infill plate. First, variation of the two selected post yielding parameters is demonstrated through validation of two unstiffened SPSW specimens (Vian and Bruneau 2005; Choi and Park 2008).

3.9.1 Analysis of Single Storey SPSW Tested by Vian and Bruneau (2005)

The single storey specimen tested by Vian and Bruneau (2005) and is shown in Fig. 3.15(a) is chosen as the first specimen for validation of the numerical model. The infill plate thickness was 2.6mm and the panel aspect ratio (ratio of bay width to storey height) was 2.38, which is quite close to the upper specified limit (2.5) permitted by AISC 341-16 (AISC 2016). Some other characteristics of the specimen is graphically depicted in Fig. 3.15(a) and more details can be found in Vian and Bruneau (2005).

Prediction provided by numerical model with $\varepsilon_c/\varepsilon_y = 6$ and $\alpha = 0.157$ represents a good agreement with experimental results (Fig. 3.15(b)). However, severe pinching in the experimental results is observed in comparison to negligible pinching in the strip model. Onset of yielding, capping point, and degradation backbone curve up to the end of the test are estimated accurately by the selected post yielding parameters.

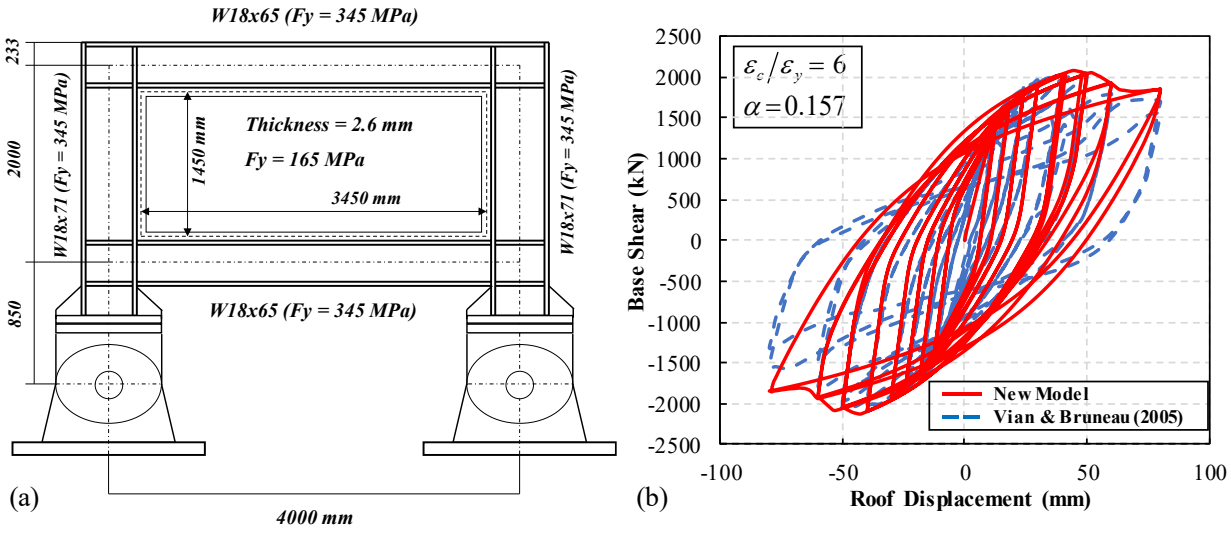

Fig. 3.15. Validation of numerical model: (a) specimen tested by Vian and Bruneau (2005); (b) comparison of numerical model with experimental result of Vian and Bruneau (2005).

3.9.2 Analysis of Three Storey SPSW Tested by Choi and Park (2008)

The second specimen used in this study was a three storey SPSW tested by Choi and Park (2008). Infill plate thickness was 4 mm in all stories and panel aspect ratio was 2.2, which is categorized as large panel aspect ratio. Fig. 3.16(a) provides additional information about the tested SPSW system. Based on the report provided by Choi and Park (2008), no fracture occurred in the boundary frame members. Ultimately, the load-carrying capacity of the specimen was decreased due to severe tearing of the infill plates. The prediction provided by the numerical model with $\varepsilon_c/\varepsilon_y = 13$ and $\alpha = 0.05$ values is presented in Fig. 3.16(b) which can be considered as a satisfactory fit.

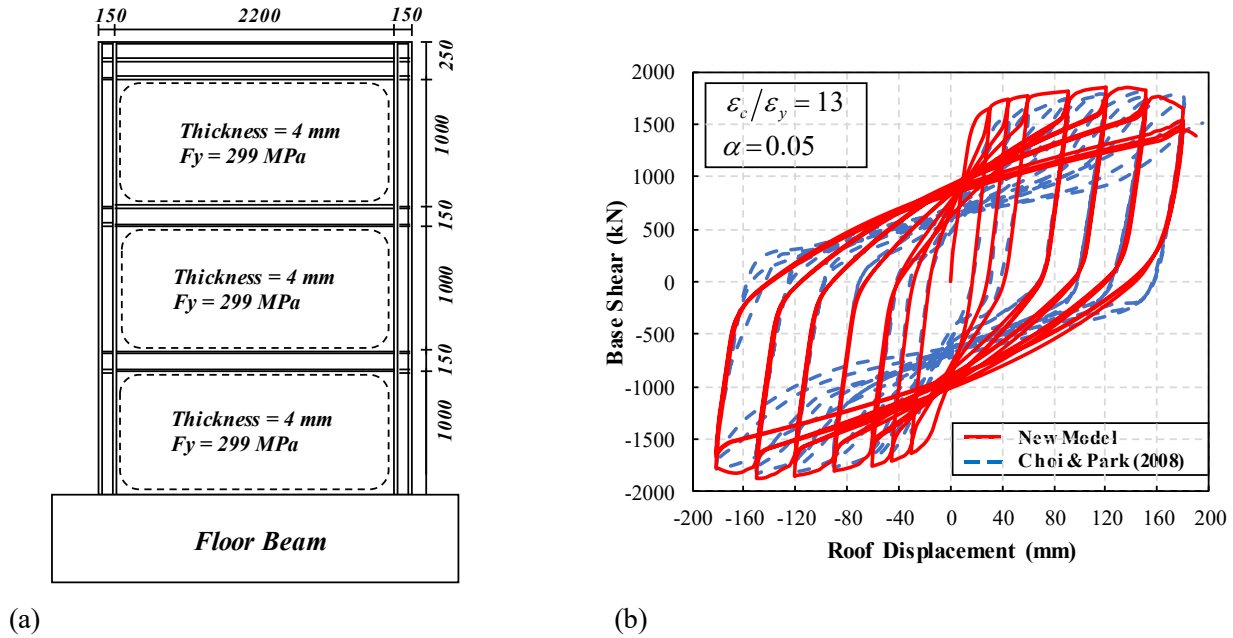

Fig. 3.16. Validation of numerical model: (a) specimen tested by Choi and Park (2008); (b) comparison of numerical model with experimental result of Choi and Park (2008).

As observed from Fig. 3.16(a,b), ductility capacity ($\varepsilon_c/\varepsilon_y$) and post-cap stiffness ratio (α) vary in numerical model to best fit with the experimental results of unstiffened SPSWs. It is worth mentioning that several factors like initiation of infill plate tearing, pattern of tear propagation in an infill plate, boundary element compactness and design procedure used to size SPSW components might affect the length of plastic behavior (ductility capacity) and the slope of degrading line (post-cap stiffness ratio) in the whole system during cyclic loading procedure.

A similar variation in post-yielding parameters can be anticipated in stiffened SPSWs, where infill plate is sufficiently stiffened by attaching a series of horizontal and vertical stiffeners. Thus, sensitivity assessment was carried out to investigate the effect of each post-yielding parameter's variation on overall performance of stiffened SPSWs. For this reason, the same three multi-storey (7-, 10-, and 13-storey) stiffened SPSWs designed earlier were used for sensitivity assessment. Nine variant models with different values of two post-yielding parameters were developed for each stiffened SPSW archetype. The variant models are shown in Table 3.7.

Table 3.7: Assigned post-yielding parameters to each variant model

Variant number	Nomenclature	Model parameters	
		Ductility, $\varepsilon_c/\varepsilon_y$	Post-cap stiffness ratio, α
1	5 - 0.05	5	0.05
2	5 – 0.15	5	0.15
3	5 – 0.3	5	0.3
4	15 – 0.05	15	0.05
5	15 – 0.15	15	0.15
6	15 – 0.3	15	0.3
7	30 – 0.05	30	0.05
8	30 – 0.15	30	0.15
9	30 – 0.3	30	0.3

IDA analyses were conducted on all variant models for each archetype and the resulting median IDA curves and fragility curves are depicted in Fig. 3.17 and Fig. 3.18. To draw a quantitative comparison between the seismic performance of all variant models in each archetype, $S_a\,(T_1, 5\%)$ value correspond with 50% probability of collapse, which is known as median collapse capacity (MCC), is taken as a benchmark.

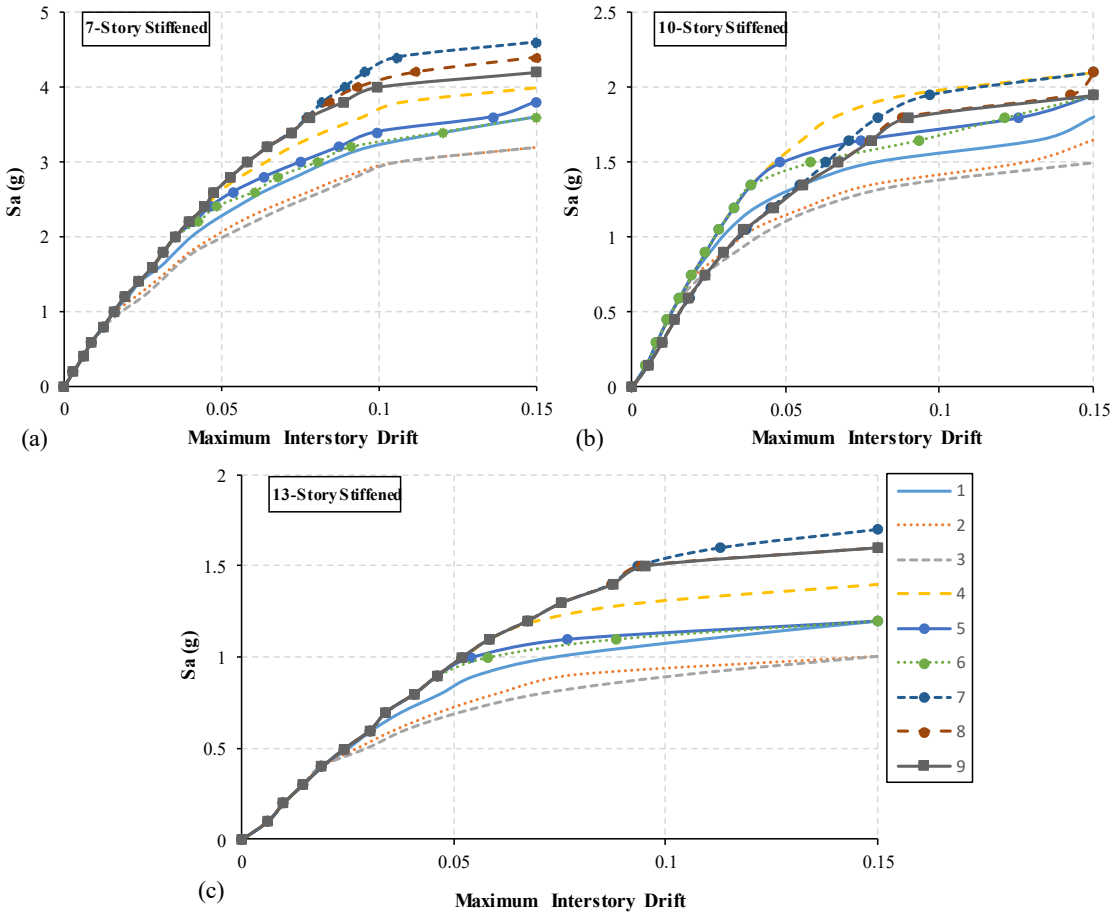

Fig. 3.17. Median IDA curves for all variant models.

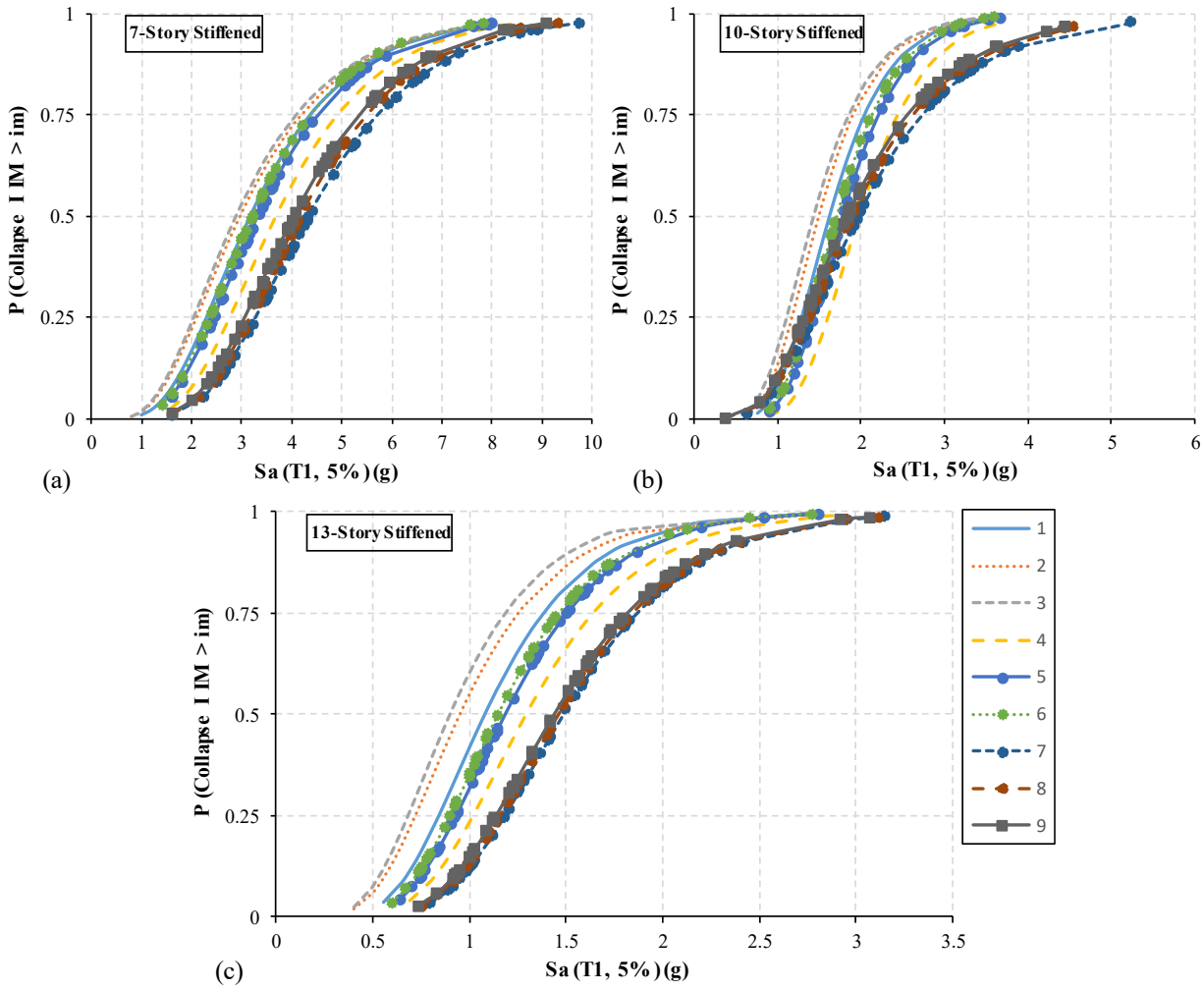

Fig. 3.18. Derived fragility curves for all variant models (variation of post-yielding parameters).

3.9.3 Sensitivity to Ductility Capacity Changes

As shown in Fig. 3.19(a), three groups were defined to assess the sensitivity of variant models to ductility capacity changes. In order to compare the MCC values obtained for individual variant models, MCC values were normalized based on the largest value obtained for MCC (variant model with minimal degradation) in each archetype. Variant number 7 (30 – 0.05) produced largest MCC values in all three stiffened SPSW archetypes. As indicated in Fig. 3.19(a), MCC increases in all archetypes as ductility capacity increases. In all three groups, ductility capacity changes from 5 to 30 while the post-cap stiffness is kept constant within each group. Group three of the variant models represents the most sensitive group to the variation of ductility

capacity. When ductility capacity of infill plate was varied from 5 to 30, about 40.5%, 28.9%, and 60.2% increase in the MCC were observed for 7-, 10-, and 13-storey stiffened SPSWs, respectively.

3.9.4 Sensitivity to Post-cap Stiffness Changes

Similar to ductility capacity, three groups of variant models were considered to assess the sensitivity of MCC to variation of post-cap stiffness ratio (Fig. 3.19(b)). Post-cap stiffness was varied from 0.05 to 0.3 in each group. It is worth mentioning that smaller value of post-cap stiffness corresponds with slight degradation in stress-strain relationship considered for infill plate. Second group of variant models was the most sensitive group to post-cap stiffness variation in 7- and 10-storey stiffened SPSWs, while first group of variants was the most critical one in 13-storey archetype. About 13.1%, 13.6%, and 16.5% reduction were observed in MCC of 7-, 10-, 13-storey stiffened SPSWs, when post-cap stiffness changes from 0.05 to 0.3. The results indicated that the capacity of stiffened SPSW is more sensitive to ductility capacity changes than to post-cap stiffness variation.

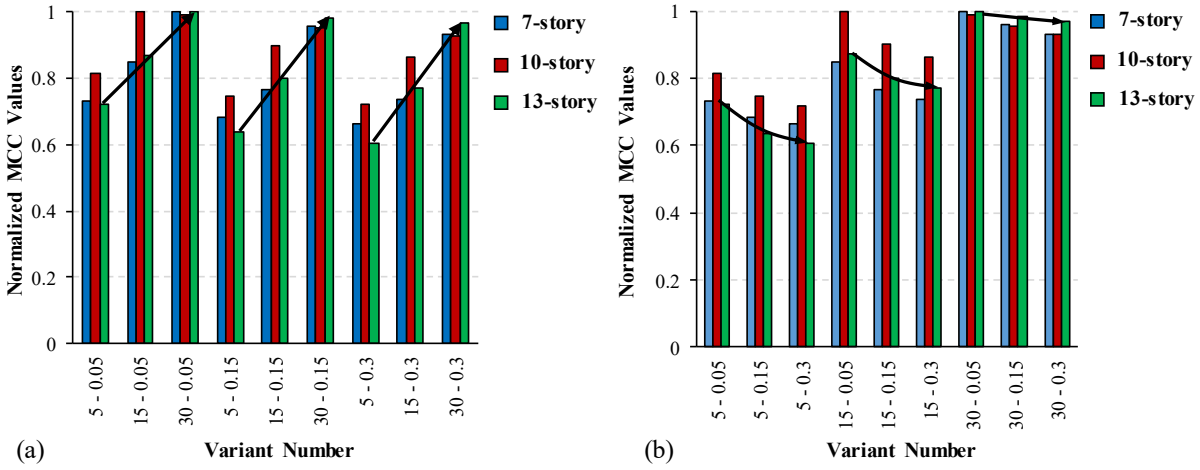

Fig. 3.19. Sensitivity of MCC to variation of post-yielding parameters in infill plate: (a) ductility capacity changes; (b) post-cap stiffness changes

3.10 Conclusion

This study presents results from nonlinear pushover analyses and Incremental dynamic analyses (IDA) using a developed deterioration model to assess the probability of collapse for stiffened SPSWs. A set of 44 artificial ground motions compatible with uniform hazard spectrum of Vancouver, Canada region were used to investigate the seismic performance of three multi-storey (7-, 10-, and 13-storey) stiffened SPSWs. Results from the study are as follows:

● The proposed strength deterioration model for stiffened infill plate and the macro modelling approach adopted in this study showed good agreement between analyses and tests conducted on stiffened SPSW (reported in the literature) under cyclic loading. Yield point, capping point, pinching, and degradation backbone curve until the end of the experiment were captured precisely by the developed numerical model.

● All archetypes studied herein showed ductile and stable behaviour and provided reliable safety margin against collapse. This was observed from comparison of ACMR values calculated for each archetype with allowable ACMR value presented in FEMA P695 (FEMA 2009). Thus, ductility-related force modification factor (R_d) of 5.0 and overstrength-related force modification factor (R_0) of 1.6, which are used to design unstiffened SPSWs, can be used for design of stiffened SPSW as well.

● The upper bound value recorded for drift in each storey in all archetypes was quite smaller than the allowable value of 2.5%, suggested by NBC (2015). This shows the effectiveness of the designed stiffened SPSW system to control the drift in all stories when subjected to strong ground motions.

● Maximum contribution of individual structural components (i.e., infill plate and boundary columns) in resisting applied lateral forces showed that a significant portion of storey shear, in some cases as high as 70%, is resisted by boundary columns. Current design approach assumes the total shear be resisted by the infill plate. This assumption will lead to more stable performance by providing a reliable backup system, which is ductile moment resisting frame, for primary load carrying component (i.e., infill plate).

● Sensitivity analysis for variation of post-yielding parameters on behavior of 7-, 10-, and 13-storey stiffened SPSWs showed that maximum variation in MCC for all archetypes due to variation of ductility capacity was significantly higher than that obtained due to post-cap stiffness changes.

It was observed that variation of ductility capacity from 5 to 30 caused a significant increase in the capacity of the system (up to 60.2 % in 13-storey stiffened SPSW), while the variation of post-cap stiffness ratio from 0.05 to 0.3 caused a maximum capacity reduction of 16.5%, which was observed in 13-storey stiffened SPSW system. This shows the lower level of participation from post-cap stiffness variation on overall performance of the stiffened SPSW system in comparison to ductility capacity changes.

It is acknowledged that the conclusions obtained in this study are based on analysis of limited number of stiffened SPSWs. Experimental as well as numerical studies on stiffened SPSWs with a with wide range of building heights, bay widths are required.

Chapter 4
Seismic Collapse Assessment of Composite Plate Shear Walls

4.1 Abstract

Collapse evaluation of composite plate shear walls (C-PSWs) under seismic loading requires a reliable analytical model that can accurately capture deterioration in the strength and stiffness of the system. In this study, research is carried out to develop a macro-modelling approach for C-PSW. Nonlinear time history analyses of six multistorey (7-, 10-, and 13-storey) C-PSWs (traditional and innovative) located in Western Canada are performed. It is observed that a significant portion of the storey shear is resisted by boundary members, while the RC panel does not contribute enough in resisting applied lateral forces (less than 10% of total storey shear). To estimate the seismic response parameters (i.e., ductility-related force modification factor and overstrength-related force modification factor) for designing C-PSW, incremental dynamic analysis (IDA) is performed for all archetypes following the procedure presented in FEMA P695. It is observed that all archetypes provide significant safety margin against collapse (large collapse margin ratio values) and satisfy the requirements of FEMA P695. In addition, a sensitivity study is conducted and effects of post-yielding parameters (ductility capacity and post-capping stiffness) for infill plate and post-cracking parameters (shear strain corresponding to maximum shear stress, yielding shear strain, and residual stress) adopted for the RC panel on seismic collapse capacities of traditional C-PSWs are investigated. It is observed that difference in values of post-yielding parameters for the steel infill plate can affect the seismic response of C-PSW. On the other hand, variation of post-cracking parameters of the concrete panel has a minor effect on seismic collapse capacity of the C-PSW system.

Author Keywords: Composite plate shear wall; Macro-modeling approach; Nonlinear time history analysis; Incremental dynamic analysis; OpenSees; FEMA P695; Seismic collapse performance.

4.2 Introduction

Steel plate shear walls (SPSWs) have been rapidly gaining interests as an effective lateral load resisting system in recent years. Three common types of SPSWs that are widely used in construction of multistorey buildings are unstiffened, stiffened, and composite plate shear walls (C-PSWs). Unstiffened SPSW consists of a thin infill plate and is connected to the surrounding boundary elements (beams and columns) using fillet welds or bolts. Several studies have been conducted on unstiffened SPSWs to assess the overall performance of the system (Driver et al. 1997; Roberts and Sabouri-Ghomi 1991; Astaneh-Asl 2001; Berman 2011; Bhowmick et al. 2008; Choi and Park 2010). In unstiffened SPSWs, the thin infill plates tend to buckle with a very small applied lateral load. This can reduce initial stiffness, strength, and energy dissipation capacity of the whole SPSW system. In order to postpone buckling of the infill plate, two general methods can be used. The first method is to use a stiffened infill plate. However, stiffeners are not cost effective to use in construction. In addition, both unstiffened and stiffened SPSWs experience larger inelastic rotation in their connections when subjected to cyclic loading (Allen and Bulson 1980). The second method is to attach a reinforced concrete (RC) panel to one or both sides of the thin infill plate. This system is known as composite plate shear wall (C-PSW) or composite plate shear wall-concrete encased (C-PSW/CE). The presence of RC panel in C-PSW reduces the vulnerability of the system to fire and blast loads. Very limited research has been conducted on C-PSW (or C-PSW/CE), more specifically macro modelling of C-PSW. Research on C-PSWs started from experimental study of Zhao and Astaneh-Asl (2004) on two different configurations (Traditional and Innovative) of C-PSWs. In the innovative C-PSW, there is a small gap between the RC panel and the surrounding boundary elements, while in the traditional one, the RC panel is in direct contact with the surrounding boundary members (Fig. 4.1(a,b)). Main components of both systems are thin steel infill plates, RC panels, boundary members (beam and column), and shear connectors (shear stud or bolt), as shown in Fig. 4.1(c). Zhao and Astaneh-Asl (2004) tested two half-scale 3-storey specimens with and without gap. Both specimens were subjected to a similar cyclic loading pattern. Their tests indicated that addition of the RC panel increased the energy dissipation capacity of the C-PSW system. It was also observed that the extent of damage to the RC panel in an innovative system was much less severe than that for the traditional system (because of gap between RC panel and boundary members). Rahai and Hatami (2009) investigated the effects of

variation in middle beam rigidity, shear stud spacing, and type of beam to column connection on overall performance of C-PSWs. Their study showed that by increasing the shear stud spacing up to a specific value, ductility and energy absorption capacity of the system could be increased. Furthermore, the effect of middle beam rigidity and beam to column connections (pin or rigid) on the performance of the C-PSW system was found to be negligible.

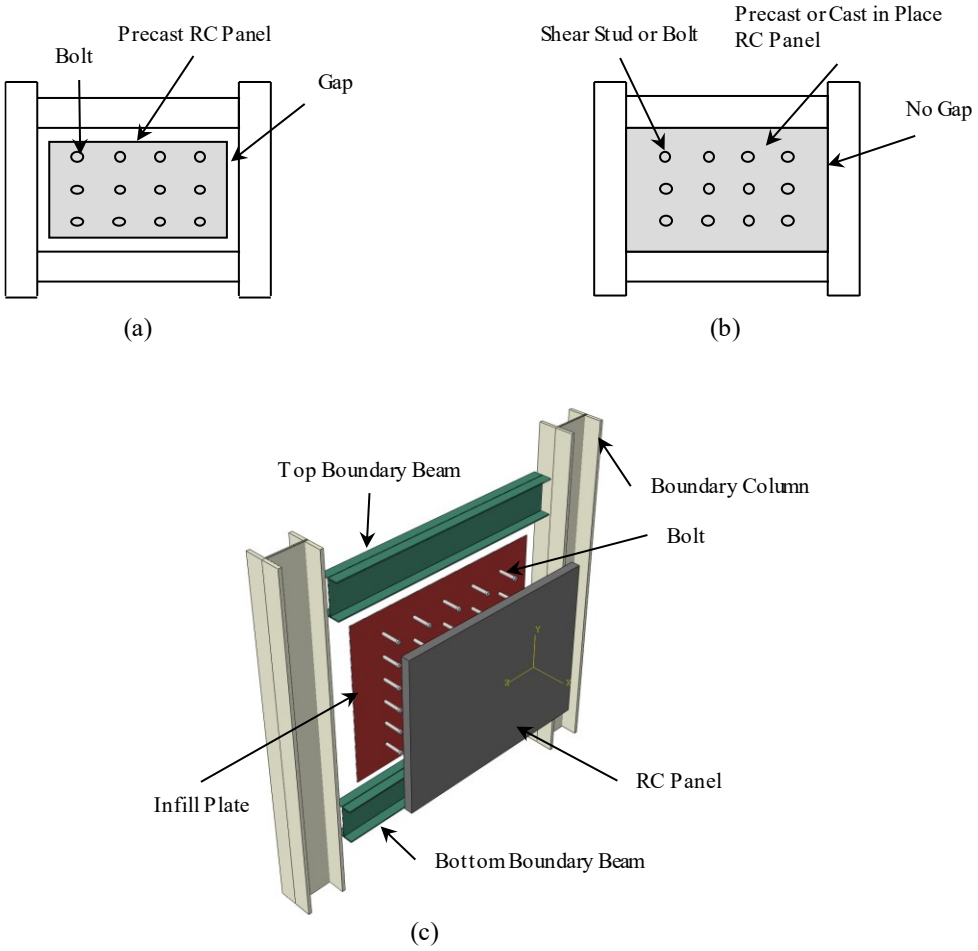

Fig. 4.1. (a) Innovative C-PSW; (b) traditional C-PSW; (c) components of C-PSW

This paper investigates the seismic collapse assessment of C-PSWs. Reinforced concrete (RC) panel connected to one side of the thin infill plate is only considered in this study. Seismic collapse assessment is done following a procedure similar to the one presented in FEMA P695 (FEMA 2009). FEMA P695 provides a rational framework to assess the probability of collapse under maximum considered earthquake (MCE) ground motions. This methodology can be used to evaluate the accuracy of response parameters such as response modification coefficient (R-factor),

overstrength factor (Ω), and deflection amplification factor (C_d). One of the key components of FEMA P695 (FEMA 2009) methodology is to develop a simple and accurate numerical model to use for incremental dynamic analysis. This paper presents development of a 2D macro analytical model for analysing C-PSWs (traditional and innovative) using *Open System for Earthquake Engineering Simulation* (*OpenSees*) (McKenna et al. 2013). Experimental studies available in the literature are used to verify the accuracy of the proposed model. After validating the numerical model, a total of three multistorey C-PSWs (7-, 10-, and 13-storey) in two different configurations (with and without gap) are designed according to CSA S16-14 (CSA 2014) and NBC (2015). While AISC 341-16 (AISC 2016) provides guidelines for analysis and design of C-PSW, at the time of this writing, there is no specific recommendations for seismic performance factors (i.e., ductility-related force modification factor, R_d, and overstrength-related force modification factor, R_0) for C-PSW in NBC (2015). Many engineers in Canada currently use the same R_d and R_0 values as of unstiffened SPSW to design C-PSWs. This study investigates the applicability of using the same R_d and R_0 as of ductile unstiffened SPSWs for designing of C-PSWs. Thus, all C-PSWs are designed using the same seismic performance factors as of unstiffened SPSW and then the probability of collapse of each archetype is assessed. For collapse assessment of C-PSW, incremental dynamic analyses of all archetypes are carried out using a group of 44 artificial ground motions developed by Atkinson (2009) for western Canada.

In addition, nonlinear time history analysis (NTHA) is carried out for all designed C-PSWs. Maximum contributions of different elements of C-PSW (steel infill, columns, and RC panel) in resisting shear are calculated from seismic analyses. Also, seismic collapse performance of C-PSWs to different values of two post-yielding parameters (ductility capacity and post-capping stiffness) for the steel plate and three post-cracking parameters for the RC panel (i.e., shear strain corresponding to maximum shear stress, yielding shear strain, and residual stress of the RC panel) are carried out for the three selected traditional C-PSWs.

4.3 Modelling Approach

4.3.1 Thin Steel Infill Plate

In unstiffened SPSW, the shear is mainly resisted by the infill plate through tension field action after the plate is buckled. Fig. 4.2(a) presents a solid infill plate subjected to pure shear. To find

the principal stresses acting on the infill plate before buckling, a small segment was chosen and rotated by 45^0 to find maximum tensile and compressive stresses. Analysis of unstiffened SPSWs are currently done by the strip model proposed by Thorburn et al (1983). In strip model, a series of strips along the direction of the tension field action, α, is used to represent the infill plate behaviour. The width of each strip can be calculated as ($L\,cos\alpha + h\,sin\alpha$) divided by number of strips in each storey, where L and h are width and height of the panel, respectively (Fig. 4.2(b)). In multistorey SPSW, changes in the value of tension field action in different stories will result in staggered node points on the beams. This will create an artificial bending on beams at any intermediate floors. One way to overcome this is to use the average of tension field angle calculated at each storey. Such approximation does not have much effect on the overall behaviour of the SPSW structures (Dastfan and Driver 2008).

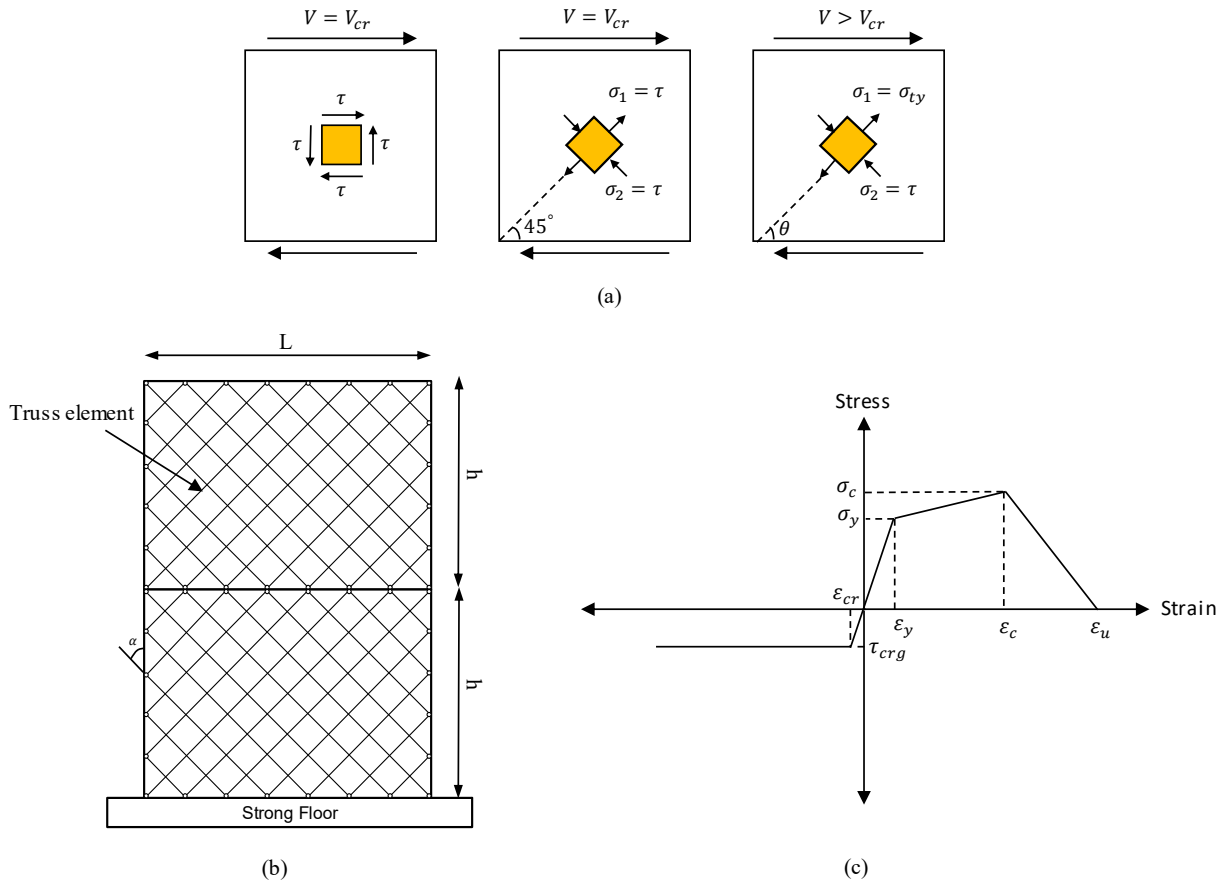

Fig. 4.2. (a) Stresses in infill plate before and after buckling; (b) strip model representation for SPSW; (c) deterioration model for strips

In the proposed macro model, strip model concept was used for the infill plate. As indicated in Fig. 4.2(c), a trilinear material model for tension and a bilinear material model for compression were considered. In the tri-linear material model, the behaviour in tension is elastic up to yielding point (ε_y,σ_y) and then strain hardening of steel material occurs up to capping point (ε_c,σ_c), followed by initiation of degradation in tension up to the ultimate point (ε_u, 0). In the compression zone, the behavior remains elastic up to buckling point (ε_{cr},τ_{crg}), where τ_{crg} is the global buckling stress and is calculated based on classical buckling theory.

4.3.2 Reinforced Concrete Panel

The RC panel can be installed in one or both sides of the thin infill plate. To be consistent with the experimental study conducted by Zhao and Astaneh-Asl (2004), analytical model for the RC panel was proposed with an assumption of one-sided connection only. The RC panel is capable of adding to total strength and stiffness of the whole system by compression field action. Also, depending on the reinforcement ratio in the RC panel, it can enhance the ductility of the whole C-PSW system.

In analytical model, as shown in Fig. 4.3, the RC panel was idealized using a displacement-based beam- column element. Beam-column element with displacement-based formulation is based on the assumption of constant axial strain and linear distribution for curvature (hypothesis of the planar cross-sections). This element is capable of considering both axial elongation as well as combination of axial and bending moment acting on the element. The main drawback of the element is that most of the fibers do not take into account the effect of shear deformation which occurs due to lateral loads. To account for shear deformation and enhance the accuracy of the proposed analytical model, a translational spring was added in the middle of each beam-column element (as shown in Fig. 4.3). Force-deformation relationship adopted for spring was modelled using the Pinching4 material model available in the library of *OpenSees*. The nonlinear behavior assigned to spring in each storey was specified by a multi-linear (quadlinear) envelope curve which includes: (i) cracking (cracking force, V_{cr}; displacement corresponding to initiation of crack, d_{cr}); (ii) yielding (yielding force, V_y; yielding displacement, d_y); (iii) maximum strength (the force at which degradation initiates in the RC panel due to crushing), V_{max} and corresponding displacement, d_{max}; (iv) residual strength, V_{res} and corresponding displacement, d_{res}.

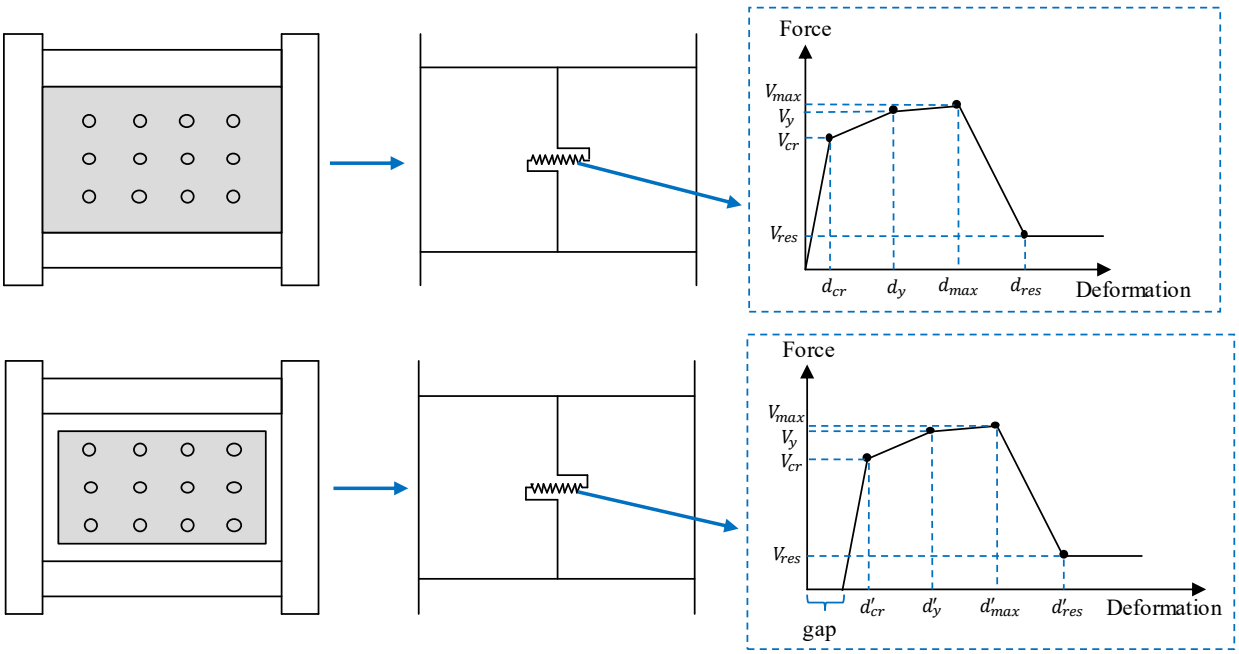

Fig. 4.3. Analytical model of RC panel and corresponding force-deformation relationship for shear-dominated RC panels

Analytical model developed for the RC panel in both traditional and innovative systems were similar. The only difference was in the force-deformation relationship that was adopted for these two systems. As indicated in Fig. 4.3, a gap was considered at the beginning of the force-deformation relationship for the innovative C-PSW to represent that the RC panel was not active from the beginning of the loading.

4.3.3 Boundary Elements

Columns and beams are termed as vertical boundary elements (VBEs) and horizontal boundary elements (HBEs) in SPSWs. In addition to resisting gravity loads, which is the primary function of these elements, they also provide anchor points for tension field developed in the thin infill plate. Tension forces that act on intermediate beams are not crucial since a significant portion of the tension forces from adjacent stories will be counteracted. But this effect is crucial for top and bottom beams since they are connected to infill plates from one-side only. A displacement-based fiber element (distributed-plasticity) with Menegotto-Pinto steel material in OpenSees was used for boundary members.

4.4 Model Validation

Model verification was carried out against two experimental tests conducted by Zhao and Astaneh-Asl (2004). Both C-PSWs (traditional and innovative) were half-scale three stories, one bay structure with moment resisting frame as boundary members and a composite shear wall embedded inside the frame. The composite shear wall was comprised of the RC panel, which was connected to the steel infill plate by bolts. Two middle panels represented two whole stories, while top and bottom panels represented as two half stories. Details of both test specimens can be found in Zhao and Astaneh-Asl (2004).

Both specimens were modelled in *OpenSees* and monotonic pushover as well as cyclic analyses were conducted. Material properties were assigned as the one reported by the authors such as yield stress of 345 MPa (50 ksi) for boundary members and 248 MPa (36 ksi) for steel infill plate. Nominal compressive strength of concrete was considered as 28 MPa (4000 psi). Fig. 4.4(a) presents the stress-strain relationship considered in this study for strips. For the RC panel, as shown in Fig. 4.4(b), an idealized tri-linear force-deformation relationship was considered in the first phase of the study by neglecting the yielding in the RC panel. Residual strength of the RC panel was assumed as 20% of the maximum shear strength. Force-deformation relationship assigned to the RC panel in this study is similar to that considered by Gogus and Wallace (2015) for the shear-dominated RC panels. In Fig. 4.4(c), base shear-overall drift relation from the test is compared with the results obtained from analytical model for traditional C-PSW. As depicted in the figure, there is a good agreement between analytical and experimental results. Zhao and Astaneh-Asl (2007) described behaviour of each specimen tested under cyclic loading. During the traditional C-PSW test, it was observed that at an overall drift of 3%, the RC panel crushed at corners and lots of major cracks were formed in the middle of the panel. This point was designated as “Onset of degrading line” in the force-deformation relationship. Slope of the degrading line was calibrated in such a way that at an overall drift of 4.2%, the RC panels in both stories lost 80% of their strength. For the infill plate, fracture was the main source of degradation, which occurred at an overall drift of 4.2% and caused 20% degradation in total strength of the whole system.

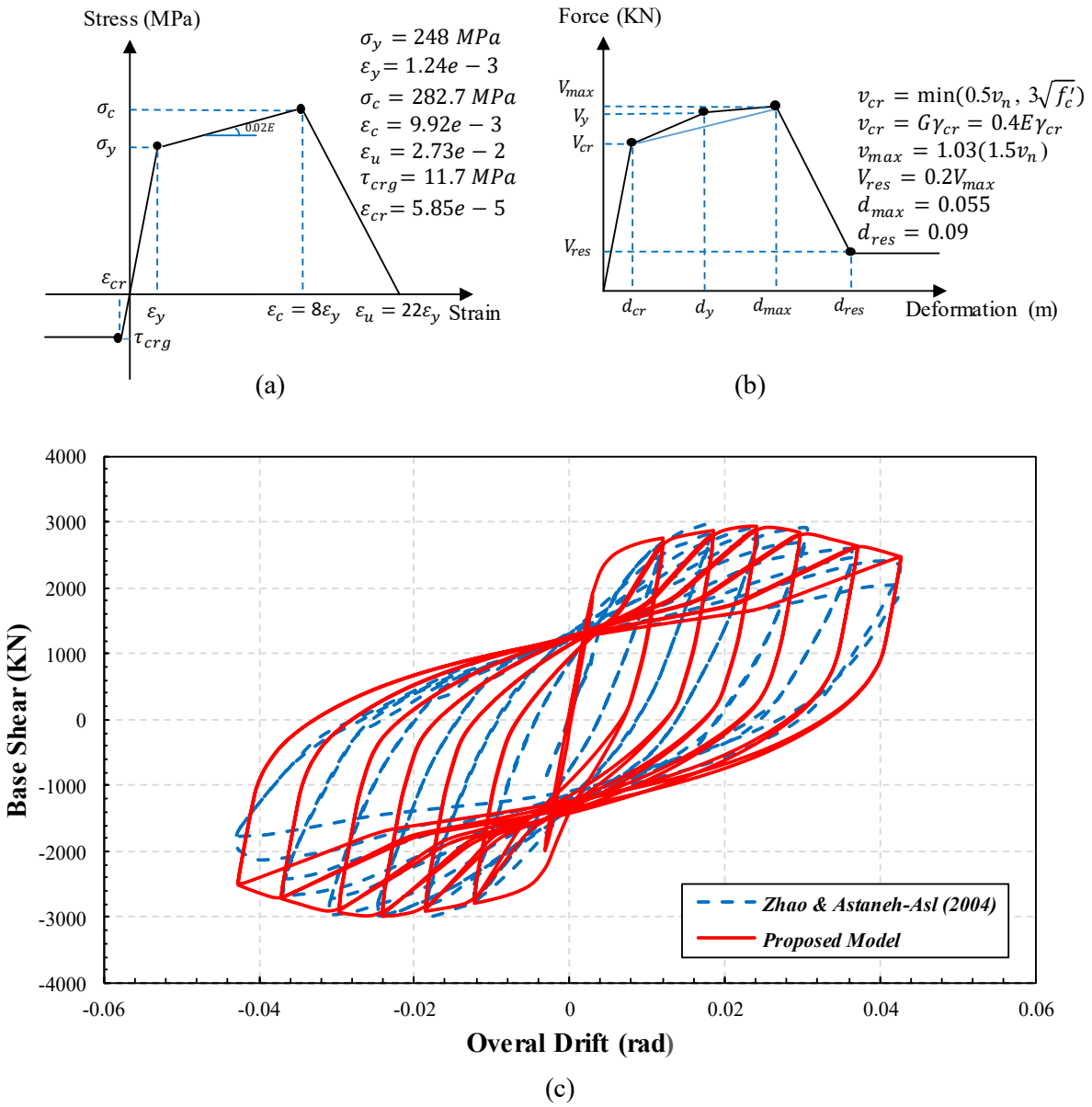

Fig. 4.4. (a) Stress-strain relationship for strips; (b) force-deformation relationship for RC panel; (c) comparison of the results from numerical model and test data for traditional composite shear wall

Fig. 4.5 compares the results obtained from test with that predicted by *OpenSees* for the innovative C-PSW. Moreover, cyclic behavior of the RC panels in both systems were plotted for comparison. Both the RC panels in the traditional C-PSW (second and third stories) experienced severe damages at the end of the test, which caused 80% strength loss from the maximum strength.

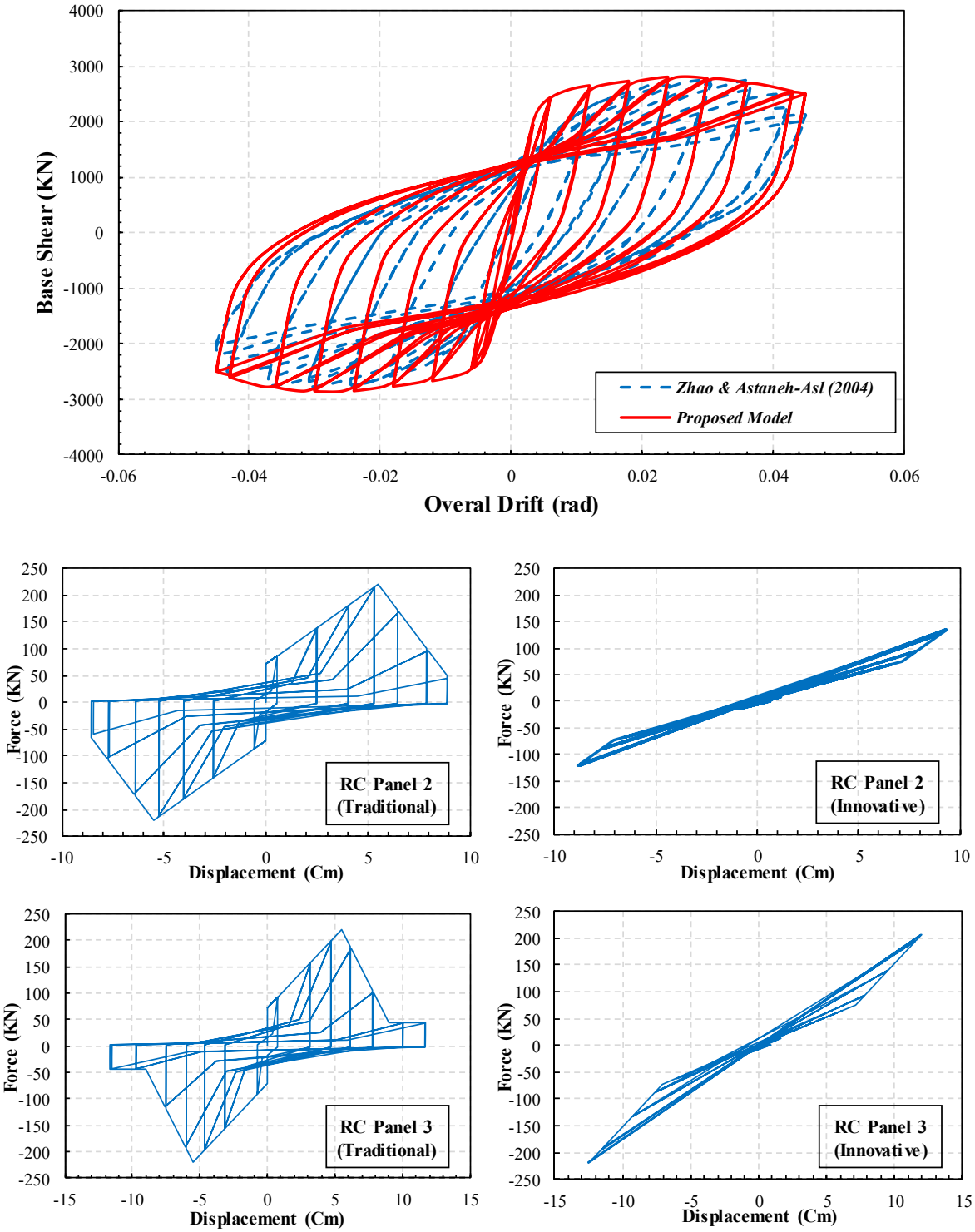

Fig. 4.5. Comparison of the results from numerical model and experimental data for innovative composite shear wall along with RC panel cyclic behavior in C-PSWs

4.5 Seismic Design of Composite Shear Walls

4.5.1 Configuration of Studied Composite Shear Walls

The buildings considered herein were three multistorey (7-, 10-, 13-stories) C-PSW systems with and without gap. These buildings were hypothetical residential buildings located in Vancouver, Canada and have 30 x30 m square plan (9682.6 ft^2). Each building has two C-PSWs resisting lateral loads in each direction (Fig. 4.6(a)). Each C-PSW was 5 m (16.4 ft) wide, measured from center to center of the columns and has equal storey height of 3.6 m (11.8 ft) (panel aspect ratio of 1.39). The buildings were assumed to be located on site class C. As per NBC (2015), site class C consists of very dense soil or soft rock in which the average shear wave velocity is considered to be within 360-760 m/s (1181-2493 ft/s), soil undrained shear strength higher than 100 kPa (14.5 psi), and average standard penetration resistance of 50 or more. A dead load of 4.1 kPa was used for each floor and 3.3 kPa for roof level. The live load on all floors was taken as 2.4 kPa. The snow load was calculated as 1.64 kPa at the roof level. An infill plate thickness of 2.0 mm (0.079 in.) was considered as the minimum thickness based on handling and welding considerations.

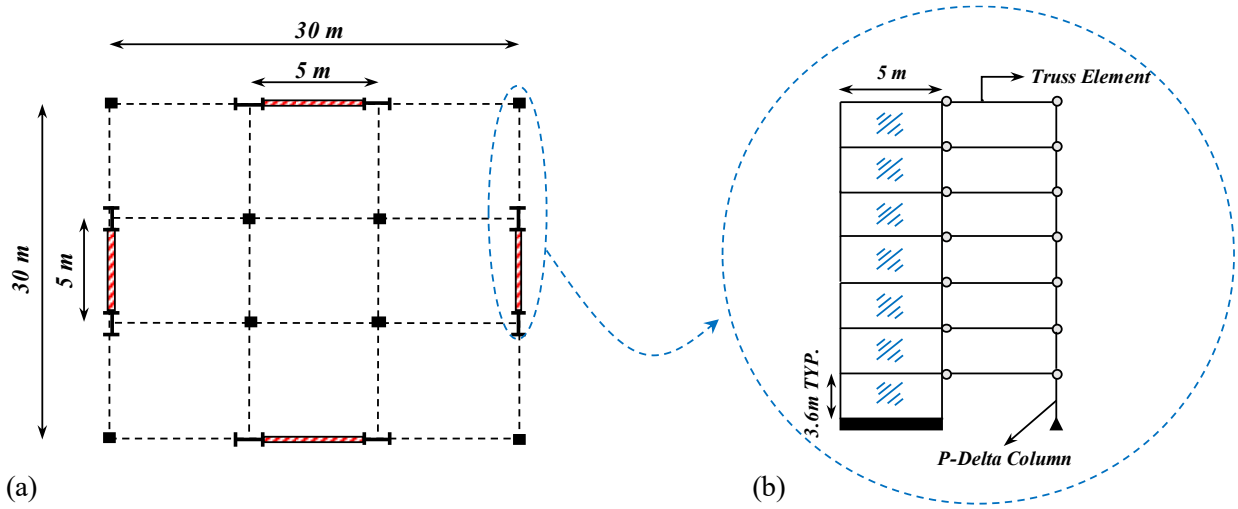

Fig. 4.6. (a) Plan view of sample buildings; (b) analytical model for 7-storey C-PSW along with gravity column

The analytical model in *OpenSees* includes one C-PSW and a leaning column, as shown in Fig. 4.6(b). The leaning column was designed so as not to provide any lateral stiffness to the system and was connected to the C-PSW in every storey with rigid links. In *OpenSees* software,

elastic beam column element (EBC) was used to model the leaning column. Two rotational springs were located at the top and bottom of each EBC and their rotational stiffness were set as a small value to apply the pin ended connections for each EBC. To account for P-delta effects, tributary area and associated gravity loads for the gravity columns were calculated and applied on the leaning column at each floor. NBC (2015) recommends use of load combination '1.0D + 1.0E + 0.5L or 0.25S' (where D = dead load, L = live load, E = earthquake load, and S = snow load). Thus, load combination '1.0D + 1.0E + 0.5L' was used for the floors and load combination '1.0D + 1.0E + 0.25S' was used for roof. Truss elements were used in each storey level to connect the C-PSW system to the leaning columns.

4.5.2 Design Consideration for Composite Shear Walls

The selected C-PSWs were designed as per NBC (2015) and CSA S16-14 (CSA 2014). Same seismic performance factors as of ductile SPSW were used for design as currently these factors are not available for C-PSW. Thus, a ductility-related force modification factor, R_d, of 5.0 and an overstrength related force modification factor, R_0, of 1.6 were used in design of C-PSW. AISC341-16 (AISC 2016) does not consider the contribution of the RC panel in determining the shear strength of the composite wall and assume the infill plate as the main energy dissipating component of C-PSW. Thus, as presented in steel design guide 20 (Sabelli and Bruneau 2007), the strength of the C-PSW is based on yielding of infill plate in shear:

$$V_r = 0.6\,\emptyset\,F_y\,t_w\,L_{cf} \tag{4.1}$$

where $\emptyset = 0.9$; F_y is the yield strength of the infill plate; t_w is the infill thickness; L_{cf} is the clear span between columns.

In C-PSW, design of boundary members is controlled by both stiffness and strength. Stiffness requirement is intended to prevent excessive in-ward deformation and ensure that the whole capacity of infill plate is reached by forming a uniform tension field action. Regarding strength requirement, boundary members must remain essentially elastic under expected shear yielding of infill plate ($0.6\,R_yF_yt_wL_{cf}$, where R_y is equal to 1.1) except that plastic hinges are allowed at the ends of beams. The boundary members were designed according to the capacity design method by Berman and Bruneau (2008). Table 4.1, Table 4.2, and Table 4.3 present geometric properties of all the selected C-PSWs. The concrete panel selected was of 75 mm

thickness. A reinforcement ratio of 0.0093, with 100 mm spacing between longitudinal reinforcements, was considered. Rebar #3 with an area equal to 71.26 mm^2 was used, which resulted in total of 49 longitudinal reinforcements in the RC panel. The concrete used in all the RC panels had a nominal compressive strength, f_c', of 28 MPa (4000 psi).

Table 4.1. Design Summary of 7-storey C-PSW

Level	Infill plate (mm)	Beam	Column
7	2	W360x287	W360x509
6	2	W310x67	W360x592
5	2	W310x67	W360x634
4	2	W310x67	W360x634
3	2	W310x67	W360x634
2	3	W360x179	W360x634
1	3	W310x79	W360x818
0	NA	W360x382	NA

Table 4.2. Design Summary of 10-storey C-PSW

Level	Infill plate (mm)	Beam	Column
10	2	W360x287	W360x509
9	2	W310x67	W360x634
8	2	W310x67	W360x677
7	2	W310x67	W360x744
6	2	W310x67	W360x744
5	3	W360x179	W360x744
4	3	W310x79	W360x744
3	3	W310x79	W360x744
2	3	W310x79	W360x744
1	3	W310x79	W360x900
0	NA	W360x382	NA

Table 4.3. Design Summary of 13-storey C-PSW

Level	Infill plate (mm)	Beam	Column
13	2	W360x314	W1000x296
12	2	W310x67	W1000x412
11	2	W310x67	W1000x483
10	2	W310x67	W1000x539
9	2	W310x67	W1000x554
8	2	W310x67	W1000x591
7	3	W360x179	W1000x642
6	3	W310x79	W1000x748
5	3	W310x79	W1000x748
4	3	W310x79	W1000x748
3	3	W310x79	W1000x748
2	3	W310x79	W1000x883
1	3	W310x79	W40x655[a]
0	NA	W360x421	NA

4.6 Seismic Performance Assessment

Nonlinear time history analyses and incremental dynamic analyses were conducted on all designed C-PSWs. The ground motion selection and scaling method adopted in this study are presented in the following section.

4.6.1 Selection and Scaling of Ground Motions

Selection of adequate number of ground motions for collapse assessment is always a challenge. The studied C-PSW buildings are located in Western Canada and thus a group of 44 artificial ground motions developed by Atkinson (2009) for western Canada was used for NTHA and incremental dynamic analysis. The selected earthquake records included far field records with two different magnitudes, $M = 6.5$ and $M = 7.5$. Details of the earthquake records and their main characteristics such as magnitude, M, closest distance to fault rupture, R_{fault}, peak ground acceleration, PGA, and the ratio of maximum velocity to maximum acceleration, $^{v}/_{a}$, are presented elsewhere (Farahbakhshtooli and Bhowmick 2019).

All the selected ground motions must be scaled to ensure comparable results for IDA and NTHA. In NBC (2015), there is no specific procedure for scaling of ground motions. However, it is indicated that the scale factor must be applied to all ground motions to obtain comparable results. Moreover, this scale factor needs to be calculated in such a way that the mean spectrum resulting from response spectra of a group of ground motions must lie or be above the uniform hazard spectrum (UHS) at any points. Thus, the scaling method presented in ASCE/SEI-7 (ASCE 2016) was employed to scale the ground motions. ASCE/SEI states that the scale factor must be calculated in such a way that the mean spectrum of the selected earthquake records is above the UHS within interval $0.2T_1$ to $1.5T_1$, where T_1 is the fundamental period of vibration obtained from *OpenSees* modal analysis. Fig. 4.7 presents 5% damped pseudo-acceleration response spectra of the selected ground motions.

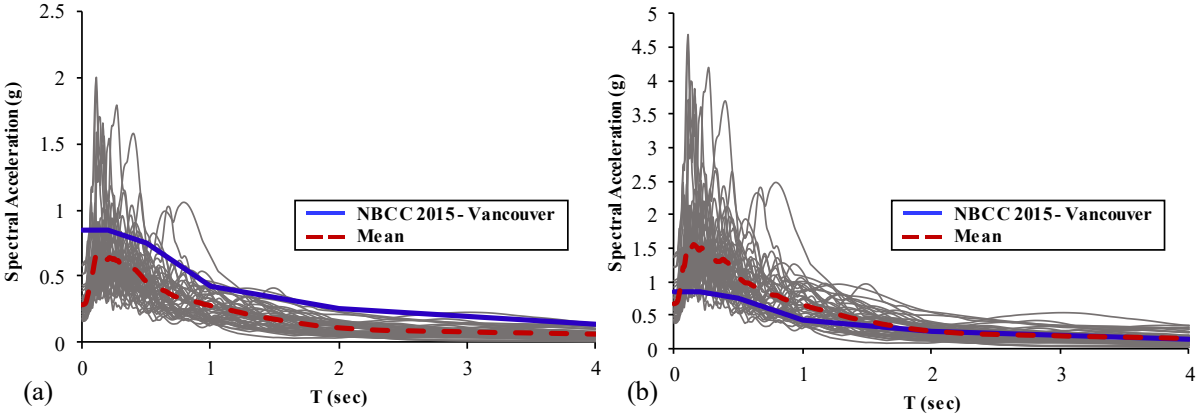

Fig. 4.7. 5% damped pseudo-acceleration response spectra of selected earthquake records: (a) unscaled; (b) scaled

4.6.2 Results of Time History Analyses

Maximum interstorey drifts were obtained from seismic analyses of all archetypes. The results are shown in terms of box plot in Fig. 4.8. As shown in Fig. 4.8, the box represents the interquartile range (Q1-Q3), which starts at first quartile and finishes at third quartile. The solid line inside the box shows the median of the data and the two solid lines outside the box represent the lower and upper bound of the interstorey drift recorded for the corresponding storey. Each figure compares the variation of interstorey drift in two different configurations of C-PSWs considered in this study

(with and without gap). In most of the stories in all C-PSWs, median interstorey drift recorded for traditional system was slightly smaller than that for innovative system. Further investigation indicated that due to existence of gap in the innovative system, the RC panel was not activated in any storey except in the third storey of the 10-storey innovative system when subjected to one of the ground motions (west7c1.26). As can be seen in Fig. 4.8, peak median values of 0.72 and 0.796% were recorded for 7-storey traditional and innovative systems respectively, while for 10- and 13-storey, values of about 0.95 and 1.16% were obtained for both traditional and innovative systems, respectively. Thus, based on the median values of interstorey drift, both configuration of C-PSWs (with and without gap) exhibit similar behavior with minor variation. This is due to the fact that a significant portion of the RC panel capacity was not involved during moderate excitations in traditional system to decrease interstorey drift.

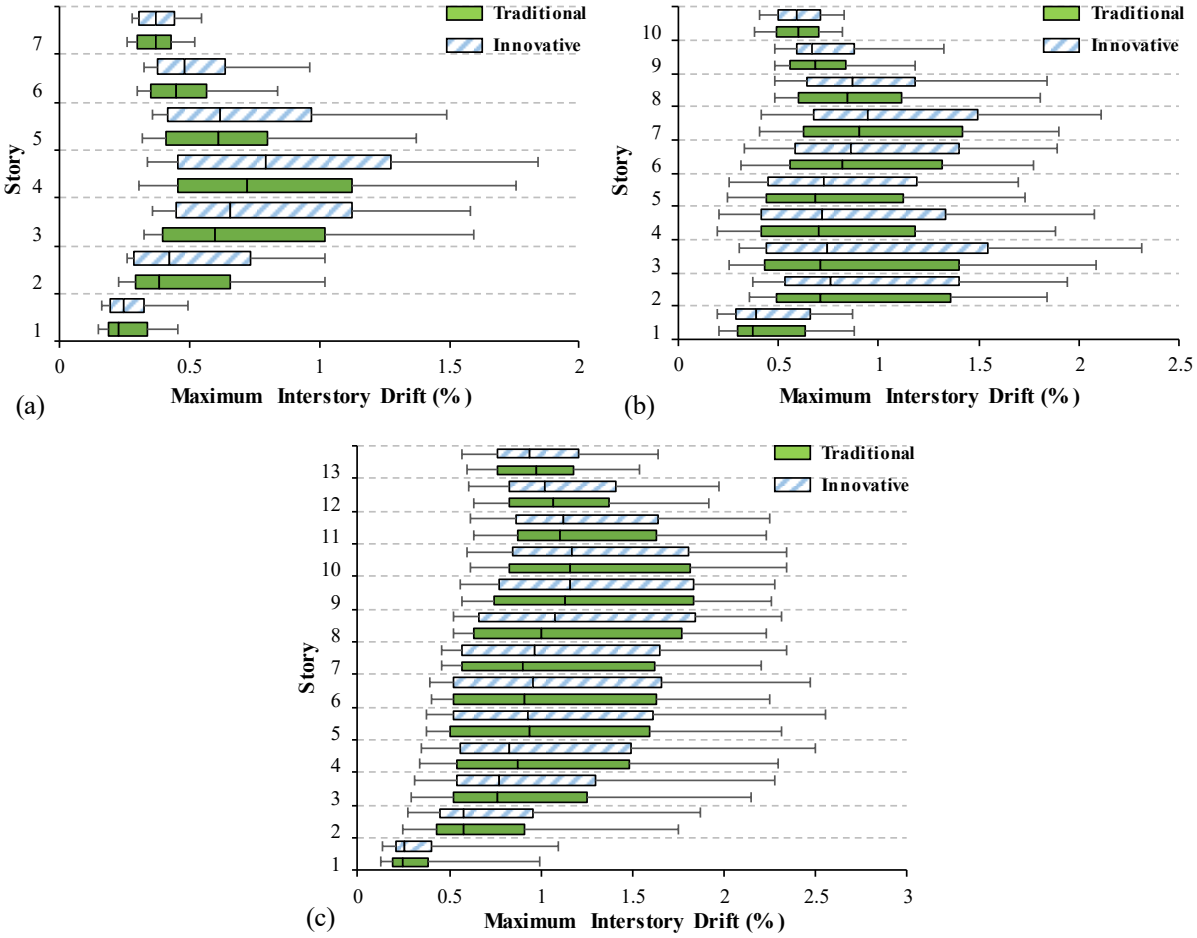

Fig. 4.8. Comparison of interstorey drifts for traditional and innovative C-PSWs

In addition to interstorey drift, maximum shears taken by different structural elements of C-PSW were determined from seismic analyses and are shown in Fig. 4.9. Since none of the RC panels in the innovative system contribute in resisting applied lateral forces (except one case addressed earlier), results of the RC panels participation in the innovative systems are not presented. The values presented in Fig. 4.9 were normalized by the corresponding maximum storey shear for each ground motion. As shown in Fig. 4.9, in 7- and 10-storey buildings, the contributions of infill plates were significantly higher than that for boundary columns in all the stories. For instance, maximum participation of infill plate was 84 and 94% in 7-storey traditional and innovative systems, respectively, which was approximately twice the corresponding values calculated for boundary columns (42% as maximum contribution of boundary members in 7-storey buildings). In general, the difference in contribution of infill plate and boundary columns in each storey gets smaller in the upper floors. Fig. 4.9(e,f) shows that upper bound and median values of shear contributions from boundary columns in the first storey of the 13-storey building are quite higher than those observed in the infill plates. Thus, a significant portion of the shear is resisted by boundary columns, which is not considered in the current design procedure of C-PSW. The total shear is assumed to be resisted by steel infill plate and the contribution of other structural components are ignored. Purba and Bruneau (2014) investigated the effect of sharing the storey shear between the infill plate and the vertical boundary members of unstiffened SPSW and observed that some of the designed SPSWs failed the performance evaluation as per FEMA P695 (FEMA 2009). Thus, similar to SPSWs, neglecting the contributions from columns in capacity design of C-PSWs will provide more stable performance.

Participation of the RC panels in resisting lateral loads were less than 10% in all archetypes. Maximum contribution of the RC panels was 8.2%, which was observed in the RC panel located in the fourth floor of 7-storey traditional C-PSW when subjected to the last artificial ground motion (west7c2.14).

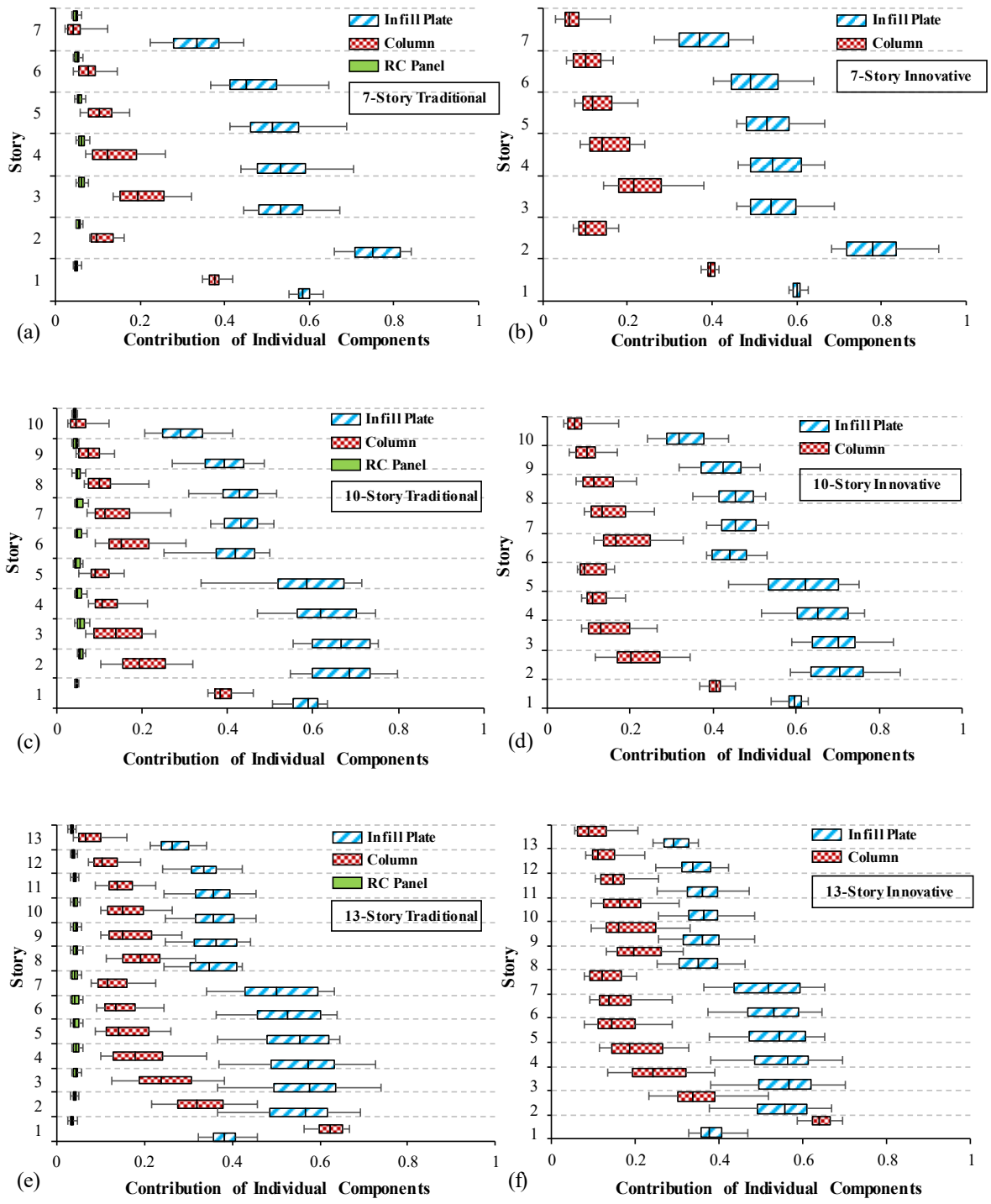

Fig. 4.9. Maximum seismic shear in different components of C-PSWs

4.6.3 Nonlinear Pushover Analysis and Incremental Dynamic Analysis

Nonlinear pushover analysis was conducted for all C-PSWs to estimate system overstrength, Ω_0, and period-based ductility, μ_T, factors. These factors were calculated using the following equations:

$$\Omega_0 = {V_{max}}/{V_d} \tag{4.2}$$

$$\mu_T = {\Delta_u}/{\Delta_y} \tag{4.3}$$

where V_{max} and V_d are the maximum and design base shear strength, respectively; Δ_u and Δ_y are ultimate and effective yield roof displacement, respectively. As indicated in Table 4.4, in all the selected C-PSWs, period-based ductility for innovative C-PSW is higher than that of the traditional one. This increase is due to late activation of the RC panel in resisting lateral forces. On the other hand, for all archetypes, the overstrength factor calculated for traditional system was slightly higher than that for innovative system. This is mainly because of early contribution of the RC panel in resisting lateral forces, which adds to the stiffness and strength of the system from the beginning of the loading.

To determine the probability of collapse for each archetype, IDA analyses were performed on all the structures. This method was first introduced by Luco and Cornell (1998) and explained later in detail by Vamvatsikos and Cornell (2002). Selecting the appropriate number of ground motions for IDA analysis is always a challenge. Sufficient number of ground motions that should be considered for an appropriate seismic assessment depends on various parameters like the accuracy of the adopted analysis, type of the response chosen for comparison, and considered limit states. For instance, it is clear that the dispersion of the responses taken from an occupancy limit state for a specific structure is much less than that extracted for the same structure in a collapse condition. The extent of nonlinearity in the structure can also affect the total number of needed ground motions for seismic assessment of the structure. In the current study, the same set of 44 ground motions used for NTHA was considered for IDA analysis. Fig. 4.10 presents the results of IDA analyses for all archetypes considered in this study. The IDA analyses were performed using maximum interstorey drift as the engineering demand parameter (EDP) and 5% damped spectral acceleration of the buildings first-mode period as the intensity measure (IM).

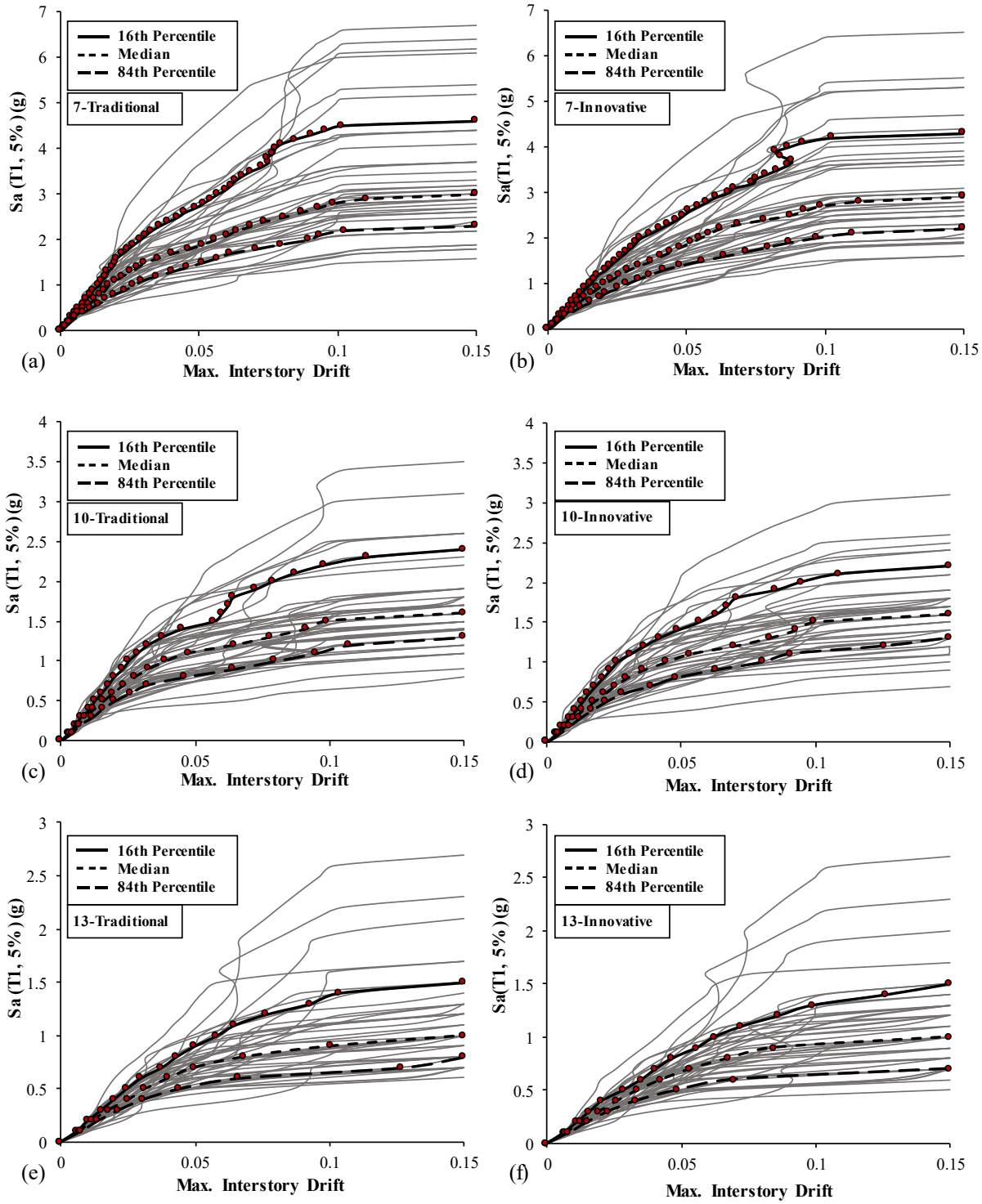

Fig. 4.10. IDA results of C-PSWs: (a) 7-storey traditional; (b) 7-storey innovative; (c) 10-storey traditional; (d) 10-storey innovative; (e) 13-storey traditional; (f) 13-storey innovative IDA results were used to calculate the probability of collapse under MCE ground motions.

The probability of collapse can be derived by subjecting the structure to a suite of ground motions whose IM values are scaled to be equal or greater than specific values. Thus, for each ground motion, there is a specific value of IM that corresponds to onset of collapse in the structure. Fragility function parameters were estimated by the following equations given by Ibarra and Krawinkler (2005):

$$ln\theta = \frac{1}{n}\sum_{i=1}^{n} \ln IM_i \tag{4.4}$$

$$\beta = \sqrt{\frac{1}{n}\sum_{i=1}^{n} (\ln(IM_i/\theta))^2} \tag{4.5}$$

where n is the total number of ground motions; IM_i is the IM value associated with onset of collapse in ith ground motion; $ln\theta$ and β are mean and standard deviation, respectively. A lognormal distribution function was used to define fragility function (Eq. (4.6)).

$$P\ (C \parallel IM = IM_i) = \Phi\left(\frac{\ln\left(\frac{x}{\theta}\right)}{\beta}\right) \tag{4.6}$$

where $P\ (C \parallel IM = IM_i)$ is the probability of structure's collapse that is subjected to a ground motion with IM value equal to IM_i; Φ is standard cumulative distribution function (CDF). The derived fragility curves for the selected buildings are presented in Fig. 4.11.

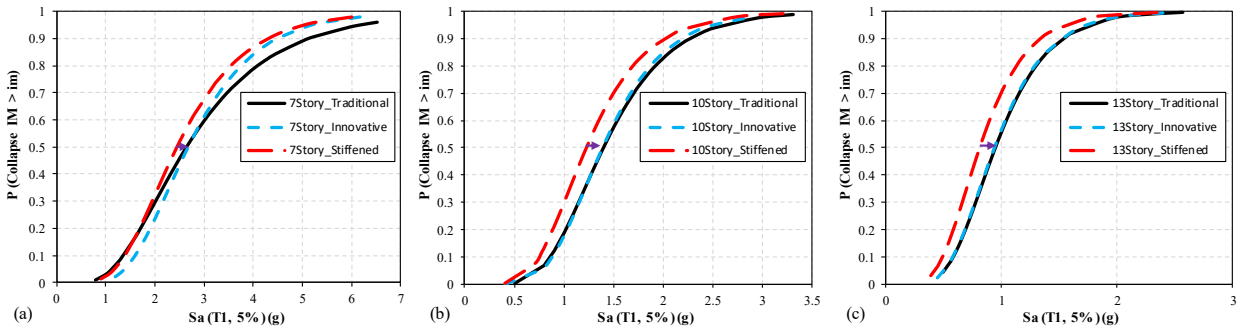

Fig. 4.11. Fragility curves from IDA analyses for traditional, innovative, and stiffened archetypes: (a) 7-storey; (b) 10-storey; (c) 13-storey

Results of the fragility curves were used to calculate collapse margin ratio (CMR), which is a primary parameter to assess the safety of structure against collapse. CMR is defined as S_{CT}/S_{MT}, where S_{CT} is the median collapse capacity of the structure obtained from fragility curve and S_{MT}

is the maximum considered ground motion intensity corresponding to the fundamental period of the structure. FEMA P695 (FEMA 2009) prescribes modification of CMR by a factor, known as spectral shape factor (SSF). SSF depends on period-based ductility of the system (μ_T), fundamental period, and seismic design category. FEMA P695 (FEMA 2009) provides spectral shape factor (SSF) values to determine adjusted collapse margin ratio (ACMR). These SSF values were determined for the FEMA P695 ground motions. Since the 44 earthquake records, developed for western Canada, used in this study are different from FEMA P695 ground motions, the SSF values suggested by FEMA P695 were not directly used in this study. However, the SSF value in the table provided in FEMA P695 are all greater than 1.0. For performance evaluation purposes, FEMA P695 considers four different types of uncertainties: uncertainty related to design requirements (β_{DR}), uncertainty related to modelling (β_{MDL}), uncertainty related to test data selected for validation of developed model (β_{TD}), and uncertainty related to variations in ground motions (β_{RTR}). The values for uncertainties were obtained from recommendations by FEMA P695. Thus, design requirements uncertainty (β_{DR}) was considered as B (good) and a value of 0.2 was assigned. The nonlinear model developed for C-PSW was considered as good and thus β_{MDL} was taken as 0.2. As mentioned earlier, very limited number of tests on C-PSW are currently available and thus $\beta_{TD}$was rated as D (poor): $\beta_{TD} = 0.5$. Finally, β_{RTR} was taken as 0.4 since the C-PSW system has a period-based ductility, $\mu_T \geq 3$. After quantifying all the uncertainties, the total system collapse uncertainty (β_{TOT}) was calculated as 0.7 using the following equation:

$$\beta_{TOT} = \sqrt{\beta_{RTR}^2 + \beta_{DR}^2 + \beta_{TD}^2 + \beta_{MDL}^2} \tag{4.7}$$

As presented in the table in FEMA, the acceptable ACMR for 10% probability ($ACMR_{10\%}$) of collapse for β_{TOT} of 0.7 is 2.45. Purba and Bruneau (2014) previously calculated allowable ACMR as 2.16 for unstiffened SPSWs. In this study, as presented in Table 4.4, the smallest calculated CMR value was 3.9 for the 13-storey innovative C-PSW system. If a value of SSF 1.0 is used, the smallest ACMR would be 3.9, which would be greater than the allowable ACMR given by FEMA P695. In addition, as given in the table in FEMA P695, the maximum $ACMR_{10\%}$ is 3.38 (for $\beta_{TOT} = 0.95$). Thus, both the traditional and the innovative C-PSW systems showed a significant safety margin against collapse.

In addition, as observed in Table 4.4, similar values of CMR were obtained for traditional and innovative systems. Further investigation on the RC panels in both systems (with and without gap) indicated that most of the RC panels reached ultimate capacities and experienced significant damages at collapse condition. Therefore, both systems exhibited similar performances in terms of safety against collapse. Thus, leaving a small gap between the RC panel and the surrounding boundary members did not affect the overall performance of the C-PSW system in collapse condition.

In addition to traditional and innovative systems, the fragility curve was also obtained for a third case, denoted as "stiffened SPSW" and is shown in Fig. 4.11. In stiffened SPSW, the RC panel was not considered, and instead, the infill plate was assumed to be fully braced out-of-plane. As can be seen in Fig. 4.11(a,b,c), median collapse capacity is increased by 8.5%, 14%, and 16.9% for 7-, 10-, and 13-storey traditional C-PSWs, respectively (when RC panel contributions are considered).

Table 4.4. Summary of Performance Evaluation for C-PSW Archetypes

Archetype	Pushover						IDA		
	$\Delta_y\ (mm)$	$\Delta_u\ (mm)$	μ_T	$V_d\ (kN)$	$V_{max}\ (kN)$	Ω_0	$S_{MT}\ (g)$	$S_{CT}\ (g)$	CMR
7-Traditional	75.6	762.8	10.09	1243.7	4250.01	3.42	0.464	2.654	5.72
7-Innovative	76.57	937.3	12.24	1243.7	3956.11	3.18	0.464	2.68	5.77
10-Traditional	145.44	828.5	5.7	1502.65	4428.66	2.95	0.341	1.396	4.09
10-Innovative	142.56	951.5	6.67	1502.65	4121.53	2.74	0.341	1.387	4.07
13-Traditional	266.06	1676.8	6.3	1616.23	4744.17	2.94	0.242	0.953	3.94
13-Innovative	264.4	1899.7	7.18	1616.23	4505.96	2.79	0.242	0.944	3.9

4.7 Sensitivity Assessment

Since the parameters used for the proposed deterioration model can vary, sensitivity of different parameters on capacity of C-PSWs were studied. Variation of two post-yielding parameters for the infill plate and three post-cracking parameters for the RC panel were considered in this study.

4.7.1 Effect of Post-yielding Parameters for Infill Plate

In order to study the effects of two post-yielding parameters, three unstiffened SPSWs (Vian and Bruneau 2005; Sabouri-Ghomi and Asad-Sajjadi 2012; Choi and Park 2010) were analysed. Fig. 4.12 presents the comparison between numerical models and test results for three aforementioned unstiffened SPSWs. It is observed that ductility capacity ($\varepsilon_c/\varepsilon_y$) and post-capping stiffness (α), which represents the severity of degradation, vary between different tests.

Due to limited experimental studies available for C-PSWs (with the RC panel attached to one side only) in comparison to unstiffened one, a sensitivity analysis was deemed crucial to investigate the effects of variation of two aforementioned parameters on overall performance of C-PSWs. Sensitivity analyses were carried out using the same three traditional C-PSWs that were designed previously. In each archetype, nine models were developed by changing the post-yielding parameters (Table 4.5). The lower and upper bound considered herein for post-yielding parameters were chosen to avoid any convergence issue (sudden degradation in the deterioration curve for strips can cause significant convergence issues). In addition, these values were selected based on engineering judgement and available data extracted during calibration process of both unstiffened and stiffened SPSWs.

For each C-PSW, IDA analyses were performed for all developed models in Table 4.5. The resulting fragility curves from IDA analyses are shown in Fig. 4.13. To investigate the effects of variation of post-yielding parameters in each archetype, $S_a(T_1, 5\%)$, spectral acceleration corresponding to 50% probability of collapse and which is also known as median collapse capacity (MCC), was taken as the benchmark.

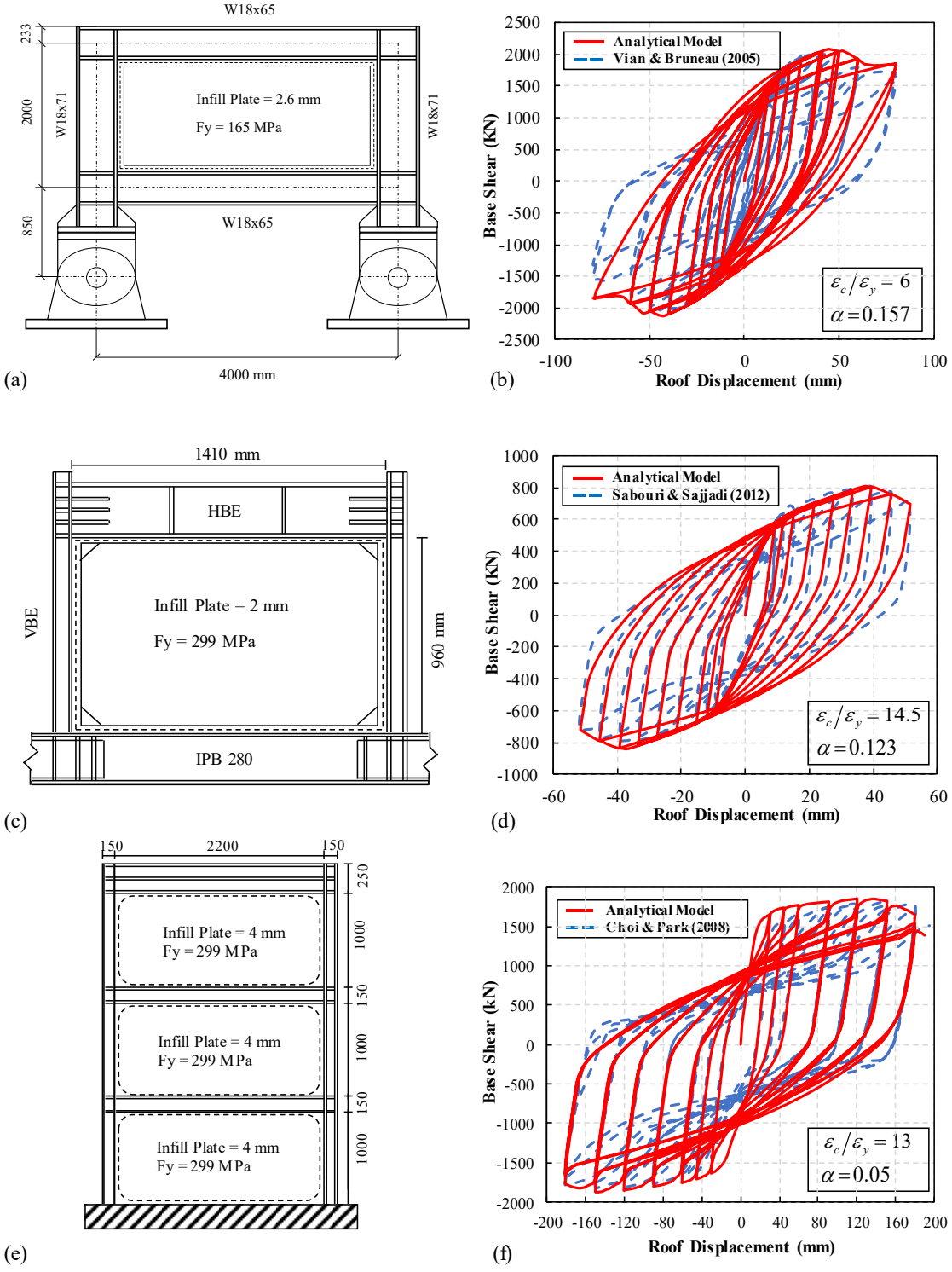

Fig. 4.12. Model validation against SPSW specimens: (a) specimen of Vian and Bruneau (2005); (b) comparison of analysis with test results of Vian and Bruneau (2005); (c) specimen of Sabouri and Sajjadi (2012); (d) comparison of analysis with test results of Sabouri and Sajjadi (2012); (e) specimen of Choi and Park (2008); (f) comparison of analysis with test results of Choi and Park (2008)

Table 4.5. Parametric Matrix for Effect of Post-yielding Parameters for Infill Plate

Case	Designation	Model parameters	
		Ductility, $\varepsilon_c/\varepsilon_y$	Post-cap stiffness ratio, α
1	5 - 0.05	5	0.05
2	5 – 0.15	5	0.15
3	5 – 0.3	5	0.3
4	15 – 0.05	15	0.05
5	15 – 0.15	15	0.15
6	15 – 0.3	15	0.3
7	30 – 0.05	30	0.05
8	30 – 0.15	30	0.15
9	30 – 0.3	30	0.3

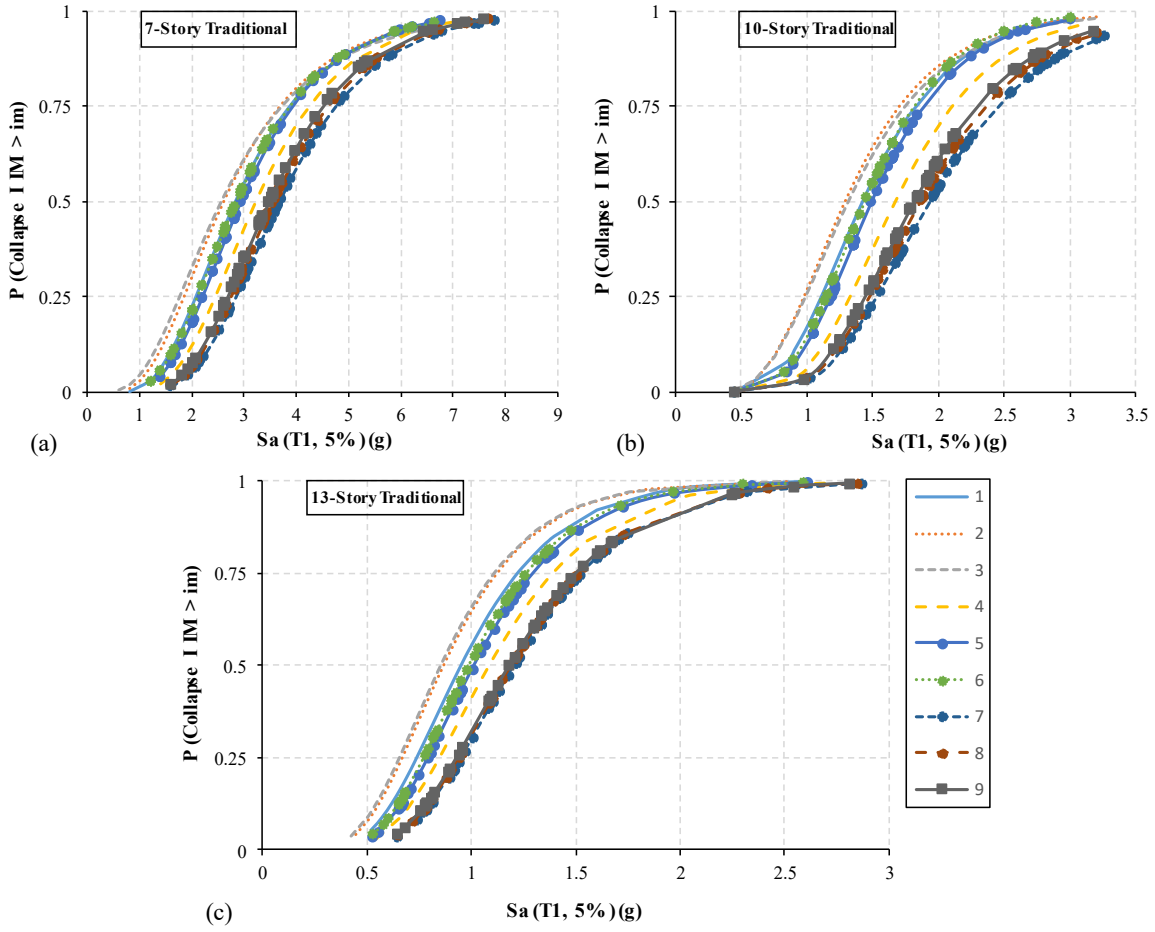

Fig. 4.13. Fragility curves for each archetype for effect of post-yielding parameters for infill plate

4.7.1.1 Effect of Ductility Capacity

In order to investigate the effect of ductility capacity on collapse capacity of C-PSW, ductility capacity was changed from 5 to 30 while post-capping stiffness remained constant. For comparison purposes, MCC values in each archetype were divided by the maximum MCC value obtained for each archetype. Fig. 4.14(a) shows that MCC increases in all C-PSWs as ductility capacity increases. This was a clear trend in all three groups of variant models selected for this study. It was observed that case 7 designated as (30 – 0.05), in Table 4.5, produced the maximum MCC values in all three C-PSWs. Thus, when ductility capacity was varied from 5 to 30, the collapse capacities of 7-, 10-, and 13-storey C-PSWs increased by 36.4%, 44.7%, and 37.8%, respectively.

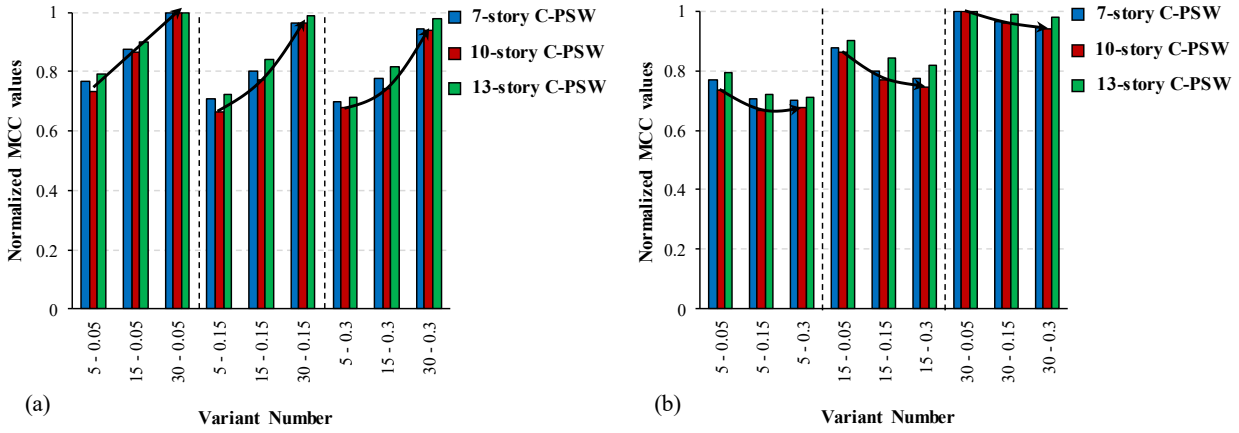

Fig. 4.14: Effect of post-yielding parameters of steel infill on MCC of traditional C-PSW: (a) ductility capacity variation; (b) post capping stiffness variation

4.7.1.2 Effect of Post-capping Stiffness

For investigating the effect of post-capping stiffness on collapse capacity of C-PSW, the parameter (post-capping stiffness), as shown in Table 4.5, was varied from 0.05 to 0.3. The larger post-capping stiffness value corresponds to sudden degradation in stress-strain relationship considered for strips. As shown in Fig. 4.14(b), C-PSW capacity is less sensitive to the post-capping stiffness in comparison to the ductility capacity. It was observed that when the post-capping stiffness was varied from 0.05 to 0.3, the collapse capacities (MCC) of C-PSWs decreased by about 11.6%, 13.8%, and 10.2% for the 7-, 10-, and 13-storey C-PSWs.

4.7.2 Sensitivity Assessment for the Variation of Reinforced Concrete Panel Parameters

As explained earlier, a macroscale model was proposed in this study to simulate the performance of the RC panel attached to the infill plate. The proposed model consisted of a displacement-based beam-column element with a translational spring located at the mid-height to capture the shear behavior. Assigned stress-strain relationship for spring follows a multilinear (quadlinear) relationship, which was idealized by a trilinear one (by neglecting the yielding of the RC panel) during validation of the test conducted by Zhao and Astaneh-Asl (2004). Due to the limited number of experimental tests available for C-PSW (traditional and innovative with the RC panel attached to one side of the infill plate) and lack of individual component tests to capture the behavior of individual elements under cyclic loading, especially the shear behavior of the RC panel attached to the infill plate of the C-PSW system, a sensitivity assessment was deemed necessary. Thus, in the second phase of sensitivity assessment study, research was carried out to investigate the effect of variation of three post-cracking parameters (i.e., yielding, residual stress, and strain corresponding to initiation of degradation in the RC panel) on overall performance of C-PSW. Fifteen models with different combination of post-cracking parameters were considered for the traditional C-PSWs (i.e. 7-, 10-, and 13-storey). Table 4.6 presents the values of post-cracking parameters in each variant model. IDA analyses were conducted and resulting fragility curves, as shown in Fig. 4.15, were extracted for all variant models.

4.7.2.1 Sensitivity to Variation of Shear Strain Corresponding to Maximum Shear Stress

As shown in Fig. 4.16(a), for each C-PSW, maximum shear strain, $\gamma_{\max}$, was varied from 0.015 to 0.2. Collapse capacities (MCC) for all variant models for each archetype were normalized by the maximum MCC value obtained for each archetype. Variant number 15 (0.2 – 0.5 – 0.2), in Table 4.6, produced the largest MCC value among all the archetypes. In general, by increasing the maximum shear strain ($\gamma_{\max}$) from 0.015 to 0.2, MCC increased in all groups except group four where the capacity of all three archetypes remained constant. This is due to the fact that no degradation was considered for the RC panel in group four. Group two represented the most sensitive group to γ_{max}, where with an increase of γ_{max} from 0.015 to 0.2, the collapse capacities increased by 14%, 10.8%, and 10%, for 7-, 10-, and 13-storey C-PSWs, respectively.

Table 4.6. Parametric Matrix for Effect of Post-cracking Parameters for RC Panel

Case	Designation	Model parameters		
		$\gamma_{\max}$ [a]	γ_y [b]	v_{res} [c]
1	0.015 – 0 – 0.2	0.015	– –	$0.2v_{\max}$
2	0.015 – 0.1 – 0	0.015	$0.1\gamma_{\max}$	0
3	0.015 – 0.1 – 0.2	0.015	$0.1\gamma_{\max}$	$0.2v_{\max}$
4	0.015 – 0.1 – 1	0.015	$0.1\gamma_{\max}$	$v_{\max}$ [d]
5	0.015 – 0.5 – 0.2	0.015	$0.5\gamma_{\max}$	$0.2v_{\max}$
6	0.05 – 0 – 0.2	0.05	– –	$0.2v_{\max}$
7	0.05 – 0.1 – 0	0.05	$0.1\gamma_{\max}$	0
8	0.05 – 0.1 – 0.2	0.05	$0.1\gamma_{\max}$	$0.2v_{\max}$
9	0.05 – 0.1 – 1	0.05	$0.1\gamma_{\max}$	$v_{\max}$
10	0.05 – 0.5 – 0.2	0.05	$0.5\gamma_{\max}$	$0.2v_{\max}$
11	0.2 – 0 – 0.2	0.2	– –	$0.2v_{\max}$
12	0.2 – 0.1 – 0	0.2	$0.1\gamma_{\max}$	0
13	0.2 – 0.1 – 0.2	0.2	$0.1\gamma_{\max}$	$0.2v_{\max}$
14	0.2 – 0.1 – 1	0.2	$0.1\gamma_{\max}$	$v_{\max}$
15	0.2 – 0.5 – 0.2	0.2	$0.5\gamma_{\max}$	$0.2v_{\max}$

[a] Shear strain correspond to $v_{\max}$; [b] Yielding shear strain

[c] Residual shear stress; [d] Maximum shear stress

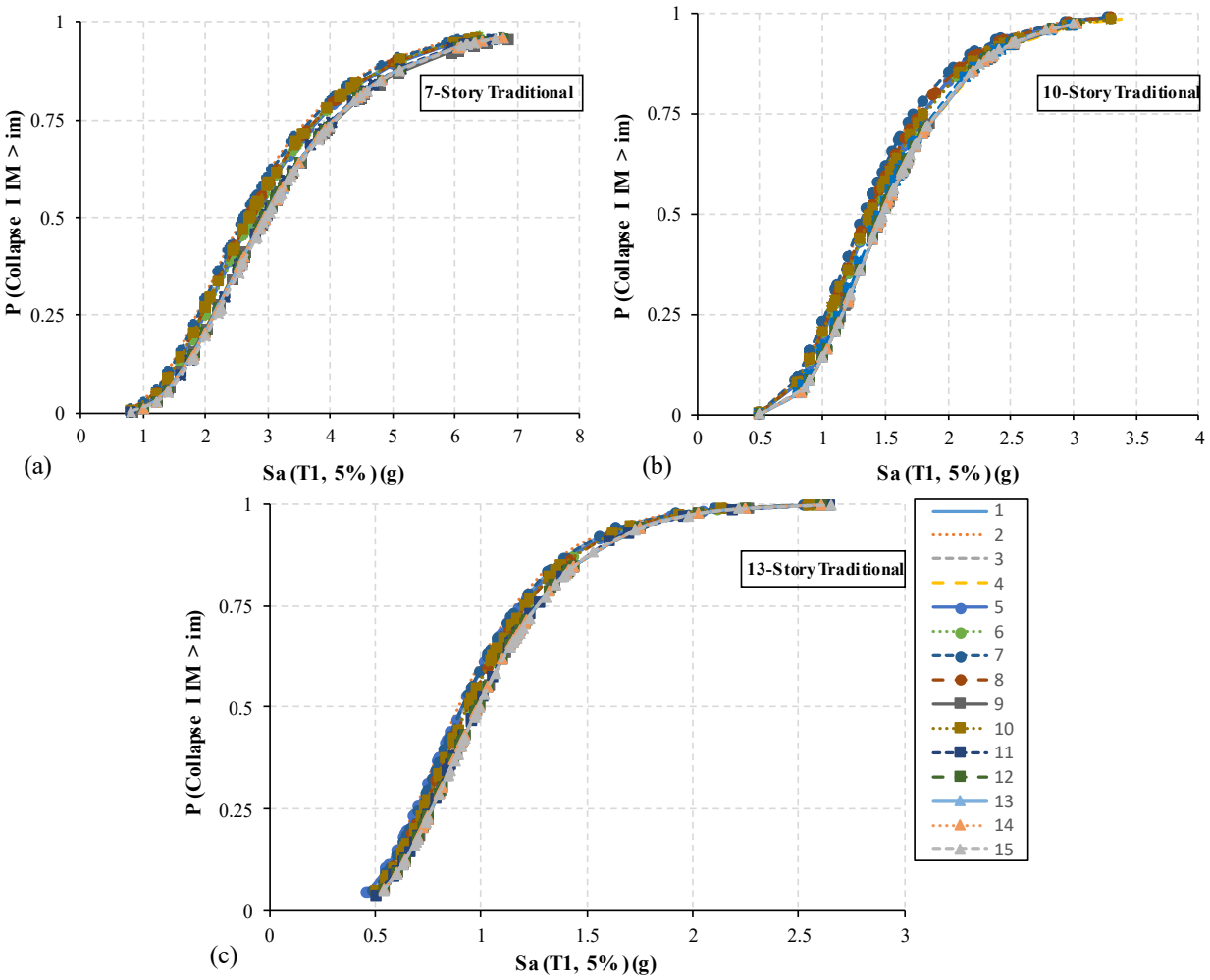

Fig. 4.15. Fragility curves for each archetype for changes in post-cracking parameters for RC panel

4.7.2.2 Sensitivity to Yielding Point

Fig. 4.16(b) presents the results of sensitivity analyses of each C-PSW for the variation of yielding shear strain in the RC panel. Three sets were defined and in each set, yielding shear strain was varied from 0 to 0.5 times γ_{max} keeping the two other post-cracking variables constant. Term "0" assigned to yielding shear strain of the RC panel in several variant numbers presented in Table 4.6 refers to the condition that quadlinear relationship adopted for spring was idealized by a trilinear relationship neglecting the yielding point. It was observed that by changing yielding shear strain from 0 to 0.5 times γ_{max}, maximum percentage of MCC changes were 2%, 1.4%, and 1% for 7-, 10-, and 13-storey C-PSW systems, respectively. It was also observed that replacing a

quadlinear stress-strain relationship with a trilinear one did not affect the overall performance of the system. On the other hand, this simplification reduced the complexity of the numerical model and decreased the required time to analyze C-PSWs.

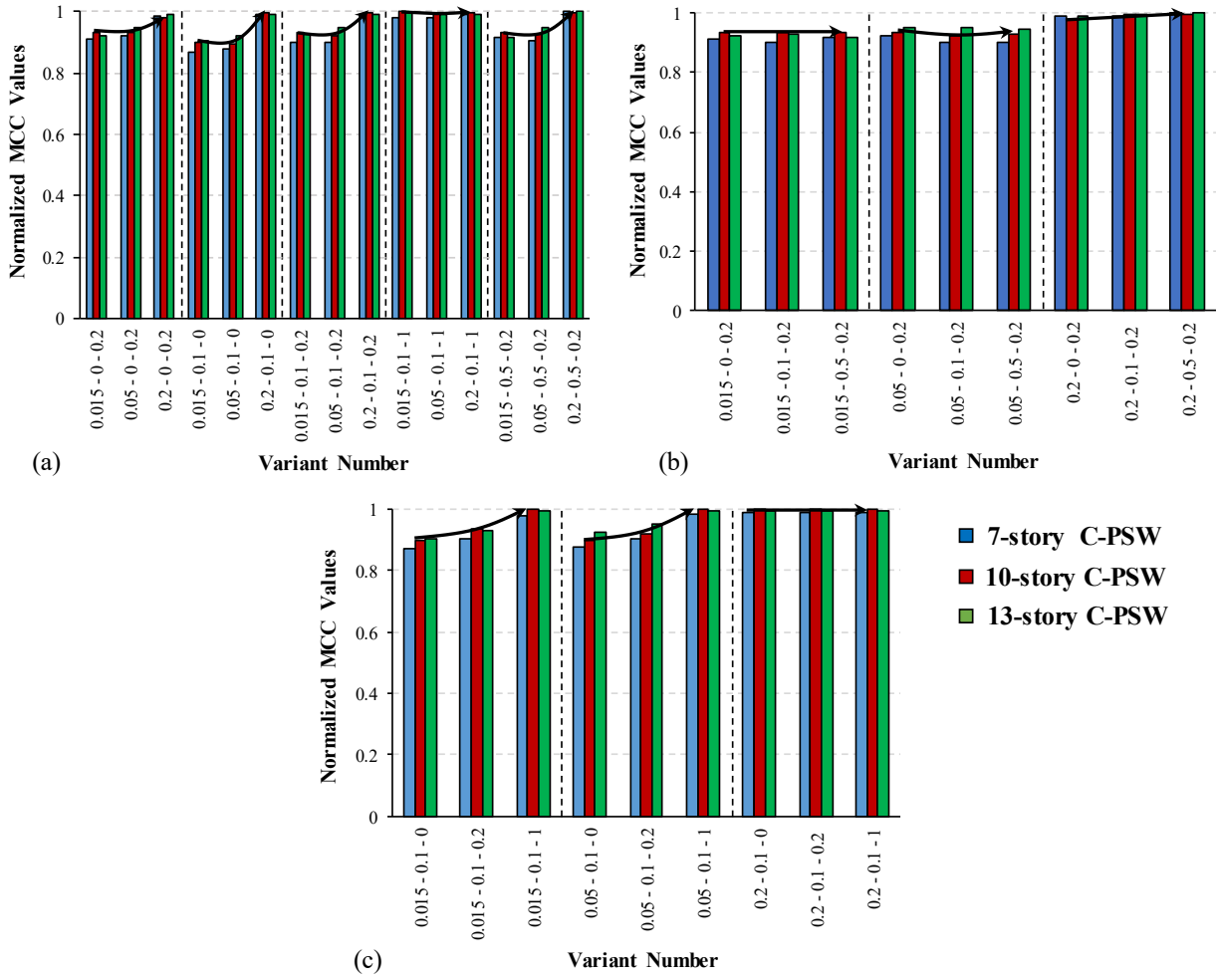

Fig. 4.16. Effect of post-cracking parameters of RC panel on MCC of traditional C-PSW: (a) variation of shear strain corresponding to v_{max}(b) yielding shear strain changes; (c) residual strength changes

4.7.2.3 Sensitivity to Variation of Residual Stress of the RC Panel

At collapse condition, due to friction between different parts of crushed RC panels, the RC panel can have some residual shear strength and this residual shear strength can vary. To address the effect of variation of residual shear strength in RC panel on overall performance of the C-PSW system, three groups were considered. Residual strength of the RC panel was varied from 0 to

100% of maximum strength. For comparison purposes, the variation of residual stress was assumed between 0 to 20% of maximum stress. It was observed that when residual stress was changed from 0 to 20%, maximum increase in MCC was 3.8%, 3.8%, and 3% for 7-, 10-, and 13-storey C-PSWs, respectively. The results indicated that variation of residual stress from 0 to 20% did not have any significant effect on the overall performance of the C-PSW system.

4.8 Conclusion

This study presented results from nonlinear time history and IDA analyses of traditional and innovative C-PSWs using a nonlinear macro-modelling approach. A total of 50800 nonlinear analyses were performed on 7-, 10-, and 13-storey C-PSWs (with and without gap). The main findings of the study are as follows:

- The proposed deterioration model for C-PSW was shown to provide a very good prediction of the cyclic behaviour of the available tests. Thus, elements and the modelling considerations adopted in this study are able to capture all essential features of the behavior of C-PSWs.
- In all C-PSWs, the maximum interstorey drift was lower than the permissible value of 2.5% given by NBC (2015). This shows effectiveness of the C-PSW system in controlling storey drift.
- Inelastic dynamic analyses showed that boundary columns resist a significant portion of the storey shear. The contribution of boundary columns is not considered in the current design procedure of C-PSWs. It is expected that the extra strength and stiffness contributions of columns will provide a valuable back up to the infill plate, which is the main fuse of the C-PSW system. On the other hand, maximum participation of the RC panel in resisting storey shear was less than 10% in all archetypes.
- All archetypes assessed in this study showed a CMR of more than 3.9, which passes the acceptable ACMR value proposed by FEMA P695 (FEMA 2009). Thus, the seismic force modification factors ($R_d = 5.0$ and $R_o = 1.6$) used in this study for C-PSWs are adequate and these values are recommended for NBC (2015). In addition, similar values of CMR were obtained for both traditional and innovative C-PSWs. This was due to fact that the RC panels (with and without gap) in all archetypes reached to their ultimate capacities and experienced significant damages in collapse condition.
- Sensitivity analyses of 27 variant models showed that, among the two post yielding parameters for infill plate, ductility capacity has more effect on the collapse capacity of C-PSW than the post-

capping stiffness. It was observed that a change in ductility capacity from 5 to 30 resulted in a significant increase in the capacity of entire C-PSW system (45% increase in 10-storey). On the other hand, when post-capping stiffness ratio was varied from 0.05 to 0.3, a maximum of 14% reduction (in case of 10-storey) in the capacity of the C-PSW system was observed.

● Among the three selected post-cracking parameters for RC panel, shear strain corresponding to maximum shear stress (γ_{max} variation) has more effect on MCC of C-PSW. Thus, when γ_{max} was increased from 0.015 to 0.2, increase in MCC for 7-, 10-, and 13-storey C-PSWs were 14%, 10.8%, and 10%, respectively. On the other hand, maximum change in the MCC due to change in values of the two other post-cracking parameters, yielding shear strain and residual stress, was less than 5% in all cases.

● Sensitivity analysis showed that a trilinear model rather than a quadlinear one can be used to simulate the shear behavior of the RC panel. This will reduce the complexity level of the proposed model and decrease the required time to analyze C-PSW buildings.

● Sensitivity analysis also showed no significant effect on the behaviour of the C-PSW when residual stress was varied between 0 to 20% of maximum stress (less than 5% variation in MCC). It is thus recommended to use 20% residual stress in shear behavior for the spring in the RC panel to account for shear aggregate interlock, which might occur at ultimate condition due to friction between different parts of the crushed RC panel.

The results obtained in this study, especially regarding the applicability of ductility-related force modification factor, R_d, of 5 and overstrength-related force modification factor, R_0, of 1.6 for designing of C-PSW (or C-SPSW-CE), are based on analysis of limited number of C-PSWs and only for seismic region of Western Canada (equivalent to seismic region D in ASCE). More studies on C-PSWs with different geometry are needed. In addition, ground motions suggested by FEMA P695 (FEMA 2009) methodology and other seismic regions (low and moderate seismic regions) need to be considered to generalize the conclusions about seismic force modification factors (R_d and R_0 values).

Finally, as required by FEMA P695 methodology, the study presented here requires an independent peer review. The peer review shall examine adequacy and quality of the test data, available design information, analytical modeling, selection of earthquake records, nonlinear analysis procedure and finally, appropriateness of the proposed seismic force modification factors.

Chapter 5

Nonlinear Seismic Analysis of Perforated Steel Plate Shear Walls using a Macro-model

5.1 Abstract

Steel plate shear wall (SPSW) with regularly spaced circular perforations has recently been developed. While the current edition of AISC 341-16 and CSA S16-14 have adopted perforated SPSW (P-SPSW) in their design standards, no simple numerical model is currently available for analysing this SPSW system. A reliable macro-model is developed for regularly spaced circular perforations. The proposed macro-model is validated against available experimental data. Performance of three multi-storey (4-, 7-, and 10-storey) perforated SPSWs designed according to CSA S16-14 and NBC 2015 is further investigated through conducting a series of time history analyses using a suite of 44 ground motions developed for western Canada. When compared with seismic analysis results of solid SPSWs, it is observed that the median shear envelopes for P-SPSWs are slightly less than that for solid ones. Also, on contrary to solid SPSW archetypes, the contribution of boundary columns in resisting the storey shear is found higher than the infill plate in most of the stories in P-SPSW archetypes. Finally, a sensitivity assessment is performed to evaluate the effect of perforation diameter on different responses of P-SPSWs, such as peak column axial forces, peak column bending moments, and maximum interstorey drift. It is observed that with an increase in the hole diameter, column axial force demand decreases, while the bending moment remains almost same. Also, since adding perforations to the infill plate reduces stiffness and strength of the P-SPSW system, interstorey drift ratio is increased in comparison to solid SPSW.

Keywords: Steel plate shear wall; Perforated infill plate; Macro-model; Seismic analysis; Shear envelopes; Sensitivity assessment.

5.2 Introduction

Steel plate shear walls (SPSWs) have been rapidly gaining interests as an effective lateral load resisting system in recent years. The infill plates provide high initial stiffness, excellent ductility, and energy dissipation capacity for the whole system through post buckling behavior and tension field action. Thorburn et al. (1983) proposed an analytical model to predict the behavior of unstiffened SPSWs. The suggested analytical model consists of a series of parallel truss elements, known as strips, which are aligned in the direction of tension field action. As per capacity design, surrounding boundary members (i.e., beams and columns) are designed based on yielding of the infill plates. It is observed that minimum infill plate thickness used in construction are usually higher than the required infill plate thickness and this imposes significant demand on the surrounding boundary members, which will increase the size of beams and columns. To overcome this problem, a number of solutions, such as use of light-gauge shear walls with cold rolled infill plate (Berman and Bruneau 2005), have been proposed by the researchers. Light-gauge shear walls with cold rolled infill plate can be a suitable option to improve the economy of the system (Berman and Bruneau 2005). Use of low-yield steel has also been found to reduce the demand on the surrounding boundary members (Vian and Bruneau 2004). Another alternative which has got a lot of attention in recent years is to have circular perforations (Vian and Bruneau 2004; Roberts and Sabouri-Ghomi 1991; Purba 2006; Bhowmick et al. 2014) or rectangular openings (Sabouri-Ghomi and Mamazizi 2015; Sabouri-Ghomi et al. 2016; Hosseinzadeh and Tehranizadeh 2012) in the infill plate. These perforations in the infill plate can accommodate passing of the utilities like electric lines and water pipes through the infill plate. In addition, it can ease lifting, handling, and installation process of the infill plate in the construction site.

Current edition of AISC 341-16 (AISC 2016) and CSA S16-14 (CSA 2014) have design guidelines for SPSW with regularly spaced circular perforations in the infill plate. However, very limited research is currently available for P-SPSWs. Also, the available numerical studies are all based on detailed finite element (FE) model. When conducting collapse assessment or performance-based design of buildings, it is not suitable to adopt a detailed FE model. Thus, a macro-model for simulation of the behavior of P-SPSWs subjected to lateral loads needs to be developed. This paper presents development of a 2D macro-model for analyzing P-SPSW using a refined strip model approach, which was originally proposed for the solid infill plate, using Open

System for Earthquake Engineering Simulation (OpenSees) (McKenna et al. 2013). The accuracy of the proposed macro-modelling approach is validated against available experimental results. The validated macro-model is then used to study seismic performance of three multi-storey (4-, 7-, and 10-storey) P-SPSWs with multiple regularly-spaced circular perforations of equal diameter in the infill plate. To compare the results of perforated SPSWs with SPSWs with no perforations, three similar multi-storey SPSWs with solid infill plates are also analysed. The SPSWs (i.e., solid and perforated) were designed according to CSA S16-14 (CSA 2014) and NBC (2015). Nonlinear time history analyses are performed on all code designed solid and perforated SPSWs using a group of 44 artificial ground motions that were developed for Western Canada. Storey shear envelopes, peak column axial forces, peak column bending moments, and maximum contribution of individual components (i.e., infill plates and boundary columns) in resisting the storey shear are extracted from nonlinear seismic analyses of perforated SPSWs and are compared with solid SPSWs. In addition to seismic analyses, nonlinear pushover analyses are carried out on all studied archetypes to estimate period-based ductility and overstrength factor for both SPSW systems.

Finally, in order to assess the effect of the hole diameter on the overall response of the P-SPSW structure, a series of sensitivity assessment is performed. For each studied archetype, 6 variant models are developed by changing the hole diameter from 0 mm (solid infill plate) to 250 mm. Variation of different responses of studied archetypes, such as peak column axial forces, peak column bending moments, and maximum interstorey drifts, are examined when the hole diameter is varied between 0 mm and 250 mm.

5.3 Proposed Macro-modelling Approach

Thorburn et al. (1983) proposed an analytical model, strip model, to obtain post-buckling behavior of unstiffened solid SPSW. The macro-model developed in this paper is based on the strip model. The following two subsections presents strip model implementation in unstiffened solid infill plate as well as in unstiffened perforated infill plate.

5.3.1 Macro-model for Unstiffened Solid Infill Plate

In an unstiffened SPSW, it is considered that the column overturning moment is resisted by axial coupling loads in columns and the shear is resisted by the infill plate through the post-

buckling behavior and tension field action. Fig. 5.1(a) represents a solid infill plate subjected to pure shear. To find the principal stresses acting on the infill plate before buckling, a small segment is chosen and rotated by 45 degrees. After buckling, the infill plate is not capable of carrying the compressive stresses that are higher than the critical shear stress (τ_{cr}). Thus, tension field action gradually forms and develops in the entire infill plate to resist the loads, as indicated in Fig. 5.1(b). Fig. 5.1(c) presents the superposition of stresses before and after buckling of the infill plate.

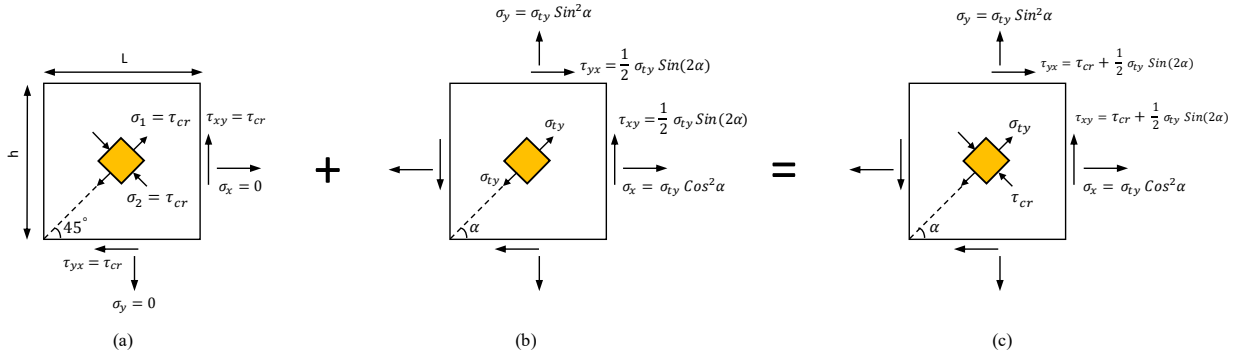

Fig. 5.1. State of stresses in an infill plate at different stages of loading: (a) stresses before buckling; (b) stresses due to tension field action; (c) post-buckling stresses

In macro-scale modelling of unstiffened solid SPSW, the infill plate is idealized using a minimum of 10 truss members in each direction to represent the behavior of the infill plate when subjected to cyclic loading, such as earthquake. The truss members, known as strips, are oriented in the direction of tension field action, α, to resist the lateral loads. Using the principle of least work, tension field angle measured from the vertical direction is calculated as (Timler and Kulak 1983):

$$\alpha = tan^{-1}\sqrt[4]{\left(1+\frac{tL}{2A_c}\right)\left[1+th\left(\frac{1}{A_b}+\frac{h^3}{360\,I_cL}\right)\right]^{-1}} \tag{5.1}$$

where t is the thickness of plate; A_c is the cross sectional area of the column, also known as vertical boundary element (VBE); A_b is the cross sectional area of the beam, also known as horizontal boundary element (HBE); L is the distance between the VBE centerlines; h is the distance between the HBE centerlines; I_c is the moment of inertia of a VBE. As indicated in Eq. (5.1), the tension field angle depends on the geometric properties of the surrounding boundary

members as well as the thickness of the infill plate. In multi-storey buildings, tension field angle might vary from one level to the other since the geometric properties of the surrounding boundary members and infill plate thickness vary. If exact tension field angles are used, tension strips from the panels above and below any intermediate beam do not necessarily coincide. The staggered node points on the beam will increase the number of beam segments and will produce artificial bending moment along the length of the beam. To avoid this phenomenon, it is recommended to average the tension field angle along the height of the building and use the average value for all stories in the building. This approach is valid when the same bay width is used and storey heights are similar in the building and also, the calculated tension field angle in each level is within 5^o of the average tension field angle (Dastfan and Driver 2008). Fig. 5.2 shows a sample 2-storey unstiffened solid SPSW along with the cross section of each strip and their connections to the surrounding boundary members. As shown in Fig. 5.2(b), width of each strip, when there are n number of equally spaced strips, is calculated as:

$$\Delta_x = \frac{[L + h\ tan\alpha]}{n} \tag{5.2}$$

The cross sectional area of each strip is calculated based on Eq. (5.3):

$$A_s = \frac{[L\ cos\alpha + h\ sin\alpha]\ t}{n} \tag{5.3}$$

In addition, compressive stresses are developed in the plate perpendicular to the tensile stresses. After buckling, maximum principle compressive stress (σ_{cp}) becomes constant and is very close to the critical shear stress. The critical shear stress is a function of material properties, bay width, and thickness of the infill plate, and is calculated as:

$$\tau_{cr} = k_s \frac{\pi^2\ E_s}{12\ (1 - \vartheta^2)} \left(\frac{t}{L}\right)^2 \tag{5.4}$$

where E_s is the modulus of elasticity of steel; ϑ is the Poisson's ratio of steel plate; k_s is the buckling coefficient which is the function of panel aspect ratio and is calculated using Eq. (5.5):

$$k_s = \begin{pmatrix} 5.6 + 8.98\left(\frac{L}{h}\right)^2 & for\left(\frac{L}{h}\right) \geq 1 \\ 8.98 + 5.6\left(\frac{L}{h}\right)^2 & for\left(\frac{L}{h}\right) \leq 1 \end{pmatrix} \tag{5.5}$$

Maximum principle tensile stress after buckling (σ_{ty}) is significantly higher than the critical shear stress and slightly less than the yield stress of steel material (σ_y). By using the von Mises yield criterion, maximum principle tensile stress after buckling can be calculated using Eq. (5.6) and Eq. (5.7):

$$\left[\sigma_{ty} - \left(-\sigma_{cp}\right)\right]^2 + {\sigma_{ty}}^2 + (-\sigma_{cp})^2 - 2{\sigma_y}^2 = 0 \tag{5.6}$$

$$\sigma_{ty} = \sqrt{\sigma_y^2 - 0.75\sigma_{cp}^2} - 0.5\sigma_{cp} \tag{5.7}$$

Fig. 5.2(d) shows the stress-strain relationship that is assigned to each diagonal strip in both solid and perforated SPSWs. A trilinear relationship in tension and a bilinear relationship in compression is assigned to each diagonal strip. Tri-linear stress-strain behavior initiates with the elastic behavior until yielding occurs in tension, then plastic behavior takes place by forming the

tension field action and finally web tearing begins, causing significant degradation in the strength of the entire SPSW system.

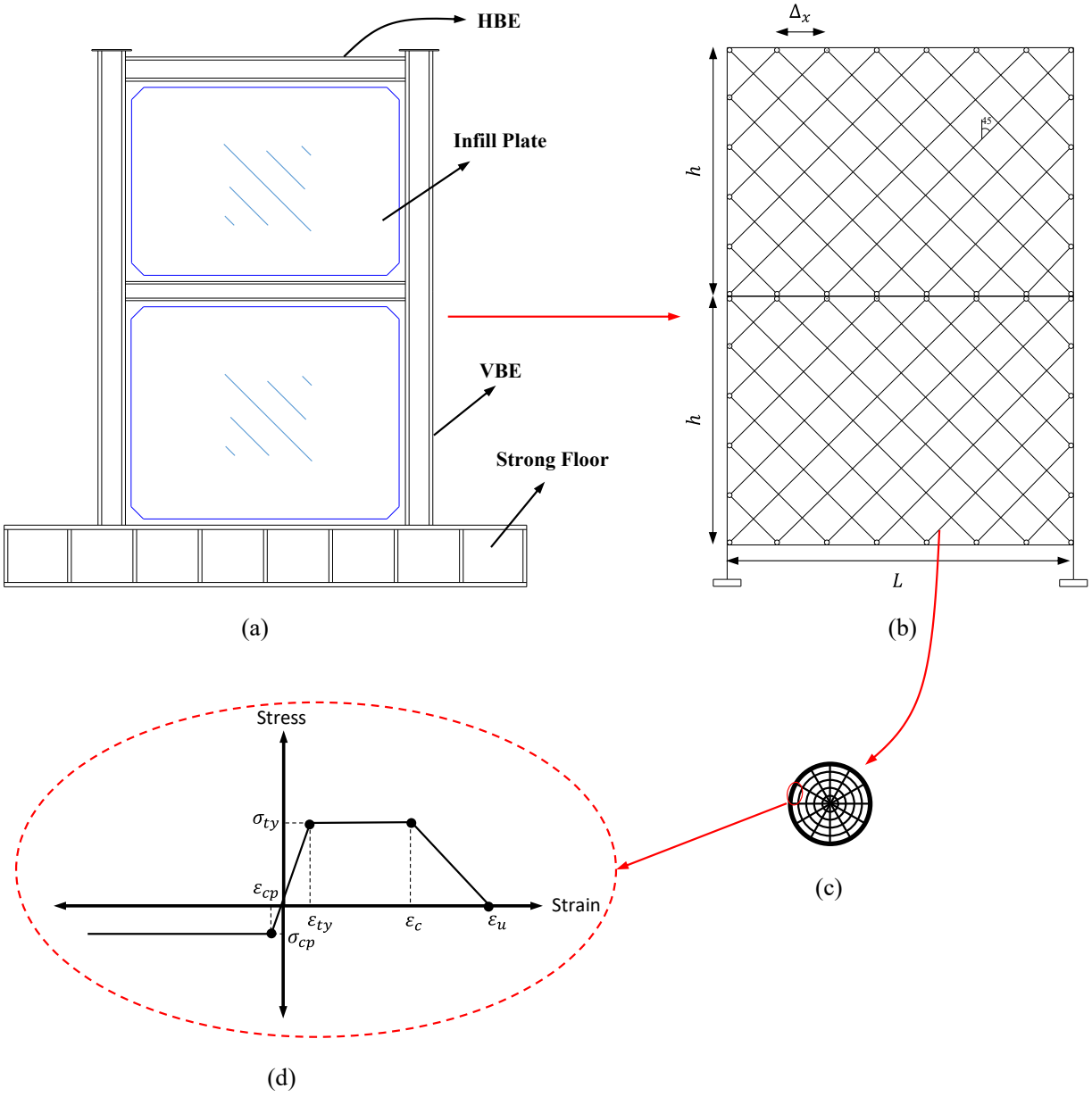

Fig. 5.2. (a) General configuration of a 2-storey unstiffened solid SPSW; (b) analytical macro-model for unstiffened solid SPSW; (c) cross section of each strip along with fiber discretization; (d) assigned stress-strain relationship to each fiber

5.3.2 Macro-model for Unstiffened Perforated Infill Plate

Roberts and Sabouri-Ghomi (1991) conducted a study on SPSW with single perforation. They conducted a series of quasi-static cyclic loading tests on centrally placed circular perforation and proposed a reduction factor to be applied to the strength and stiffness of the solid infill plate to calculate corresponding values for the perforated infill plate. The reduction factor was a function of perforation diameter and specimen width. Vian and Bruneau (2004) tested a single bay, single storey low yield steel SPSW specimen with regularly spaced 200 mm-diameter perforations in the infill plate. Fig. 5.3 shows a typical single storey perforated SPSW with a diagonal strip. To develop uniform tension field action in the perforated infill plate, the perforations must be made with the same diameter and must be equally spaced with a diagonal width S_{diag}, arranged at an angle of 45 degree with respect to the column axis. A typical strip is defined as the region within a tributary width of $\frac{1}{2}\ S_{diag}$ on either side of a perforation layout line, which is indicated by a shaded region in Fig. 5.3.

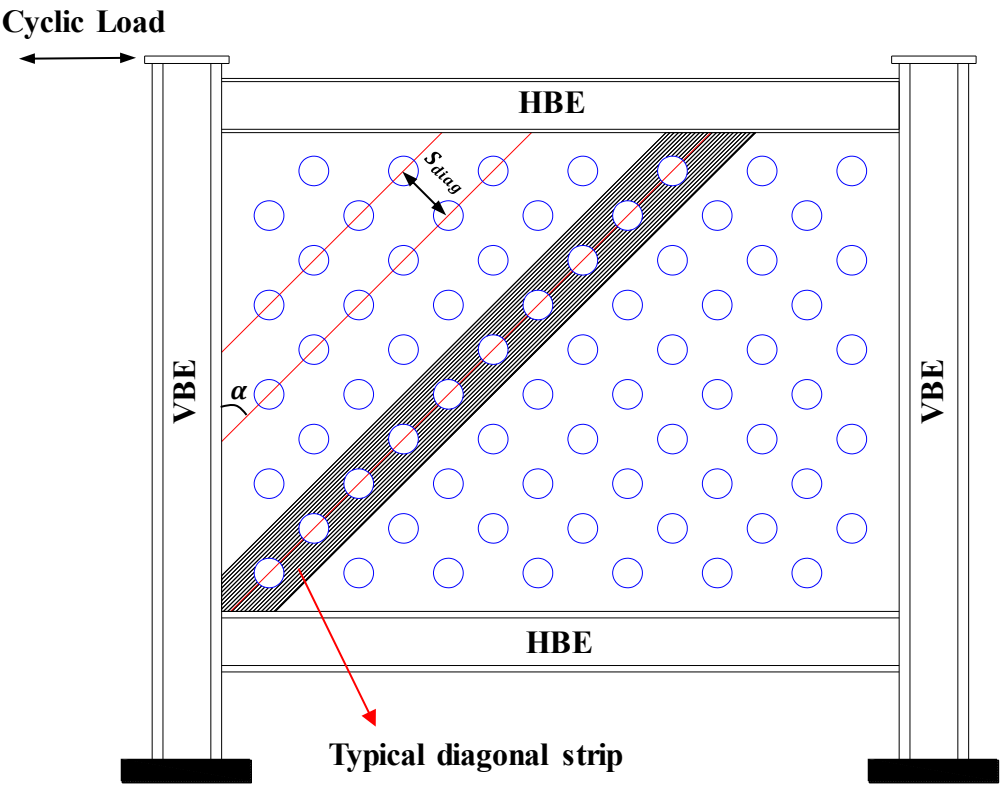

Fig. 5.3. Single storey perforated SPSW with a typical diagonal strip

Both CSA S16-14 (CSA 2014) and AISC 341-16 (AISC 2016) have adopted the regularly spaced perforation layout proposed by Vian and Bruneau (2004). In perforated SPSW, typical diagonal strips from adjacent stories do not necessarily coincide at a common node at the beam level. The similar pattern can also be observed in the columns since strips are formed in the two perpendicular directions due to cyclic nature of the earthquake loading. Barua and Bhowmick (2019) conducted a study on two different layouts of strip model for perforated SPSWs. One was exact layout and the other was crosshatch layout. Exact layout was the result of actual positioning of strips on surrounding boundary members while in the crosshatch layout, a minor change in the orientation of strips was made to share common nodes on the boundary members. It was observed that the exact layout provided a better estimation of the initial stiffness, post-yielding behavior, and ultimate strength of the perforated SPSW system. However, as discussed earlier, staggered node points formed on the boundary members can produce an extra bending moment and this can increase the demand on the boundary columns. This study investigates the demand on the boundary columns when the perforated SPSW system is subjected to a group of 44 ground motions.

5.4 Validation of the Macro-model

Vian and Bruneau (2004) tested single storey solid and perforated SPSWs subjected to quasi-static cyclic loading. The specimens were named as “S” and “P”, where “S” referred to the specimen with the solid infill plate without perforations and “P” referred to the specimen with regularly placed circular perforations. In this study, specimen “S” and “P” are utilized to validate the accuracy of the proposed modelling approach for solid and perforated SPSWs, respectively.

Both “S” and “P” specimens had infill plate thickness of 2.6 mm, which was made of low yield steel with yield stress of 165 MPa. The center to center distance between the VBEs was 4000 mm and center to center distance between the HBEs was 2000 mm. The boundary members were made of I-shaped sections, W18x71 for columns and W18x65 for beams, with specified yield strength of 345 MPa. The beams were connected to the columns using reduced beam section (RBS) connections. Fig. 5.4(a) and Fig. 5.4(c) present the general configuration of specimen “S” tested by Vian and Bruneau (2004) along with the numerical model developed for the specimen using *OpenSees* software. Fig. 5.4(e) shows the stress-strain relationship assigned to the individual strips in the numerical model. As discussed in section 5.3.1, maximum principle compressive stress (σ_{cp})

is calculated based on Eq. (5.4). Maximum principle tensile stress (σ_{ty}) is calculated based on von Mises yield criterion and is equal to 161.7 MPa, which is slightly less than the yield stress of the infill plate. As indicated in Fig. 5.4(b), the perforated SPSW had a total of 20 circular openings with 200 mm diameter and 300 mm center to center distance between the perforations. Thus, a diagonal strip width (S_{diag}) of 424.26 mm was used to develop the numerical model. At the end of the experiment, minor fractures were observed at the panel corners. The test was terminated after a drift of 3%, when a weld in the continuity plate failed at the top of a column. Fig. 5.4(d) shows the modified strips orientation and their connections to the surrounding boundary members. As previously discussed, the strips did not reach to a common node on the surrounding boundary members since tension field action was formed in a width of S_{diag} which is equal to center to center distance between the perforations (not edge to edge distance). As shown in Fig. 5.4(e), the assigned stress-strain relationship to the strips in the perforated SPSW is exactly the same as the solid one. Fig. 5.4(f) compares the load-displacement data from the experimental test with solid infill plate (specimen "S") with the corresponding data obtained from the numerical model. A good agreement between the test and the developed macro-model is observed. Fig. 5.4(g) compares the cyclic behavior of the perforated SPSW obtained from the experiment with that from the macro-model. As can be seen, there is a good agreement between the proposed model and the experimental data in terms of both elastic stiffness and inelastic response of the P-SPSW system.

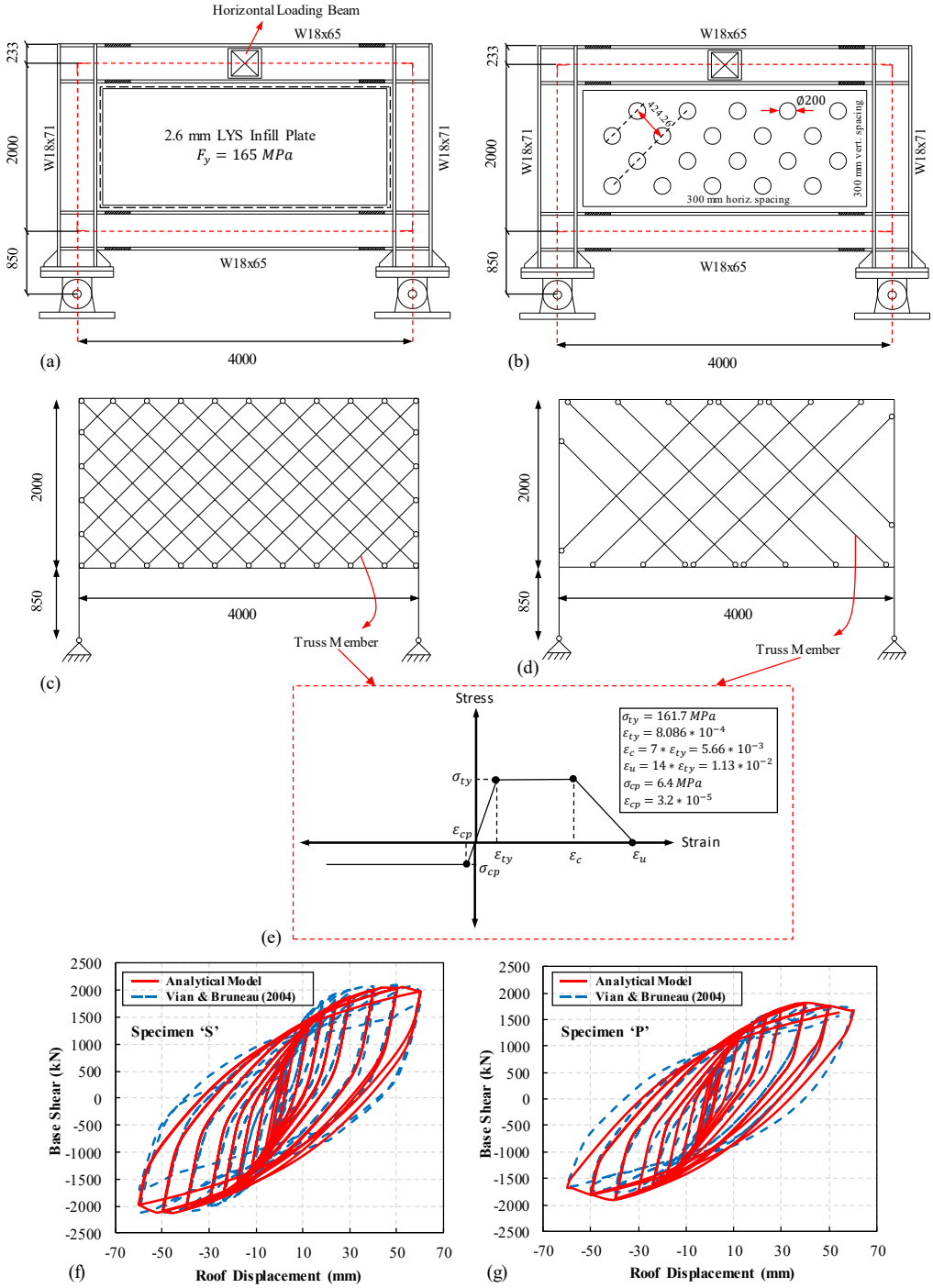

Fig. 5.4. Validation of numerical models: (a, b) General configuration of tested specimens; (c, d) developed analytical models; (e) assigned stress-strain relationship to strips; and (f, g) validation of numerical models for solid and perforated specimens

5.5 Selection of Solid and Perforated SPSWs

To assess the seismic performance of both perforated and solid SPSWs, a total of six multi-storey (4-, 7-, and 10-storey) steel shear walls (solid and perforated) were studied. The SPSW buildings are hypothetical residential buildings located in Vancouver, BC. The buildings, as shown in Fig. 5.5, have a square plan of 35 m x 35 m, with two unstiffened SPSWs in each direction to resist the lateral loads. The studied archetypes have equal storey height of 3.6 m and a bay width of 5 m.

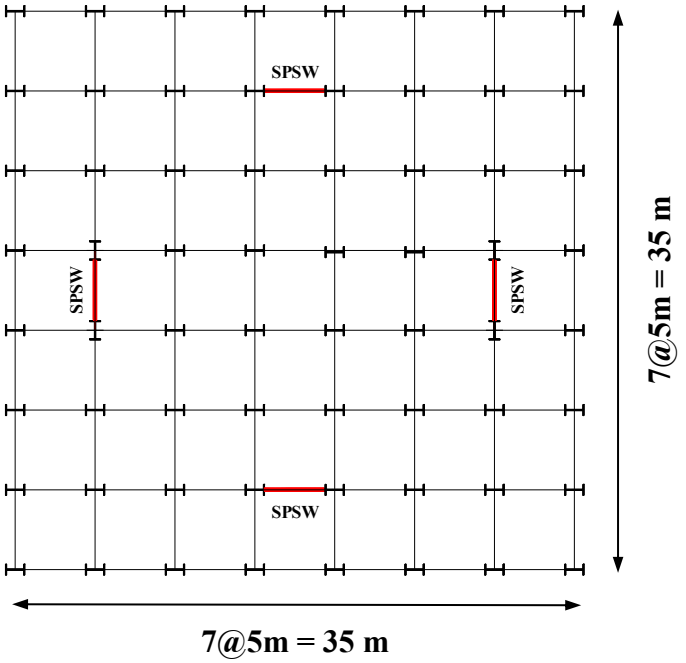

Fig. 5.5. Typical floor plan of the hypothetical SPSW building

The foundation of each building was assumed to be located on site class C. As per NBC (2015), site class C is the reference soil consisting of very dense soil or soft rock with an average shear wave velocity of 360-760 m/s, soil undrained shear strength greater than 100 kPa, and average standard penetration resistance of 50 or more. All archetypes were designed according to CSA S16-14 (CSA 2014) and NBC (2015). The yield stress for the boundary members and the infill plates was taken as 345 MPa and 235 MPa, respectively. A dead load of 4.1 kPa for each floor and 3.3 kPa for roof level were considered. A live load of 2.4 kPa was assigned to all stories

(other than roof level). A snow load of 1.64 kPa was calculated at the roof level. Seismic forces and storey shears for each archetype were calculated using the equivalent static force procedure presented in NBC (2015). An infill plate thickness of 2 mm was considered as the minimum thickness based on handling and welding considerations. In each storey, the total shear was assumed to be resisted by the infill plate only. As presented in AISC 341-16 (AISC 2016), the factored shear resistance for perforated infill plate with circular perforations was determined using Eq. (5.8):

$$V_r = 0.42\, F_y\, t\, L_{cf} \left(1 - \frac{0.7\, D}{S_{diag}}\right) \tag{5.8}$$

where V_r is the factored shear strength; F_y is the yield stress of the steel material; L_{cf} is the clear length of the infill plate between the VBE flanges; D is the perforation diameter; S_{diag} is the shortest center-to-center distance between the perforations.

Design of the surrounding boundary members were carried out using the capacity design method presented by Berman and Bruneau (2008). In the capacity design approach, a part of the system is defined as seismic fuse and is responsible for dissipating the energy due to external loads like earthquake. In SPSW system, the infill plate acts as the seismic fuse and experiences extensive inelastic deformation during the strong ground motions. Surrounding boundary members (beams and columns) are designed based on resulting inward forces due to yielding of the infill plate. When designing the boundary members, both stiffness and strength requirements must be satisfied. Stiffness requirement is intended to prevent excessive in-plane deformation of the boundary members so that a uniform tension field action can be developed in the infill plate. In order to ensure the stiffness adequacy for the surrounding boundary members, the following minimum moment of inertia for beams and columns, given in Eq. (5.9) and Eq. (5.10), respectively, are recommended.

$$I_b \geq 0.003\, \frac{\Delta t\, L^4}{h} \tag{5.9}$$

$$I_c \geq 0.00307\, \frac{t\, h^4}{L} \tag{5.10}$$

where I_b is the moment of inertia of the HBE; Δt is the difference in infill plate thicknesses above and below the HBE. Regarding the strength requirement, the boundary members must remain essentially elastic under expected yielding of the infill plate. Plastic hinges are also allowed at the end of HBEs as well as at the base of the columns. Table 5.1, Table 5.2, and Table 5.3 present the size of boundary members and the thicknesses of infill plate used in the selected solid and perforated SPSWs. In these tables, t_w is the thickness selected for the corresponding storey based on practical considerations and constructability point of view. $t_{w,req}$ is the required thickness for the corresponding storey, which is calculated based on the assumption that the whole storey shear is resisted by the infill plate.

Table 5.1. Selected boundary members and infill plates for both solid and perforated 4-storey SPSWs

Storey	$t_w\,(mm)$	$\frac{t_w}{t_{w,req}}$	HBE Section	VBE Section
4	2	2.44	W360x287	W360x421
3	2	1.33	W310x67	W360x463
2	2	1.03	W310x67	W360x463
1	3	1.38	W360x162	W360x592
0	NA	NA	W360x347	NA

Table 5.2. Selected boundary members and infill plates for both solid and perforated 7-storey SPSWs

Storey	$t_w\,(mm)$	$\frac{t_w}{t_{w,req}}$	HBE Section	VBE Section
7	2	2.35	W360x287	W360x509
6	2	1.2	W310x67	W360x592
5	3	1.3	W360x162	W360x634
4	3	1.05	W310x79	W360x634
3	4	1.23	W360x162	W360x634
2	4	1.14	W310x79	W360x634
1	4	1.1	W310x79	W360x900
0	NA	NA	W360x463	NA

Table 5.3. Selected boundary members and infill plates for both solid and perforated 10-storey SPSWs

Storey	$t_w\,(mm)$	$\frac{t_w}{t_{w,req}}$	HBE Section	VBE Section
10	2	2.15	W360x287	W1000x296
9	2	1.23	W310x67	W1000x371
8	3	1.34	W360x162	W1000x483
7	3	1.08	W310x79	W1000x554
6	4	1.23	W360x162	W1000x642
5	4	1.1	W310x79	W1000x642
4	4	1.02	W310x79	W1000x642
3	5	1.2	W360x162	W1000x748
2	5	1.15	W310x107	W1000x883
1	5	1.14	W310x107	W40x655*
0	NA	NA	W360x592	NA

* Imperial designation

Fig. 5.6 shows the elevation view of the studied P-SPSWs. In this study, similar to the P-SPSW tested by Vian and Bruneau (2004), circular openings of 200 mm diameter and a 300 mm center to center distance between the perforations were considered. In addition, based on the requirements of AISC 341-16 (AISC 2016), an edge distance between diameter (D) and ($D + 0.7S_{diag}$) was maintained from the boundary members to the perforations.

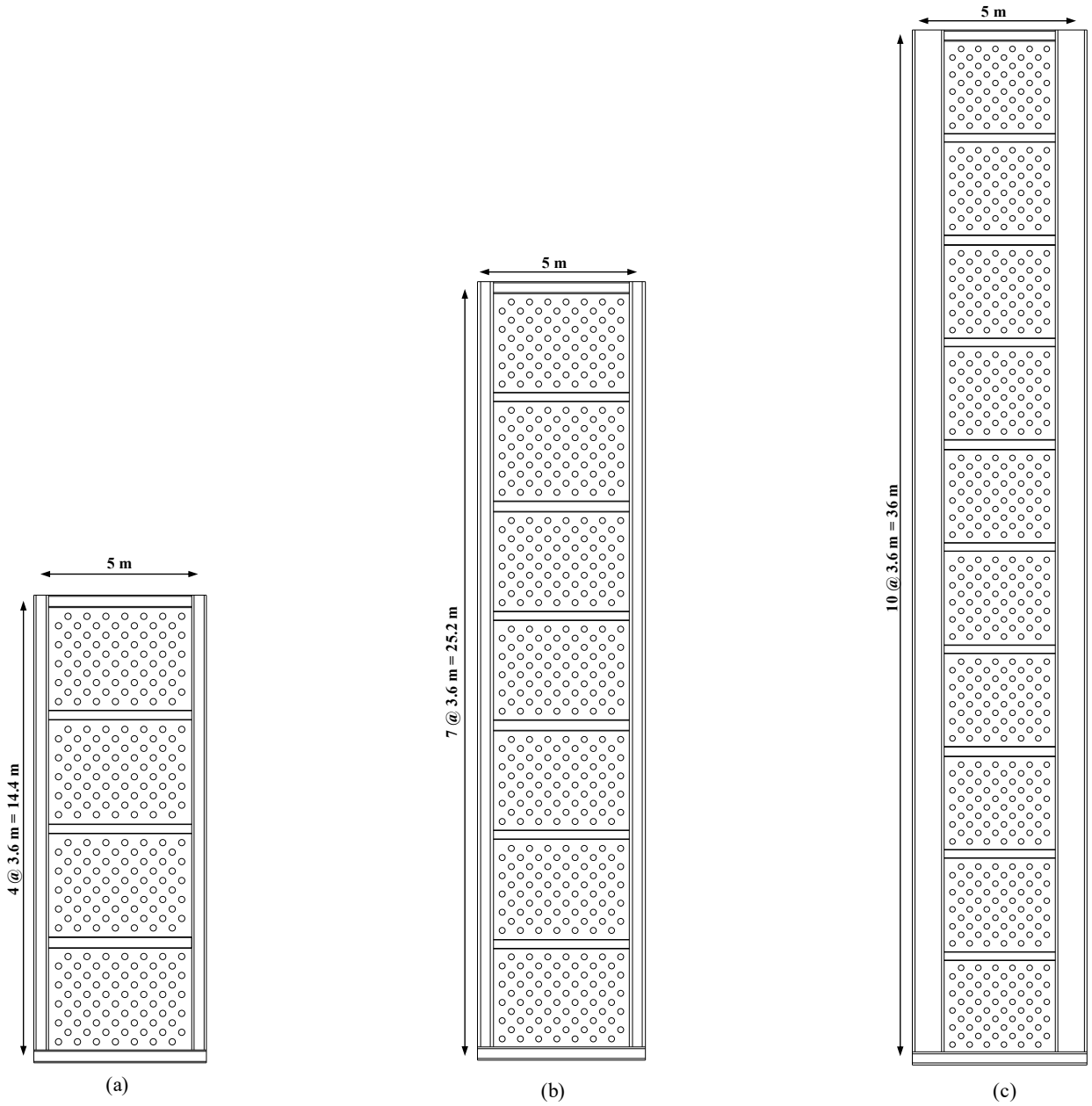

Fig. 5.6. Typical elevation view of studied P-SPSWs; (a) 4-storey; (b) 7-storey; (c) 10-storey

As shown in Fig. 5.7, the numerical model includes a gravity column in order to accurately capture the effect of gravity loads on the walls (Lignos and Krawinkler 2012). The gravity column is not a part of the lateral load resisting system, but its presence is vital to capture the destabilizing $P-\Delta$ effect associated with the gravity loads. In *Opensees*, elastic beam column (EBC) element was implemented to model the gravity column. The gravity column was designed not to provide any lateral stiffness to the SPSW system and had pinned support condition at the base. Truss members

were used in each storey level to connect the main system to the gravity column. To prevent any axial deformation in the truss members and to satisfy the requirements of the rigid links in connecting the system to the gravity column, the cross sectional area of the truss members was increased by 100 times of the largest HBE available in the model. All seismic masses were assigned to the P-SPSW by considering two equal concentrated mass at the right and left joints at every storey. The gravity load assigned to the gravity column were calculated based on the tributary area which is equal to the half of the plan area of the building, in which the tributary area of the P-SPSW is excluded.

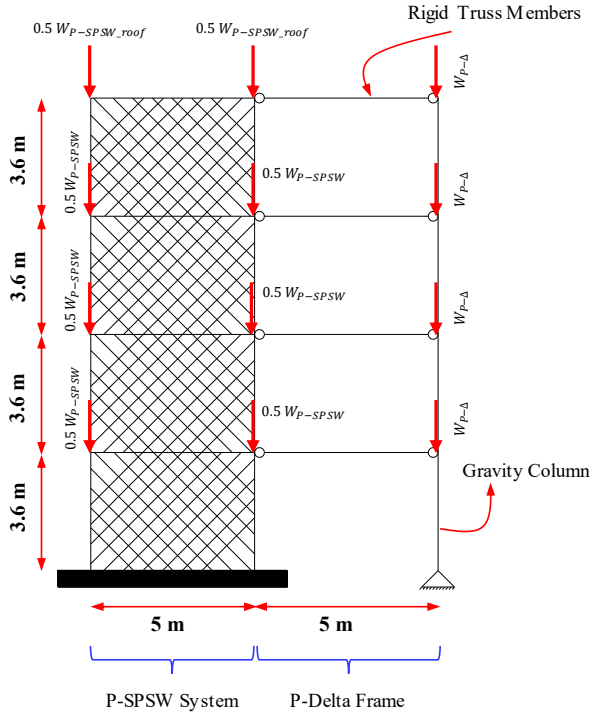

Fig. 5.7. Typical numerical model for 4-storey archetype

5.6 Analysis of Selected SPSW Archetypes

5.6.1 Nonlinear Static Pushover Analysis

To estimate storey shear and deformation capacity of both solid and perforated SPSWs, nonlinear pushover analysis was performed. The analysis was carried out using a lateral load pattern proportional to the fundamental mode shape. Fig. 5.8 shows base shear versus roof displacement for all studied archetypes. For pushover curves, normalized base shear and roof displacement are presented instead of absolute values. Base shear was normalized based on design base shear and roof displacement was normalized with respect to building's height.

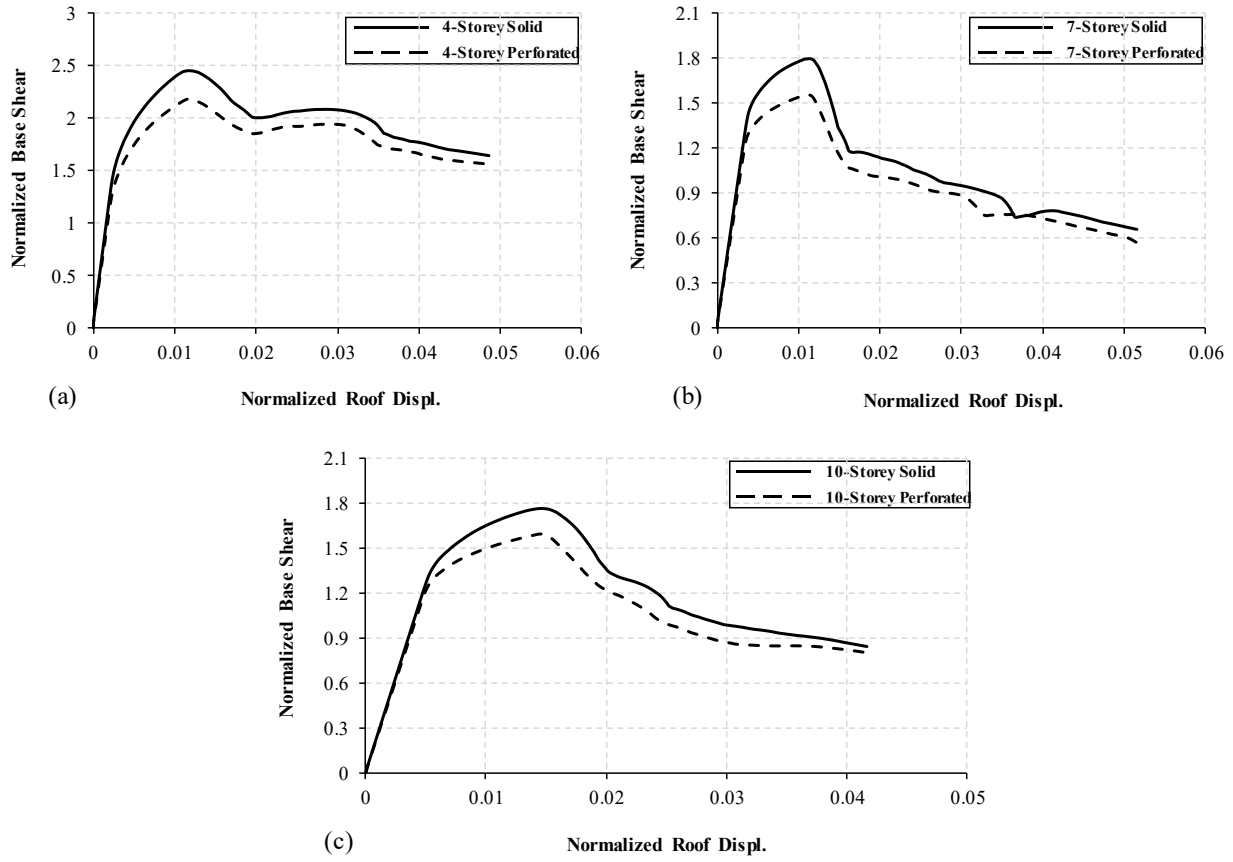

Fig. 5.8. Monotonic pushover analysis results for selected SPSWs

From comparison of the pushover curves (capacity curves), it is observed that the initial stiffness of both archetypes (solid and perforated) are almost identical. However, the lateral load capacity of the P-SPSW system is decreased. For the selected perforated SPSWs, reduction in

lateral load capacity was around 11%, 13.5%, and 9.7% in 4-, 7-, and 10-storey, respectively. Thus, adding perforations to the infill plate did not significantly affect the lateral load capacity of the SPSW system. Overstrength of the structure, Ω, and period-based ductility, μ, are two important parameters that can be derived directly from pushover analysis. Overstrength factor, given in Eq. (5.11), is defined as the ratio of maximum base shear (V_{max}) obtained from pushover analysis to the design base shear (V_d) calculated from the equivalent static force procedure.

$$\Omega = \frac{V_{max}}{V_d} \tag{5.11}$$

As shown in Table 5.4, overstrength factors are calculated for all archetypes. The 4-storey archetypes had larger overstrength factor. This was because of selection of higher than required infill plate thickness. For all P-SPSW archetypes, circular perforations in the infill plate slightly reduced the overstrength factor. Period-based ductility, μ, defined in Eq. (5.12), is the ratio of ultimate roof displacement (δ_u) to the roof yield displacement ($\delta_{y,eff}$).

$$\mu = \frac{\delta_u}{\delta_{y,eff}} \tag{5.12}$$

Ultimate roof displacement was calculated from the pushover analysis results. This is the displacement when the maximum base shear is reduced by 20%. The roof yield displacement was obtained based on the following formula:

$$\delta_{y,eff} = C_o \frac{V_{max}}{W} \left[\frac{g}{4\,\pi^2}\right] [\max(T, T_1)]^2 \tag{5.13}$$

where C_o is a coefficient which relates the spectral displacement of an equivalent single degree of freedom (SDOF) system to the roof displacement of the multi degree of freedom (MDOF) system according to ASCE 41-06 (ASCE 2006); $\frac{V_{max}}{W}$ maximum normalized base shear; g = gravity constant; T = fundamental period of the structure based on empirical formula; T_1 = fundamental period of the structure obtained from eigenvalue analysis in *OpenSees*.

As shown in Table 5.4, period-based ductility in perforated archetypes are higher than the solid ones. This was due to early yielding of the perforated SPSW which increased the period-based ductility. It should be noted that all studied archetypes exhibited stable performance and high level of ductility during nonlinear static pushover analysis.

Table 5.4. Summary of the results taken from pushover analysis

Archetype	$\delta_{y,eff}(mm)$	$\delta_u\,(mm)$	μ	$V_d\,(kN)$	$V_{\max}\,(kN)$	Ω
4-storey solid	44.6	496	11.1	1049.4	2578	2.46
4-storey perforated	39.7	503	12.7	1049.4	2292.2	2.18
7-storey solid	74.4	363	4.88	1755.2	3156	1.8
7-storey perforated	64.3	357	5.55	1755.2	2726.6	1.55
10-storey solid	114.66	699	6.1	2119.2	3735	1.76
10-storey perforated	107.18	683	6.37	2119.2	3371.9	1.59

5.6.2 Nonlinear Time History Analysis

All designed archetypes were subjected to a group of 44 artificial ground motions that were developed for western Canada by Atkinson (2009). These ground motions included far field records with two different magnitudes, $M = 6.5$ and $M = 7.5$. The selected earthquake records and their main characteristics like magnitude, M, closest distance to fault rupture, R_{fault}, peak ground acceleration, PGA, and the ratio of maximum velocity to maximum acceleration, v/a, are presented elsewhere (Farahbakhshtooli and Bhowmick 2019). Before conducting time history analyses, all ground motions were scaled using the methodology addressed by ASCE/SEI 7-16 (ASCE 2016).

Nonlinear time history analyses of the selected solid and perforated SPSWs were conducted with the scaled earthquake records. Fig. 5.9 shows seismic shear demand in every storey for all the selected solid and perforated SPSWs. The 16th and 84th percentiles of the responses are also shown in this figure. Fig. 5.10 compares the median shear envelopes of solid and perforated SPSWs. As shown in Fig. 5.10, median shear envelope in perforated SPSW is slightly less than the solid one in all studied archetypes. Median base shear was calculated as 2498 kN and 2248 kN for 4-storey solid and perforated SPSWs, respectively. The maximum reduction in the shear demand due to perforations was around 10%. Similar trend was observed in the 7- and 10-storey

archetypes where the maximum reduction in the shear demand was around 10% and 8% in 7- and 10-storey perforated SPSWs, respectively.

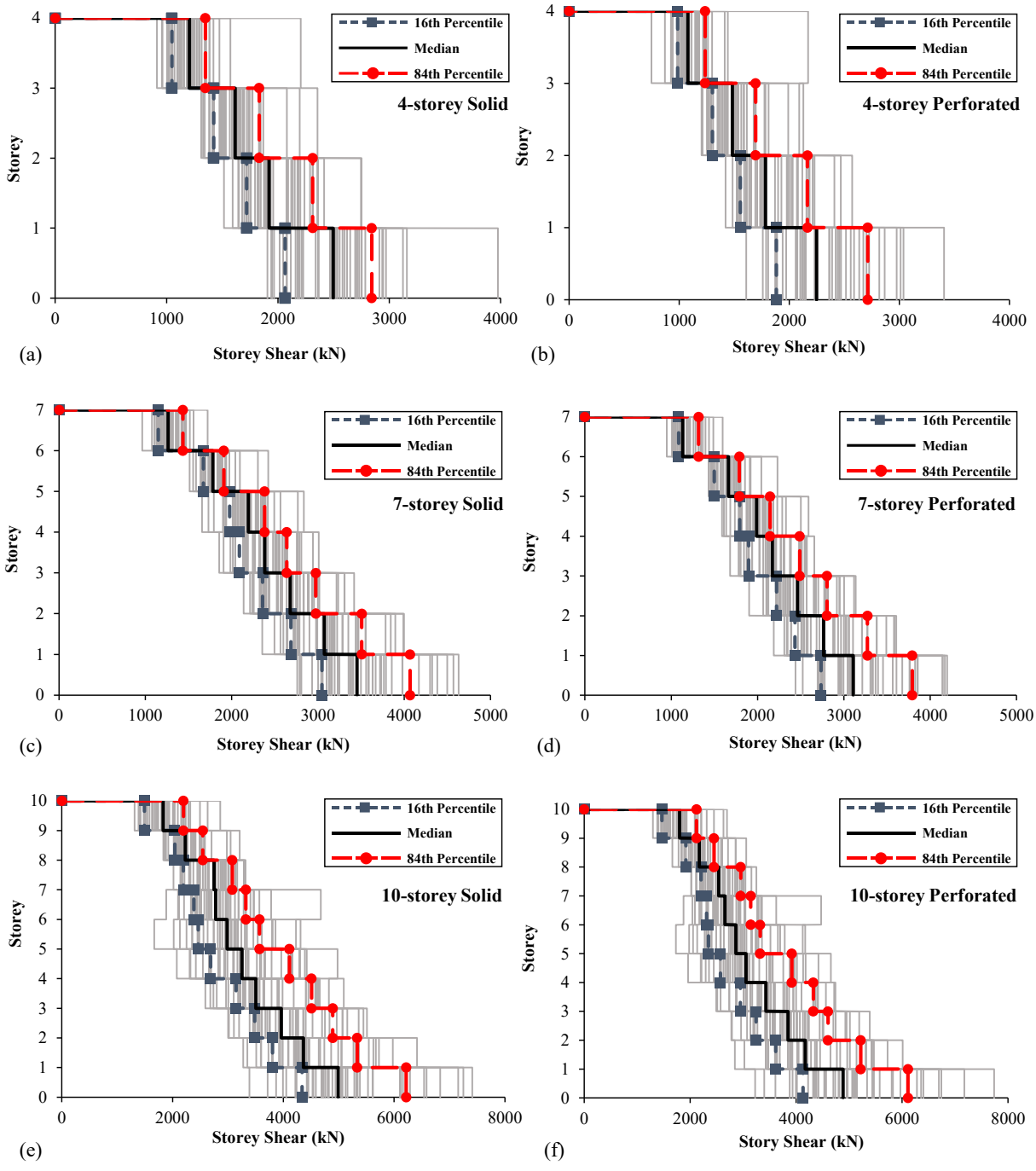

Fig. 5.9. Shear envelopes of SPSWs (solid and perforated) subjected to ground motions

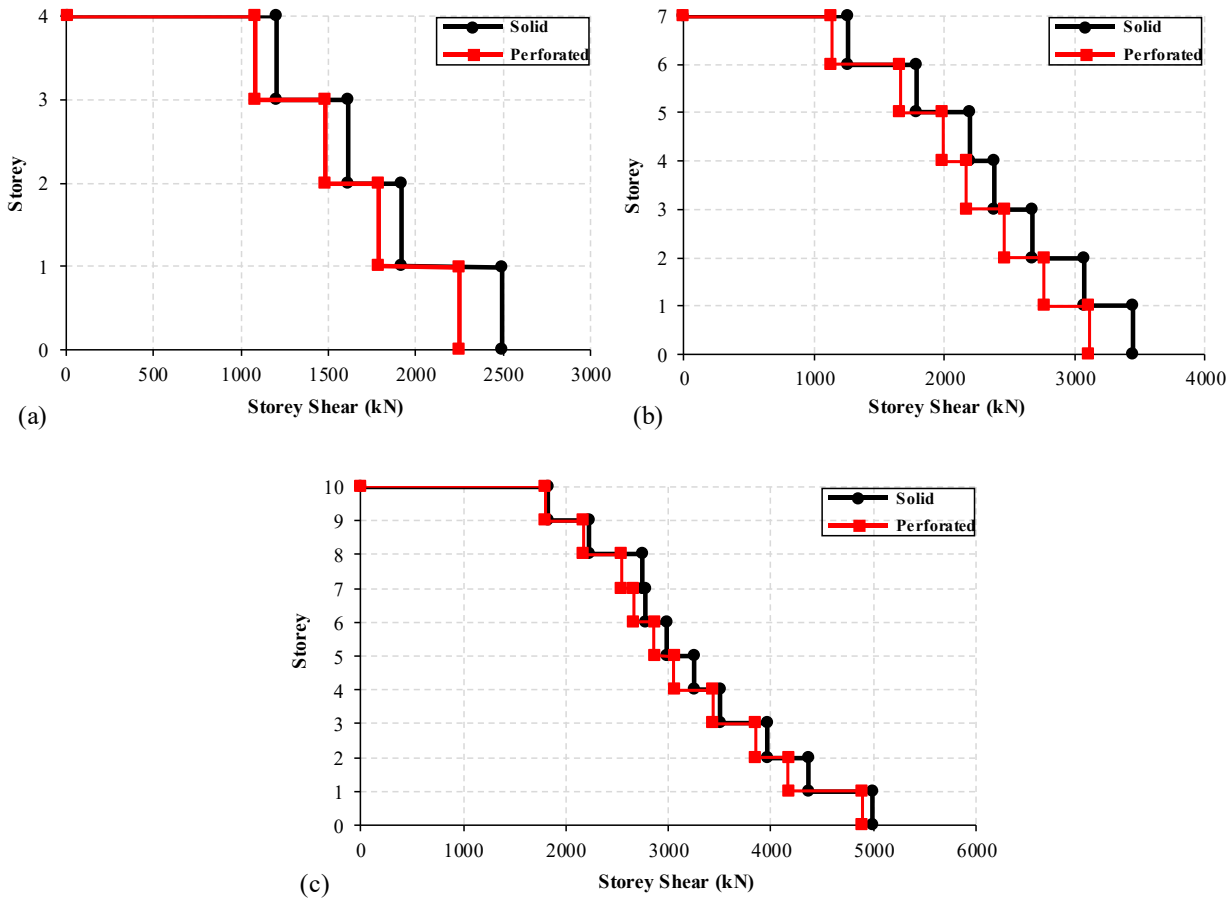

Fig. 5.10. Comparison of median shear envelopes of solid and perforated SPSWs

Seismic envelopes for axial force and bending moment for the boundary columns were obtained for all SPSWs, Fig. 5.11 shows only the results of 7-storey solid and perforated SPSWs, where the envelope of peak column axial forces and peak column bending moments (which do not necessarily occur simultaneously) are indicated. The results are compared with the design values calculated based on capacity design principle. By comparing the median responses with the design values for both column axial force and bending moment, it is understood that the capacity design method proposed by Berman and Bruneau (2008) to size the surrounding boundary members is able to accurately estimate the demand on the surrounding boundary members since the design values are larger than the median values calculated for peak column axial forces and bending

moments. Due to the variation of responses under individual ground motions, the median responses were used for comparison between solid and perforated specimens.

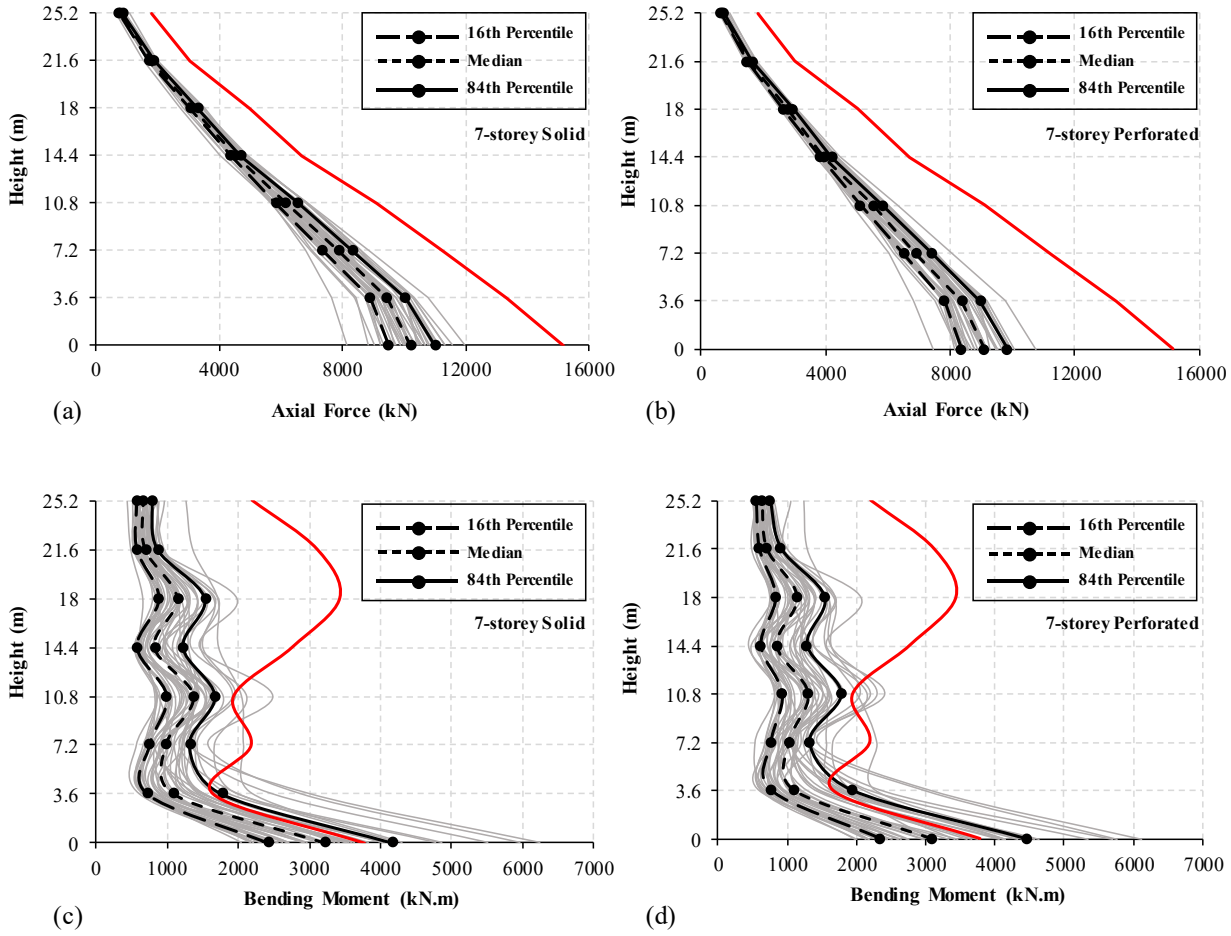

Fig. 5.11. Peak column axial forces and bending moments for 7-storey archetypes (solid and perforated)

Fig. 5.12 presents the median peak column moments in each storey extracted from nonlinear time history analysis. As shown in Fig. 5.12, the median responses are identical in both solid and perforated SPSWs in all studied archetypes. The results showed that adding perforations to the studied archetypes did not reduce the bending moment demand on columns. As discussed in section 5.3.2, typical diagonal strips that are used to model the perforated infill plates do not necessarily coincide at the beam levels. The similar pattern can also be observed in columns since strips are created in two perpendicular directions due to the cyclic nature of the earthquake load. Because of the distance between staggered points, extra bending moments will be added to the existing bending moments acting on columns in perforated SPSWs. The extra bending moments

developed at several locations along the height of the column will compensate the decrease in demand due to perforation in the system.

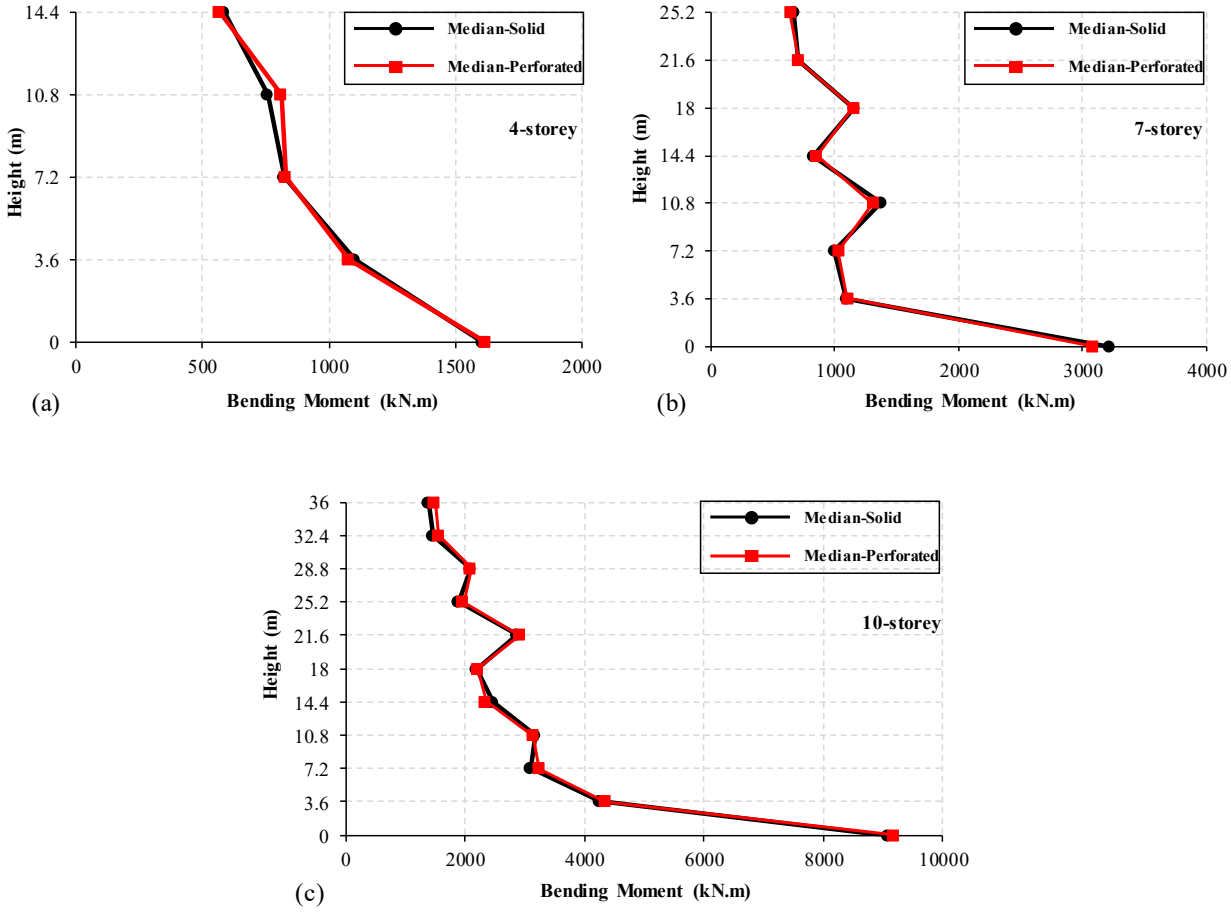

Fig. 5.12. Comparison between median peak column bending moments for solid and perforated SPSWs

However, decrease in demand on the surrounding columns were observed for axial forces (Fig. 5.13). Fig. 5.13 compares the median peak axial forces in each storey for both solid and perforated SPSWs. The maximum reduction of axial force demand was 14.2%, 14.1%, and 8.5% in 4-, 7-, and 10-storey P-SPSWs, respectively.

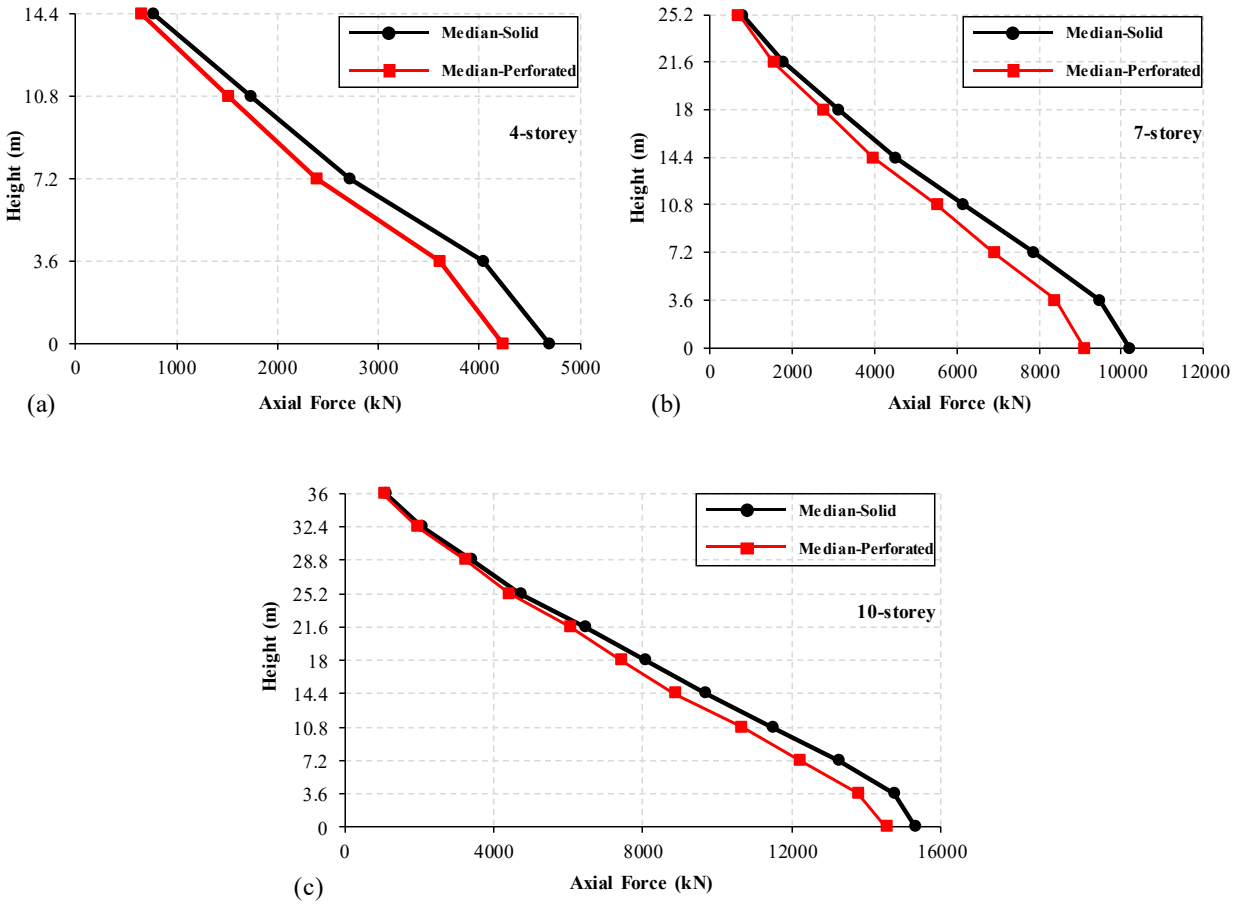

Fig. 5.13. Comparison between median peak column axial forces for solid and perforated SPSWs

As discussed earlier, Fig. 5.9 presents the shear envelope (storey shear) for all studied archetypes. To calculate the contribution of each component (i.e., infill plates and boundary columns) in resisting the storey shear in each level, maximum shear carried by each component during each ground motion was divided by the maximum storey shear resulted from corresponding ground motion. Since each archetype was subjected to 44 ground motions, there were 44 data in every storey. Thus, the results are shown in the form of boxplot (Fig. 5.14). As shown in Fig. 5.14, the box indicates the interquartile range (Q1-Q3), which starts from the first quartile and finishes at the third quartile. The small solid line inside the box represents the median of data and the two solid lines located outside of the box shows the lower and upper bounds of data that were recorded in the corresponding storey. As observed from Fig. 5.14, for solid SPSW archetypes, the contribution of infill plate in resisting the storey shear is higher than the corresponding value in

the boundary columns. This is an obvious trend in all solid SPSW archetypes in all stories except the first level of the 10-storey SPSW where the contribution of boundary columns is higher than the infill plate. On the contrary, the contribution of boundary columns is higher than the infill plate in resisting the storey shear in most of the stories in P-SPSW archetypes. As discussed earlier, the maximum reduction in shear demand due to perforations was around 10%, which is not a significant reduction in the demand. On the other hand, as given by Eq. (5.8), the factored shear strength of a perforated infill plate is reduced by a factor of $(1 - \frac{0.7D}{S_{diag}})$ in comparison to a similar solid infill plate. Thus, for perforation diameter (D) of 200 mm and for a shortest center-to-center distance between the perforations (S_{diag}) of 424.26 mm, a reduction factor of 0.67 should be obtained. This means that the capacity of the perforated infill plate should be reduced by 33%. However, the maximum shear demand reduction observed for the selected P-SPSWs was about 10%. The difference between the demand and the capacity of storey shear in perforated SPSWs can be attributed to the increased shear contributions by the boundary members. This is why the

contribution of boundary members in resisting storey shear was higher than the infill plate in most of the stories in P-SPSWs.

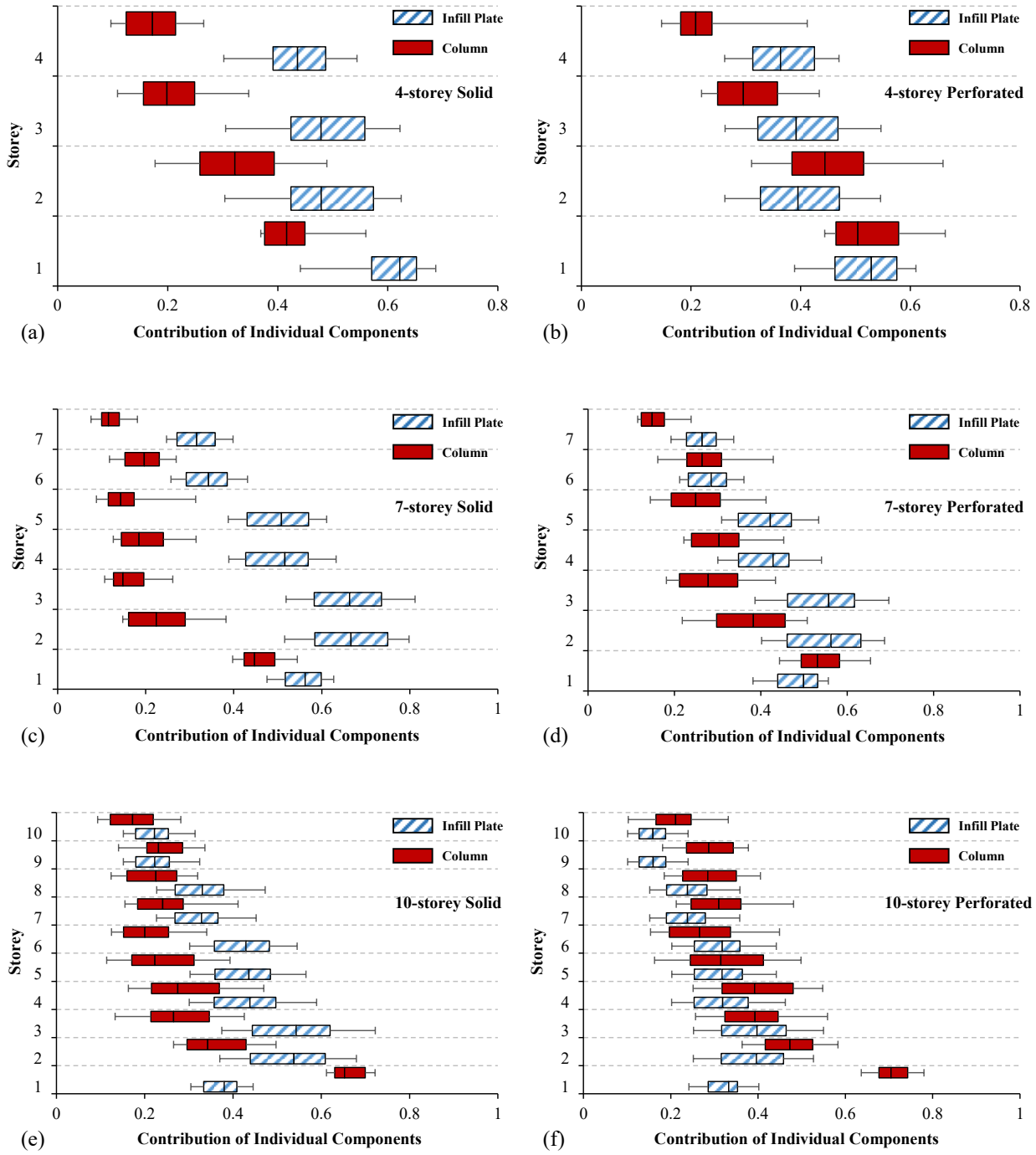

Fig. 5.14: Maximum contribution of storey shear in infill plates and columns

5.7 Sensitivity Assessment

Purba and Bruneau (2009) assessed the behavior of several individual perforated strips using ABAQUS (2003). They showed that there is no interaction between adjacent strips that could affect the stress distribution in each strip. In other words, each strip performs independently. Thus, it was proposed that the hole diameter be less than 60% of the strip width ($\frac{D}{S_{diag}} \leq 0.6$). In this study, a sensitivity assessment is carried out to evaluate the sensitivity of several responses (i.e., peak column axial force, peak column bending moment, and maximum interstorey drift) to the variation of hole diameter in the studied archetypes. For the sensitivity assessment, the strip width was kept a constant value of 424.26 mm, which is identical to the aforementioned studied three P-SPSWs. Perforation diameter was varied from 50 mm to 250 mm with an increment of 50 mm. Maximum diameter of 250 mm was chosen so that the proportion of hole diameter to strip width remained less than 0.6 ($\frac{250}{424.26} = 0.59$), as suggested by the standards (AISC 341-16; CSA S16-14). Thus, for each archetype, 6 variant models were developed with diameter from 0 mm (solid SPSW) to 250 mm. In each variant model, the area of strip was modified based on the hole diameter. In total, 18 variant models were developed for all studied archetypes (4-, 7-, and 10-storey archetypes). Each variant model was subjected to the same set of 44 artificial ground motions that were introduced in section 5.6.2. Peak column axial forces, peak column bending moments, and maximum interstorey drifts were recorded from seismic analyses for all variant models. For comparison, the median responses were selected to assess the sensitivity of each variant model to the variation in hole diameter. Fig. 5.15 presents the median peak axial forces in columns for all studied archetypes. As clearly observed, in all buildings, by changing the perforation diameter from 0 mm to 250 mm, axial force demand on columns decreases in all stories. Furthermore, reduction in axial force demand was more obvious in the lower stories than the upper stories. In the first storey, near the base, the reduction in axial force demand in column was 13.8%, 16.8%, and 9.5% in the 4-, 7-, and 10-storey archetypes, respectively, when the hole diameter was increased from 0 mm to 250 mm. Thus, perforations are suitable alternative to reduce the axial force demand on the surrounding boundary members.

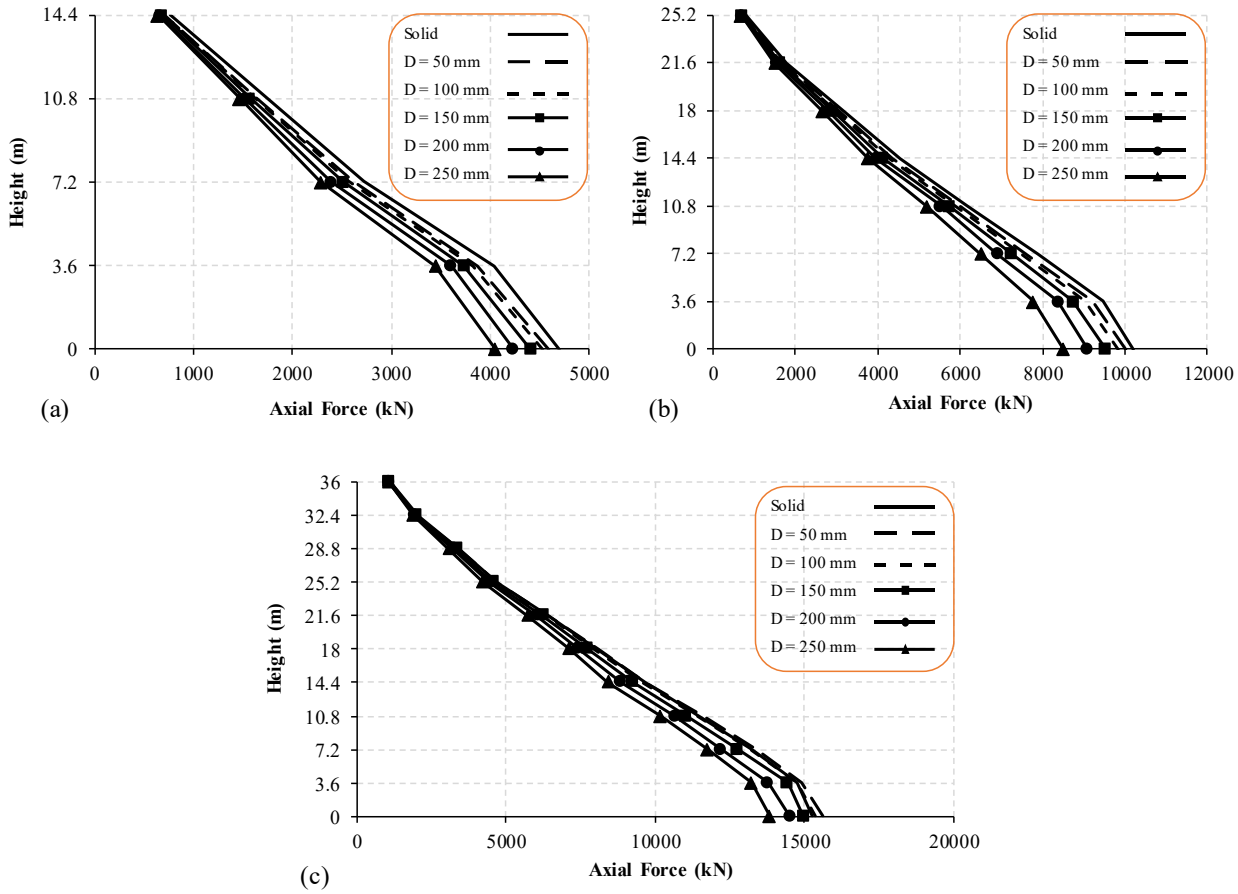

Fig. 5.15. Median peak column axial forces in each storey for different perforation diameter: (a) 4-storey; (b) 7-storey; (c) 10-storey

As shown in Fig. 5.16, the flexural (bending moment) demand in the columns was approximately same for all perforation diameters. Thus, the hole diameter does not have any effect on the bending moment demand of columns due to seismic excitations.

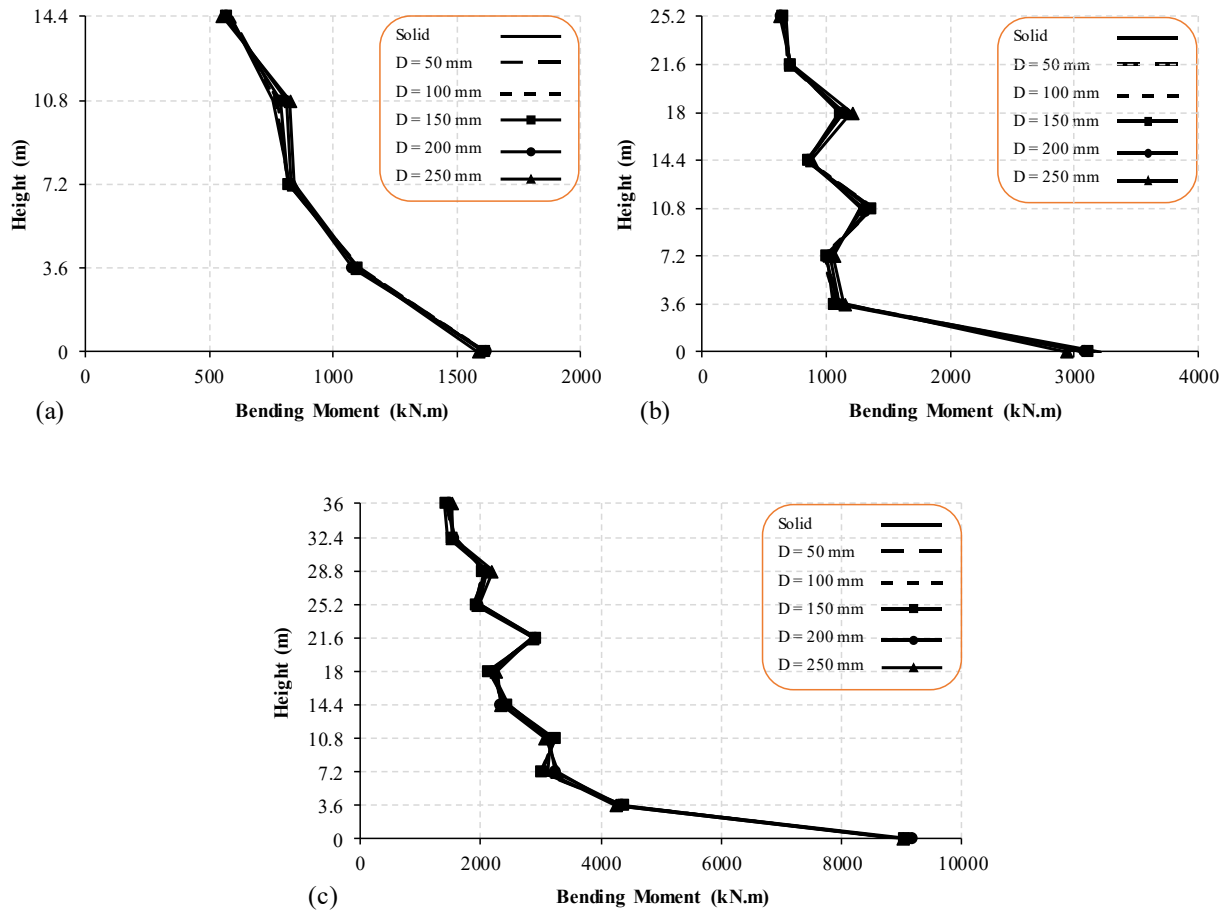

Fig. 5.16. Median peak column bending moments in each storey for different perforation diameter: (a) 4-storey; (b) 7-storey; (c) 10-storey

Past studies conducted on solid SPSWs showed that SPSW system is capable of controlling interstorey drifts during strong ground motions since the infill plate provides sufficient stiffness to the whole SPSW system. In the case of P-SPSW, due to perforations, the stiffness and strength of the system decrease and thus can lead to higher interstorey drift values than the solid infill plate. In performance-based earthquake engineering, interstorey drift is an important indicator in estimating the extent of damage to structural components and to assess the overall condition of the structure after earthquake excitation. In order to investigate the effect of hole diameter on the interstorey drift, the hole diameter was varied from 0 mm to 250 mm, with a 50 mm increment. Fig. 5.17 shows the variation in median maximum interstorey drift for different hole diameter. For all archetypes, the interstorey drift increases when the hole diameter is increased from 0 mm to 250 mm. NBC (2015) suggests interstorey drift limit of 2.5% to ensure the life safety of residents

during and after strong ground motions. As shown in Fig. 5.17, all studied variant models, even archetypes with 250 mm hole diameter, experienced interstorey drifts significantly smaller than the code limit. This highlights the suitability of both solid and perforated SPSWs in controlling the interstorey drift during strong ground motions.

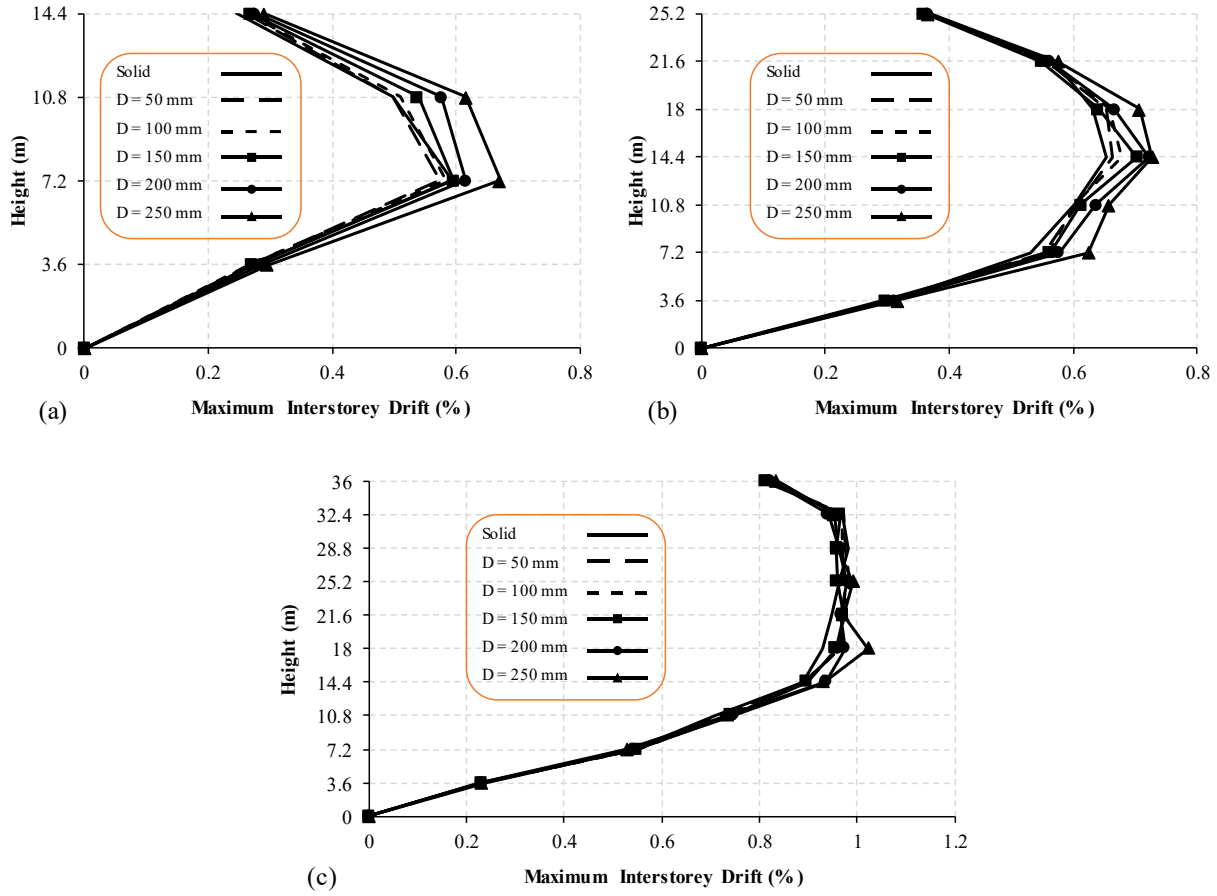

Fig. 5.17. Interstorey drift variation for different perforation diameter: (a) 4-storey; (b) 7-storey; (c) 10-storey

5.8 Conclusion

Nonlinear seismic performance of six code designed SPSWs (4-, 7-, and 10-storey) (solid and perforated) were assessed in this study using monotonic pushover and time history analyses. A macro-model was developed based on the strip model for solid infill plate. Then, the developed macro-model was modified to be applicable for perforated SPSWs by considering the effect of perforations on the area of each strip. The accuracy of the adopted modelling approach was validated against both solid and perforated SPSW tests. Results from this study are as follows:

● Monotonic pushover analyses showed stable and ductile behavior of both solid and perforated SPSWs. It was also observed that circular perforations in the infill plate can slightly reduce the overstrength of the SPSW system.

● As observed from nonlinear time history analyses, maximum reduction in shear demand in SPSWs due to circular perforations was 10%, 10%, and 8% in 4-, 7-, and 10-storey SPSWs, respectively.

● Median peak column axial forces and bending moments obtained from nonlinear time history analyses were smaller than the design values and this shows the accuracy of the adopted procedure to size the surrounding boundary members. In addition, holes in the infill plates reduced the axial force demand acting on the boundary columns, but they did not considerably affect the bending moment demand of the columns.

● Maximum contribution of each individual component in resisting storey shear resulting from seismic excitations indicated that in solid SPSWs, the contribution of infill plates was higher than those for boundary members in all stories except the first storey of 10-storey building. Conversely, contribution of boundary members was higher than those for infill plates in perforated SPSWs. Thus, when the capacity of the perforated infill plate was reduced by 33%, shear demand of the P-SPSW system was only reduced by about 10%. The boundary members compensated for the difference between demand and capacity.

● Results from sensitivity assessment showed that variation of hole diameter from 0 mm to 250 mm did not affect the bending moment demand on the surrounding boundary columns, but it reduced the axial force demand on the columns. Also, maximum interstorey drift increased when

the hole diameter was changed from 0 mm to 250 mm, in both 4- and 7-storey archetypes; however, the changes in interstorey drift was not considerable in the selected 10-storey building. In addition, all archetypes (solid and perforated) satisfied the requirement of NBC (2015) to ensure the life safety of residents during seismic excitations by having less than 2.5% of interstorey drift in all levels.

Chapter 6
Summary, Conclusions, and Recommendations for Future Work

6.1 Summary

The purpose of current study was to investigate the seismic response of steel shear walls by focusing on developing macro-models to simulate the behavior of unstiffened (solid and perforated), stiffened, and composite SPSWs. To the best of the author's knowledge, very limited numerical studies have been carried out to develop macro-models for stiffened and composite SPSWs. Proposed analytical models were verified against available experimental results. Several multi-storey SPSWs were designed and the nonlinear behavior was assessed through conducting a series of nonlinear analyses such as pushover, time history, and IDA. A collapse risk assessment for stiffened and composite SPSWs were performed to extract the collapse capacity of the systems.

Past studies has shown that infill plate thickness requirement for SPSW (i.e., solid unstiffened, stiffened, and composite) to resist storey shear is usually low, especially in low-to-mid-rise buildings. From constructability point of view, it is often observed that the minimum plate thickness used in construction is larger than the required infill plate thickness. When larger than required infill plate thickness is used, the demand on surrounding boundary members will increase significantly and consequently will increase the sizes of boundary members. One of the solutions is to use regularly-spaced circular perforations. In this study, a macro-model was developed to simulate the performance of perforated SPSW which takes into account the area reduction in each strip due to the existence of perforation.

The numerical studies included the followings:

- Develop an analytical model to simulate the performance of traditional and innovative C-PSWs. The proposed model is capable of considering both functions (i.e., adding to strength and stiffness as well as providing a brace to prevent out-of-plane buckling) of RC panel.

- Assess the suitability of implementing ductility-related force modification factor, R_d, of 5 and overstrength-related force modification factor, R_o, of 1.6 for designing of stiffened and composite SPSWs since these two factors are originally proposed for unstiffened SPSWs. The assessment was performed using the performance evaluation given by FEMA P695 (FEMA 2009).
- A series of sensitivity assessments were carried out on variation of two parameters in infill plate (i.e., ductility capacity ratio, and post-cap stiffness ratio) and three parameters in RC panel (i.e., yield point, shear strain correspond to maximum shear stress, and residual stress) to assess the overall sensitivity of the structure to the changes of aforementioned parameters.
- Performing monotonic pushover analyses on both solid and perforated SPSWs to estimate the percentage of reduction in maximum strength due to perforation.
- Compare the demand on surrounding boundary members (i.e., axial force and bending moment) with the design values resulting from capacity design method as well as capturing different responses of the structure such as maximum interstorey drift and variation of shear storey along the height of the building.
- Performing a series of sensitivity analysis to assess the effect of variation in hole diameter on overall response of the structure such as axial force demand, bending moment demand, and maximum interstorey drift.

6.2 Conclusion

The main findings of the research are categorized in three subsections for stiffened, composite, and perforated SPSWs, respectively.

6.2.1 Conclusions obtained for stiffened SPSWs

This section presents the conclusions drawn from the stiffened SPSWs:

- Macro-modelling approach proposed for simulating the behavior of stiffened SPSWs provided a good agreement with experimental results. Yield point, capping point, pinching,

and degradation backbone curve until the end of the experiment were captured precisely by the developed numerical model.

- Performance evaluation of studied archetypes was carried out using the procedure given by FEMA P695 (FEMA 2009). All studied archetypes showed stable and reliable performance under strong ground motions. The median collapse capacity resulted from IDA analysis was implemented to calculate adjusted collapse margin ratio. Calculated adjusted collapse margin ratios were significantly higher than the allowable limit given by FEMA P695. Based on the results, it is suggested to use ductility-capacity force modification factor, R_d, of 5 and overstrength-related force modification factor, R_0, of 1.6 for designing of stiffened SPSWs.
- Maximum contribution of individual structural components (i.e., infill plate and boundary columns) in resisting applied lateral forces showed that a significant portion of storey shear, in some cases as high as 70%, is resisted by boundary columns. Current design approach assumes the total shear be resisted by the infill plate. This assumption will lead to more stable performance by providing a reliable backup system, which is ductile moment resisting frame, for primary load carrying component (i.e., infill plate).
- A series of sensitivity analyses were performed on variation of two post-yielding parameters (i.e., ductility capacity and post-cap stiffness ratio). The results indicated that the median collapse capacity of the system is more sensitive to variation of ductility capacity. It was observed that variation of ductility capacity from 5 to 30 caused a significant increase in the capacity of the system (up to 60.2 % in 13-storey stiffened SPSW), while the variation of post-cap stiffness ratio from 0.05 to 0.3 caused a maximum capacity reduction of 16.5%, which was observed in 13-storey stiffened SPSW system. This shows the lower level of participation from post-cap stiffness variation on overall performance of the stiffened SPSW system in comparison to ductility capacity changes.

6.2.2 Conclusions obtained for C-PSWs

- The proposed deterioration model for C-PSW was shown to provide a very good prediction of the cyclic behaviour of the available tests. Thus, elements and the modelling considerations adopted in this study are able to capture all essential features of the behavior of C-PSWs.

- Reinforced concrete panel was modelled using displacement-based fiber element by locating a spring in the middle of the element which enable the element to consider the shear-dominated behavior of the RC panel. Cyclic behavior of RC panel was in good agreement with the experimental results which validates the accuracy of the RC modelling in both adding to the stiffness and strength of the whole system as well as providing a brace to prevent out-of-plane buckling of the infill plate.
- Inelastic dynamic analyses showed that boundary columns resist a significant portion of the storey shear. The contribution of boundary columns is not considered in the current design procedure of C-PSWs. It is expected that the extra strength and stiffness contributions of columns will provide a valuable back up to the infill plate, which is the main fuse of the C-PSW system. On the other hand, maximum participation of the RC panel in resisting storey shear was less than 10% in all archetypes.
- Similar to stiffened SPSWs, all studied C-PSWs (traditional and innovative) were subjected to IDA analysis to extract the median collapse capacity of the system. Collapse margin ratio was calculated based on the median collapse capacity to assess the performance of the studied archetypes. Calculated CMR values indicated that all studied archetypes provide significant safety margin against collapse.
- Three post-cracking parameters (i.e., yield point, shear strain correspond to maximum shear stress (γ_{max}), and residual stress) were chosen to assess the sensitivity of C-PSWs to variation of these parameters. γ_{max} has the most effect on the variation of median collapse capacity of C-PSWs. Thus, when γ_{max} was increased from 0.015 to 0.2, increase in MCC for 7-, 10-, and 13-storey C-PSWs were 14%, 10.8%, and 10%, respectively. On the other hand, maximum change in the MCC due to change in values of the two other post-cracking parameters, yielding shear strain and residual stress, was less than 5% in all cases.
- Sensitivity analysis showed that a trilinear model rather than a quadlinear one can be used to simulate the shear behavior of the RC panel. This will reduce the complexity level of the proposed model and decrease the required time to analyze C-PSW buildings.
- The results of sensitivity assessment indicated that the variation of residual stress between 0% to 20% does not significantly affect the capacity of the whole system (less than 5%). Thus, it is recommended to use 20% residual stress in shear behavior for the spring in the

RC panel to account for shear aggregate interlock, which might occur at ultimate condition due to friction between different parts of the crushed RC panel.

6.2.3 Conclusions obtained for perforated SPSWs

Nonlinear seismic performance of six code designed SPSWs (4-, 7-, and 10-storey) (solid and perforated) were assessed in this study using monotonic pushover and time history analyses. Results from this study is as follow:

- Monotonic pushover analyses showed stable and ductile behavior of both solid and perforated SPSWs. It was also observed that circular perforations in the infill plate can slightly reduce the overstrength of the system.
- Results of nonlinear time history analysis indicated that maximum shear demand reduction due to perforation in SPSWs was around 10%, 10%, and 8% in 4-, 7-, and 10-storey SPSWs respectively.
- Peak column axial forces and bending moments obtained from nonlinear time history analysis were compared with design values which were calculated using capacity design method. The results indicated that the median of peak column axial forces and bending moments are smaller than design values which confirmed the accuracy of adopted procedure to size the boundary members.
- Maximum contribution of infill plates and boundary columns in resisting the storey shear was calculated for both solid and perforated SPSWs. In solid SPSWs, the contribution of infill plates was higher than boundary columns (except the first storey of 10-storey archetype) while in perforated SPSWs, contribution of boundary columns were higher than those for infill plates. By calculating the shear strength of perforated SPSW and compare it with solid SPSW, it was observed that the capacity of the perforated infill plate was reduced by 33% while shear demand of the P-SPSW system was only reduced by about 10%. Thus, in the case of severe ground motions and yielding of perforated infill plate, the boundary members compensated for the difference between demand and capacity.

- Sensitivity assessment was performed to assess the variation in axial force and bending moment (acting on boundary columns) when hole diameter was changed from 0 (solid infill plate) to 250 mm. Results showed that the peak column axial force decreased when hole diameter increased. On the other hand, variation in hole diameter does not affect the column's bending moment demand. As previously discussed, Because of the distance between staggered points, extra bending moments will be added to the existing bending moments acting on columns in perforated SPSWs. The extra bending moments developed at several locations along the height of the column will compensate the decrease in demand due to perforation in the system.

6.3 Recommendations for Future Research

The conclusions of current study were limited to the parameters that were being analyzed and tested. However, to further expand the knowledge in this field, other parameters may be considered. Thus, several recommendations for future research works are list as following:

- Innovative C-PSW is known as a smart structure. Smart structures have a distinguished feature which is not available in common structures. The gap exists between RC panel and surrounding boundary members is an adjustable parameter which can significantly affect the overall performance of the structure. Thus, sensitivity assessment can be carried out on variation of gap to find the optimum gap to reach the best performance in the system.
- The macro-scale performance of unstiffened SPSWs with a circular perforation in the center of the infill plate is not established yet. This is due to complexity of stress distribution in infill plate especially around the perforation. Proposing an analytical model which can simulate the real behavior and true inward forces acting on surrounding boundary members can have a significant impact in understanding the behavior of the system in both component and structural levels.
- Evaluate the seismic resilience of steel plate shear walls under expected collapse risk to estimate total loss and required recovery time for the structure after strong ground motions.

- Extending the numerical methodology developed in this study for C-PSWs to investigate the effects of design variables such as compressive strength of the concrete, yield strength of reinforcement, yield strength of infill plate and boundary members, and detailing of reinforcement in RC panel.

References

ABAQUS theory manual. (2003). Version 6.9. Hibbitt, Karlsson and Sorensen, Inc. Pawtucket, R.I.

AISC. (2016). "*Seismic provisions for structural steel buildings.*" ANSI/AISC 341-16, Chicago.

Allen, H.G., and Bulson, P.S. (1980). Background to buckling. U.K.: McGraw Hill Book Company.

Ali, M. M., Osman, S. A., Husam, O. A., and Al-Zand, A.W. (2018). "Numerical study of the cyclic behavior of steel plate shear wall systems (SPSWs) with differently shaped openings", Steel Compos. Struct., Int. J., 26(3), 361-373.

Alinia, M.M., and Sarraf-Shirazi, R. (2009). "On the design of stiffeners in steel plate shear walls." J Constr Steel Res; 65 (10-11): 2069-2077.

ANSYS Inc. (2010): Theory Reference for the Mechanical APDL and Mechanical Applications. Canonsburg, PA.

ASCE. 41-17. (2017). *Seismic rehabilitation of existing buildings.* ASCE/SEI 41-17. Reston, VA.

ASCE. (2016). *Minimum design loads for buildings and other structures*. ASCE/SEI 7-16. Reston, VA: ASCE.

Astaneh-Asl, A. (2001). "Seismic behavior and design of steel shear walls." Rep. Prepared for Structural Steel Education Council, Univ. of California at Berkeley, Berkeley, Calif.

Atkinson, G. (2009). "Earthquake time histories compatible with the 2005 National Building Code of Canada uniform hazard spectrum." Can. J. Civ. Eng. 36 (6): 991–1000. https://doi.org/10.1139/L09-044.

Barkhordari, M.A., Hosseinzadeh, S.A.A., and Seddighi, M. (2014), "Behavior of steel plate shear walls with stiffened full-height rectangular openings", Asian J. Civil Eng., 15(5), 741-759.

Barua, K., Bhowmick, A.K. (2019). "Nonlinear seismic performance of code designed perforated steel plate shear walls." Steel and Composite Structures; 31(1): 85–98.

Basler, K. (1961). Strength of Plate Girders under Combined Bending and Shear. Engineering Laboratory Rep. No. 186, Dept. of Civil Engineering, Univ. of Lehigh, Pennsylvania.

Berman, J., and Bruneau, M. (2003). Plastic Analysis and Design of Steel Plate Shear Walls. *Journal of Structural Engineering*, ASCE, 129(11), 1448–1456

Berman J.W, and Bruneau M. (2005). "Experimental investigation of light-gauge steel plate shear walls." Journal of Structural Engineering, 131(2): 259-267.

Berman, J. W., and Bruneau, M. (2008). “Capacity design of vertical boundary elements in steel plate shear walls.” *Eng. J.* 45(1), 57–71.

Bhowmick, A. K., Driver, R. G., and Grondin, G. Y. (2008). “Seismic analysis of steel plate shear walls considering strain rate and P-delta effects.” J. Construct. Steel Res., 65(12), 1149-1159.

Bhowmick, A. K, Grondin, G. Y., and Driver, R. G. (2014). “Nonlinear seismic analysis of perforated steel plate shear walls.” J Constr Steel Res; 94: 103–113.

Caccese, V., Elgaaly, M., and Chen, R. (1993). Experimental Study of Thin Steel Plate Shear Walls under Cyclic Load. *Journal of Structural Engineering*, 119(2), 573–587.

Choi, I. R., and Park, H. G. (2008). Steel Plate Shear Walls with Various Infill Plate Designs. *Journal of Structural Engineering*, ASCE, 135(7), 785-796.

Choi, I.R., and Park, H.G. (2010). “Hysteresis Model of Thin Infill Plate for Cyclic Nonlinear Analysis of Steel Plate Shear Walls.” *J. Struct. Eng*., 10.1061/(ASCE)ST.1943-541X.0000244, 1423–1434.

CSA (Canadian Standards Association). (2014). Limit states design of steel structures. CAN/CSA-S16-14. Toronto, Ontario, Canada.

Dastfan, M., and Driver, R. G. (2008). “Flexural stiffness limits for frame members of steel plate shear wall systems.” *Proc., Annual Stability Conf., Nashville*, Structural Stability Research Council, Rolla, MO.

Dey, S., and Bhowmick, A. (2016). Seismic Performance of Composite Plate Shear Walls. *Journal of Structures*, Elsevier, 6, 59-72.

Driver, R.G., Kulak, G.L., Kennedy, D.J.L., Elwi, A.E. (1997). “Seismic Behavior of Steel Plate Shear Walls,” *Structural Engineering Rep. No. 215,* Dept. of Civil Engineering, Univ. of Alberta, Edmonton.

Elgaaly, M. (1998). “Thin steel plate shear walls behavior and analysis.” Thin-Walled Struct., 32, 151–180.

Farahbakhshtooli, A., Bhowmick, A.K. (2018). “Seismic collapse analysis of stiffened steel plate shear walls.” *6th Annual Canadian Society of Civil Engineers Conference*, 13-16 June, Fredericton, New Brunswick, Canada.

Farahbakhshtooli, A., Bhowmick, A.K. (2018). “Development of deterioration model for analysis of unstiffened steel shear walls.” *6th Annual Canadian Society of Civil Engineers Conference*, 13-16 June, Fredericton, New Brunswick, Canada.

Farahbakhshtooli, A., Bhowmick, A.K. (2019). “Collapse assessment of stiffened steel plate shear walls using FEMA P695 Methodology.” *12th Canadian Conference on Earthquake Engineering*, 17-20 June, Quebec City, Quebec, Canada.

Farahbakhshtooli A, Bhowmick A.K. (2019). “Seismic collapse assessment of stiffened steel plate shear walls using FEMA P695 methodology.” *Engineering Structures*, 200, 1-19.

FEMA. (2000). Pre-standard and Commentary for Seismic Rehabilitation of Buildings. *FEMA Rep. No. 356*, ASCE for FEMA, Washington, United States.

FEMA. (2009). *Quantification of building seismic performance factors*. FEMA P695. Washington, DC: FEMA.

Galambos, T.V. (1998). “Guide to Stability Design Criteria for Metal Structures,” (5th Edition), John Wiley & Sons, New York, NY, USA.

Gholipour, M., and Alinia, M. M. (2016). “Behavior of Multi-Storey Code-Designed Steel Plate Shear Wall Structures Regarding Bay Width.” *Journal of Constructional Steel Research*, Elsevier, 122, 40–56.

Gogus, A., and Wallace, J. W. (2015). “Seismic safety evaluation of reinforced concrete walls through FEMA P695 methodology.” *J. Struct. Eng*., 10.1061/(ASCE)ST.1943-541X.0001221, 04015002.

Hosseinzadeh, S.A.A, Tehranizadeh, M. (2012). “Introduction of stiffened large rectangular openings in steel plate shear walls.” J Constr Steel Res; 77: 180–192.

Ibarra, L. F., and Krawinkler, H. (2005). “Global collapse of frame structures under seismic excitations.” *John A. Blume Earthquake Engineering Center, Technical Rep. No. 152*, Dept. of Civil Engineering, Stanford Univ., Stanford, CA.

Kharrazi, M. H. K., Ventura, C. E., Prion, H. G. L. (2011). “Analysis and design of steel plate walls: experimental evaluation.” *Canadian Journal of Civil Engineering*; 38(1): 60–70.

Lignos, D.G., Krawinkler, H. (2011). “Prediction and validation of sideway collapse of two scale models of a 4-storey steel moment frame.” Earthquake Engineering and Structural Dynamics; 40(7): 807–825.

Lubell, A. S., Prion, H. G. L., Ventura, C. E., and Rezai, M. (2000). "Unstiffened steel plate shear wall performance under cyclic loading." J. Struct. Eng., 126(4), 453–460.

Luco, N., and Cornell, C. A. (1998). "Effects of random connection fractures on demands and reliability for a 3-storey pre-Northridge SMRF structure." *Proc., 6th U.S. National Conf. on Earthquake Engineering*, Earthquake Engineering Research Institute, Seattle.

McKenna, F., Fenves, G., and Scott., M. (2013). *Computer program OpenSees: Open system for earthquake engineering simulation*. Berkeley, CA: Pacific Earthquake Engineering Center, Univ. of California.

NBC (National Building Code of Canada). (2015). *National building code of Canada, National research council of Canada. Ottawa*: NBC.

Park, H. G., Kwack, J. H., Jeon, S. W., and Choi, I. R. (2007). "Framed Steel Plate Wall Behavior under Cyclic Lateral Loading." J. Struct. Eng., 133(3), 378-388.

Purba, RH. (2006). "Design recommendations for perforated steel plate shear walls." M.Sc. Thesis, Buffalo, New York, USA: State University of New York at Buffalo.

Purba, R., and Bruneau, M. (2009). "Finite-element investigation and design recommendations for perforated steel plate shear walls." Journal of Structural Engineering; 135(11): 1367–1376.

Purba, R., and Bruneau, M. (2014a). "Seismic performance of steel plate shear walls considering two different design philosophies of infill plates. I: Deterioration model development." J. Struct. Eng., 10.1061/(ASCE) ST.1943-541X.0001098, 04014160.

Purba, R., and Bruneau, M. (2014b). "Seismic performance of steel plate shear walls considering two different design philosophies of infill plates. II: Assessment of collapse potential." *J. Struct. Eng.*, 10.1061/(ASCE)ST .1943-541X.0001097, 04014161.

Qu, B., and Bruneau, M. (2008). Seismic Behavior and Design of Boundary Frame Members of Steel Plate Shear Walls. *Technical Rep. MCEER-08-0012,* Multidisciplinary Center for Earthquake Engineering Research, Buffalo, United States.

Qu, B., and Bruneau, M. (2009). Design of Steel Plate Shear Walls Considering Boundary Frame Moment Resisting Action. *Journal of Structural Engineering*, ASCE, 135(12), 1511–1521.

Rahai, A., and Hatami, F. (2009). "Evaluation of composite shear wall behavior under cyclic loadings." J. Constr. Steel Res., 65(7), 1528–1537.

Rahmzadeh, A., Ghassemieh, M., and Park, Y., Abolmaali A. (2016). "Effect of stiffeners on steel plate shear wall systems." Steel and Composite Structures; 20(3): 545–569.

Roberts, T., and Sabouri-Ghomi, S. (1991). “Hysteretic characteristics of unstiffened plate shear panels.” *Thin Walled Struct*., 12(2), 145–162.

Roberts, T., and Sabouri-Ghomi, S. (1992). “Nonlinear dynamic analysis of steel plate shear walls including shear and bending deformations.” *Engineering Structures*, 14(5), 309–317.

Sabelli, R., and Bruneau, M. (2015). “Steel design guide 20: steel plate shear walls.” American Institute of Steel Construction, Chicago, IL.

Sabouri-Ghomi, S., Kharrazi, M. H. K., Mamazizi, S. E. D., Sajjadi, R.A. (2008). “Buckling behavior improvement of steel plate shear wall systems.” Struct Des Tall Special Build; 17(4): 823–837.

Sabouri-Ghomi, S., Mamazizi, S. (2015). “Experimental investigation on stiffened steel plate shear walls with two rectangular openings.” Thin-Walled Structures; 86: 56–66.

Sabouri-Ghomi S, Mamazizi S, Alavi M. (2016). “An investigation into linear and nonlinear behavior of stiffened steel plate shear panels with two openings.” Advances in Structural Engineering, 18(5): 687–700.

Sabouri-Ghomi, S. and Sajjadi, S.R.A. (2012). “Experimental and theoretical studies of steel shear walls with and without stiffeners.” *J. Constr. Steel Res*., 75, 152–159.

SeismoSoft. (2014). SeismoStruct – User Manual For version 7.0. www.seismosoft.com, Pavia, Italy.

Shekastehband, B., Azaraxsh, A.A., and Showkati, H. (2017), “Hysteretic behavior of perforated steel plate shear walls with beam-only connected infill plates”, Steel Compos. Struct., Int. J., 25(4), 505-521.

Soltani, N., Abedi, K., Poursha, M., and Golabi, H. (2017). “An investigation of seismic parameters of low yield strength steel plate shear walls”, Eartq. Struct., Int. J., 12(6), 713-723.

Song, J. K., and Pincheira, J. A. (2000). Seismic Analysis of Older Reinforced Concrete Columns. *Journal of Earthquake Spectra*, ASCE, 15(2), 817-851.

Takahashi, Y., Takeda, T., Takemoto, Y., and Takagai, M. (1973). “Experimental study on thin steel shear walls and particular steel bracing under alternating horizontal loading.” IABSE, Symposium on resistance and ultimate deformability of structures acted on by well-defined repeated loads, Lisbon, Portugal, 185-19.

Thorburn, L. J., Kulak, G. L., and Montgomery, C. J. (1983). "Analysis of steel plate shear walls." *Structural Engineering Rep. No. 107*, Dept. of Civil Engineering, Univ. of Alberta, Edmonton, AB, Canada.

Timler, P. A., and Kulak, G. L. (1983). Experimental Study of Steel Plate Shear Walls. *Structural Engineering Rep. No. 114*, Dept. of Civil Engineering, Univ. of Alberta, Edmonton.

Timoshenko, SP., and Gere, J.M. (1961) "Theory of elastic stability." New York: McGraw-Hill.

Vamvatsikos, D., and Cornell, C. A. (2002). The Incremental Dynamic Analysis and Its Application to Performance-Based Earthquake Engineering. 12th European Conference on Earthquake Engineering, London, United Kingdom, **1:** 479-488.

Vamvatsikos, D., and Cornell, C. A. (2002). "Incremental dynamic analysis." *Earthquake Eng. Struct. Dyn.*, 31(3), 491–514.

Vian, D., and Bruneau, M. (2004). "Testing of Special LYS Steel Plate Shear Walls. In *Proc., 13th World Conf. on Earthquake Engineering*. Vancouver, BC, Canada, 978-987.

Zhao, Q., and Astaneh-Asl, A. (2002). ''Cyclic behavior of traditional and an innovative composite shear wall,'' *Rep. No. UCB-Steel-01/2002*, Dept. of Civil and Environmental Engineering, Univ. of California, Berkeley, Calif.

Zhao, Q., and Astaneh-Asl, A. (2004). "Cyclic behavior of traditional and innovative composite shear walls." J. Struct. Eng., 130(2), 271–284.

Zhao, Q., and Astaneh-Asl, A. (2007). "Seismic behavior of composite shear wall systems and application of smart structures technology." *Journal of Steel Structures*, 7, 69–75.